Impact of Osmotic Stressors on the Metabolic Activity of *Methylocystis* sp. Strain SC2

Dissertation

„Kumulativ“

zur Erlangung des Grades eines
Doktor der Naturwissenschaften
(Dr. rer. nat.)

des Fachbereichs Biologie

der Philipps-Universität Marburg

Vorgelegt von

Kangli Guo

Aus Yibin, China

Marburg/Lahn, Deutschland | 2022

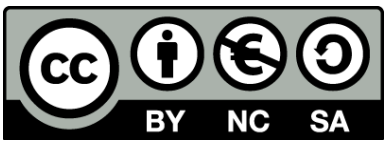

Die vorliegende Dissertation wurde von Oktober 2018 bis Oktober 2022 am Max Planck-Institut für terrestrische Mikrobiologie in Marburg/Lahn unter der Leitung von Herrn PD Dr. Werner Liesack angefertigt.

Vom Fachbereich Biologie
der Philipps-Universität Marburg in Marburg/Lahn
(Hochschulkennziffer 1180) als Dissertation
angenommen am **25. Oktober, 2022**

Erstgutachter(in):	Herr PD Dr. Werner Liesack
Zweitgutachter(in):	Herr Prof. Dr. Martin Thanbichler

Weitere Mitglieder der Prüfungskommission:
Herr PD Dr. Gert Bange
Herr Prof. Dr. Lennart Randau
Tag der Disputation: **13. Januar, 2023**

Die in dieser Dissertation beschriebenen Ergebnisse sind in folgenden Publikationen veröffentlicht bzw. zur Veröffentlichung vorgesehen:

Guo K, Hakobyan A, Glatter T, Paczia N, Liesack W*. (**2022**) *Methylocystis* sp. strain SC2 acclimatizes to increasing NH_4^+ levels by a precise rebalancing of enzymes and osmolyte composition, e0040322.

Guo K, Glatter T, Paczia T*, Liesack W*. Asparagine uptake: a cellular strategy of *Methylocystis* spp. to combat severe salt stress. (***submitted***) (*corresponding authors)

ERKLÄRUNG

Hiermit versichere ich, dass ich meine Dissertation mit dem Titel "Impact of osmotic stressors on the metabolic activity of *Methylocystis* sp. strain SC2 " selbständig und ohne unerlaubte Unterstützung angefertigt und mich dabei keiner anderen als der von mir ausdrücklich bezeichneten Quellen und Hilfen bedient habe.

Die Dissertation wurde weder in der jetzigen noch in einer ähnlichen Form bei einer anderen Hochschule eingereicht und hat keinen sonstigen Prüfungszwecken gedient.

Marburg, den 25. Oktober, 2022

Kangli Guo

Dedicated to my beloved parents and family members.

“Insight must precede application.”

— Max Planck

Summary

Proteobacterial methane-oxidizing bacteria, or methanotrophs, have the unique ability to grow on methane as their sole source of carbon and energy. Among these, *Methylocystis* spp. belong to the family *Methylocystaceae* within the *Alphaproteobacteria*. Their key enzyme is the particulate methane monooxygenase (pMMO), which oxidizes methane to methanol. *Methylocystis* spp. are among the ecologically most relevant methanotroph populations in terrestrial environments and are widely distributed in diverse habitats. In consequence, *Methylocystis* spp. require a range of physiological capabilities that allow them to respond and acclimatize to fluctuations in abiotic and biotic factors in their native environment. However, to date there still exist major gaps in our knowledge of their metabolic potential, in particular with regard to their ability to acclimatize to environmental change and to cope with abiotic stress.

In my first project, we used a recently developed proteome workflow to elucidate the cellular mechanisms underlying the acclimatization of *Methylocystis* sp. strain SC2 to high NH_4^+ load (added as NH_4Cl). Relative to 1 mM NH_4^+, high (50 mM and 75 mM) NH_4^+ load under CH_4-replete conditions significantly increased the lag phase duration required for proteome adjustment, while the addition of 100 mM NH_4^+ completely inhibited growth of strain SC2. The number of differentially regulated proteins was highly significantly correlated to the increase in NH_4^+ load. The cellular responses involved the significant upregulation of stress-responsive proteins, the K^+ "salt-in" strategy, the synthesis of compatible solutes (glutamate and proline), and the glutathione metabolism. The apparent K_m value for CH_4 oxidation significantly increased with the NH_4^+ load. This observation was indicative of an increased pMMO-based oxidation of NH_3 to toxic hydroxylamine. In consequence, the detoxifying activity of hydroxlyamine oxidoreductase (HAO) increased with the NH_4^+ concentration and led to a significant accumulation of NO_2^- and, with delay, N_2O. Significant production of N_2O occurred only after the oxygen concentration had dropped to low or unmeasurable levels. Thus, high NH_4^+ load had a dual effect on the activity of strain SC2, with one being general phenomenon of ionic-osmotic stress and the other being the competitive inhibition effect

of NH_3 on pMMO-based methane oxidation. Although strain SC2 precisely rebalanced enzymes and osmolyte composition in response to the increase in NH_4^+ load, the need to simultaneously combat both ionic-osmotic stress and the toxic effects of hydroxylamine may be the reason why its acclimatization capacity is limited to 75 mM NH_4^+.

Starting point of my second project was the knowledge that the growth of strain SC2 is completely inhibited at medium concentrations ≥ 1.5% NaCl. Sodium chloride is an important ionic-osmotic stressor in bulk and rhizosphere soils. We therefore tested various amino acids and other osmolytes for their potential to act as a compatible solute or osmoprotectant under otherwise inhibitory NaCl conditions. The addition of 10 mM asparagine to the growth medium had the greatest stress relief effect under severe salinity (1.5% NaCl), leading to a partial growth recovery of strain SC2. The analysis of the exo-metabolome revealed that asparagine was taken up quantitatively by strain SC2. This resulted in an intracellular concentration of 264 ± 57 mM asparagine. Under severe salinity (1.5% NaCl), the uptake of asparagine induced major proteome rearrangements related to the KEGG level 2 categories energy metabolism, amino acid metabolism, and cell growth and death. In particular, various proteins involved in cell division and peptidoglycan synthesis showed a positive expression response. The incorporation of asparagine-derived ^{13}C-carbon into nearly all amino acids indicated that asparagine acted as a source for cell biomass under severe salinity (1.5% NaCl), with glutamate being a major hub between central carbon and amino acid pathways.

Zusammenfassung

Die zu den *Proteobacteria* gehörenden methanoxidierenden Bakterien, oder auch Methanotrophe, sind durch ihre Fähigkeit charakterisiert Methan gleichzeitig als Energie- und Kohlenstoffquelle nutzen zu können. Ihr Schlüsselenzym ist die partikuläre Methan-Monooxygenase (pMMO), welches Methan zu Methanol oxidiert. *Methylocystis* spp., welche zur Familie *Methylocystaceae* innerhalb der *Alphaproteobacteria* gehören, zählen zu den funktionell bedeutendsten Methanotrophen in terrestrischen Ökosystemen. Tatsächlich sind Mitglieder der Gattung *Methylocystis* in Standorten mit stark variierenden Umweltbedingungen weit verbreitet. Grundlage hierfür ist ihr physiologisches Potential sich schnell an wechselnde abiotische und biotische Umwelteinflüsse anpassen zu können. Allerdings existiert bis heute ein Mangel an Kenntnissen über die zellulären Mechanismen, mit denen *Methylocystis* spp. auf abiotischen Stress zu reagieren vermögen.

Daher sollten in meinem ersten Projekt die zellulären Mechanismen aufgeklärt werden, welche es *Methylocystis* sp. Stamm SC2 erlaubt sich an eine hohe Ammoniumbelastung (zugefügt als NH_4Cl) anzupassen. Ausgangspunkt war die Kenntnis, dass das Wachstum von Stamm SC2 bereits durch eine Belastung mit 100 mM NH_4^+ vollständig gehemmt wird. Zur Anwendung kam eine kürzlich entwickelte Methode, mit der das Proteom von Stamm SC2 effizient analysiert werden kann. Eine hohe (50 mM und 75 mM) Belastung mit NH_4^+ im Medium führte, relativ zu 1 mM NH_4^+, unter nicht limitierenden Methanbedingungen zu einer signifikant erhöhten Dauer der lag-Phase. Korrespondierend dazu erhöhte sich die Anzahl differentiell regulierter Proteine mit der Ammoniumbelastung signifikant. Die zelluläre Antwort beinhaltete eine erhöhte Expression von Stress-Proteinen, der K^+ "Salz-in" Strategie und des Glutathion-Metabolismus sowie eine Akkumulation kompatibler Solute (Glutamat und Prolin). Verursacht durch die vermehrte pMMO-basierte Oxidation von NH_4^+ zum toxischen Hydroxlyamin (NH_2OH) erhöhte sich der apparente K_m-Wert der Methanoxidation mit zunehmender Ammoniumbelastung signifikant. Korrespondierend dazu erhöhte sich die Aktivität der Hydroxylamin-Oxidoreduktase (HAO), welches zu einer Akkumulation von Nitrit und Distickstoffoxid (N_2O) führte. Eine signifikante Produktion von N_2O fand erst statt, nachdem die Sauerstoffkonzentration auf ein sehr niedriges Niveau gefallen war. Offensichtlich hatte eine hohe Ammoniumbelastung einen doppelten Effekt auf die Aktivität von Stamm SC2. Dies war zum einen der durch NH_4Cl verursachte osmotische

Stress und zum anderen die kompetitive Hemmung der pMMO-basierten Methanoxidation durch Ammoniak; letzteres ein spezifisches Phänomen methanotropher Bakterien. Obgleich Stamm SC2 fähig war Proteom und kompatible Solute der steigenden Ammoniumbelastung exakt anzupassen, ist die Notwendigkeit sowohl auf osmotischen Stress als auch auf den toxischen Effekt von Hydroxylamin reagieren zu müssen vermutlich der Grund, warum eine zelluläre Akklimatisation nur bis zu einer Belastung mit 75 mM NH_4^+ im Medium möglich war.

Ausgangspunkt meines zweiten Projekts war die Kenntnis, dass das Wachstum von Stamm SC2 bei einer Konzentration von 1,5% NaCl im Medium vollständig gehemmt ist. Natriumchlorid ist ein wichtiger osmotischer Stressor im Boden und Rhizosphäre. Wir testeten daher eine Reihe von Aminosäuren und anderer Osmolyte auf ihre Schutzwirkung als kompatibles Solut. Dabei zeigte die Zugabe von 10 mM Asparagin in das Medium die größte stressmindernde Wirkung auf Stamm SC2 bei Inkubation mit 1.5% NaCl, was eine teilweise Wachstumswiederbelebung zur Folge hatte. Die Analyse des Exo-Metaboloms bestätigte eine vollständige Aufnahme des Asparagins in die Zellen. Dies resultierte in eine intrazelluläre Konzentration von 264 ± 57 mM Asparagin. Die zelluläre Aufnahme von Asparagin unter Salzstress (1,5% NaCl) induzierte eine erhebliche Proteomantwort, die insbesondere Proteine mit Bezug zum Energie-Metabolismus, Aminosäure-Stoffwechsel sowie Zellteilung und Zelltod betraf. So wurde die Synthese einer Reihe von Proteinen, welche in Zellteilung und Peptidoglykan-Synthese involviert sind, aufreguliert. Der Nachweis von ^{13}C-Kohlenstoff, abgeleitet von markiertem Asparagin, in nahezu allen freien intrazellulären Aminosäuren lieferte Evidenz, dass Asparagin unter Salzstress zur Bildung von Zellbiomasse beiträgt und die Umsetzung von Glutamat ein entscheidendes Bindeglied zwischen dem zentralen Kohlenstoff-Metabolismus und dem Aminosäure-Stoffwechsel ist.

Chapter 1: Introduction

1 Introduction

1.1 Methane in the Global Carbon Cycle

1.1.1 Methane budget

Next to carbon dioxide (CO_2), methane (CH_4) is the most important greenhouse gas, responsible for about 30% of the rise in global warming since the industrial revolution (Jackson et al., 2020; Arias et al., 2021). CO_2 remains in the atmosphere for hundreds to thousands of years and thus much longer than CH_4 (around nine years). However, since CH_4 absorbs thermal infrared radiation from the sun more efficiently than CO_2, it has 84-87 times more global warming potential than CO_2 over a 20-year timeframe (GWP_{20}) (Dean et al., 2018). Furthermore, methane affects the air quality because it is an ingredient in the formation of tropospheric ozone (West et al., 2006). Atmospheric CH_4 concentrations have accelerated in recent years, reaching approximately 1888.3 parts per billion in 2021 which is likely to be among the largest annual increases ever recorded (Fig 1.1) (NOAA, 2021). The most recent estimate suggests that global CH_4 emissions are around 570 million tons per year (Reay et al., 2018). Understanding global CH_4 sources and sinks is a prerequisite for the design of strategies to counteract global warming.

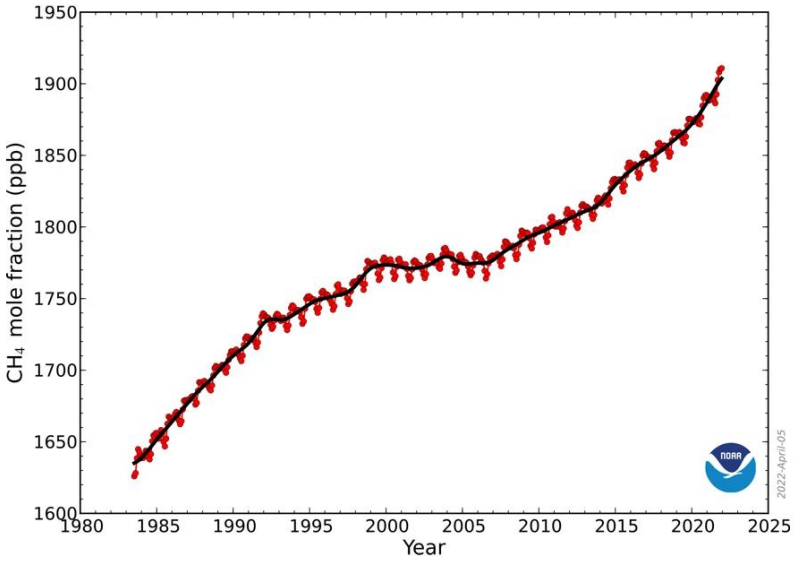

Fig. 1.1 The annual increase in atmospheric CH_4 since systematic measurements began in 1983. Figure adopted from (NOAA, 2021, https://www.noaa.gov/).

CH_4 is emitted in a variety of biotic and abiotic processes, involving anthropogenic and natural sources. Anthropogenic emissions, caused by direct human activity, include agriculture, waste management, and fossil-fuel-related activities, which collectively contribute 60% to the total CH_4 emission (Jackson et al., 2020). The natural sources of CH_4 can be divided into "wetlands" and "other natural" emissions such as non-wetland inland waters, wild animals, termites, land geological sources, oceanic geological and biogenic sources, and terrestrial permafrost (Saunois et al., 2020). Collectively, these natural sources contribute 40% to the total CH_4 emission (Fig 1.2).

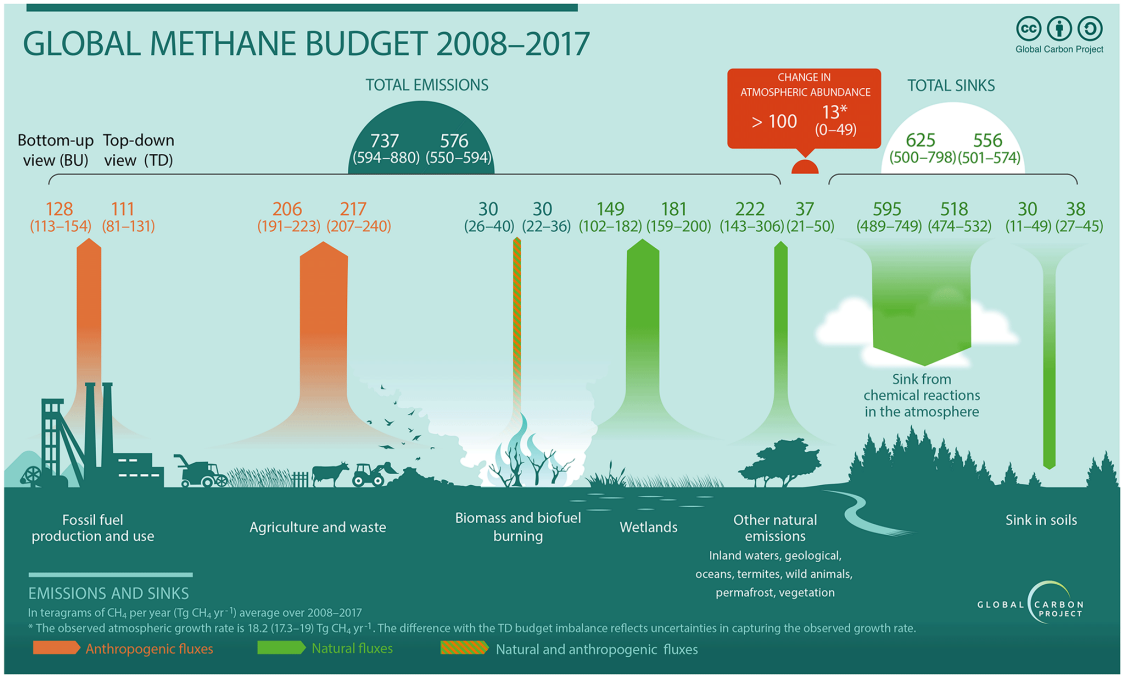

Fig. 1.2 Methane emissions and sinks. Figure adopted from (Saunois et al., 2020).

1.1.2 Methanogen ecology

Indeed, both anthropogenic and natural sources are associated with biogenic and abiogenic CH_4 emissions (Fig 1.2). The biogenic sources, including rice fields and natural wetlands, account for almost half of the total (44%) global CH_4 budget. Here, CH_4 is the final product of the anoxic decomposition of organic matter by methanogenic archaea (methanogens) (Chen and Prinn, 2005; Conrad, 2007; Saunois et al., 2020). Other methanogenic sources are the intestines of ruminants and termites (20%), landfills, and other waste treatment systems (10%). Thus, 75% of the total atmospheric CH_4 originates from the activity of methanogens in various anoxic environments (Knapp et al., 2014).

As strict anaerobes, methanogens have long been believed to be limited to anoxic habitats. However, recent studies have shown that some methanogens produce CH_4 in

oxic environments (Lyu et al., 2018). Most recently, it was shown that in the presence of oxygen, many organisms across all domains of life could form CH_4, including plants, fungi, algae, and cyanobacteria (Ernst et al., 2022). The formation of CH_4 by these non-methanogenic organisms is triggered by free iron and reactive oxygen species (ROS). ROS-induced methyl radicals are key intermediates for CH_4 production (Ernst et al., 2022). However, these sources make only a small contribution to the global CH_4 budget.

Methanogenesis is a form of anaerobic respiration carried out by microorganisms that belong to the phylum *Euryarchaeota* within the domain *Archaea*. Methanogens can be classified into three group based on their substrate. These are aceticlastic (acetate), hydrogenotrophic (H_2/CO_2) and methylotrophic (methylated compounds) methanogens. Taxonomically, they are organized into eight orders: *Methanosarcinales*, *Methanomicrobiales*, *Methanopyrales*, *Methanocellales*, *Methanococcales*, *Methanobacteriales*, *Methanonatronarchaeales*, and *Methanomassiliicoccales* (Balch et al., 1979; Sakai et al., 2008; Dridi et al., 2012; Iino et al., 2013). Aceticlastic methanogenesis can be found only in the order *Methanosarcinales*. In contrast, hydrogenotrophic methanogenesis is present in almost all methanogenic orders with the exception of the *Methanomassiliicoccales*. Methylotrophic methanogenesis is found in the orders *Methanosarcinales*, *Methanomicrobiales*, and *Methanomassiliicoccales*. Over the last decade, methanogenesis has been recognized no longer to be restricted to the *Euryarchaeota* but also to be present in the *Bathyarchaeota* (Guerrero-Cruz et al., 2021). In addition, methanogenic archaea have representatives in three superphyla: TACK (*Thaumarchaeota*, *Aigarchaeota*, *Crenarchaeota*, and *Korarchaeota*) (Lloyd, 2015; Berghuis et al., 2019), DPANN (*Diapherotrites*, P*arvarchaeota*, *Aenigmarchaeota*, *Nanoarchaeota*, and *Nanohaloarchaeota*) (Castelle and Banfield, 2018), and the Asgard superphylum (Evans et al., 2015; Guerrero-Cruz et al., 2021). However, all data regarding methanogenesis outside of the *Euryarchaeota* is based on genome analysis and require laboratory studies which at present are not possible due to the lack of isolates.

The methanogens show diversity in regard to their substrates (Fig. 1.3). Acetate-consuming methanogens are fairly well studied and contribute to approximately 2/3 of the global biomethane production (Conrad, 2005). The *Methanosarcina* and *Methanosaeta* ("*Methanothrix*") genera are the only aceticlastic methanogens known to date. The *Methanosaeta* genus is strictly dependent on acetate showing high affinity to

the

substrate (Jetten et al., 1990; Rotaru et al., 2014). *Methanosaeta* is the most abundant aceticlastic methanogen in environments where a low acetate concentration is observed (Jetten et al., 1990). In contrast, *Methanosarcina* has a high growth rate and low affinity for acetate, making their enrichment much easier using routine isolation procedures. Moreover, *Methanosarcina* has a versatile substrate range, including methanol and methylated amines, and the ability for hydrogenotrophic growth. It can be considered a generalist (Stams et al., 2019).

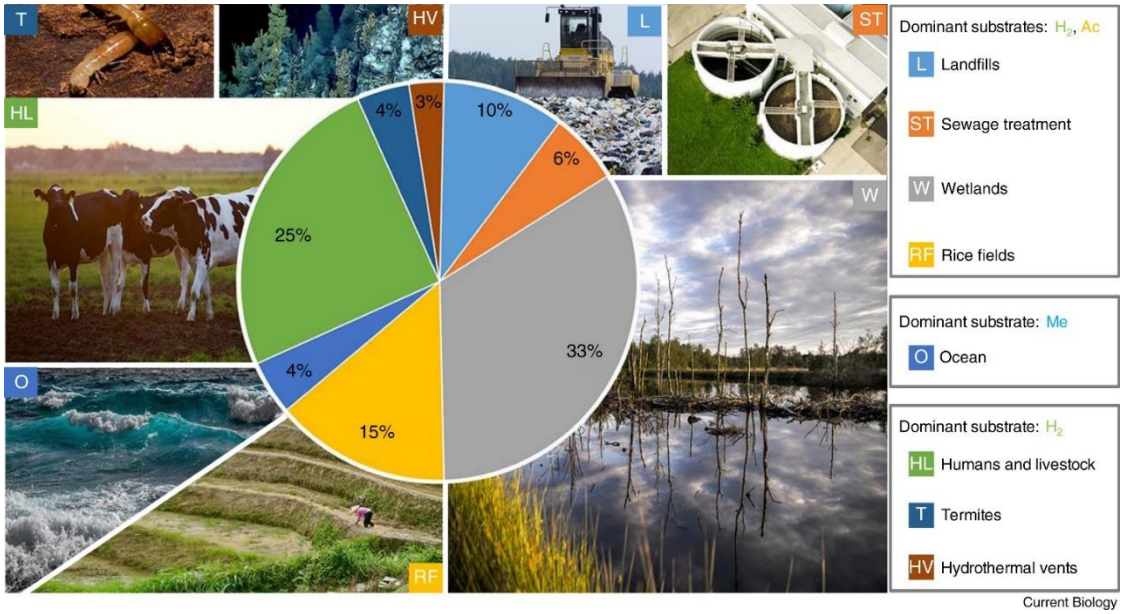

Fig. 1.3 Sources of biogenic methane emissions to the atmosphere. Figure adopted from (Lyu et al., 2018).

Hydrogenotrophic methanogenesis is most dominant in terms of both CH_4 emissions and community composition, with 1/3 contribution to the total global biomethane production (Fig. 1.4) (Conrad, 2005). *Methanosarcinales*, *Methanomicrobiales*, *Methanopyrales*, *Methanocellales*, *Methanococcales*, and *Methanobacteriales* utilize H_2 and CO_2 to produce CH_4 via the methyl branch of the archaeal type Wood–Ljungdahl pathway (WLP) or the reductive methyl-CoM reduction. Hydrogen can be replaced by formate, carbon monoxide (CO), or alcohols as substrates (Conrad, 2020). It is postulated that hydrogenotrophic methanogenesis is the ancestral form of CH_4 production due to its broad distribution (Bapteste et al., 2005; Berghuis et al., 2019).

Methylotrophic methanogenesis uses certain methylated compounds (methylamines and methylated sulfides) and is common in marine systems and in hypersaline, sulfate-rich environments (Fig. 1.4) (Alcolombri et al., 2015; Lyu et al., 2018). The environmental production of methanol is different from acetate, CO_2, and H_2. Methylotrophic methanogenesis is less frequently detected and thus remains poorly understood (Xiao et al., 2018).

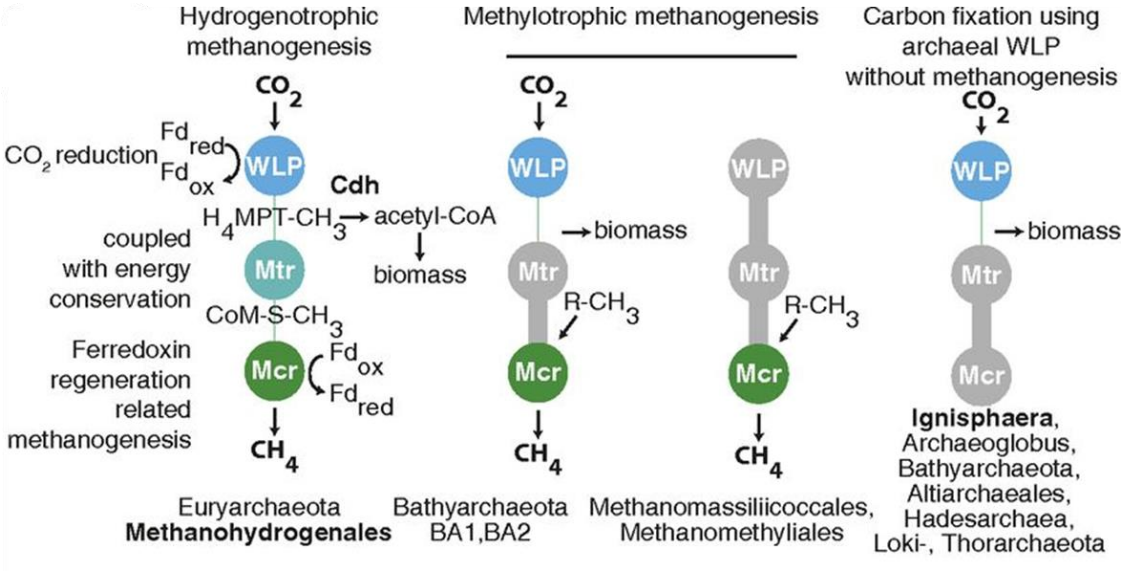

Fig. 1.4 Pathways of methanogenesis. Abbreviations: Mtr, coenzyme M methyltransferase; Mcr, methyl-coenzyme M reductase; MLP, Wood–Ljungdahl pathway; Fd, ferredoxin. Figure adopted from (Berghuis et al., 2019).

The ratio of aceticlastic and methylotrophic methanogenesis is tightly regulated by substrate quantity and quality. An overview about the environmental significance of hydrogenotrophic and aceticlastic methanogenesis for CH_4 production can be found in a review by Conrad (2020). If the degradation of complex organic matter is complete, the fermentation pathways result in the production of acetate and H_2, which favors > 67% aceticlastic methanogenesis and 33% hydrogenotrophic methanogenesis (Smith and Mah, 1966; Conrad, 2020). If organic matter is incompletely degraded or complex organic substrates and recalcitrant organic matter increase in soil or sediment, their degradation occurs predominantly by (> 50%) hydrogenotrophic methanogenesis (Conrad et al., 2010; Ji et al., 2016). These results provided insights into why a transition from aceticlastic to hydrogenotrophic methanogenesis might have occurred.

1.1.3 Methanotroph ecology

In terrestrial and aquatic environments, only a fraction of produced CH_4 is emitted to the atmosphere. Most of CH_4 is oxidized to reduce global CH_4 emission to the atmosphere (Saunois et al., 2020). CH_4 oxidation can occur in both oxic and anoxic environments using oxygen or alternative terminal electron acceptors; however, this involves both completely different biochemical processes and very different microbial groups.

Anaerobic CH_4 oxidation. Anaerobic oxidation of methane (AOM) is a major biological sink in anoxic marine and natural sediments (Conrad, 2009). Briefly, anaerobic methane oxidation (ANME) is coupled to the reduction of sulfate, nitrate/nitrite, iron, manganese, or organic electron accepters as the terminal electron acceptor (Cui et al., 2015; Guerrero-Cruz et al., 2021; Karthikeyan et al., 2021). Several archaeal lineages have been shown to mediate AOM, which are phylogenetically related to different methanogenic archaea. ANME-1 and ANME-2 archaea are the most abundant groups of ANME. ANME-1 archaea are distantly related to the orders *Methanosarcinales* and *Methanomicrobiales*. ANME-2 archaea belong to the order *Methanosarcinales*. ANME-3 archaea are mostly present in submarine mud volcanoes and related to the genera *Methanococcoides* of *Methanosarcinales* order (Wang et al., 2014). The biological process of anaerobic methane oxidation was described as sulfate-dependent anaerobic methane oxidation (S-DAMO) which is performed by a microbial consortium consisting of sulfate-reducing bacteria (SRB) and methanotrophic archaea (S-DAMO). ANME-1 and ANME-2 archaea are associated with SRB of the genera *Desulfosarcina and Desulfococcus*, while ANME-3 archaea are associated with SRB of the *Desulfobulbus* branch. The ANME group for S-DAMO is further divided into subgroups, including ANME-1a and ANME-1b, ANME-2a, ANME-2b, and ANME-2c. No subgroups are shown for ANME-3.

In freshwater sediments, abundant nitrate and nitrite thermodynamically favor CH_4 oxidation relative to sulfate reduction. The anaerobic methanotrophs that use nitrate or nitrite as the electron donor for CH_4 oxidation are referred to as nitrogen-dependent anaerobic methane oxidation (N-DAMO) group (Norði and Thamdrup, 2014). The methanotrophic representatives of the candidate phylum NC10, such as *Candidatus* Methylomirabilis oxyfera, were shown to perform nitrite-dependent anaerobic methane oxidation (Luesken Francisca et al., 2011; Versantvoort et al., 2018). The new mechanism of N-DAMO involves an “intra-aerobic” pathway of nitrite reduction to NO and O_2 by

Candidatus Methylomirabilis oxyfera in anoxic habitats (Ettwig et al., 2010). The O_2 is used as terminal electron acceptor for the intra-aerobic pathway of CH_4 oxidation (Ettwig et al., 2010). Subsequently, the archaea ANME-2d partner of the NC10 bacteria named *Candidatus* Methanoperedens nitroreducens was identified to use nitrate rather than nitrite as the terminal electron acceptor, which is different from *M. oxyfera*. For comparisons between *Candidatus* Methylomirabilis oxyfera (*M. oxyfera*) and *Candidatus* Methanoperedens nitroreducens (*M. nitroreducens*), the reader is referred to a review article (Cui et al., 2015). Metal ions, i.e. manganese (Mn^{4+}) and iron (Fe^{3+}), are abundant in marine methane-seep sediments and act as electron acceptors for AOM (M-DAMO). The M-DAMO may play an important role in global marine AOM although its mechanism still remains unclear (Cui et al., 2015).

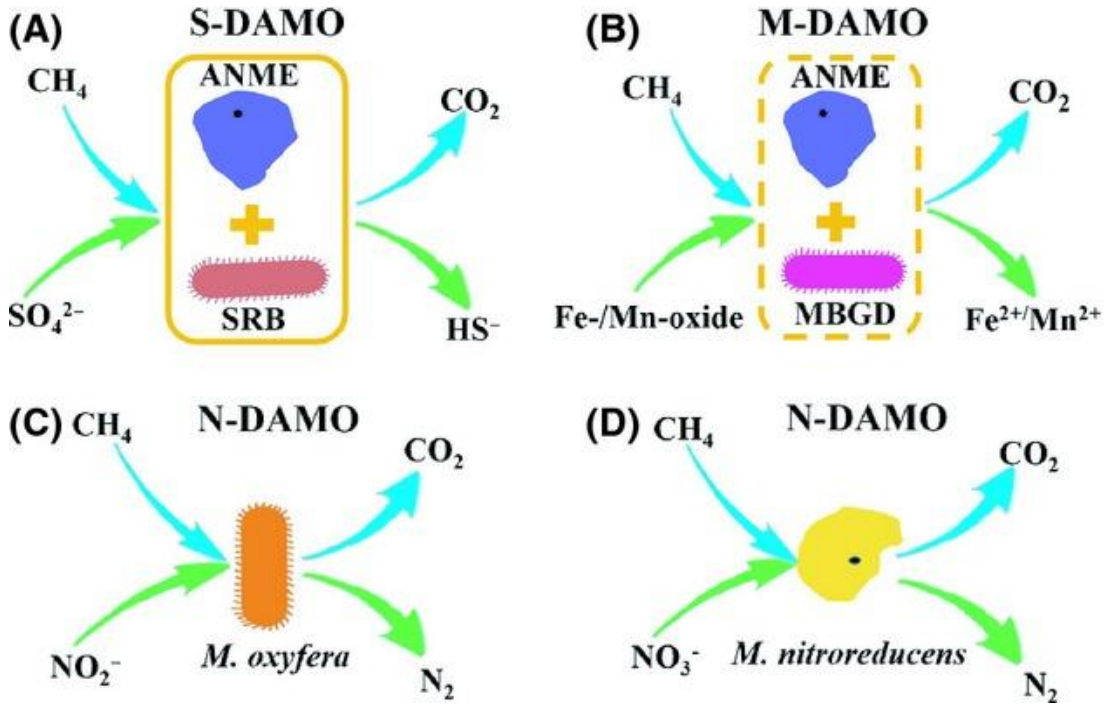

Fig 1.5 Three electron-accepting processes coupled to anaerobic methane oxidation (AOM) in natural environments: (A) sulfate-dependent anaerobic methane oxidation (S-DAMO); (B) metal ion (Mn^{4+} and Fe^{3+})-dependent anaerobic methane oxidation (M-DAMO); and (C, D) nitrate/nitrite-dependent anaerobic methane oxidation (N-DAMO). Abbreviations: ANME, anaerobic methane oxidation; SRB, sulfate-reducing bacteria; *M. oxyfera*, *Candidatus* Methylomirabilis oxyfera; *M. nitroreducens*, *Candidatus* Methanoperedens nitroreducens; MBGD, marine benthic group D. Figure adopted from (Cui et al., 2015).

Aerobic CH_4 oxidation. Aerobic methanotrophic bacteria typically inhabit anoxic-oxic interfaces (Brune et al., 2000; Reim et al., 2012). Extensive enrichment and isolation

work by Whittenbury et al. led to the isolation of a large variety of methanotrophs into pure culture (Whittenbury et al., 1970). With the increasing availability of molecular methods for the identification and classification of microorganisms, the number of methanotroph cultures has doubled over the last 10 years. Nearly all the aerobic methanotrophs have been identified to belong to the phylum *Proteobacteria* (Knief, 2015). A limited number of isolates, however, further expanded our knowledge of the phylum *Verrucomicrobia* for bacteria that are able to utilize CH_4 as the sole carbon and energy source (Dunfield et al., 2007; Pol et al., 2007; Camp, 2009).

Proteobacterial methanotrophs are classified into two major groups, type I (*Gammaproteobacteria*) and type II (*Alphaproteobacteria*) methanotrophs based on morphology, ultrastructure, phylogeny, and metabolic pathways (Whittenbury and Dalton, 1981). The carbon fixation mechanism via the ribulose monophosphate pathway (RuMP, type I) or serine pathway (type II) is still a distinctive feature to differentiate type I and type II methanotrophs (Knief, 2015; Dedysh and Knief, 2018), while other traits found in various genera and species do not longer exclusively differentiate between type I and type II methanotrophs.

To date, 23 methanotrophic genera and 56 different species with validly published names within the *Proteobacteria* have been proposed, with five genera being described in the *Alphaproteobacteria* (Fig 1.6) (Knief, 2015; Dedysh and Knief, 2018). Alphaproteobacterial methanotrophs belong to the families *Methylocystaceae* (type IIa), including the genera *Methylocystis* and *Methylosinus*, and *Beijerinckiaceae* (type IIb), including the genera *Methylocella*, *Methylocapsa*, and *Methyloferula* (Knief, 2015). Members of the genus *Methylocystis* are strictly aerobic bacteria with type II intracytoplasmic membranes (ICM). They are among the most ecologically relevant methanotroph populations in terrestrial habitats (Bowman, 2015) and commonly found in diverse environments, such as different soils, rice paddies, peatlands, landfills, and freshwater sediments (Belova et al., 2013; Bowman, 2015; Leng et al., 2015; Tikhonova et al., 2021). At species level, *Methylocystis* species that are related to *Methylocystis rosea*, *Methylocystis hirsuta*, and *Methylocystis echinoides* have most frequently been isolated.

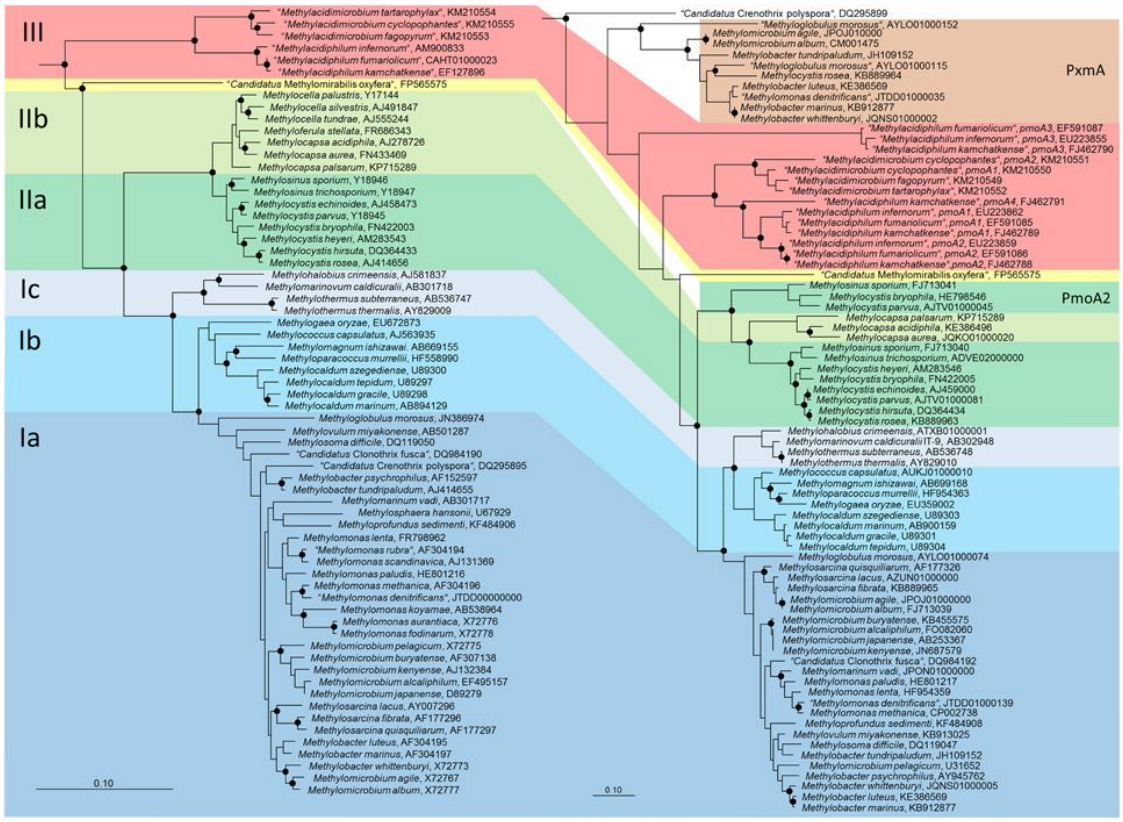

Fig 1.6 Phylogenetic trees showing the phylogeny of methantrophic type strains based on sequences of both 16S rRNA gene and *pmoA*. The Neighbor-Joining trees were calculated using the ARB software package (Ludwig et al., 2004) based on 1556 nucleotide positions (16S rRNA gene) with Jukes Cantor correction and 160 amino acid positions (PmoA) with Kimura correction, respectively. PmoA sequences of *Methylobacter luteus*, *Methylobacter whittenburyi*, and *Methylomicrobium pelagicu* are not available from the type strains, but were taken from a different strain representing the species. The 16S rRNA gene tree was rooted with sequences of methanogenic *Archaea* (AB301476, M60880, AB065296, AM114193, AB196288), while the PmoA tree was rooted with AmoA sequences of ammonia-oxidizing bacteria (NC_004757, X90822). Dots label branch points that were confirmed in Maximum-Likelihood trees. The scale bars display 0.10 changes per nucleotide or amino acid position. Figure adopted from (Knief, 2015).

In addition to act as a biofilter for CH_4 produced in methanogenic sites, another environmentally relevant activity is the oxidation of atmospheric CH_4 in unsaturated soils (Conrad, 2009). Upland soils act as a CH_4 sink for 9 to 45 Tg atmospheric CH_4 $year^{-1}$, thereby balancing for about 1 to 7 % of the global annual CH_4 emission (Knief et al., 2003). Atmospheric CH_4 consumption is performed by bacteria with high affinity to CH_4. Initial molecular-ecology research identified two as-yet-uncultured methanotroph clades as the major biological sink for atmospheric CH_4 in forest and grassland soils. These were termed upland soil clusters alpha and gamma (USCα and USCγ) (Holmes Andrew et al.,

1999; Knief and Dunfield, 2005; Kolb, 2009). The USCα and USCγ clusters are phylogenetically affiliated to *Alpha*- and *Gammaproteobacteria* and use the particulate methane monooxygenase (pMMO) for atmospheric CH_4 oxidation (Cai et al., 2020). Most recently, *Methylocapsa gorgona* MG08 has been described (Tveit et al. 2019). This isolate is (i) able to oxidize atmospheric CH_4, (ii) globally distributed in upland soils, (iii) closely related to USCα, and (iv) exhibits an higher estimated specific affinity for CH_4 (a^0_s, $\sim 195 \times 10^{-12}$ $L \cdot cell^{-1} \cdot h^{-1}$) than other cultivated methanotrophs (Dunfield Peter and Conrad, 2000; Knief and Dunfield, 2005; Tveit et al., 2019).

Besides the members of these two uncultured methanotroph clusters, some methanotrophic strains belonging to the family *Methylocystaceae* have been shown to oxidize CH_4 at atmospheric mixing ratios (Knief and Dunfield, 2005; Täumer et al., 2022). In particular, USCα and *Methylocystis* spp. are most frequently detected in acidic soils, while USCγ and *Methylocystis* spp. are frequently detected in pH-neutral soils. *Methylocystis* sp. strain SC2 was found to oxidize atmospheric CH_4 by an alternative high-affinity pMMO2 isozyme (Dunfield et al., 2002; Ricke et al., 2004; Baani and Liesack, 2008). In addition, two *Methylocystis* strains (DWT and LR1) required the lowest amount of CH_4 for growth (10–100 ppmv) and maintained atmospheric (1.75 ppmv) CH_4 oxidation for the longest period in a study by (Knief and Dunfield, 2005). Depending on soil type and environmental factors, methanotrophic communities in unsaturated soils were dominated by USCα, USCγ, or *Methylocystis*. Their ecophysiology needs to be more specifically addressed in future studies (Kolb, 2009; Deng et al., 2019).

1.2 Metabolic versatility of aerobic methanotrophs

1.2.1 Methane oxidation

Methanotrophic bacteria use monooxygenase enzymes for the first step of CH_4 oxidation to methanol, which is then further converted to formaldehyde, formate and CO_2 by methanol, formaldehyde, and formate dehydrogenases (Hanson and Hanson, 1996). Cell carbon for growth is assimilated from formaldehyde by either the RuMP (type I) or serine pathways (type II). Two forms of CH_4 monooxygenases are known, a soluble form (sMMO) present only in a few methantroph species (Kaluzhnaya et al., 2001; Kalyuzhnaya et al., 2008; Khalifa et al., 2015) and a membrane-bound form (pMMO) present in all known methanotrophs, except members of the genera *Methylocella* and

Methyloferula (Theisen et al., 2005; Dedysh and Dunfield, 2016). A subset of type I and type IIa methanotrophs can produce both sMMO and pMMO.

The two MMO systems are evolutionarily unrelated and thus completely differ in their gene and protein sequences, their overall structure, their substrate selectivity, and their active site composition (Fig 1.7) (Holmes et al., 1995; Leahy et al., 2003; Khadka et al., 2018). The sMMO belongs to a multicomponent monooxygenase (BMM) family and is composed of a hydroxylase (MMOH), a reductase (MMOR), and a regulatory protein (MMOB). The MMOH consists of three polypeptides arranged in an $\alpha_2\beta_2\gamma_2$ dimer (Rosenzweig et al., 1993). The sMMO has a wide substrate range including halogenated alkanes, alkenes, and aromatic compounds (Semrau, 2011). The pMMO is a membrane-bound, copper- and iron-containing enzyme (Lieberman et al., 2003). The *pmoCAB* gene cluster codes for three integral membrane polypeptides of approximately 22, 24, and 42 kDa, respectively. These are arranged as a 300 kDa $\alpha_3\beta_3\gamma_3$ trimer (Gilbert et al., 2000; Sirajuddin and Rosenzweig, 2015). The PmoB subunit consists of two cupredoxin-like domains linked by two transmembrane helices, while the PmoA and PmoC subunits are primarily composed of transmembrane helices (Sirajuddin and Rosenzweig, 2015; Zhu et al., 2022). Since pMMO is the predominant CH_4 oxidation catalyst in nature, it is critically important to understand its catalytic potential to oxidize atmospheric CH_4. However, the identity of the physiological electron donor for pMMO activity is still unknown and the exact catalytic mechanism of pMMO remained elusive for many years (Kalyuzhnaya et al., 2015).

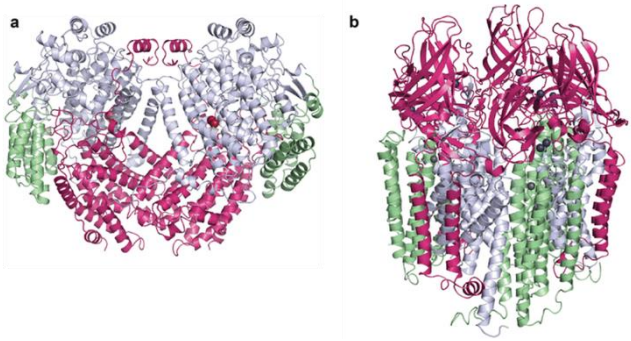

Fig 1.7 Overall structure of the two MMO forms. a *M. capsulatus* (Bath) sMMO (PDB accession code 1MTY) showing the α subunits in gray, β subunits in magenta, and γ subunits in green. Iron ions are colored red–brown. b *M. capsulatus* (Bath) pMMO (PDB accession code 3RGB) showing the PmoC subunits in green, PmoB subunits in magenta, and PmoA subunits in gray. Copper ions are dark blue and zinc ions are gray. Figure adopted from (Ross and Rosenzweig, 2017).

1.2.2 Carbon assimilation

1.2.2.1 Central carbon pathways

While gammaproteobacterial (type I) methanotrophs operate the ribulose monophosphate (RuMP) cycle for carbon assimilation, the alphaproteobacterial (type II) methanotrophs make use of the serine pathway (Fig. 1.8). Type X methanotrophs were categorized as *Gammaproteobacteria* that are distinguished from type I methanotrophs by the presence of low serine-cycle enzyme levels, in addition to the enzymes of the Calvin–Benson–Bassham (CBB) cycle. Later studies showed that type X methanotrophs use CO_2 as their sole source of carbon and energy (Khadem Ahmad et al., 2011).

Methanotrophs have the potential to play a role in future energy sustainability. The type I methanotrophs condense formaldehyde with ribulose monophosphate, thereby resulting in the production of sugar-phosphate phosphate (Trotsenko and Murrell, 2008; Kalyuzhnaya et al., 2013; Fu et al., 2017). Actually, these methanotrophs operate two variants of the RuMP cycle, with one being the Embden-Meyerhof-Parnas (EMP) variant and the other being the Entner–Doudoroff (ED) variant. Both pathways convert formaldehyde into the C3 intermediates pyruvate and phosphoenolpyruvate (PEP). Subsequently, pyruvate acts as a precursor of multi-carbon compounds.

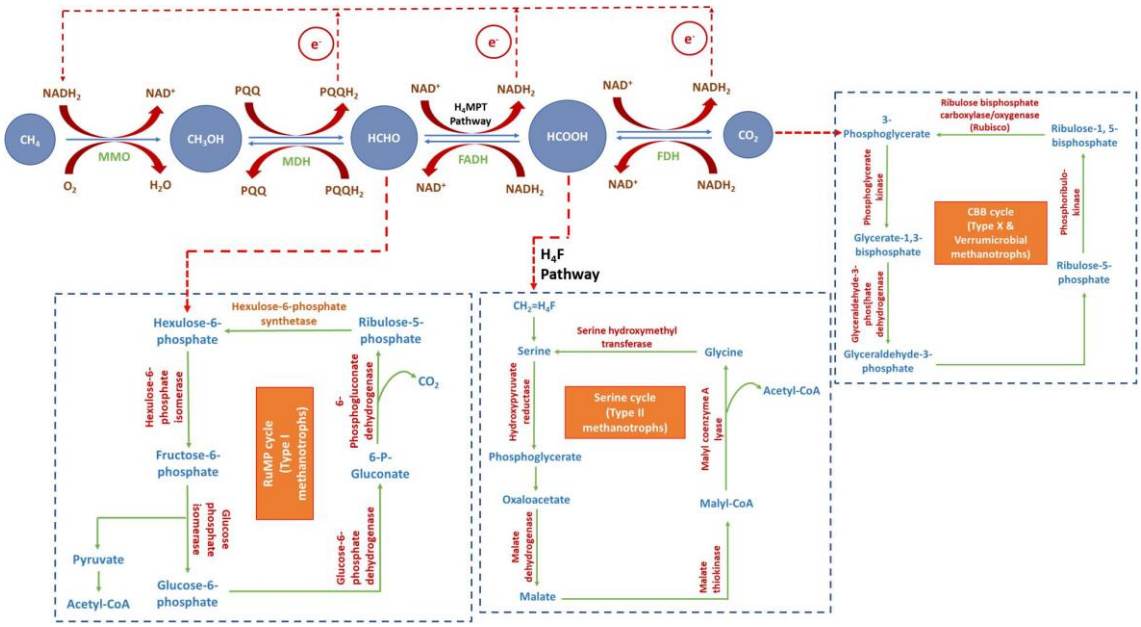

Fig. 1.8 Carbon assimilation pathway in methanotrophs. Abbreviation: MMO, methane monooxygenase; MDH, methanol dehydrogenase; FADH, formaldehyde dehydrogenase; FDH, formate dehydrogenase. Figure adopted from (Sahoo et al., 2021).

In the serine pathway, equimolar amounts of tetrahydrofolate (H_4F) and CO_2 result in the production of acetyl-CoA, which will be channeled into the ethylmalonyl-coenzyme A (EMC) pathway or the glyoxylate shunt (GS) for synthesis of amino acids, CoA derivatives, and TCA cycle intermediates. The C1 carbon assimilated via the serine pathway into the central carbon metabolism is the basis for gluconeogenesis, thereby leading to the synthesis of particular amino acids, DNA and RNA, and cell wall components. Collectively, these contribute 53% to total cell biomass (Yang et al., 2013). The second part of the serine pathway overlaps with the EMC pathway and replenishes the intermediates required for C1 carbon assimilation, including malate, acetyl-CoA, and glyoxylate. Operating the serine pathway is essential for the activity of type II methanotrophs, which are known to have a high demand for acetyl-CoA as a key metabolite for PHB biosynthesis (Jeon et al., 2019; Gęsicka et al., 2021). In addition, a significant fraction of PEP is converted to pyruvate, the precursor for alanine and the acceptor in two anaplerotic CO_2-fixation reactions. Indeed, it has been predicted that the proportion of cell carbon derived from CO_2 in type II methanotrophs (> 50%) is much greater than that of type I methanotrophs (approx. 5-15 %) (Trotsenko and Murrell, 2008a; Yang et al., 2013). Most recently, CO_2 fixation was proposed to occur via the reductive glycine pathway (Tveit et al., 2019). Since type II methanotrophs incorporate more CO_2 per unit of substrate than type I methanotrophs, they may thus represent a more suitable system for C1-based commercial production of chemicals (Yang et al., 2013).

1.2.2.2 Multi-carbon metabolism

Abiotic environmental factors, including CH_4 and oxygen concentrations, nitrogen, nutrient availability, pH, temperature, and salinity largely influence the activity of methanotrophs (Kaupper et al., 2020). Methanotrophs were initially considered to be obligates utilizing only methane or methanol for growth. Over the last two decades, discoveries greatly expanded our understanding of the methanotroph physiology. In addition to the growth on other C1 compounds such as formate and formaldehyde, strains of *Methylocystis* and *Methylocapsa*, but in particular *Methylocella* spp., have been shown to be capable of growing on compounds containing C-C bonds (Belova et al., 2011; Dedysh and Dunfield, 2011). Members of the genus *Methylocystis*, such as *M. bryophila* H2s^T, *M. heyeri* H2^T, and *M. echinoides* IMET10491^T, show slow growth on acetate and ethanol in the absence of methane (Belova et al., 2011). In contrast, *Methylocella* spp. are not only able to use methane and methanol as their sole source of energy, but also grow

on acetate, pyruvate, succinate, malate, and ethanol (Dedysh Svetlana et al., 2005; Farhan Ul Haque et al., 2020). The growth rate and carbon conversion efficiency were even higher on acetate than on methane, and acetate was the preferable substrate when both substrates were provided in excess (Dedysh Svetlana et al., 2005; Im et al., 2011).

The assimilation pathway of acetate is not yet conclusively known for members of the genus *Methylocystis* (Belova et al., 2011; Pratscher et al., 2011). The assimilation pathway of acetate in *Methylocella* spp. was considered to involve the activity of two enzymes of the glyoxylate shunt. These are isocitrate lyase (ICL) and malate synthase (MS), which are able to convert acetate into intermediates of the serine pathway such as malate and glyoxylate. The deletion of ICL or MS in *Methylocella*. *silvestris* BL2 resulted in growth defects that confirmed the incorporation of pyruvate into the central carbon metabolism via the glyoxylate shunt (Bordel et al., 2020). The sMMOs belong to a large family of di-iron carboxylate enzymes that include soluble di-iron monoxygenases (SDIMOs). The sMMO allows *Methylocella* spp. to grow on a range of short-chain alkanes, ethane, and propane (Crombie and Murrell, 2014; Farhan Ul Haque et al., 2018; Tveit et al., 2019). Interestingly, acetate repressed the sMMO expression in some facultative *Methylocella* strains (Theisen et al., 2005).

Conversely, *Methylocystis* strains H2s and SB2 constitutively expressed pMMO regardless of whether methane or acetate was available as substrate for growth. It was speculated that facultative *Methylocystis* spp. are able to use acetate as a secondary carbon or a reducing source to enable the continued expression of the pMMO, so that these strains can readily utilize methane when it becomes available (Belova et al., 2011). This newly detected metabolic flexibility suggested that some type II methanotrophs have a greater competitive advantage than previously thought and the operation of multiple pathways by *Methylocystis* spp. can be highly controlled and integrated. This facultative capability may be a further explanation of why *Methylocystis* spp. are ubiquitously distributed in oligotrophic environments such as upland soils.

1.2.2.3 Growth strategy under unbalanced nutrition conditions

Another factor that affects methanotroph selection is nutrient concentration. Almost all type IIa methanotrophs are able to convert CH_4 to poly-beta-hydroxybutyrate (PHB), the most common type of polyhydroxyalkanoates (PHAs) naturally produced in methanotrophs under nutrient-limiting conditions (e.g., carbon excess coupled to nitrogen limitation) (Pfluger et al., 2011; Pieja et al., 2011). Type IIa methanotroph cells use

intracellular PHB as a source of carbon and reducing power and as an internal substrate for cell survival during starvation periods with limited external carbon and energy sources (Fig 1.9).

Three genes, *phaCAB*, are considered crucial for PHB synthesis (Madison and Huisman, 1999). These genes encode the condensation of two acetyl-CoA molecules to acetoacetyl-CoA (*phaA*), the reduction of acetoacetyl-CoA to (R)-3-hydroxybutyryl-CoA (*phaB*), and the polymerization of (R)-3-hydroxybutyryl-CoA monomer units into PHB (*phaC*) (Madison and Huisman, 1999). These genes are well conserved among type IIa methanotrophs and have been used to screen for PHB production capacity (Sheu et al., 2000). To date, neither PHB synthesis genes nor the production of PHB have been detected in type I methanotrophs. The production of PHB has only been documented in type IIa methanotrophs of the genera *Methylocystis* and *Methylosinus* (Pfluger et al., 2011; Pieja et al., 2011; Pieja Allison et al., 2011; Bordel et al., 2019). The main precursor for PHB bioconversion is acetyl-CoA. Its synthesis via the serine pathway, which contributes 53% to cell biomass, partially explains why PHB production is limited to type IIa methanotrophs, while not found in type I methanotrophs (Yang et al., 2013).

Previous research had already shown that low nutrient level favors type IIa methanotrophs over type I methanotrophs due to PHB storage (Criddle et al., 2014). In fact, M*ethylocystis* and *Methylosinus* are known to accumulate 20% to 50% of its dry biomass in the form of poly-3-hydroxybutyrate (PHB) under nitrogen-limiting conditions (Pieja et al., 2011). Their ability to convert CH_4 to PHB not only mitigates CH_4 emission to the atmosphere but also makes type IIa methanotrophs a promising cell factory for synthesis of biodegradable polymer substitutes used in plastics production (Saratale and Oh, 2015; Yeo et al., 2018). Nowadays, great efforts are made to elucidate their metabolic potential in order to make their use in biotechnology (Trotsenko and Murrell, 2008b; Fei et al., 2014; Hakobyan et al., 2020).

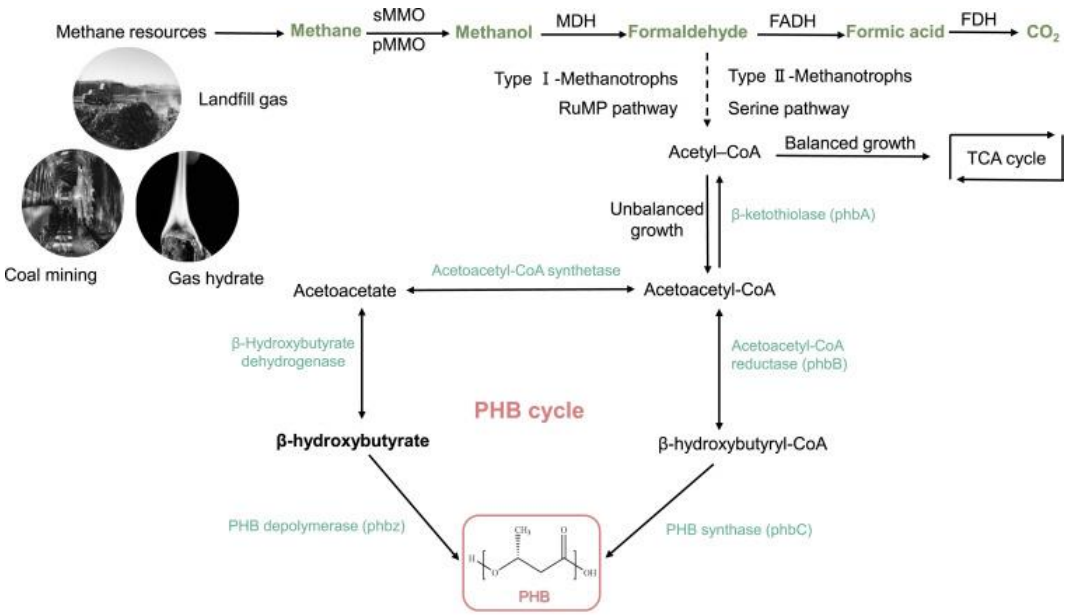

Fig 1.9 Methane metabolism in methanotrophs. Adopted from (Zhang et al., 2008; Liu et al., 2020)

1.2.3 Alternative energy sources

Atmospheric hydrogen has a mixing ratio as low as 0.53 ppmv (Greening et al., 2014). Abiogenic and biogenic processes, such as fermentation, nitrogen fixation, and photosynthesis, can continuously produce hydrogen. There are three phylogenetically distinct classes of hydrogenases. Their differentiation is based on the metals within the interior H_2-binding sites: groups 1 to 4 [NiFe]-hydrogenases, groups A to C [FeFe]-hydrogenases, and [Fe]-hydrogenases (Fig 1.10) (Shima et al., 2008; Greening et al., 2016). Low-affinity H_2 oxidation is catalyzed by microbes in habitats with relatively high H_2 availability. On the contrary, high-affinity microorganisms can oxidize atmospheric H_2. The H_2 metabolism has been recently recognized in anoxic sediments, animal guts and hydrothermal vents involving members of five different bacterial phyla: *Proteobacteria*, *Firmicutes*, *Cyanobacteria*, *Euryarchaeota* and *Chlorophyta*. Furthermore, various members of the *Actinobacteria* and *Acidobacteria* are able to persist in aerobic soils by scavenging H_2 from the lower atmosphere (Greening et al., 2014; Greening and Cook, 2014; Lubitz et al., 2014; Greening et al., 2015). The use of H_2 as an alternative energy source may help microorganisms to cope with environmental fluctuations in available energy sources (Piché-Choquette and Constant, 2019).

Our current knowledge on the evolution and diversity of hydrogenases suggests that the H_2 metabolism is more diverse and widespread across members of the domain *Bacteria* and thus among microbial communities than previously thought (Greening et

al., 2016). Hydrogen treatment of soils altered both the carbon utilization and the CH_4 oxidation. The strong negative correlation between low-affinity H_2 oxidation and high-affinity CH_4 oxidation led to the conclusion that CH_4 and H_2 oxidation might be performed by the same microorganisms that have the ability to utilize both CH_4 and H_2 as substrates (Khdhiri et al., 2017; Piché-Choquette et al., 2018).

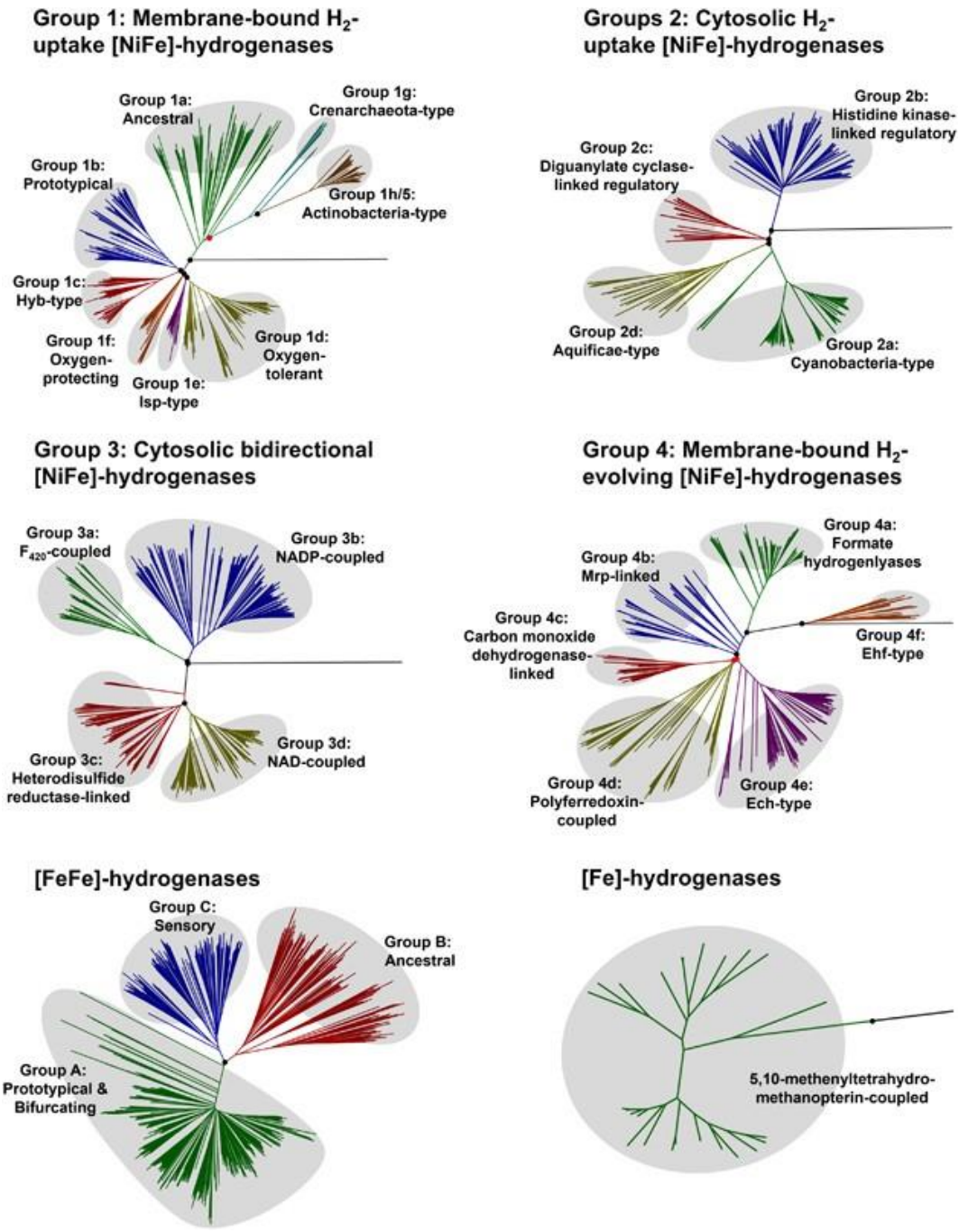

Fig. 1.10 Classification and phylogeny of hydrogenases. These Neighbor-Joining skeleton trees show the phylogenetic relationships of 3286 hydrogenases. The trees are color-coded by [NiFe]-hydrogenase subgroup and [FeFe]-hydrogenase group. The nodes separating the major clades are encircled and colored

according to their bootstrap values, that is, black circles for well-supported nodes (bootstrap values >0.75) and red circles for unsupported nodes (bootstrap values <0.75). Group A [FeFe]-hydrogenases cannot be reliably subdivided phylogenetically and can only be classified into subtypes based on their genetic organisation. Figure adopted from (Greening et al 2015).

Recently, hydrogenase-coding genes were also identified in the genomes of various alphaproteobacterial and verrucomicrobial methanotroph genomes, thereby suggesting that hydrogen oxidation is a general metabolic strategy operated by these methanotrophic bacteria (Hanczár et al., 2002; Greening et al., 2016; Carere et al., 2017). Later, the low-affinity and oxygen-sensitive membrane-bound group Id [NiFe]-hydrogenase was shown to provide the ability to switch between growth strategies on the concurrent use of H_2 and CH_4 as energy and carbon sources (Mohammadi et al., 2017; Hakobyan et al., 2020). Mixotrophy relying on H_2 as an energy source confers a flexible Knallgas-methanotrophic lifestyle that uses hydrogenases to channel electrons from hydrogen into the quinone pool, thereby providing the link between hydrogen oxidation and energy production (Piché-Choquette and Constant, 2019). Hydrogen oxidation is particularly important for the acclimatization of methanotrophs to CH_4 and oxygen limitation (Fig 1.11) (Hakobyan et al., 2020).

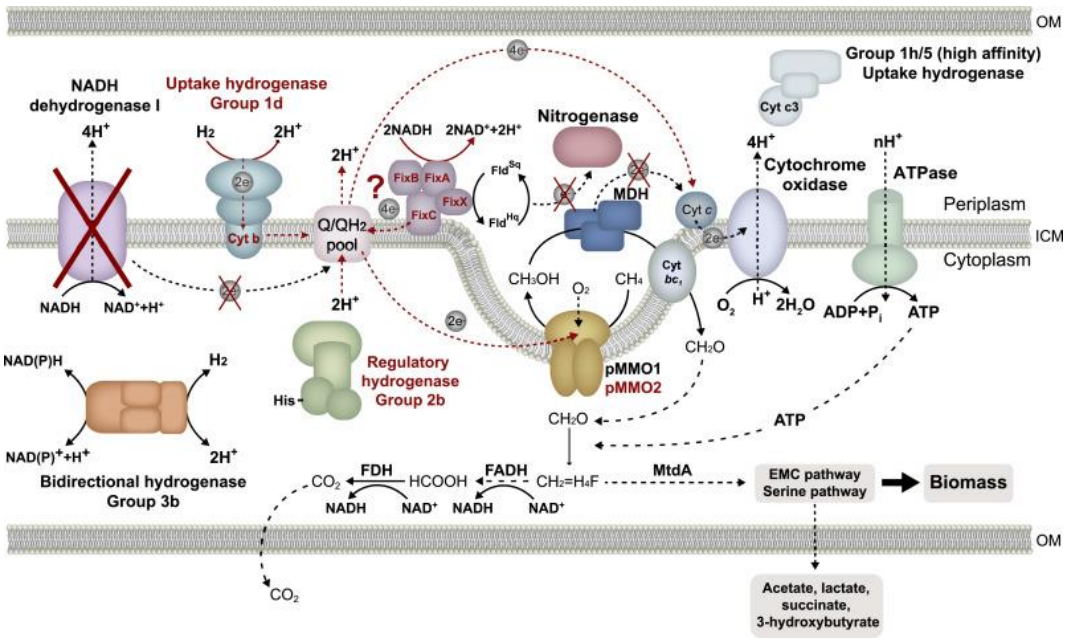

Fig. 1.11. Proposed metabolic model of how *Methylocystis* sp. strain SC2 responds to the addition of H_2 under CH_4 and O_2 limited conditions. During the growth of strain SC2, H_2 is oxidized by Group 1d uptake hydrogenase, yielding reduced quinones (QH_2) and, in consequence, a large proton-motive force for production of ATP. In addition, some of the QH_2 provides electrons for CH_4 oxidation by pMMO. Some formaldehyde oxidation via the activity of formaldehyde dehydrogenase (FADH) and formate dehydrogenase (FDH) may lead to the production of reducing equivalents (NADH) that feed the electron transport chain through the FixABCX complex, resulting in additional ATP available for growth. In

addition, certain amounts of energy in form of NADH and ATP may be generated through fermentative pathways. All the proteins and pathways that were differentially regulated are highlighted in red. The exact functional role of FixABCX should be elucidated in future studies. Figure adopted from (Hakobyan et al., 2020).

1.2.4 Nitrogen metabolism

One of the major distinctive characteristics between type I and type II methanotrophs is their nitrogen metabolism capabilities. Both NH_4^+ and NH_3, but also nitrate (NO_3^-), can be used as a nitrogen source for growth and biomass production (Bodelier et al., 2000; Tays et al., 2018). However, methanotrophic activity in soil is highly sensitive to high NH_4^+ concentrations. Whether NH_4^+ in the environment has inhibitory or stimulatory effects on methane-oxidizing bacteria, however, depends largely on the diversity, the structure, and the activity of the methanotrophic community, as well as the particular conditions in the habitat (Stein et al.; Schnell and King, 1994; Dunfield and Knowles, 1995; Bodelier et al., 2000; Mohanty et al., 2006). The application of NH_4^+ fertilizers to various soils and sediments has been shown to inhibit methanotrophic activity (vanderNat et al., 1997; Bodelier and Laanbroek, 2004). In particular, the activity of alphaproteobacterial type IIa methanotrophs (*Methylocystis* / *Methylosinus*) is inhibited or at least not stimulated in nitrogen-amended soils (Mohanty et al., 2006; Nyerges and Stein, 2009). The evolutionary relationship between the pMMO and ammonia monooxygenase (AMO) explains why, in addition to pMMO and sMMO, AMO is the only other enzyme known to oxidize CH_4 (Fisher et al., 2018). The structural homology between pMMO and AMO allows both methanotrophs and ammonia oxidizers to convert either substrates (CH_4 and NH_3), although neither is able to grow on the alternative substrate (Stein and Klotz, 2011; Versantvoort et al., 2020). The pMMO oxidizes NH_3 to hydroxylamine (NH_2OH) (Versantvoort et al., 2020). Ammonia produced from the deprotonation of liquid NH_4^+ competes with CH_4 for the same active site of pMMO (Nyerges and Stein, 2009; Yang et al., 2011). On the other hand, methanotrophs, like all bacteria, require nitrogen for growth. The fact that NH_3 acts for methanotrophs as both a nutrient and a competitive inhibitor of pMMO suggests that these bacteria need to be able to simultaneously acclimatize to various environmental triggers: assimilation of NH_4^+ nitrogen, competitive inhibition of pMMO, and NH_2OH and NO_2^- toxicity when NH_3 oxidation is favored (Stein and Klotz, 2011). Nevertheless, the acclimatization response of methanotrophs to increasing NH_4^+ load has not yet been conclusively understood at

the cellular level. This is particularly valid for type IIa methanotrophs and more specifically for *Methylocystis* spp.

Type IIa methanotrophs are known to be capable of expressing nitrogenase and utilizing N_2 as nitrogen source in many environments including forest soil, rice roots, and oligotrophic ocean; i.e., ecosystems characterized by extremely low concentrations of available nitrogen compounds (Murrell and Dalton, 1983; Auman Ann et al., 2001; Dedysh et al., 2004).

1.3 Multi-omics methods to elucidate the physiological and metabolic versatility of methanotrophs

High-throughput molecular techniques, collectively termed multi-omics techniques such as metagenomics, metatranscriptomics and metaproteomics, can be used to assess the community structure and the metabolic potential as well as the activity of methanotrophs in diverse environmental niches (Abram, 2015). Metagenomics allows us to access the environmental gene pool of methanotrophs that is not reachable through classical microbial cultivation techniques. The main purpose of metagenomics is to infer the taxonomic and functional profiles of a microbial community. However, the metagenome provides only insights into the genetic potential of a microbial community, while the metatranscriptome informs us of the genes being expressed by the community at the time of sampling (Zheng and Chistoserdova, 2019). The annotation of the mRNA transcripts provides detailed information on the functions being expressed by a community under specific environmental conditions. Metaproteomics investigates the proteins expressed within a microbiome and, together with metabolomics, provides access to ecosystem functioning (Zheng and Chistoserdova, 2019). The metabolites, collectively termed metabolome, released by members of the microbial community are a result of the interaction of these microbes with the biotic and abiotic conditions that prevail in the environment that they inhabit. The results of metaproteome and metabolome complement with each other well and can be used to construct active metabolic pathways.

The culture-independent approaches allow us to analyze the identity, genetic potential, and possible functional role of as-yet uncultured microorganisms; however, culture-based studies are still needed to reveal microbial physiology and test multi-omics-based ecological hypotheses, improve database annotations, and (3) construct genome-

scale models of metabolic capabilities and pathways in order to uncover possible applications in biotechnology (Gutleben et al., 2018).

Currently, five genera with taxonomically described members are known among the alphaproteobacterial methanotrophs: *Methylocystis* and *Methylosinus* (*Methylocystaceae*) as well as *Methylocapsa*, *Methylocella*, and *Methyloferula* (*Beijerinckiaceae*) (Knief, 2015). The genus *Methylocystis* includes seven species with validly published names: *Methylocystis echinoides* IMET 10491^T (Bowman et al., 1993), *Methylocystis rosea* SV97^T (Wartiainen et al., 2006), *Methylocystis hirsuta* CSC1^T (Lindner et al., 2007a), *Methylocystis heyer*i H2^T (Dedysh et al., 2007), *Methylocystis parvus* OBBP^T (del Cerro et al., 2012), *Methylocystis bryophila* H2s^T (Belova et al., 2013), and *Methylocystis silviterrae* FS^T (Tikhonova et al., 2021). The genus *Methylosinus* includes two species with validly published names: *Methylosinus trichosporium* OB3b^T and *Methylosinus sporium* ACM 3306^T (Bowman et al., 1993).The *Beijerinckiaceae* family comprises three genera and seven species with validly published names: *Methylocapsa acidiphila* B2^T (Dedysh et al., 2002), *Methylocapsa aurea* KYG^T (Dunfield et al., 2010), *Methylocapsa palsarum* NE2^T (Dedysh et al., 2015), *Methylocella palustris* K^T (Dedysh et al., 2000), *Methylocella silvestris* BL2^T (Dunfield et al., 2003), *Methylocella tundra* T4^T (Dedysh et al., 2004) and *Methyloferula stellata* AR4^T (Vorobev et al., 2011).

With the development of next-generation sequencing technologies, it is increasingly easy to sequence bacterial genomes of pure cultures. To date, dozens of methanotroph genomes obtained from pure cultures are available, and the databases are continuously growing (http://www.methanotroph.org/wiki/introduction/). In the following, I discuss multi-omics applied to methanotrophs: genomics, transcriptomics, proteomics, and metabolomics.

1.3.1 Genomics

The tremendous increase in the number of draft genomes requires an accurate taxonomic classification of the newly assembled genomes. Bacterial and archaeal 16S ribosomal RNA (rRNA) gene sequences, but also functional genes (e.g., *mcrA* [methanogens], *pmoA* [methanotrophs]), are frequently used as markers for the taxonomic and phylogenetic classification of microorganisms, including methanotrophs. However, phylogenetic trees

constructed based on 16S rRNA gene sequences may not be sufficiently resolving to reveal the exact evolutionary relationships among the closely related members of the genera *Methylocystis* and *Methylosinus* (*Methylocystaceae*) (Yang et al., 2016). Recently, the taxonomy placement of genome-sequenced isolates was evaluated using the Genome Taxonomy Database Toolkit (GTDB-Tk). This toolkit provides an automated and objective taxonomic classification of bacterial genomes by identifying a set of 120 marker genes (Chaumeil et al., 2020). In addition to single-amplified genomes, GTDB-Tk allows for a thorough classification of metagenome-assembled genomes (MAGs) (Bowers et al., 2017).

Implementation of genomic techniques into research on methanotrophs can provide information on their genomic potential and reveal as-yet-unknown metabolic capacities. For instance, the isoforms of particulate methane monooxygenase (Ricke et al., 2004), alternative methanol dehydrogenases (Wegner et al., 2019), hydrogenases (Mohammadi et al., 2017; Carere et al., 2017) as well as enzymes for aerobic anoxygenic photosynthesis by means of photosystem II (Miroshnikov et al., 2019) have been discovered in methanotrophic bacteria. Comparative genomic analysis of the acetate-utilizing *Methylocystis* sp. strain SB2 with other closely related *Methylocystis* strains, but also facultative strains of *Methylobacterium extorquens*, was done to elucidate the mechanisms of multicarbon compound assimilation that exist in facultative and obligate *Methylocystis* strains. Both TCA cycle and EMC pathway were found to be complete in *Methylocystis* sp. strain SB2, but also in *Methylocystis rosea* SV97^{T}, *Methylocystis* sp. strain SC2, and *Methylocystis* sp. strain Rockwell (ATCC 49242). The authors did not find any genomic evidence for a differentiation between the obligate and facultative nature of *Methylocystis* spp. (Dam et al., 2014; Vorobev et al., 2014). A phylogenetic tree based on universally conserved genes demonstrated a vertical inheritance pattern of methanotrophy and methylotrophy genes within the *Methylocystaceae* and *Beijerinckiaceae* families. However, all MMOs in the alphaproteobacterial methanotrophs are foreign in origin via lateral gene transfer (LGT) (Tamas et al., 2014). Methanotrophy got lost, and the ability to grow on multicarbon substrates was regained in some members of the *Beijerinckiaceae* (Tamas et al., 2014).

Comparative genomics also provided evidence that strains of the same bacterial or archaeal species can greatly differ in gene content, with only a fraction of genes being common to all genomes. These insights gave rise to the pangenome concept. The term ‘pangenome’ describes all the genes present in all isolates of a certain taxon. The

pangenome, i.e., the sum of core and accessory genes (soft core, shell and cloud genes), can give insights into habitat specificity and evolutionary forces shaping microbial genomes (Brockhurst et al., 2019). The core genome of *Methylocystis* spp. represents the conserved genetic backbone and basic cellular machineries (Dam et al., 2013). The genes involved in CH_4 oxidation and formaldehyde assimilation, including the serine pathway, as well as nitrogen fixation were identified as core gene clusters in *Methylocystis* spp. (Gontijo, 2022).

1.3.2 Transcriptomics

Genome-wide transcriptomics analysis was applied in combination with metabolomics to disentangle the metabolic network of methanotrophs (Matsen et al., 2013; Yang et al., 2013). For example, upon sequencing of the genome of *M. trichosporium* OB3b, transcriptome and metabolome analyses were applied to refine the central pathway for C1 utilization under growth in batch culture with no limiting carbon and nitrogen conditions (Yang et al., 2013).

The growth on C1 substrates, i.e., methane and methanol, changed the gene expression in both type I and type II methanotrophs (Vorobev et al., 2014; Nguyen et al., 2019). *Methylomonas* sp. DH-1 has been proven to be an ideal candidate for biotechnological applications using methane and methanol as the feedstock. Strain DH-1 operates the RuMP cycle and the EMP pathway for C1 assimilation but is also able to express the complete serine pathway. The latter is the typical C1 assimilation pathway of type II methanotrophs, but not common in type I methanotrophs. An increase in the flux towards the serine pathway was particularly observed in *Methylomonas* sp. DH-1 during the growth on methanol, which led to an increased production of acetyl-CoA (Nguyen et al., 2019). In contrast, the growth of *Methylocystis* sp. strain SB2 on methanol led to a significant decline in the expression of genes involved in methane oxidation and the serine pathway (Vorobev et al., 2014). Furthermore, an opposite regulation of the TCA cycle was observed for *Methylomonas* sp. DH-1 and *Methylocystis* sp. strain SB2 during their growth on methanol (Vorobev et al., 2014; Nguyen et al., 2019).

The analysis of both transcriptomics and metabolomics data revealed that the core metabolism of *Methylocystis trichosporium* OB3b consists of several tightly connected metabolic cycles, such as the serine pathway, the ethylmalonyl-CoA (EMC) pathway, and

the TCA cycle. Strain OB3b displays a high gene expression level of the H_4MTP-pathway for formaldehyde oxidation. Both metabolome and ^{13}C-labeling studies have further shown that in strain OB3b, a significantly larger portion of the cell carbon (over 60%) is derived from CO_2 than from CH_4 (Yang et al., 2013). Shifts in the central carbon metabolism were also observed for the type I methanotroph *Methylomicrobium buryatense* 5GB1 during the growth on either methane of methanol (Fu et al., 2019). A steady state ^{13}C metabolic flux analysis provided evidence that in addition to the complete TCA cycle, *M. buryatense* 5GB1 operates a partial serine pathway. The analysis of *fumA* and *fumC* knockout mutants revealed a severe growth defect in strain 5GB1, thereby suggesting that the TCA cycle not only provides precursors for biomass synthesis, but also reducing power (Fu et al., 2017). Both metabolic and ^{13}C-methane tracing experiments in *Methylomicrobium alcaliphilum* strain 20Z, a promising biocatalyst, revealed a novel model of methane utilization under oxygen-limited conditions, which allowed reconstructing the metabolic C1 utilization pathway. The oxygen-limited conditions favored operation of fermentation pathways, which led to the excretion of various products, such as formate, acetate, succinate, lactate, 3-hydroxybutyrate, and H_2 (Kalyuzhnaya et al., 2013). In contrast to other omics methods, metabolomics provides a strong link between environmental change and physiological response.

1.3.3 Proteomics

Proteins are the biofunctional molecules that govern the cellular phenotype. Neither genomics nor transcriptomics elucidate the actual production of translated proteins. Therefore, direct detection of the enzymes involved in methanotrophy by proteomics is a promising method to overcome the limitations of the other omics approaches (Abram, 2015).

Mass spectrometry (MS) in combination with a range of separation methods has been widely used as a principal methodology in proteomics. Traditional proteome analyses consist of two-dimensional electrophoresis (2-DE)-based methods. The protein mixture is either separated by two-dimensional electrophoresis followed by digestion and mass spectrometry or directly digested into peptide mixtures separated by multidimensional separation methods. Proteins are identified from their generated mass spectra using database searching. The identification and characterization of proteins by proteolytic digestion offers their in-depth analysis in complex sample mixtures and is termed the “bottom-up” approach (Fournier et al., 2007; Zhang et al., 2013). In contrast,

the "top-down" approach analyzes intact proteins (Catherman et al., 2014). The two general categories of bottom-up proteomic experiments are the data-dependent acquisition (DDA) and data-independent acquisition (DIA) methods. DDA methods have been extensively applied in proteomics since its inception (Elias and Gygi, 2007). The DIA methods select and fragment precursors regardless of their abundance in the samples. A predetermined set of wide isolation windows (e.g. 25 Da) is used to send the precursor ions in an isolation window for fragmentation (Gillet et al., 2012). In DIA experiments, the spectral library needs to be sufficiently large and the highly complex fragment spectra derived from multiple precursor ions make the data-analysis quite challenging (Goh et al., 2015). Nonetheless, recent improvements in software tools and bioinformatics now enable the accurate analysis of SWATH-DIA data.

To date, very few proteomics studies were conducted on methanotrophs. The ICAT (cleavable isotope coded affinity tag) technology in combination with off-line two-dimensional LC-MS/MS has been developed for the quantitative analysis of proteomic changes in the type I methanotroph *Methylococcus capsulatus* under different copper conditions (Kao et al., 2004). Later, for the first time, high-resolution two-dimensional gel electrophoresis and mass spectrometry have been applied to identify the outer membrane (OM) subproteome of *M. capsulatus* (Berven et al., 2006). Shortly thereafter, three comparative proteomics approaches, which enable label-free quantification, were used for the identification and relative quantification of proteins in the type IIb methanotroph *Methylocella silvestris* (Patel et al., 2009). The three approaches were (i) one-dimensional PAGE, (ii) MudPIT incorporating isobaric tags for relative and absolute quantification (iTRAQ), and (iii) a data-independent scanning LC-MS method.

Bacterial membrane proteins, or more precisely integral membrane proteins, comprise about 20% to 30% of the total proteome and perform essential physiological functions (Poetsch and Wolters, 2008). Despite the functional significance of membrane proteins in biological systems, the number of effective membrane protein studies is limited due to the methodological difficulties in the efficient solubilization and digestion of membrane-associated proteins (Kongpracha et al., 2022). In particular, type IIa methanotrophs possess a special cell wall architecture characterized by intracytoplasmic membranes (ICMs). The presence of ICMs makes global proteomics approaches highly challenging for members of the *Methylocystis*/*Methylosinus* group. However, recently an optimized proteomics workflow was developed for *Methylocystis* spp. that led to an

increase in both the protein quantification accuracy and the proteome coverage, with *Methylocystis* sp. strain SC2 being used as the model organism (Fig 1.12) (Hakobyan et al., 2018). This new crude-lysate-MS approach captured 62% of the predicted SC2 proteome, with up to 10-fold increase in membrane-associated proteins relative to less effective conditions. Moreover, the use of crude cell lysate for downstream analysis showed to be highly efficient not only for strain SC2 but also for other members of the family *Methylocystaceae* (Hakobyan et al., 2018).

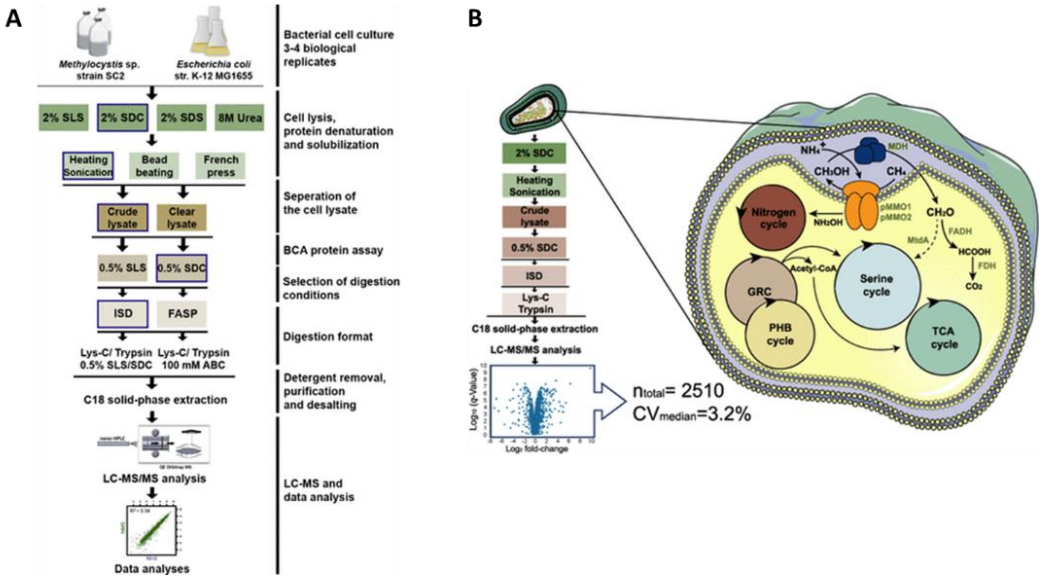

Fig 1.12. Flowchart illustrating the different solubilization and digestion conditions, and procedural steps used to obtain an optimized proteomics workflow for *Methylocystis* sp. strain SC2. Cell pellets of strain SC2, reference methanotrophs, and *E. coli* were reconstituted in different buffer systems. Different cell disruption techniques were applied. Cell debris were either removed or maintained in the lysate to obtain clear and crude lysates, respectively. The protein extraction efficiency was assessed by BCA protein assay. After determining the optimal solubilization conditions, crude-MS performance was tested under in-solution or FASP digestion conditions. All peptides derived from the individual assessment steps were purified using C18 solid phase extraction and analyzed via LC–MS. All experiments were performed in at least three biological replicates. Figure adopted from (Hakobyan et al., 2018).

1.4 Our model organism: *Methylocystis* sp. strain SC2

Strain SC2 was isolated in 1978 from the highly polluted river Saale near Wichmar, Germany (Dunfield et al., 2002; Heyer et al., 2002). The whole-genome sequence of strain SC2 was determined by shotgun sequencing using the 454 GS-FLX Titanium platform (Dam et al., 2013). Strain SC2^T contains three replicons, including the circular chromosome (3.77 Mbp) and two plasmids of 0.23 Mbp (pBSC2-1) and 0.14 Mbp

(pBSC2-2) in size. The average G+C content of the circular chromosome and the two plasmids is 63%, 61%, and 60%, respectively (Dam et al., 2012). Their nucleotide sequences have been deposited with the EMBL, GenBank, and DDBJ databases under the accession numbers HE956757 (chromosome), FO000001 (pBSC2-1), and FO000002 (pBSC2-2), respectively (Fig 1.13).

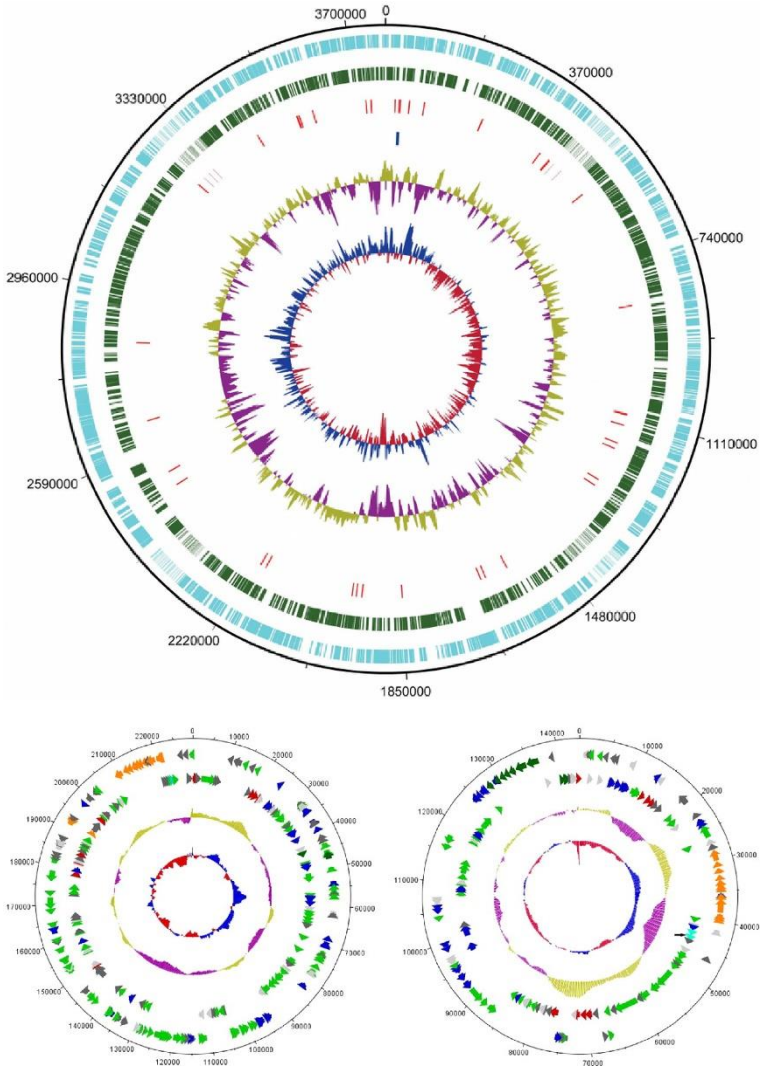

Fig 1.13 Circular representation of the gap-closed genome of strain SC2 with two plasmids, pBSC2-1 and pBSC2-2. Open reading frames (ORFs) are colored according to their function: red, plasmid replication and maintenance; orange, conjugation; light green, ORFs having homology to some functional proteins; dark green, nitrogen metabolism; blue, transposase-like proteins; light gray, hypothetical proteins; dark gray, conserved hypothetical proteins. The singleton pmoC (marked with an arrow) and its upstream regulatory gene in pBSC2-2 are colored sky blue. Adopted from (Dam et al., 2012b).

All genes required for a methanotrophic lifestyle were identified in strain SC2. Our model organism is able produce two pMMO isozymes with different affinities to

methane, the low-affinity pMMO1 and the high-affinity pMMO2 (Fig 1.14) (Ricke et al., 2004; Baani and Liesack, 2008). The low-affinity pMMO1 is encoded by two *pmoCAB1* gene clusters, while the high-affinity pMMO2 is encoded by a single *pmoCAB2* gene cluster. The apparent *Km* value of pMMO2 for methane oxidation is 0.11 μM, which corresponds well to *Km(app)* values measured in soils acting as a sink for atmospheric methane (Bender and Conrad, 1992; Baani and Liesack, 2008).

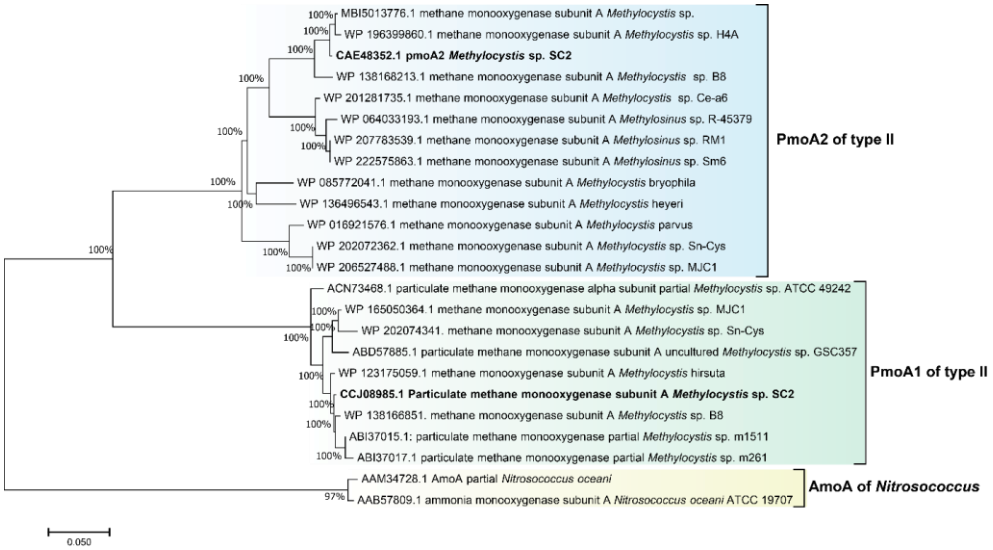

Fig 1.14. Phylogenetic tree of PmoA1 and PmoA2 of *Methylocystis* sp. SC2 and related strains. The phylogenetic tree was constructed using the Maximum-Likelihood method with a JTT model. The tree was built with 21 amino acid sequences. Bootstrap values (100 replications) are shown at the nodes. The evolutionary analysis was conducted in MEGA 7. The outgroup was AmoA of *Nitrosococcus oceani* strains. Bar: 0.05 substitutions per amino acids site.

Likewise, all the genes involved in the serine pathway were identified. These are the serine-glyoxylate aminotransferase (Xiao et al.), the hydroxypyruvate reductase (Hpr), two subunits of malate thiokinase (MtkAB), the acetyl-coenzyme A (acetyl-CoA)-independent phosphoenol pyruvate carboxylase (Ppc), and the malyl-CoA lyase (Mcl). Strain SC2 shows diverse nitrogen metabolism capabilities such as the transport and assimilation of nitrate and ammonium, hydroxylamine detoxification, denitrification, and dinitrogen fixation (Dam et al., 2013; Dam et al., 2014). The full complement of 34 genes involved in N_2 fixation and a complete denitrification pathway, including the plasmid-born *nosRZDFYX* operon, were identified in the SC2 genome (Dam et al., 2013). Furthermore, the genome harbors a complete set of genes encoding PHB-related enzymes, including the PHB depolymerase, the polyhydroxyalkonate synthesis repressor (PhbR), the acetyl-CoA acetyltransferase (PhbA), the acetoacetyl-CoA reductase (Phb),

and phasin homologs. Strain SC2 was shown to be a strong PHB producer, with PHB (mg/ mg total suspected solids) making a 30% contribution to the total cell biomass under N_2 fixation condition (Pieja et al., 2011). In addition, the genome of strain SC2 encodes various hydrogenase types (Ia, Id, 2b, 3b, 1h/5) and accessory proteins (Fig 1.15).

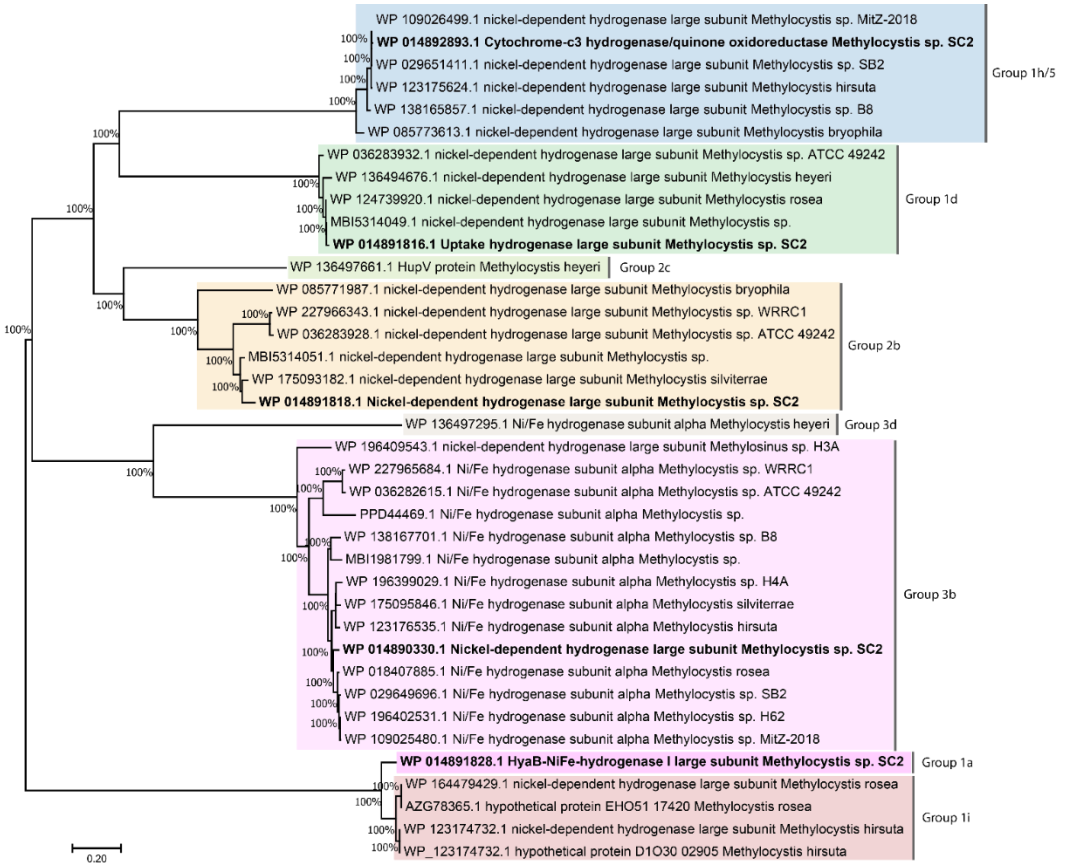

Fig 1.15. Phylogenetic tree of hydrogenases based on the amino acid sequence of *Methylocystis* sp. SC2 and related strains. The tree was conducted in MEGA7 using the Neighbor-Joining method. Bar: 0.20 substitutions per amino acid site.

1.5 Objectives of the study

Members of the genus *Methylocystis* are widely distributed in oxic-anoxic interfaces of methanogenic soils in which they play a key role in reducing methane emissions to the atmosphere. A systematic knowledge of their physiology, proteome, and thus metabolic capabilities is crucial for understanding their methane mitigation potential. Despite the fact that methanotrophs have been studied for decades, there still exist major gaps in our knowledge of their metabolism; in particular with regard to their acclimatization capacity to environmental change. Ammonium may have a dual function, with one being osmotic stressor and the other, after deprotonation, being competitive inhibitor of pMMO activity. The impact of increasing NH_4^+ load on the activity of *Methylocystis* spp. may be of particular importance in agricultural soils supplied with nitrogenous fertilizers. Here, our research on strain SC2 combined growth experiments with global proteomics, amino acid profiling, and the measurement of nitrite and nitrous oxide release (**Chapter 2**). A related aspect is the effect of increasing environmental salinity on the activity of *Methylocystis* spp. The activity of *Methylocystis* sp. strain SC2 has been reported to be sensitive to an increase in salinity, with *Methylocystis* spp. generally exhibiting a low salt tolerance. The tolerance range is from 0.2% to 1% NaCl (Han et al., 2017). In my PhD study, we thus tested a series of canonical amino acids and known compatible solutes for their potential to enhance the salt and osmotic stress tolerance of strain SC2 by modulating the glutamate metabolism and/or the central carbon metabolism. The research combined growth experiments with global proteomics, metabolomics, and ^{13}C-labeling experiments (**Chapter 3**).

1.6 References

Abram, F. (2015) Systems-based approaches to unravel multi-species microbial community functioning. *Computational and Structural Biotechnology Journal* **13**: 24-32.

Alcolombri, U., Ben-Dor, S., Feldmesser, E., Levin, Y., Tawfik, D.S., and Vardi, A. (2015) Identification of the algal dimethyl sulfide–releasing enzyme: A missing link in the marine sulfur cycle. *Science* **348**: 1466-1469.

Arias, P., Bellouin, N., Coppola, E., Jones, R., Krinner, G., Marotzke, J. et al. (2021) Climate Change 2021: The Physical Science Basis. Contribution of Working Group14 I to the Sixth Assessment Report of the Intergovernmental Panel on Climate Change; Technical Summary.

Auman Ann, J., Speake Catherine, C., and Lidstrom Mary, E. (2001) nifH Sequences and Nitrogen Fixation in Type I and Type II Methanotrophs. *Applied and Environmental Microbiology* **67**: 4009-4016.

Baani, M., and Liesack, W. (2008) Two isozymes of particulate methane monooxygenase with different methane oxidation kinetics are found in *Methylocystis* sp. strain SC2. *Proceedings of the National Academy of Sciences* **105**: 10203-10208.

Balch, W., Fox, G.E., Magrum, L.J., Woese, C.R., and Wolfe, R. (1979) Methanogens: reevaluation of a unique biological group. *Microbiological reviews* **43**: 260-296.

Bapteste, É., Brochier, C., and Boucher, Y. (2005) Higher-level classification of the Archaea: evolution of methanogenesis and methanogens. *Archaea* **1**: 353-363.

Belova, S.E., Kulichevskaya, I.S., Bodelier, P.L., and Dedysh, S.N. (2013) Methylocystis bryophila sp. nov., a facultatively methanotrophic bacterium from acidic Sphagnum peat, and emended description of the genus Methylocystis (ex Whittenbury et al. 1970) Bowman et al. 1993. *International journal of systematic and evolutionary microbiology* **63**: 1096-1104.

Belova, S.E., Baani, M., Suzina, N.E., Bodelier, P.L.E., Liesack, W., and Dedysh, S.N. (2011) Acetate utilization as a survival strategy of peat-inhabiting Methylocystis spp. *Environmental Microbiology Reports* **3**: 36-46.

Bender, M., and Conrad, R. (1992) Kinetics of Ch4 Oxidation in Oxic Soils Exposed to Ambient Air or High Ch4 Mixing Ratios. *Fems Microbiology Ecology* **101**: 261-270.

Berghuis, B.A., Yu, F.B., Schulz, F., Blainey, P.C., Woyke, T., and Quake, S.R. (2019) Hydrogenotrophic methanogenesis in archaeal phylum Verstraetearchaeota reveals the shared ancestry of all methanogens. *Proceedings of the National Academy of Sciences* **116**: 5037-5044.

Berven, F.S., Karlsen, O.A., Straume, A.H., Flikka, K., Murrell, J.C., Fjellbirkeland, A. et al. (2006) Analysing the outer membrane subproteome of Methylococcus capsulatus (Bath) using proteomics and novel biocomputing tools. *Archives of Microbiology* **184**: 362-377.

Bodelier, P.L.E., and Laanbroek, H.J. (2004) Nitrogen as a regulatory factor of methane oxidation in soils and sediments. *FEMS Microbiology Ecology* **47**: 265-277.

Bodelier, P.L.E., Roslev, P., Henckel, T., and Frenzel, P. (2000) Stimulation by ammonium-based fertilizers of methane oxidation in soil around rice roots. *Nature* **403**: 421-424.

Bordel, S., Rojas, A., and Muñoz, R. (2019) Reconstruction of a Genome Scale Metabolic Model of the polyhydroxybutyrate producing methanotroph Methylocystis parvus OBBP. *Microbial Cell Factories* **18**: 104.

Bordel, S., Crombie, A.T., Muñoz, R., and Murrell, J.C. (2020) Genome Scale Metabolic Model of the versatile methanotroph Methylocella silvestris. *Microbial Cell Factories* **19**: 144.

Bowers, R.M., Kyrpides, N.C., Stepanauskas, R., Harmon-Smith, M., Doud, D., Reddy, T. et al. (2017) Minimum information about a single amplified genome (MISAG) and a metagenome-assembled genome (MIMAG) of bacteria and archaea. *Nat Biotechnol* **35**: 725-731.

Bowman, J.P. (2015) Methylocystis. In *Bergey's Manual of Systematics of Archaea and Bacteria*, pp. 1-7.

Bowman, J.P., Sly, L.I., Nichols, P.D., and Hayward, A.C. (1993) Revised Taxonomy of the Methanotrophs: Description of Methylobacter gen. nov., Emendation of Methylococcus, Validation of Methylosinus and Methylocystis Species, and a Proposal that the Family Methylococcaceae Includes Only the Group I Methanotrophs. *International Journal of Systematic and Evolutionary Microbiology* **43**: 735-753.

Brockhurst, M.A., Harrison, E., Hall, J.P.J., Richards, T., McNally, A., and MacLean, C. (2019) The Ecology and Evolution of Pangenomes. *Curr Biol* **29**: R1094-R1103.

Brune, A., Frenzel, P., and Cypionka, H. (2000) Life at the oxic–anoxic interface: microbial activities and adaptations. *FEMS Microbiol Rev* **24**: 691-710.

Cai, Y., Zhou, X., Shi, L., and Jia, Z. (2020) Atmospheric Methane Oxidizers Are Dominated by Upland Soil Cluster Alpha in 20 Forest Soils of China. *Microbial Ecology* **80**: 859-871.

Camp, H.D. (2009) Minireview Environmental, genomic and taxonomic perspectives on methanotrophic Verrucomicrobia.

Carere, C.R., Hards, K., Houghton, K.M., Power, J.F., McDonald, B., Collet, C. et al. (2017) Mixotrophy drives niche expansion of verrucomicrobial methanotrophs. *The ISME Journal* **11**: 2599-2610.

Castelle, C.J., and Banfield, J.F. (2018) Major New Microbial Groups Expand Diversity and Alter our Understanding of the Tree of Life. *Cell* **172**: 1181-1197.

Catherman, A.D., Skinner, O.S., and Kelleher, N.L. (2014) Top Down proteomics: facts and perspectives. *Biochem Biophys Res Commun* **445**: 683-693.

Chaumeil, P.-A., Mussig, A.J., Hugenholtz, P., and Parks, D.H. (2020) GTDB-Tk: a toolkit to classify genomes with the Genome Taxonomy Database. *Bioinformatics* **36**: 1925-1927.

Chen, Y.-H., and Prinn, R.G. (2005) Atmospheric modeling of high- and low-frequency methane observations: Importance of interannually varying transport. *Journal of Geophysical Research: Atmospheres* **110**.

Conrad, R. (2005) Quantification of methanogenic pathways using stable carbon isotopic signatures: a review and a proposal. *Organic Geochemistry* **36**: 739-752.

Conrad, R. (2007) Microbial Ecology of Methanogens and Methanotrophs. In *Advances in Agronomy*: Academic Press, pp. 1-63.

Conrad, R. (2009) The global methane cycle: recent advances in understanding the microbial processes involved. *Environ Microbiol Rep* **1**: 285-292.

Conrad, R. (2020) Importance of hydrogenotrophic, aceticlastic and methylotrophic methanogenesis for methane production in terrestrial, aquatic and other anoxic environments: A mini review. *Pedosphere* **30**: 25-39.

Conrad, R., Claus, P., and Casperb, P. (2010) Stable isotope fractionation during the methanogenic degradation of organic matter in the sediment of an acidic bog lake, Lake Grosse Fuchskuhle. *Limnol Oceanogr* **55**: 1932-1942.

Criddle, C.S., Billington, S.L., and Frank, C. (2014) *Renewable Bioplastics and Biocomposites From Biogas Methane and Waste-Derived Feedstock: Development of Enabling Technology, Life Cycle Assessment, and Analysis of Costs: Contractor's Report*: Department of Resources Recycling and Recovery.

Crombie, A.T., and Murrell, J.C. (2014) Trace-gas metabolic versatility of the facultative methanotroph Methylocella silvestris. *Nature* **510**: 148-151.

Cui, M., Ma, A., Qi, H., Zhuang, X., and Zhuang, G. (2015) Anaerobic oxidation of methane: an "active" microbial process. *MicrobiologyOpen* **4**: 1-11.

Dam, B., Dam, S., Blom, J., and Liesack, W. (2013) Genome analysis coupled with physiological studies reveals a diverse nitrogen metabolism in *Methylocystis* sp strain SC2. *Plos One* **8**: e74767.

Dam, B., Dam, S., Kim, Y., and Liesack, W. (2014) Ammonium induces differential expression of methane and nitrogen metabolism-related genes in *Methylocystis* sp strain SC2. *Environmental Microbiology* **16**: 3115-3127.

Dam, B., Dam, S., Kube, M., Reinhardt, R., and Liesack, W. (2012) Complete Genome Sequence of Methylocystis sp. Strain SC2, an Aerobic Methanotroph with High-Affinity Methane Oxidation Potential. *Journal of Bacteriology* **194**: 6008-6009.

Dean, J.F., Middelburg, J.J., Röckmann, T., Aerts, R., Blauw, L.G., Egger, M. et al. (2018) Methane Feedbacks to the Global Climate System in a Warmer World. *Rev Geophys* **56**: 207-250.

Dedysh, S.N., and Dunfield, P.F. (2011) Facultative and obligate methanotrophs how to identify and differentiate them. *Methods Enzymol* **495**: 31-44.

Dedysh, S.N., and Dunfield, P.F. (2016) Methyloferula. In *Bergey's Manual of Systematics of Archaea and Bacteria*, pp. 1-5.

Dedysh, S.N., and Knief, C. (2018) Diversity and Phylogeny of Described Aerobic Methanotrophs. In *Methane Biocatalysis: Paving the Way to Sustainability*. Kalyuzhnaya, M.G., and Xing, X.-H. (eds). Cham: Springer International Publishing, pp. 17-42.

Dedysh, S.N., Ricke, P., and Liesack, W. (2004) NifH and NifD phylogenies: an evolutionary basis for understanding nitrogen fixation capabilities of methanotrophic bacteria. *Microbiology* **150**: 1301-1313.

Dedysh, S.N., Didriksen, A., Danilova, O.V., Belova, S.E., Liebner, S., and Svenning, M.M. (2015) Methylocapsa palsarum sp. nov., a methanotroph isolated from a subArctic discontinuous permafrost ecosystem. *International journal of systematic and evolutionary microbiology* **65**: 3618-3624.

Dedysh, S.N., Khmelenina, V.N., Suzina, N.E., Trotsenko, Y.A., Semrau, J.D., Liesack, W., and Tiedje, J.M. (2002) Methylocapsa acidiphila gen. nov., sp. nov., a novel methane-oxidizing and dinitrogen-fixing acidophilic bacterium from Sphagnum bog. *International Journal of Systematic and Evolutionary Microbiology* **52**: 251-261.

Dedysh, S.N., Liesack, W., Khmelenina, V.N., Suzina, N.E., Trotsenko, Y.A., Semrau, J.D. et al. (2000) Methylocella palustris gen. nov., sp. nov., a new methane-oxidizing acidophilic bacterium from peat bogs, representing a novel subtype of serine-pathway methanotrophs. *International Journal of Systematic and Evolutionary Microbiology* **50**: 955-969.

Dedysh, S.N., Berestovskaya, Y.Y., Vasylieva, L.V., Belova, S.E., Khmelenina, V.N., Suzina, N.E. et al. (2004) Methylocella tundrae sp. nov., a novel methanotrophic bacterium from acidic tundra peatlands. *International Journal of Systematic and Evolutionary Microbiology* **54**: 151-156.

Dedysh, S.N., Belova, S.E., Bodelier, P.L.E., Smirnova, K.V., Khmelenina, V.N., Chidthaisong, A. et al. (2007) Methylocystis heyeri sp nov., a novel type II methanotrophic bacterium possessing 'signature' fatty acids of type I methanotrophs. *International Journal of Systematic and Evolutionary Microbiology* **57**: 472-479.

Dedysh Svetlana, N., Knief, C., and Dunfield Peter, F. (2005) Methylocella Species Are Facultatively Methanotrophic. *Journal of Bacteriology* **187**: 4665-4670.

del Cerro, C., García Jesús, M., Rojas, A., Tortajada, M., Ramón, D., Galán, B. et al. (2012) Genome Sequence of the Methanotrophic Poly-β-Hydroxybutyrate Producer Methylocystis parvus OBBP. *Journal of Bacteriology* **194**: 5709-5710.

Deng, Y., Che, R., Wang, F., Conrad, R., Dumont, M., Yun, J. et al. (2019) Upland Soil Cluster Gamma dominates methanotrophic communities in upland grassland soils. *Science of The Total Environment* **670**: 826-836.

Dridi, B., Fardeau, M.-L., Ollivier, B., Raoult, D., and Drancourt, M. (2012) Methanomassiliicoccus luminyensis gen. nov., sp. nov., a methanogenic archaeon isolated from human faeces. *International journal of systematic and evolutionary microbiology* **62**: 1902-1907.

Dunfield, P., and Knowles, R. (1995) Kinetics of inhibition of methane oxidation by nitrate, nitrite, and ammonium in a humisol. *Applied and Environmental Microbiology* **61**: 3129-3135.

Dunfield Peter, F., and Conrad, R. (2000) Starvation Alters the Apparent Half-Saturation Constant for Methane in the Type II MethanotrophMethylocystis Strain LR1. *Applied and Environmental Microbiology* **66**: 4136-4138.

Dunfield, P.F., Khmelenina, V.N., Suzina, N.E., Trotsenko, Y.A., and Dedysh, S.N. (2003) Methylocella silvestris sp. nov., a novel methanotroph isolated from an acidic forest cambisol. *International Journal of Systematic and Evolutionary Microbiology* **53**: 1231-1239.

Dunfield, P.F., Belova, S.E., Vorob'ev, A.V., Cornish, S.L., and Dedysh, S.N. (2010) Methylocapsa aurea sp. nov., a facultative methanotroph possessing a particulate methane monooxygenase, and emended description of the genus Methylocapsa. *International journal of systematic and evolutionary microbiology* **60**: 2659-2664.

Dunfield, P.F., Yimga, M.T., Dedysh, S.N., Berger, U., Liesack, W., and Heyer, J. (2002) Isolation of a Methylocystis strain containing a novel pmo A-like gene. *FEMS Microbiology Ecology* **41**: 17-26.

Dunfield, P.F., Yuryev, A., Senin, P., Smirnova, A.V., Stott, M.B., Hou, S. et al. (2007) Methane oxidation by an extremely acidophilic bacterium of the phylum Verrucomicrobia. *Nature* **450**: 879-882.

Elias, J.E., and Gygi, S.P. (2007) Target-decoy search strategy for increased confidence in large-scale protein identifications by mass spectrometry. *Nat Methods* **4**: 207-214.

Ernst, L., Steinfeld, B., Barayeu, U., Klintzsch, T., Kurth, M., Grimm, D. et al. (2022) Methane formation driven by reactive oxygen species across all living organisms. *Nature* **603**: 482-+.

Ettwig, K.F., Butler, M.K., Le Paslier, D., Pelletier, E., Mangenot, S., Kuypers, M.M. et al. (2010) Nitrite-driven anaerobic methane oxidation by oxygenic bacteria. *Nature* **464**: 543-548.

Evans, P.N., Parks, D.H., Chadwick, G.L., Robbins, S.J., Orphan, V.J., Golding, S.D., and Tyson, G.W. (2015) Methane metabolism in the archaeal phylum Bathyarchaeota revealed by genome-centric metagenomics. *Science* **350**: 434-438.

Farhan Ul Haque, M., Xu, H.J., Murrell, J.C., and Crombie, A. (2020) Facultative methanotrophs - diversity, genetics, molecular ecology and biotechnological potential: a mini-review. *Microbiology (Reading)* **166**: 894-908.

Farhan Ul Haque, M., Crombie, A.T., Ensminger, S.A., Baciu, C., and Murrell, J.C. (2018) Facultative methanotrophs are abundant at terrestrial natural gas seeps. *Microbiome* **6**: 118.

Fei, Q., Guarnieri, M.T., Tao, L., Laurens, L.M.L., Dowe, N., and Pienkos, P.T. (2014) Bioconversion of natural gas to liquid fuel: Opportunities and challenges. *Biotechnol Adv* **32**: 596-614.

Fisher, O.S., Kenney, G.E., Ross, M.O., Ro, S.Y., Lemma, B.E., Batelu, S. et al. (2018) Characterization of a long overlooked copper protein from methane- and ammonia-oxidizing bacteria. *Nature Communications* **9**: 4276.

Fournier, M.L., Gilmore, J.M., Martin-Brown, S.A., and Washburn, M.P. (2007) Multidimensional separations-based shotgun proteomics. *Chemical Reviews* **107**: 3654-3686.

Fu, Y., Li, Y., and Lidstrom, M. (2017) The oxidative TCA cycle operates during methanotrophic growth of the Type I methanotroph Methylomicrobium buryatense 5GB1. *Metabolic Engineering* **42**: 43-51.

Fu, Y., He, L., Reeve, J., Beck David, A.C., and Lidstrom Mary, E. (2019) Core Metabolism Shifts during Growth on Methanol versus Methane in the Methanotroph Methylomicrobium buryatense 5GB1. *mBio* **10**: e00406-00419.

Gęsicka, A., Oleskowicz-Popiel, P., and Łężyk, M. (2021) Recent trends in methane to bioproduct conversion by methanotrophs. *Biotechnol Adv* **53**: 107861.

Gilbert, B., McDonald Ian, R., Finch, R., Stafford Graham, P., Nielsen Allan, K., and Murrell, J.C. (2000) Molecular Analysis of the pmo (Particulate Methane Monooxygenase) Operons from Two Type II Methanotrophs. *Applied and Environmental Microbiology* **66**: 966-975.

Gillet, L.C., Navarro, P., Tate, S., Röst, H., Selevsek, N., Reiter, L. et al. (2012) Targeted data extraction of the MS/MS spectra generated by data-independent acquisition: a new concept for consistent and accurate proteome analysis. *Mol Cell Proteomics* **11**: O111.016717.

Goh, W.W.B., Guo, T., Aebersold, R., and Wong, L. (2015) Quantitative proteomics signature profiling based on network contextualization. *Biology Direct* **10**: 71.

Greening, C., and Cook, G.M. (2014) Integration of hydrogenase expression and hydrogen sensing in bacterial cell physiology. *Curr Opin Microbiol* **18**: 30-38.

Greening, C., Berney, M., Hards, K., Cook, G.M., and Conrad, R. (2014) A soil actinobacterium scavenges atmospheric H2 using two membrane-associated, oxygen-dependent [NiFe] hydrogenases. *Proceedings of the National Academy of Sciences* **111**: 4257-4261.

Greening, C., Biswas, A., Carere, C.R., Jackson, C.J., Taylor, M.C., Stott, M.B. et al. (2016) Genomic and metagenomic surveys of hydrogenase distribution indicate H2 is a widely utilised energy source for microbial growth and survival. *The ISME Journal* **10**: 761-777.

Greening, C., Carere, C.R., Rushton-Green, R., Harold, L.K., Hards, K., Taylor, M.C. et al. (2015) Persistence of the dominant soil phylum Acidobacteria by trace gas scavenging. *Proceedings of the National Academy of Sciences* **112**: 10497-10502.

Guerrero-Cruz, S., Vaksmaa, A., Horn, M.A., Niemann, H., Pijuan, M., and Ho, A. (2021) Methanotrophs: discoveries, environmental relevance, and a perspective on current and future applications. *Frontiers in Microbiology* **12**: 678057.

Gutleben, J., Chaib De Mares, M., van Elsas, J.D., Smidt, H., Overmann, J., and Sipkema, D. (2018) The multi-omics promise in context: from sequence to microbial isolate. *Crit Rev Microbiol* **44**: 212-229.

Hakobyan, A., Liesack, W., and Glatter, T. (2018) Crude-MS strategy for in-depth proteome analysis of the methane-oxidizing *Methylocystis* sp. strain SC2. *J Proteome Res* **17**: 3086-3103.

Hakobyan, A., Zhu, J., Glatter, T., Paczia, N., and Liesack, W. (2020) Hydrogen utilization by *Methylocystis* sp. strain SC2 expands the known metabolic versatility of type IIa methanotrophs. *Metabolic Engineering* **61**: 181-196.

Han, D., Link, H., and Liesack, W. (2017) Response of Methylocystis sp. Strain SC2 to Salt Stress: Physiology, Global Transcriptome, and Amino Acid Profiles. *Appl Environ Microbiol* **83**: e00866-00817.

Hanczár, T., Csáki, R., Bodrossy, L., Murrell, C.J., and Kovács, K.L. (2002) Detection and localization of two hydrogenases in Methylococcus capsulatus (Bath) and their potential role in methane metabolism. *Archives of Microbiology* **177**: 167-172.

Hanson, R.S., and Hanson, T.E. (1996) Methanotrophic bacteria. *Microbiological Reviews* **60**: 439-671.

Heyer, J., Galchenko, V.F., and Dunfield, P.F. (2002) Molecular phylogeny of type II methane-oxidizing bacteria isolated from various environmentsThe GenBank accession numbers for the nearly complete 16S rRNA gene sequences for the isolates are AJ458466 to AJ458510. Partial sequences of the pmoA, mxaF and mmoX genes have been deposited under the accession numbers AJ458994–AJ459052, AJ459053–AJ459100 and AJ458511–AJ458535, respectively. Where multiple strains contained identical sequences, only one has been deposited. *Microbiology* **148**: 2831-2846.

Holmes, A.J., Costello, A., Lidstrom, M.E., and Murrell, J.C. (1995) Evidence that particulate methane monooxygenase and ammonia monooxygenase may be evolutionarily related. *FEMS Microbiol Lett* **132**: 203-208.

Holmes Andrew, J., Roslev, P., McDonald Ian, R., Iversen, N., Henriksen, K., and Murrell, J.C. (1999) Characterization of Methanotrophic Bacterial Populations in Soils Showing Atmospheric Methane Uptake. *Applied and Environmental Microbiology* **65**: 3312-3318.

Iino, T., Tamaki, H., Tamazawa, S., Ueno, Y., Ohkuma, M., Suzuki, K.-i. et al. (2013) Candidatus Methanogranum caenicola: a novel methanogen from the anaerobic digested sludge, and proposal of Methanomassiliicoccaceae fam. nov. and Methanomassiliicoccales ord. nov., for a methanogenic lineage of the class Thermoplasmata. *Microbes Environ*: ME12189.

Im, J., Lee, S.-W., Yoon, S., DiSpirito, A.A., and Semrau, J.D. (2011) Characterization of a novel facultative Methylocystis species capable of growth on methane, acetate and ethanol. *Environmental Microbiology Reports* **3**: 174-181.

Jackson, R.B., Saunois, M., Bousquet, P., Canadell, J.G., Poulter, B., Stavert, A.R. et al. (2020) Increasing anthropogenic methane emissions arise equally from agricultural and fossil fuel sources. *Environmental Research Letters* **15**: 071002.

Jeon, Y.C., Nguyen, A.D., and Lee, E.Y. (2019). Bioproduction of Isoprenoids and Other Secondary Metabolites Using Methanotrophic Bacteria as an Alternative Microbial Cell Factory Option: Current Stage and Future Aspects [WWW document].

Jetten, M.S., Stams, A.J., and Zehnder, A.J. (1990) Acetate threshold values and acetate activating enzymes in methanogenic bacteria. *FEMS Microbiology Ecology* **6**: 339-344.

Ji, Y., Angel, R., Klose, M., Claus, P., Marotta, H., Pinho, L. et al. (2016) Structure and function of methanogenic microbial communities in sediments of Amazonian lakes with different water types. *Environ Microbiol* **18**: 5082-5100.

Kaluzhnaya, M., Khmelenina, V., Eshinimaev, B., Suzina, N., Nikitin, D., Solonin, A. et al. (2001) Taxonomic characterization of new alkaliphilic and alkalitolerant methanotrophs from soda lakes of the Southeastern Transbaikal region and description of Methylomicrobium buryatense sp. nov. *Systematic and applied microbiology* **24**: 166-176.

Kalyuzhnaya, M.G., Puri, A.W., and Lidstrom, M.E. (2015) Metabolic engineering in methanotrophic bacteria. *Metabolic Engineering* **29**: 142-152.

Kalyuzhnaya, M.G., Khmelenina, V., Eshinimaev, B., Sorokin, D., Fuse, H., Lidstrom, M., and Trotsenko, Y. (2008) Classification of halo (alkali) philic and halo (alkali) tolerant methanotrophs

provisionally assigned to the genera Methylomicrobium and Methylobacter and emended description of the genus Methylomicrobium. *International journal of systematic and evolutionary microbiology* **58**: 591-596.

Kalyuzhnaya, M.G., Yang, S., Rozova, O.N., Smalley, N.E., Clubb, J., Lamb, A. et al. (2013) Highly efficient methane biocatalysis revealed in a methanotrophic bacterium. *Nature Communications* **4**.

Kao, W.-C., Chen, Y.-R., Yi, E.C., Lee, H., Tian, Q., Wu, K.-M. et al. (2004) Quantitative Proteomic Analysis of Metabolic Regulation by Copper Ions in Methylococcus capsulatus (Bath)*[boxs]. *Journal of Biological Chemistry* **279**: 51554-51560.

Karthikeyan, O.P., Smith, T.J., Dandare, S.U., Parwin, K.S., Singh, H., Loh, H.X. et al. (2021) Metal(loid) speciation and transformation by aerobic methanotrophs. *Microbiome* **9**: 156.

Kaupper, T., Luehrs, J., Lee, H.J., Mo, Y., Jia, Z., Horn, M.A., and Ho, A. (2020) Disentangling abiotic and biotic controls of aerobic methane oxidation during re-colonization. *Soil Biol Biochem* **142**: 107729.

Khadem Ahmad, F., Pol, A., Wieczorek, A., Mohammadi Seyed, S., Francoijs, K.-J., Stunnenberg Henk, G. et al. (2011) Autotrophic Methanotrophy in Verrucomicrobia: Methylacidiphilum fumariolicumSolV Uses the Calvin-Benson-Bassham Cycle for Carbon Dioxide Fixation. *Journal of Bacteriology* **193**: 4438-4446.

Khadka, R., Clothier, L., Wang, L., Lim, C.K., Klotz, M.G., and Dunfield, P.F. (2018) Evolutionary History of Copper Membrane Monooxygenases. *Frontiers in Microbiology* **9**.

Khalifa, A., Lee, C.G., Ogiso, T., Ueno, C., Dianou, D., Demachi, T. et al. (2015) Methylomagnum ishizawai gen. nov., sp. nov., a mesophilic type I methanotroph isolated from rice rhizosphere. *International Journal of systematic and evolutionary microbiology* **65**: 3527-3534.

Khdhiri, M., Piché-Choquette, S., Tremblay, J., Tringe Susannah, G., and Constant, P. (2017) The Tale of a Neglected Energy Source: Elevated Hydrogen Exposure Affects both Microbial Diversity and Function in Soil. *Applied and Environmental Microbiology* **83**: e00275-00217.

Knapp, J.R., Laur, G.L., Vadas, P.A., Weiss, W.P., and Tricarico, J.M. (2014) Invited review: Enteric methane in dairy cattle production: Quantifying the opportunities and impact of reducing emissions. *J Dairy Sci* **97**: 3231-3261.

Knief, C. (2015) Diversity and habitat preferences of cultivated and uncultivated aerobic methanotrophic bacteria evaluated based on *pmoA* as molecular marker. *Frontiers in Microbiology* **6**: 1346.

Knief, C., and Dunfield, P.F. (2005) Response and adaptation of different methanotrophic bacteria to low methane mixing ratios. *Environmental Microbiology* **7**: 1307-1317.

Knief, C., Lipski, A., and Dunfield, P.F. (2003) Diversity and activity of methanotrophic bacteria in different upland soils. *Applied and environmental microbiology* **69**: 6703-6714.

Kolb, S. (2009) The quest for atmospheric methane oxidizers in forest soils. *Environmental Microbiology Reports* **1**: 336-346.

Kongpracha, P., Wiriyasermkul, P., Isozumi, N., Moriyama, S., Kanai, Y., and Nagamori, S. (2022) Simple But Efficacious Enrichment of Integral Membrane Proteins and Their Interactions for In-Depth Membrane Proteomics. *Molecular & Cellular Proteomics* **21**.

Leahy, J.G., Batchelor, P.J., and Morcomb, S.M. (2003) Evolution of the soluble diiron monooxygenases. *FEMS Microbiol Rev* **27**: 449-479.

Leng, L., Chang, J., Geng, K., Lu, Y., and Ma, K. (2015) Uncultivated Methylocystis species in paddy soil include facultative methanotrophs that utilize acetate. *Microbial ecology* **70**: 88-96.

Lieberman, R.L., Shrestha, D.B., Doan, P.E., Hoffman, B.M., Stemmler, T.L., and Rosenzweig, A.C. (2003) Purified particulate methane monooxygenase from Methylococcus capsulatus (Bath) is a dimer with both mononuclear copper and a copper-containing cluster. *Proceedings of the National Academy of Sciences* **100**: 3820-3825.

Lindner, A.S., Pacheco, A., Aldrich, H.C., Staniec, A.C., Uz, I., and Hodson, D.J. (2007) Methylocystis hirsuta sp nov., a novel methanotroph isolated from a groundwater aquifer. *International Journal of Systematic and Evolutionary Microbiology* **57**: 1891-1900.

Lloyd, K. (2015) Beyond known methanogens. *Science* **350**: 384-384.

Lubitz, W., Ogata, H., Rüdiger, O., and Reijerse, E. (2014) Hydrogenases. *Chemical Reviews* **114**: 4081-4148.

Ludwig, W., Strunk, O., Westram, R., Richter, L., Meier, H., Yadhukumar, a. et al. (2004) ARB: a software environment for sequence data. *Nucleic acids research* **32**: 1363-1371.

Luesken Francisca, A., Zhu, B., van Alen Theo, A., Butler Margaret, K., Diaz Marina, R., Song, B. et al. (2011) pmoA Primers for Detection of Anaerobic Methanotrophs. *Applied and Environmental Microbiology* **77**: 3877-3880.

Lyu, Z., Shao, N., Akinyemi, T., and Whitman, W.B. (2018) Methanogenesis. *Curr Biol* **28**: R727-R732.

Madison, L.L., and Huisman, G.W. (1999) Metabolic engineering of poly (3-hydroxyalkanoates): from DNA to plastic. *Microbiol Mol Biol Rev* **63**: 21-53.

Matsen, J.B., Yang, S., Stein, L.Y., Beck, D., and Kalyuzhnaya, M.G. (2013) Global Molecular Analyses of Methane Metabolism in Methanotrophic Alphaproteobacterium, Methylosinus trichosporium OB3b. Part I: Transcriptomic Study. *Front Microbiol* **4**: 40.

Miroshnikov, K.K., Belova, S.E., and Dedysh, S.N. (2019) Genomic Determinants of Phototrophy in Methanotrophic Alphaproteobacteria. *Microbiology* **88**: 548-555.

Mohammadi, S., Pol, A., van Alen, T.A., Jetten, M.S.M., and Op den Camp, H.J.M. (2017) Methylacidiphilum fumariolicum SolV, a thermoacidophilic 'Knallgas' methanotroph with both an oxygen-sensitive and -insensitive hydrogenase. *The ISME Journal* **11**: 945-958.

Mohanty, S.R., Bodelier, P.L.E., Floris, V., and Conrad, R. (2006) Differential effects of nitrogenous fertilizers on methane-consuming microbes in rice field and forest soils. *Applied and Environmental Microbiology* **72**: 1346-1354.

Murrell, J.C., and Dalton, H. (1983) Nitrogen Fixation in Obligate Methanotrophs. *Microbiology* **129**: 3481-3486.

Nguyen, A.D., Kim, D., and Lee, E.Y. (2019) A comparative transcriptome analysis of the novel obligate methanotroph Methylomonas sp. DH-1 reveals key differences in transcriptional responses in C1 and secondary metabolite pathways during growth on methane and methanol. *BMC Genomics* **20**: 130.

Norði, K.á., and Thamdrup, B. (2014) Nitrate-dependent anaerobic methane oxidation in a freshwater sediment. *Geochimica et Cosmochimica Acta* **132**: 141-150.

Nyerges, G., and Stein, L.Y. (2009) Ammonia cometabolism and product inhibition vary considerably among species of methanotrophic bacteria. *FEMS Microbiology Letters* **297**: 131-136.

Patel, V.J., Thalassinos, K., Slade, S.E., Connolly, J.B., Crombie, A., Murrell, J.C., and Scrivens, J.H. (2009) A Comparison of Labeling and Label-Free Mass Spectrometry-Based Proteomics Approaches. *Journal of Proteome Research* **8**: 3752-3759.

Pfluger, A.R., Wu, W.-M., Pieja, A.J., Wan, J., Rostkowski, K.H., and Criddle, C.S. (2011) Selection of Type I and Type II methanotrophic proteobacteria in a fluidized bed reactor under non-sterile conditions. *Bioresource technology* **102**: 9919-9926.

Piché-Choquette, S., and Constant, P. (2019) Molecular hydrogen, a neglected key driver of soil biogeochemical processes. *Applied and Environmental Microbiology* **85**: e02418-02418.

Piché-Choquette, S., Khdhiri, M., and Constant, P. (2018) Dose-response relationships between environmentally-relevant H2 concentrations and the biological sinks of H2, CH4 and CO in soil. *Soil Biol Biochem* **123**: 190-199.

Pieja, A.J., Sundstrom, E.R., and Criddle, C.S. (2011) Poly-3-hydroxybutyrate metabolism in the type II methanotroph Methylocystis parvus OBBP. *Applied and environmental microbiology* **77**: 6012-6019.

Pieja Allison, J., Sundstrom Eric, R., and Criddle Craig, S. (2011) Poly-3-Hydroxybutyrate Metabolism in the Type II Methanotroph Methylocystis parvus OBBP. *Applied and Environmental Microbiology* **77**: 6012-6019.

Poetsch, A., and Wolters, D. (2008) Bacterial membrane proteomics. *Proteomics* **8**: 4100-4122.

Pol, A., Heijmans, K., Harhangi, H.R., Tedesco, D., Jetten, M.S., and Op den Camp, H.J. (2007) Methanotrophy below pH 1 by a new Verrucomicrobia species. *Nature* **450**: 874-878.

Pratscher, J., Dumont, M.G., and Conrad, R. (2011) Assimilation of acetate by the putative atmospheric methane oxidizers belonging to the USCα clade. *Environmental Microbiology* **13**: 2692-2701.

Reay, D.S., Smith, P., Christensen, T.R., James, R.H., and Clark, H. (2018) Methane and Global Environmental Change. *Annual Review of Environment and Resources* **43**: 165-192.

Reim, A., Lüke, C., Krause, S., Pratscher, J., and Frenzel, P. (2012) One millimetre makes the difference: high-resolution analysis of methane-oxidizing bacteria and their specific activity at the oxic–anoxic interface in a flooded paddy soil. *The ISME Journal* **6**: 2128-2139.

Ricke, P., Erkel, C., Kube, M., Reinhardt, R., and Liesack, W. (2004) Comparative analysis of the conventional and novel pmo (particulate methane monooxygenase) operons from Methylocystis strain SC2. *Applied and environmental microbiology* **70**: 3055-3063.

Rosenzweig, A.C., Frederick, C.A., Lippard, S.J., Nordlund, P., and auml (1993) Crystal structure of a bacterial non-haem iron hydroxylase that catalyses the biological oxidation of methane. *Nature* **366**: 537-543.

Ross, M.O., and Rosenzweig, A.C. (2017) A tale of two methane monooxygenases. *JBIC Journal of Biological Inorganic Chemistry* **22**: 307-319.

Rotaru, A.-E., Shrestha, P.M., Liu, F., Shrestha, M., Shrestha, D., Embree, M. et al. (2014) A new model for electron flow during anaerobic digestion: direct interspecies electron transfer to Methanosaeta for the reduction of carbon dioxide to methane. *Energy & Environmental Science* **7**: 408-415.

Sahoo, K.K., Goswami, G., and Das, D. (2021) Biotransformation of Methane and Carbon Dioxide Into High-Value Products by Methanotrophs: Current State of Art and Future Prospects. *Frontiers in Microbiology* **12**.

Sakai, S., Imachi, H., Hanada, S., Ohashi, A., Harada, H., and Kamagata, Y. (2008) Methanocella paludicola gen. nov., sp. nov., a methane-producing archaeon, the first isolate of the lineage 'Rice Cluster I', and proposal of the new archaeal order Methanocellales ord. nov. *International Journal of Systematic and Evolutionary Microbiology* **58**: 929-936.

Saratale, G.D., and Oh, M.-K. (2015) Characterization of poly-3-hydroxybutyrate (PHB) produced from Ralstonia eutropha using an alkali-pretreated biomass feedstock. *International journal of biological macromolecules* **80**: 627-635.

Saunois, M., Stavert, A.R., Poulter, B., Bousquet, P., Canadell, J.G., Jackson, R.B. et al. (2020) The Global Methane Budget 2000–2017. *Earth Syst Sci Data* **12**: 1561-1623.

Schnell, S., and King, G.M. (1994) Mechanistic Analysis of Ammonium Inhibition of Atmospheric Methane Consumption in Forest Soils. *Applied and Environmental Microbiology* **60**: 3514-3521.

Semrau, J.D. (2011) Bioremediation via methanotrophy: overview of recent findings and suggestions for future research. *Frontiers in Microbiology* **2**.

Sheu, D.-S., Wang, Y.-T., and Lee, C.-Y. (2000) Rapid detection of polyhydroxyalkanoate-accumulating bacteria isolated from the environment by colony PCR. *Microbiology* **146**: 2019-2025.

Shima, S., Pilak, O., Vogt, S., Schick, M., Stagni, M.S., Meyer-Klaucke, W. et al. (2008) The Crystal Structure of [Fe]-Hydrogenase Reveals the Geometry of the Active Site. *Science* **321**: 572-575.

Sirajuddin, S., and Rosenzweig, A.C. (2015) Enzymatic Oxidation of Methane. *Biochemistry* **54**: 2283-2294.

Smith, P.H., and Mah, R.A. (1966) Kinetics of acetate metabolism during sludge digestion. *Appl Microbiol* **14**: 368-371.

Stams, A.J.M., Teusink, B., and Sousa, D.Z. (2019) Ecophysiology of Acetoclastic Methanogens. In *Biogenesis of Hydrocarbons*. Stams, A.J.M., and Sousa, D.Z. (eds). Cham: Springer International Publishing, pp. 109-121.

Stein, L.Y., and Klotz, M.G. (2011) Nitrifying and denitrifying pathways of methanotrophic bacteria. *Biochemical Society Transactions* **39**: 1826-1831.

Stein, L.Y., Roy, R., and Dunfield, P.F. Aerobic Methanotrophy and Nitrification: Processes and Connections. In *eLS*.

Tamas, I., Smirnova, A.V., He, Z., and Dunfield, P.F. (2014) The (d)evolution of methanotrophy in the Beijerinckiaceae—a comparative genomics analysis. *The ISME Journal* **8**: 369-382.

Täumer, J., Marhan, S., Groß, V., Jensen, C., Kuss, A.W., Kolb, S., and Urich, T. (2022) Linking transcriptional dynamics of CH4-cycling grassland soil microbiomes to seasonal gas fluxes. *The ISME Journal* **16**: 1788-1797.

Tays, C., Guarnieri, M.T., Sauvageau, D., and Stein, L.Y. (2018) Combined effects of carbon and nitrogen source to optimize growth of proteobacterial methanotrophs. *Frontiers in Microbiology* **9**.

Theisen, A.R., Ali, M.H., Radajewski, S., Dumont, M.G., Dunfield, P.F., McDonald, I.R. et al. (2005) Regulation of methane oxidation in the facultative methanotroph Methylocella silvestris BL2. *Molecular Microbiology* **58**: 682-692.

Tikhonova, E.N., Grouzdev, D.S., Avtukh, A.N., and Kravchenko, I.K. (2021) *Methylocystis silviterrae* sp.nov., a high-affinity methanotrophic bacterium isolated from the boreal forest soil. *Int J Syst Evol Microbiol* **71**.

Trotsenko, Y.A., and Murrell, J.C. (2008) Metabolic aspects of aerobic obligate methanotrophy⋆. *Adv Appl Microbiol* **63**: 183-229.

Tveit, A.T., Hestnes, A.G., Robinson, S.L., Schintlmeister, A., Dedysh, S.N., Jehmlich, N. et al. (2019) Widespread soil bacterium that oxidizes atmospheric methane. *Proceedings of the National Academy of Sciences* **116**: 8515-8524.

vanderNat, F.J.W.A., deBrouwer, J.F.C., Middelburg, J.J., and Laanbroek, H.J. (1997) Spatial distribution and inhibition by ammonium of methane oxidation in intertidal freshwater marshes. *Applied and Environmental Microbiology* **63**: 4734-4740.

Versantvoort, W., Pol, A., Jetten, M.S.M., Niftrik, L.v., Reimann, J., Kartal, B., and Camp, H.J.M.O.d. (2020) Multiheme hydroxylamine oxidoreductases produce NO during ammonia oxidation in methanotrophs. *Proceedings of the National Academy of Sciences* **117**: 24459-24463.

Versantvoort, W., Guerrero-Cruz, S., Speth, D.R., Frank, J., Gambelli, L., Cremers, G. et al. (2018) Comparative Genomics of Candidatus Methylomirabilis Species and Description of Ca. Methylomirabilis Lanthanidiphila. *Frontiers in Microbiology* **9**.

Vorobev, A., Jagadevan, S., Jain, S., Anantharaman, K., Dick Gregory, J., Vuilleumier, S., and Semrau Jeremy, D. (2014) Genomic and Transcriptomic Analyses of the Facultative Methanotroph

Methylocystis sp. Strain SB2 Grown on Methane or Ethanol. *Applied and Environmental Microbiology* **80**: 3044-3052.

Vorobev, A.V., Baani, M., Doronina, N.V., Brady, A.L., Liesack, W., Dunfield, P.F., and Dedysh, S.N. (2011) Methyloferula stellata gen. nov., sp. nov., an acidophilic, obligately methanotrophic bacterium that possesses only a soluble methane monooxygenase. *International Journal of Systematic and Evolutionary Microbiology* **61**: 2456-2463.

Wang, F.-P., Zhang, Y., Chen, Y., He, Y., Qi, J., Hinrichs, K.-U. et al. (2014) Methanotrophic archaea possessing diverging methane-oxidizing and electron-transporting pathways. *The ISME Journal* **8**: 1069-1078.

Wartiainen, I., Hestnes, A.G., McDonald, I.R., and Svenning, M.M. (2006) Methylocystis rosea sp nov., a novel methanotrophic bacterium from Arctic wetland soil, Svalbard, Norway (78 degrees N). *International Journal of Systematic and Evolutionary Microbiology* **56**: 541-547.

Wegner, C.-E., Gorniak, L., Riedel, S., Westermann, M., and Küsel, K. (2019) Lanthanide-Dependent Methylotrophs of the Family Beijerinckiaceae: Physiological and Genomic Insights. *Applied and Environmental Microbiology* **86**: e01830-01819.

West, J.J., Fiore, A.M., Horowitz, L.W., and Mauzerall, D.L. (2006) Global health benefits of mitigating ozone pollution with methane emission controls. *Proceedings of the National Academy of Sciences* **103**: 3988-3993.

Whittenbury, R., and Dalton, H. (1981) The methylotrophic bacteria. In *The prokaryotes*: Springer, pp. 894-902.

Whittenbury, R., Phillips, K., and Wilkinson, J. (1970) Enrichment, isolation and some properties of methane-utilizing bacteria. *Microbiology* **61**: 205-218.

Xiao, K.-Q., Beulig, F., Røy, H., Jørgensen, B.B., and Risgaard-Petersen, N. (2018) Methylotrophic methanogenesis fuels cryptic methane cycling in marine surface sediment. *Limnol Oceanogr* **63**: 1519-1527.

Yang, B., Wang, Y., and Qian, P.-Y. (2016) Sensitivity and correlation of hypervariable regions in 16S rRNA genes in phylogenetic analysis. *BMC Bioinformatics* **17**: 135.

Yang, N., Lü, F., He, P., and Shao, L. (2011) Response of methanotrophs and methane oxidation on ammonium application in landfill soils. *Applied Microbiology and Biotechnology* **92**: 1073-1082.

Yang, S., Matsen, J.B., Konopka, M., Green-Saxena, A., Clubb, J., Sadilek, M. et al. (2013) Global Molecular Analyses of Methane Metabolism in Methanotrophic Alphaproteobacterium, Methylosinus trichosporium OB3b. Part II. Metabolomics and 13C-Labeling Study. *Front Microbiol* **4**: 70.

Yeo, J.C.C., Muiruri, J.K., Thitsartarn, W., Li, Z., and He, C. (2018) Recent advances in the development of biodegradable PHB-based toughening materials: Approaches, advantages and applications. *Materials Science and Engineering: C* **92**: 1092-1116.

Yimga, M.T., Dunfield, P.F., Ricke, P., Heyer, J., and Liesack, W. (2003) GENETICS AND MOLECULAR BIOLOGY-Wide Distribution of a Novel pmoA-Like Gene Copy among Type II Methanotrophs, and Its Expression in Methylocystis Strain SC2. *Applied and Environmental Microbiology* **69**: 5593-5602.

Zhang, Y.Y., Fonslow, B.R., Shan, B., Baek, M.C., and Yates, J.R. (2013) Protein Analysis by Shotgun/Bottom-up Proteomics. *Chemical Reviews* **113**: 2343-2394.

Zheng, Y., and Chistoserdova, L. (2019) Multi-omics Understanding of Methanotrophs. In *Methanotrophs: Microbiology Fundamentals and Biotechnological Applications*. Lee, E.Y. (ed). Cham: Springer International Publishing, pp. 121-138.

Zhu, Y., Koo, C.W., Cassidy, C.K., Spink, M.C., Ni, T., Zanetti-Domingues, L.C. et al. (2022) Structure and activity of particulate methane monooxygenase arrays in methanotrophs. *Nature Communications* **13**: 5221.

Chapter 2:

Methylocystis sp. Strain SC2 Acclimatizes to Increasing NH_4^+ Levels by a Precise Rebalancing of Enzymes and Osmolyte Composition

mSystems. 2022: e0040322. https://doi.org/10.1128/msystems.00403-22

Kangli Guo[1], Anna Hakobyan[1¥], Timo Glatter[2], Nicole Paczia[3], Werner Liesack[1,4*]

*Corresponding author

Chapter 2 is written in research manuscript style. It was published as research article in mSystems in August 2022. My contribution to the chapter 2 involved the experimental design, laboratory experiments, the proteomics data analysis, the writing and the revision of corresponding parts of the manuscript, including the design of the figures.

[1]Research group "Methanotrophic Bacteria and Environmental Genomics/Transcriptomics", Max Planck Institute for Terrestrial Microbiology, Marburg, D-35043, Germany

[2]Core Facility for Mass Spectrometry and Proteomics, Max Planck Institute for Terrestrial Microbiology, Marburg, D-35043, Germany

[3]Core Facility for Metabolomics and Small Molecule Mass Spectrometry, Max Planck Institute for Terrestrial Microbiology, Marburg, D-35043, Germany

[4]Center for Synthetic Microbiology (SYNMIKRO), Philipps-Universität Marburg, Marburg, D-35043, Germany

[¥]Present Address

INRES - Molecular Biology of the Rhizosphere, University of Bonn, Nussallee 13, 53115 Bonn

2.1 Abstract

High NH_4^+ load is known to inhibit bacterial methane oxidation. This is due to a competition between CH_4 and NH_3 for the active site of particulate methane monooxygenase (pMMO), which converts CH_4 to CH_3OH. Here we combined global proteomics with amino acid profiling and NOx measurements to elucidate the cellular acclimatization response of *Methylocystis* sp. strain SC2 to high NH_4^+ levels. Relative to 1 mM NH_4^+, high (50 mM and 75 mM) NH_4^+ load under CH_4 replete conditions significantly increased lag phase duration required for proteome adjustment. The number of differentially regulated proteins was highly significantly correlated to increasing NH_4^+ load. The cellular responses to increasing ionic and osmotic stress involved significant upregulation of stress-responsive proteins, K^+ "salt in" strategy, synthesis of compatible solutes (glutamate and proline), and induction of the glutathione metabolism pathway. A significant increase in the apparent K_m value for CH_4 oxidation during the growth phase was indicative of increased pMMO-based oxidation of NH_3 to toxic hydroxylamine. The detoxifying activity of hydroxlyamine oxidoreductase (HAO) led to a significant accumulation of NO_2^- and, upon decreasing O_2 tension, N_2O. Nitric oxide reductase and hybrid cluster proteins (Hcps) were the candidate enzymes for the production of N_2O. In summary, strain SC2 has the capacity to precisely rebalance enzymes and osmolyte composition in response to increasing NH_4^+ exposure, but the need to simultaneously combat both ionic-osmotic stress and the toxic effects of hydroxylamine may be the reason why its acclimatization capacity is limited to 75 mM NH_4^+.

IMPORTANCE In addition to reducing CH_4 emissions from wetlands and landfills, the activity of alphaproteobacterial methane oxidizers of the genus *Methylocystis* contributes to the sink capacity of forest and grassland soils for atmospheric methane. The methane-oxidizing activity of *Methylocystis* spp. is, however, sensitive to high NH_4^+ concentrations. This is due to the competition of CH_4 and NH_3 for the active site of particulate methane monooxygenase, thereby resulting in the production of toxic hydroxylamine with increasing NH_4^+ load. An understanding of the physiological and molecular response mechanisms of *Methylocystis* spp. is therefore of great importance. Here, we combined global proteomics with amino acid profiling.

and NOx measurements to disentangle the cellular mechanisms underlying the acclimatization of *Methylocystis* sp. strain SC2 to increasing NH_4^+ load.

Keywords: Methanotrophs; *Methylocystis*; methane; ammonia; particulate methane monooxygenase; hydroxylamine oxidoreductase; proteomics

2.2 Introduction

Aerobic methanotrophic bacteria, or methanotrophs, are crucial players in the global cycle of the greenhouse gas methane. These bacteria are defined by their ability to utilize methane as their sole energy source for growth (Knief, 2015). Among the known methane oxidizers, proteobacterial methanotrophs have been unequivocally proven to be functionally important in natural and anthropogenic terrestrial environments (Knief, 2015; Guerrero-Cruz et al., 2021). Indeed, their activity acts in aerobic interfaces of methanogenic environments as a methane biofilter through which the emission of this greenhouse gas to the atmosphere is greatly mitigated (Cébron et al., 2007; Shiau et al., 2018; Guerrero-Cruz et al., 2021). Another environmentally relevant activity is their ability to act as a sink for atmospheric CH_4 in unsaturated soils (Conrad, 2009). Their key enzyme is particulate methane monooxygenase (Baani and Liesack), which converts CH_4 to methanol (CH_3OH). The pMMO is integral part of an extensive intracytoplasmic membrane system (ICM), which is a particular characteristic of proteobacterial methanotrophs (Lindner et al., 2007; Tikhonova et al., 2021).

Historically, these bacteria have been classified into type I and type II methanotrophs. This differentiation was particularly based on the type of ICM, biochemical pathways of carbon fixation, the capability of nitrogen fixation, the formation of resting stages, and the phospholipid fatty acid composition (Whittenbury and Dalton, 1981; Hanson and Hanson, 1996). Phylogenetic analysis of their 16S rRNA gene sequences confirmed the initial classification into type I (*Gammaproteobacteria*) and type II (*Alphaproteobacteria*) methanotrophs. Besides phylogeny, the carbon fixation pathway, however, remained the only major feature of the above-mentioned criteria that validly differentiates between type I and type II methanotrophs. As suggested by Knief (2015), we therefore use these terms only as synonyms for the phylogenetic groups of *Gamma-* and *Alphaproteobacteria*. The methanotrophic *Alphaproteobacteria* were further divided into type IIa (*Methylocystaceae*) and type IIb (*Beijerinckiaceae*) methanotrophs (Deng et al., 2013; Dumont et al., 2014). Various members of the *Methylocystaceae* are able to produce two pMMO isozymes that exhibit different methane oxidation kinetics (Yimga et al., 2003; Baani

and Liesack, 2008). These methanotrophs are widely distributed in natural wetlands and rice paddies, but have also been shown to be abundantly present in upland (e.g., forest) and grasslands soils where they may oxidize atmospheric CH_4 (Knief et al., 2003; Knief and Dunfield, 2005; Knief et al., 2005). Indeed, recent research has unambiguously shown that *Methylocystis* spp. contribute via the expression of their high-affinity pMMO to the atmospheric CH_4 sink in grasslands, in addition to USCα and USCγ (Täumer et al., 2022).

Like all microorganisms, methanotrophs require nitrogen for growth. Most of them utilize either NO_3^- or NH_4^+ as nitrogen source for growth. The structural homology between pMMO and ammonia monooxygenase, however, allows both methanotrophs and ammonia oxidizers to convert either substrates (CH_4 and NH_3), although neither is able to grow on the alternative substrate (Bédard and Knowles, 1989; Stein and Klotz, 2011a; Versantvoort et al., 2020). The pMMO oxidizes NH_3 to hydroxylamine (NH_2OH) (Stein and Klotz, 2011a). Ammonia produced from the deprotonation of liquid NH_4^+ competes with CH_4 for the same active site of pMMO (Nyerges and Stein, 2009; Yang et al., 2011). Whether NH_4^+ in the environment has inhibitory or stimulatory effects on methane-oxidizing bacteria depends largely on the diversity, structure and activity of the methanotrophic community, as well as the particular conditions in the habitat (Schnell and King, 1994; Dunfield and Knowles, 1995; Mohanty et al., 2006).

The inhibitory effects of NH_3 oxidation by pMMO on methanotrophic activity occur through toxic nitrogen products such as NH_2OH and nitrite (NO_2^-). Although the affinity of pMMO for NH_3 is generally lower than for CH_4 (Bédard and Knowles, 1989), aerobic methanotrophs with high tolerance to these nitrogen products need the ability to quickly detoxify them by both nitrifying and denitrifying processes (Stein et al., 2010; Stein and Klotz, 2011a). Both the detailed survey of genes involved in nitrogen metabolism in methanotrophic bacteria and physiological studies suggest that methanotrophs with efficient hydroxylamine detoxification pathways show increased competitiveness under high NH_4^+-N conditions (Lopez et al., 2019; Ho et al., 2020; van Dijk et al., 2021). Nevertheless, the acclimatization response of methanotrophs to increasing NH_4^+ load has not yet been conclusively understood at the cellular level. This is particularly valid for type IIa methanotrophs and more specifically for *Methylocystis* spp.

Therefore, we here aimed to elucidate the cellular mechanisms underlying the acclimatization response of *Methylocystis* sp. strain SC2 to increasing NH_4^+ load. In particular, we aimed (i) to determine the NH_4^+ threshold level to which strain SC2 is able to acclimatize and (ii) to assess the cellular adjustment processes triggered by this threshold level. We expected to observe a dual response of strain SC2, with the first one being a general response to increasing ionic-osmotic stress and the second one being a methanotroph-specific response to hydroxylamine stress. Recently we developed a new analytical proteomics workflow for strain SC2, which captures 62% of the predicted SC2 proteome under standard growth conditions (Hakobyan et al., 2018). This workflow tackles the major challenges related to the high amount of integral membrane proteins that need to be efficiently solubilized and digested for downstream analysis. Thus, our research combined SC2 growth experiments under increasing NH_4^+ load (1 to 100 mM) with global proteomics, analysis of intracellular amino acids (metabolomics), and measurement of NOx compounds (Fig. 2.1).

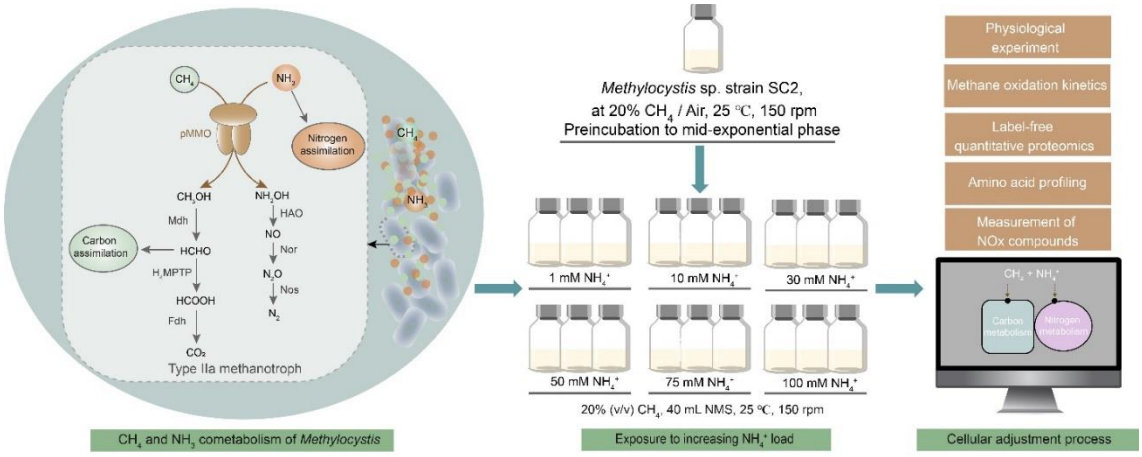

Fig. 2.1 Experimental design set up to elucidate the physiological and cellular responses of Methylocystis sp. strain SC2 to increasing NH_4^+ load. Detailed information on the experimental approach is given in Materials and Methods.

2.3 Results

The following subsections describe the effects of increasing NH_4^+ load on the activity of *Methylocystis* sp. strain SC2. This involves the impact on its growth response and apparent *Km* value of CH_4 oxidation, global proteome, and the concentration of intracellular amino acids. The effects of 10, 30, 50, and 75 mM NH_4^+ on the physiology and global proteome of strain SC2 were inferred by comparison to the reference standard growth conditions (1 mM NH_4^+). Finally, we quantified the NO_2^- and N_2O production by strain SC2 in relation to both increasing NH_4^+ load and incubation time.

2.3.1 Growth response

To assess increasing concentration levels of ammonium on SC2 growth, cells of strain SC2 were incubated in strict batch incubation mode with a CH_4:air mixing ratio of 20:80 % (v/v) (Fig. 2.2). Cell density (OD_{600}) and the headspace concentrations of both CH_4 and CO_2 were regularly measured during the complete incubation period of up 336 h (14 d), ranging from early lag phase to late stationary phase (Fig. 2.2). The addition of 1 mM NH_4^+ prompted immediate growth of strain SC2, while the addition of 10 mM and 30 mM NH_4^+ also had nearly no delay effect on the growth response of strain SC2 (Fig. 2.2). Supplementation with NH_4^+ levels higher than 30 mM triggered significant delays in the growth response with lag phase durations of 75 h (50 mM NH_4^+) and 125 h (75 mM NH_4^+). This was linked to a significant decrease in the growth and CH_4 consumption rates (Fig. 2.2, Table 2.1). However, regardless of the amount of ammonium added (1 to 75 mM NH_4^+), all SC2 cultures grew to the same final OD_{600} of about 0.45 (Fig. 2.2). Accordingly, total cell dry weight (CDW), total amount of CH_4 consumed and, in consequence, biomass yield did not significantly differ between the different NH_4^+ concentrations. However, the standard deviation of CDW increased with increasing NH_4^+ load, thereby suggesting an increasingly heterogeneous population response (Table 2.1). There was no significant CH_4 consumption and cell density change after the addition of 100 mM NH_4^+ (Fig. 2.2).

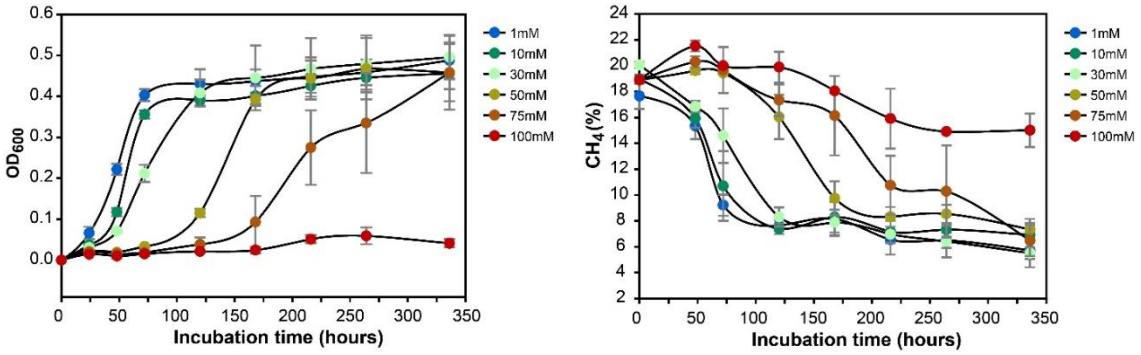

Fig. 2.2 Effect of increasing NH_4^+ concentrations on (A) growth of and (B) CH_4 consumption by Methylocystis sp. strain SC2. Growth (OD_{600}) and CH_4 concentration were regularly monitored over the whole incubation period. Measurements were done in triplicate cultures. Growth response occucrred up to 75 mM NH_4Cl, corresponding to a total ionic medium strength of 114 mM (Table S2). No growth occurred with 100 mM NH_4Cl, corresponding to a total ionic medium strength of 139 mM. Error bars show standard deviations of triplicate cultures.

Table 2.1 Physiological growth parameters of *Methylocystis* sp. strain SC2 during cultivation under different NH_4^+ concentrations

Ammonium treatment‡	**CDW† (mg)**	**Growth rate§ (mg CDW / d)**	**CH_4 consumption (mmol CH_4)**	**Biomass yield (mg CDW / mmol CH_4)**	**CH_4 consumption rate (mmol CH_4 / g CDW / d)**
1 mM	3.5±0.04	1.75±0.02	0.29±0.04	12.38±1.59	40.87±5.55
10 mM	3.32±0.13	1.66±0.07	0.27±0.03	12.29±1.72	41.22±5.68
30 mM	3.93±0.35	1.31±0.12**	0.28±0.01	14.08±1.04	23.75±1.74**
50 mM	4.26±0.54	0.71±0.09***	0.36±0.02	11.84±2.27	14.42±2.68***
75 mM	4.36±1.02	0.48±0.11***	0.35±0.04	12.4±3.21	9.34±2.2***

Note: ‡ All growth parameters were calculated based on triplicate cultures. † Cell dry weight (CDW) was calculated with 1 OD_{600} = 0.26 g CDW/L of strain SC2 culture (Hakobyan et al., 2020). § Asteriks indicate significant difference with **p*-value ≤ 0.05; ***p*-value ≤ 0.01; and ****p*-value ≤ 0.001 relative to the control treatment (1 mM NH_4^+), using Tukey's method with one-way ANOVA.

2.3.2 Apparent *Km* value of CH_4 oxidation

The CH_4:air mixing ratios adjusted to 10:90 and 20:80 (v/v) showed no significant difference in SC2 growth response when supplemented with 10 mM, 30 mM and 50 mM

NH_4^+. No increase in cell density (OD_{600}) was observed in SC2 cultures supplemented with 50 mM NH_4^+ after adjusting the CH_4:air mixing ratio to below 10:90 (v/v) (Fig. S2.1).

The SC2 growth parameters determined for the different CH_4:air mixing ratios and increasing NH_4^+ concentrations revealed that relative to the control (20:80 [v/v]), ratio values of 5:95 and 2.5:97.5 (v/v) reduced cell dry weight (CDW) production, growth rate, CH_4 consumption, and CH_4 consumption rate. This was significant ($p < 0.001$) across all physiological growth parameters for SC2 cultures supplemented with 50 mM NH_4^+ (Table S1). The increase in NH_4^+ concentration greatly altered the apparent K_m values ($K_{m(app)}$) for CH_4 oxidation, being 0.17 μM, 1.20 μM, and 1.40 μM under growth conditions with 10 mM, 30 mM and 50 mM NH_4^+, respectively (Table S2). This corresponds well to the decrease in the ratio of CH_4 to NH_3 dissolved in the liquid growth medium (Table S2). The $K_{m(app)}$ value for 75 mM NH_4^+ could not be calculated because growth of strain SC2 was completely inhibited when incubated under a headspace of 2.5% and 5% CH_4.

Table 2.2 Effect of increasing NH_4^+ load on the apparent K_m and V_{max} values of CH_4 oxidation

Incubation parameters		$K_{m(app)}$ ‡	$V_{max(app)}$
CH4 (vol/vol, %)	**NH_4^+ (mM)**	**(μM)**	**mol.cell^{-1}.h^{-1}†**
2.5–20	10	0.17	2.96E-15
2.5–20	30	1.20**	2.32E-15
2.5–20	50	1.40**	2.07E-15

Note: ‡ To test the inhibitory effect of increasing NH_4^+ concentration on CH_4 oxidation, SC2 cells were grown at 2.5%, 5%, 10%, 15%, and 20% CH_4. Exposed to 75 mM NH_4^+, growth of strain SC2 was completely inhibited when incubated with a headspace of 2.5% and 5% CH_4. Therefore, the $K_{m(app)}$ value for the treatment with 75 mM NH_4^+ could not be experimentally determined. Given the steady decline in the CH_4 consumption rates (Table 2.1), it is however reasonable to conclude that at 75 mM NH_4^+, the $K_{m(app)}$

value for CH_4 oxidation was higher than for the incubation treatments with 30 mM and 50 mM NH_4^+. Multiplication with the Oswald constant (0.03395 at 25 °C) gave the $K_{m(app)}$ value for the methane concentration in water. $K_{m(app)}$ values are shown in μM. The calculation of $K_{m(app)}$ and $V_{max(app)}$ is based on triplicate cultures. †The exponential decrease in CH_4 over incubation time was used to estimate $V_{max(app)}$ of SC2 cultures. Asterisks (**) indicate significant difference (p-value ≤ 0.01) relative to 10 mM NH_4^+ condition.

2.3.3 Whole-cell proteome

Global proteomics led to the detection of 2206 proteins, of which 438 proteins were identified to be differentially regulated proteins (DRPs) in at least one of the NH_4^+ treatments (Data Set S1). The 438 DRPs cover 10.8% of the total SC2 proteome (4040 proteins) deposited with UniProt database (https://www.uniprot.org/taxonomy/187303). Neither the PmoCAB1 subunits of low-affnity pMMO1 nor the PmoB2 subunit of the high-affinity pMMO2 showed a differential regulation. The PmoC2 and PmoA2 subunits of pMMO2 were not detectable at any of the NH_4^+ treatments (Table 2.3). Hierarchical cluster analysis and Pearson correlation coefficient values showed highly reproducible DRP profiles for all five NH_4^+ conditions (Fig. 2.3A; Fig. S2.2). The heatmap of sample-to-sample distances showed high similarities between the DRP profiles of the 1 mM and 10 mM NH_4^+ treatments, but in particular between those of the 50 mM and 75 mM NH_4^+ treatments. More specifically, the DRPs grouped into three distinct clusters comprising a total of 141, 65, and 232 proteins, respectively. The 232 proteins of DRP cluster III were significantly upregulated only under 50 mM and 75 mM NH_4^+ conditions (Fig. 2. 3A, Fig. S2.3, and Data Set S1). High DRP profile similarities between the 1mM/10mM and 50mM/75mM NH_4^+ comparisons were further evidenced by the results of Principal Component Analysis (PCA) (Fig. S2.4).

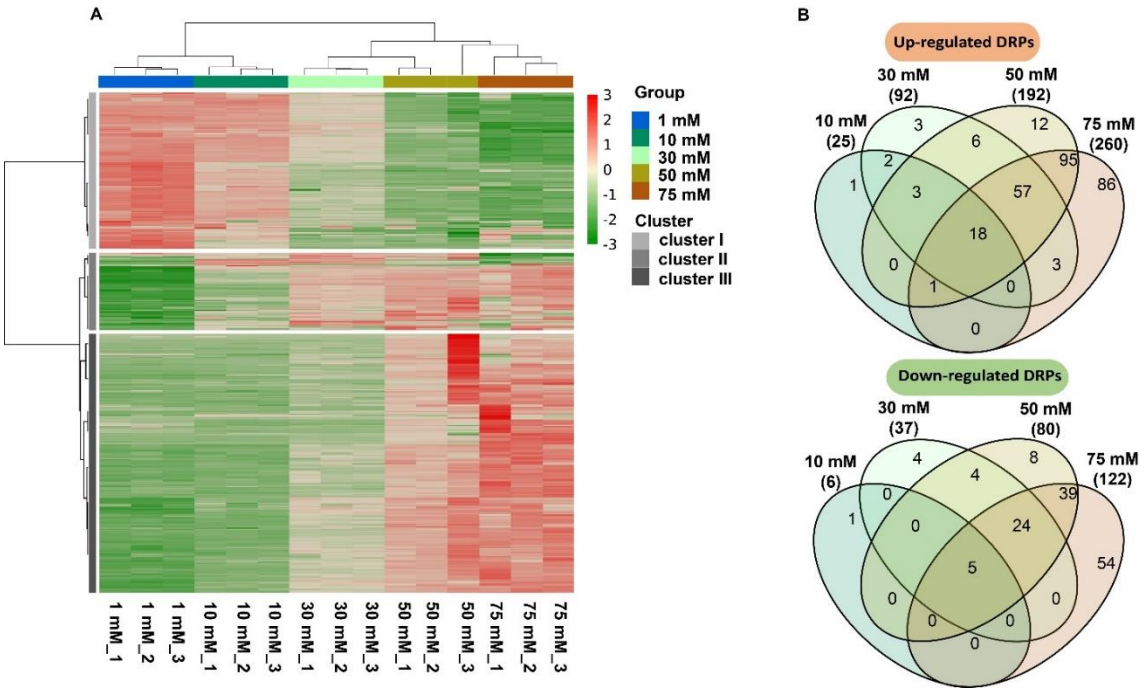

Fig. 2.3 Comparative analysis of the global label-free quantification (LFQ) proteomes. A. Heatmap showing the DRP pattern of each replicate culture in response to increasing NH_4^+ concentrations (1 mM, 10 mM, 30 mM, 50 mM, and 75 mM NH_4^+). Using Euclidean distances, the heatmap was built based on the LFQ intensities of 438 DRPs. Color scale indicates Z-score normalized LFQ intensity values. B. Venn diagram showing the overlap of up- and down-regulated DRPs among the five different NH_4^+ treatments. Further details can be found in Table S3.

A certain number of DRPs were co-regulated regardless of the initial NH_4^+ concentration. A total of 18 DRPs (10 mM NH_4^+), 57 DRPs (30 mM NH_4^+), and 95 DRPs (50 mM NH_4^+) were co-upregulated under 75 mM NH_4^+ condition (Fig. 2. 3B, Data Set S1). A similar pattern was observed for the downregulated DRPs, with 5 DRPs (10 mM NH_4^+), 24 DRPs (30 mM NH_4^+), and 39 DRPs (50 mM NH_4^+) being co-downregulated under 75 mM NH_4^+ condition (Fig. 2.3B, Data Set 1). A total of 86 and 54 DRPs were found to be significantly up- and down-regulated only under 75 mM NH_4^+ condition, respectively. This corresponds to more than 30 % (140/438) of total identified DRPs (Fig. 2.3B, Data Set S1). The number of DRPs showed a significant and positive relationship with the increase in NH_4^+ load, for both up- and down-regulated proteins (r^2 values of 0.99) (Fig. S2.5, and Data Set S2 at https://doi.org/10.6084/m9.figshare.20556600.v1).

2.3.4 Functional categorization of differentially regulated proteins

Among the 438 DRPs, functional information was available for 312 DRPs by their UniProt identifiers (Data Set S1). The remaining 126 DRPs were uncharacterized proteins based on UniProt. A survey of the 312 functionally predicted DRPs against the Kyoto Encyclopedia of Genes and Genomes (KEGG) database allowed us to annotate a total of 95 DRPs (Fig. S2.6 and Data Set S3 at https://doi.org/10.6084/m9.figshare.20556633.v1). A protein-protein interaction (PPI) network analysis revealed 121 proteins to be highly interactive (Fig. 2.4). These were partitioned into 10 functional modules including methane metabolism, nitrogen metabolism, stress response proteins, potassium transport, biosynthesis of amino acids, glutathione metabolism, transporters, porphyrin (cytochrome) metabolism, and DNA replication (Fig. 2.4). A selection of 43 DPRs is shown in Table 2.3, while information on the complete set of 121 proteins can be found in Data Set S4 at https://doi.org/10.6084/m9.figshare.20556651.v1. In addition to proteins related to glutathione metabolism and DNA replication, those involved in nitrogen metabolism were particularly enriched at high NH_4^+ concentrations (50 mM NH_4^+, q-value < 0.05; and 75 mM NH_4^+, p-value < 0.05) (Fig. S2.7). Nitrogen metabolism included proteins involved in NH_4^+ transport and assimilation, and in hydroxylamine detoxification (Table 2.3).

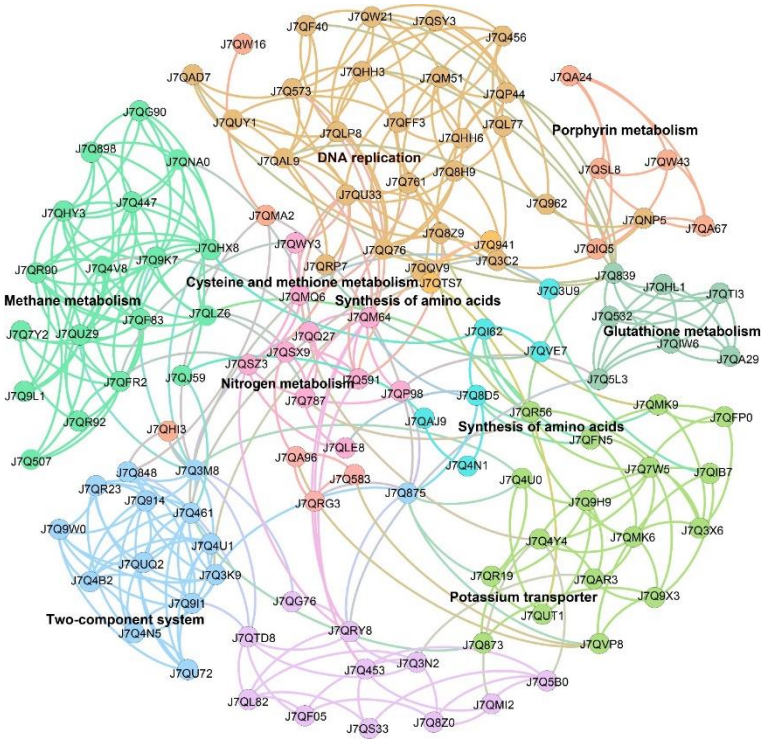

Fig. 2.4 Protein-protein interaction (Ludwig et al.) network of 121 DRPs that are connected by a total of 431 edges. The proteins were partitioned into 10 highly connected functional modules, which are highlighted by different color using the modularity class methods in Gephi. The functional categorization of the modules is based on KEGG level 3, except for general stress response and potassium transport. The size of nodes and edges is proportional to the number of connections (its degree). The protein identity of each node is indicated by the UniProt ID. The network edges indicate both functional and physical protein associations based on active interaction sources including Textming, Experiments, Databases, Co-expression, Neighborhood, Gene Fusion, and Co-occurrence. See Table S6 for details on the 121 DRPs used to construct the PPI network.

2.3.5 Amino acid profiling

Of the 16 amino acids detected, 15 amino acids showed a significant change in their intracellular concentrations across the five NH_4^+ treatments (see Data Set S5 at https://doi.org/10.6084/m9.figshare.20750203.v2). In particular, the intracellular concentration of glutamate significantly increased to 2438.69 μmol/g CDW under 50 mM NH_4^+ condition, but slightly decreased to 2020.59 μmol/g CDW under 75 mM NH_4^+ condition (Fig. 2.5, see also Data Set S5 at https://doi.org/10.6084/m9.figshare.20750203.v2). Glutamine also showed greatest intracellular accumulation at 50 mM NH_4^+, with 235.69 μmol/g CDW. Contrary to glutamate and glutamine, the intracellular concentration of proline significantly decreased from 1 mM to 50 mM NH_4^+, but showed a sharp and highly significant increase to 84.12 μmol/g CDW at 75 mM NH_4^+ (p-value≤0.001; Fig. 2.5, see also Data Set S5 at https://doi.org/10.6084/m9.figshare.20750203.v2). Concurrently, the intracellular concentration of ornithine was significantly increased and greatest (167.20 μmol/g CDW) at 75 mM NH_4^+ ($p \leq 0.001$) (Fig. 2.5, see also Data Set S5 at https://doi.org/10.6084/m9.figshare.20750203.v2). Arginine and lysine were also most enriched at 75 mM NH_4^+, with 1189.02 and 2004.68 μmol/g CDW respectively.

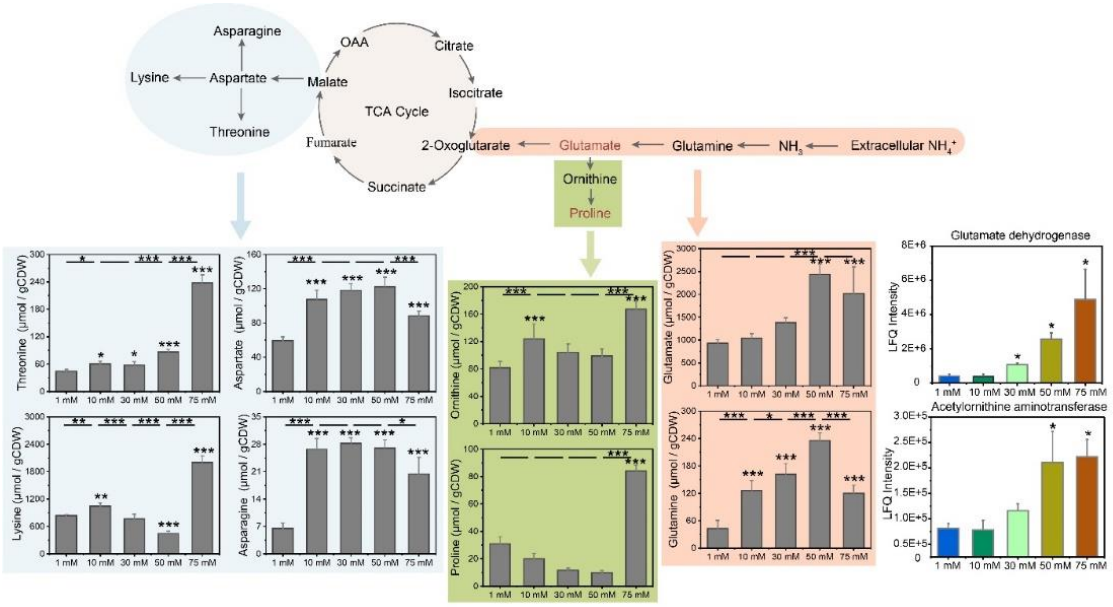

Fig. 2.5 Amino acids that show statistically significant change in their intracellular concentrations in response to increasing NH_4^+ levels. The association between particular pathway information (upper panel) and results of amino acid profiling (lower panel) is indicated by arrow and the same background color. Error bars indicate standard deviations of replicate cultures (n = 4). The lower panel asterisks (*) indicate significant difference (p-value ≤ 0.05) relative to the control treatment (1 mM NH_4^+). The upper panel asterisks (*) indicate significant difference between the stepwise increase in NH_4^+ load. Significant difference is calculated using one-way ANOVA Holm-Sidak method: *p-value ≤ 0.05; **p-value ≤ 0.01; ***p-value ≤ 0.001.

2.3.6 NO_2^- and N_2O production

Nitrite (NO_2^-) and nitrous oxide (N_2O) were detectable across all five NH_4^+ conditions (Fig. 2.6, Fig. S2.8). The production of NO_2^- significantly increased from 1mM NH_4^+ to 50 mM NH_4^+, but did not further increase at 75 mM NH_4^+. The maximum concentrations of NO_2^- that accumulated in the growth media during the incubation experiments were 4.44 μmol/L (1 mM NH_4^+), 16.99 μmol/L (10 mM NH_4^+), 23.19 μmol/L (30 mM NH_4^+), 59.95 μmol/L (50 mM NH_4^+), and 54.32 μmol/L (75 mM NH_4^+) (Fig. 2.6, Fig. S2.8, and Table S3 at https://doi.org/10.6084/m9.figshare.20559417.v1). The production of N_2O significantly increased from 1mM NH_4^+ to 75 mM NH_4^+. The maximum headspace concentrations of N_2O that accumulated during the incubation experiments were 0.65 μmol/L (10 mM NH_4^+), 1.85 μmol/L (30 mM NH_4^+), 4.93 μmol/L (50 mM NH_4^+), and 5.84 μmol/L (75 mM NH_4^+) (Fig. 2.6, Fig. S2.8, and Table S4 at https://doi.org/10.6084/m9.figshare.20589000.v1).

At high (50 mM, 75 mM) NH_4^+ levels, NO_2^- production rate was highly correlated with greatest SC2 growth activity. Compared to NO_2^- production, the accumulation of N_2O was time-shifted. Strong N_2O accumulation occurred only after NO_2^- had nearly reached its peak concentration (Fig. 2.6, Fig. S2.8).

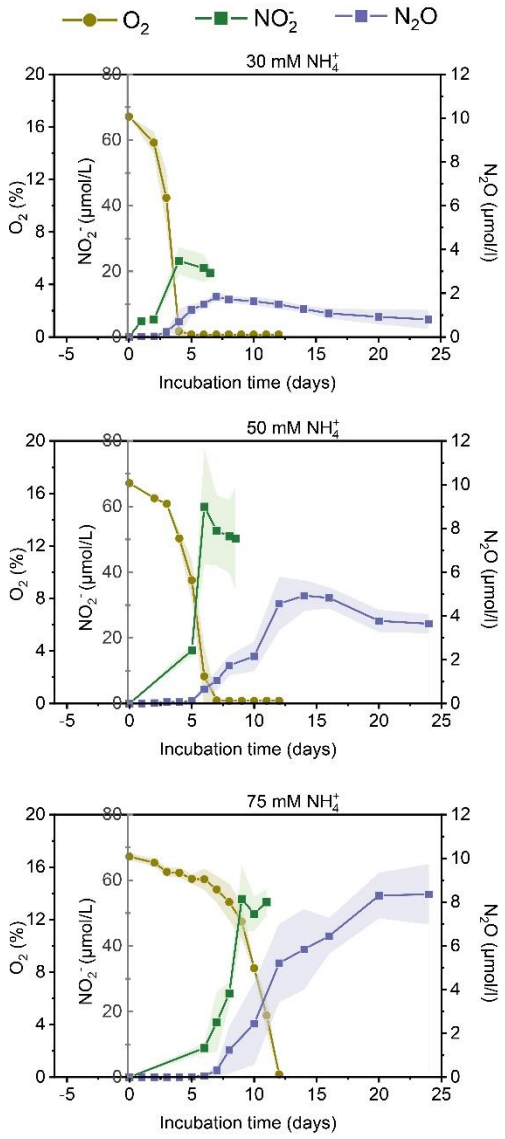

Fig.2.6 NO_2^- and N_2O production by Methylocystis sp. strain SC2 during exposure to 30 mM, 50 mM, and 75 mM NH_4^+. The stained areas indicate the standard deviations of triplicate cultures. The amounts of NO_2^- and N_2O produced during growth with 1 mM and 10 mM NH_4^+ were negligible (see Fig. S8 at https://doi.org/10.6084/m9.figshare.20750236.v3, Table S3 at https://doi.org/10.6084/m9.figshare.20559417.v1, and Table S4 at https://doi.org/10.6084/m9.figshare.20589000.v1). While we measured the accumulation of

N_2O in the gaseous headspace, it needs to be noted that N_2O is soluble in water in a ratio of 1:0.567 at 25 °C (Johnstone, 2007).

2.4 Discussion

In this study, we combined growth experiments with global proteomics, amino-acid profiling, and NOx measurements to thoroughly assess the response of *Methylocystis* sp. strain SC2 to increasing NH_4^+ concentrations. The ionic medium strength to which strain SC2 is able to acclimatize differs between NH_4Cl and NaCl as stressor. It is lower for NH_4Cl (between 114 and 139 mM; this study) than for NaCl (between 153 and 197 mM;**(Han et al., 2017)**). This may be due to the dual effect of increasing NH_4^+ load, with one being a general stress phenomenon and another being the specific inhibition effect of ammonia on methanotrophic activity. Firstly, NH_4Cl acted as an ionic and osmotic stressor, thereby leading to a tremendously increased lag phase duration with increasing NH_4^+ load. Lag phase represents the earliest stage of the bacterial growth cycle and is defined by the adjustment of metabolic fluxes and enzyme composition to given environmental conditions **(Valdez-Cruz et al., 2011; Zhang et al., 2018)**. The need for cellular adjustment processes directly depends on the level of environmental stress exposure. This view is congruous with our finding that the total number of differentially regulated proteins showed a highly positive and significant correlation with both lag phase duration and NH_4^+ load. Secondly, CH_4 consumption rate and, in consequence, growth rate significantly decreased with increasing NH_4^+ load due to the competitive inhibition of pMMO and the increasing need for detoxifying hydroxylamine, the product of pMMO-catalyzed oxidation of NH_3. Notably, all three subunits of low-affinity pMMO1 were differentially regulated neither in response to increasing NH_4^+ load nor to high NaCl stress, regardless of whether the study was done on transcriptome (Dam et al., 2014; Han et al., 2017) or proteome level (this study and (Hakobyan et al., 2018)). In the following, we firstly discuss the general stress response to increasing ionic and osmotic stress. At second we discuss the methanotroph-specific response to hydroxylamine stress.

2.4.1 General stress response to increasing ionic and osmotic stress

The cellular adjustment processes in response to increasing ionic and osmotic stress are defined by proteomic rearrangements that are widely conserved among bacteria (Lucht and Bremer, 1994; Kohlstedt et al., 2014; Bremer and Krämer, 2019). These involve the upregulation of stress-responsive proteins, K^+ "salt in" strategy, uptake and/or synthesis of compatible solutes, and induction of the glutathione metabolism pathway. The stress-

responsive proteins upregulated in response to high NH_4^+ load were the DNA-binding protein (Dps), the general stress response protein (CsbD), and heat-shock proteins. Dps has a significant role in protecting the chromosome from oxidative damage, but also from UV radiation, iron toxicity, heat, and pH stress (Nair and Finkel, 2004). The protective stress-responsive function of CsbD family proteins is not yet known (Lin et al., 2019). While the expression of various heat-shock proteins (e.g., Hsp10, [GroES], Hsp60 [GroEL], Hsp70 [DnaK], Hsp100 [ClpB]) at high constitutive level was not affected by NH_4^+, Hsp20 proteins were significantly enriched in response to high NH_4^+ load. The Hsp20 machinery prevents aggregation and misfolding of client proteins and is known to be expressed upon exposure to a stressor (Liberek et al., 2008; Bepperling et al., 2012; Yer et al., 2018).

In principle, two cellular strategies have evolved to cope with elevated osmolarity. The "salt in" strategy leads to a rapid increase in the intracellular K^+ pool followed by a concomitant increase in the cytoplasmic concentration of compounds that are compatible with cell physiology at high internal concentrations. Uptake and/or synthesis of these compatible solutes or osmoprotectants is defined as secondary response (Bremer and Kramer, 2019). Indeed, we observed a significant increase in the high-affinity (Kdp) K^+ transport system under high (75 mM) NH_4^+ load (Table 2.3). Concomitantly, global proteomics coupled with amino acids profiling revealed an intracellular glutamate pool that was significantly increased at high (50 mM and 75 mM) NH_4^+ levels (Fig. 2.5, Table 2.3). High glutamate concentrations are known to be required in a balanced osmoregulation to maintain a steady-state K^+ pool (Lucht and Bremer, 1994; Yan et al., 1996).

At 75 mM NH_4^+ load, glutamate was replaced in part by proline to act as a compatible solute, again evidenced by global proteomics coupled to amino acids profiling. Acetylornithine aminotransferase, whose expression was significantly increased at high NH_4^+ load, converts ornithine to Δ^1-pyrroline-5-carboxylate followed by the reduction to proline; with glutamate being the precursor for ornithine synthesis (Fichman et al., 2015). Previous studies have shown that the cellular osmoadaptation gradually switches from potassium-glutamate as the dominant strategy at intermediate salinities to proline at higher salinities; with a 4- to 5-fold increase in intracellular proline content (Sleator and Hill, 2002; Saum and Müller, 2007; Bremer and Krämer, 2019). This is in the same range as we observed for the increase in intracellular proline content during the exposure of strain SC2 to high (75 mM) NH_4^+ load. Thus, the intracellular

accumulation of ornithine and proline under the maximum tolerable stress condition (75 mM NH_4^+) follows a widely distributed response pattern that is also known to occur in *E. coli* and *Bacillus subtilis* (Kempf and Bremer, 1998; Hoffmann et al., 2012; Kohlstedt et al., 2014).

The stress-triggered induction of the glutathione metabolism pathway involved a significant upregulation of both glutathione peroxidase (GPX) and glutathione S-transferase (GST) under high NH_4^+ load. These enzymes have been shown to be expressed when cells are exposed to oxidative stress and hyperosmotic shock conditions. In particular, their activity is involved in detoxifying reactive oxygen (ROS) and nitrogen (Ernst et al.) species such as, for example, metal bound NO•. The latter results in the formation of nitrosothiols (RSNO) and nitrosamines (RN_2O), which are regarded as nonradical RNS (Gupta et al., 2016). Notably, the expression of two GST isoforms (UniProt IDs J7QHL1 and J7Q532, Table 2.3) were specifically and significantly upregulated in response to increasing NH_4^+ load. Their increase in expression level may be induced by the increased production of both hydroxylamine (Spooren and Evelo, 1998) and RNS such as nitrite (Stein and Klotz, 2011a; Tharmalingam et al., 2017).

Intriguingly, we also observed a differential regulation of various plasmid-encoded proteins, with most of them being upregulated (21 [pBSC2-1] and 18 [pBSC2-2]) (see Data Set S6 at https://doi.org/10.6084/m9.figshare.20750215.v2). On pBSC2-1, single-stranded DNA-binding protein (SSB), three-component CzcCBA complex, and subunits of the F_0F_1 ATPase complex were among the proteins significantly upregulated under high NH_4^+ load. SBB was the most greatly enriched (3.95-fold) plasmid-encoded protein during exposure of strain SC2 to 75 mM NH_4^+ (see Data Set S6 at https://doi.org/10.6084/m9.figshare.20750215.v2). It plays a major role in DNA replication, recombination and repair. On pBSC2-2, multicopper oxidases and the type IV secretion system (T4SS) were among the proteins most significantly upregulated under high NH_4^+ load, with the latter having functions in conjugation, DNA exchange with the extracellular space, and delivery of proteins to target cells (Wallden et al., 2010). Significant enrichment of the pBSC2-2-encoded T4SS may be linked to the differential regulation of a PmoC subunit uniquely encoded by pBSC2-2. Moderately expressed under standard (1 and 10 mM) NH_4^+ growth conditions, this PmoC subunit showed the greatest downregulation (-4.8-fold) among all differentially regulated proteins in response to high NH_4^+ load (Table 2.3), thereby providing further evidence for a particular cross

talk between the SC2 chromosome and the two plasmids. Another major functional aspect is the location of various nitrogen-cycling genes on pBSC2-2 (discussed below).

More detailed information on the differential regulation of plasmid-encoded proteins in response to high NH_4^+ load, but also on stress-responsive proteins, K^+ "salt-in" strategy, NH_4^+ assimilation and glutamate/glutamine metabolism, and glutathione metabolism, can be found Text S2.

2.4.2 Methanotroph-specific response to hydroxylamine stress

The apparent K_m value for CH_4 oxidation significantly increased with increasing NH_4^+ load (Table 2.2), which is due to the increasing inhibition of pMMO-based CH_4 oxidation by NH_3. This inhibition effect was evident for 30 mM and 50 mM NH_4^+ but most obvious for the CH_4 consumption rate at 75 mM NH_4^+ (Fig. 2.2, Table 2.2). Unfortunately, the $K_{m(app)}$ value could not be experimentally determined for the SC2 exposure to 75 mM NH_4^+ due to methodological constraints (Table 2.2). In addition, one may speculate that the increase in ionic and osmotic stress not only led to a prolonged duration of proteome adjustment, but also had adverse effects on the CH_4 oxidation activity of strain SC2.

Hydroxylamine is a highly toxic compound that has been shown to severely inhibit both the calcium- and lanthanide-dependent methanol dehydrogenases (MDHs) (Duine and Frank, 1980; Versantvoort et al., 2020). This necessitates a rapid turnover of hydroxylamine in methanotrophic bacteria, which is most likely ensured by the activity of methanotrophic hydroxylamine oxidoreductase (mHAO). In strain SC2, both mHAO subunits (mHaoAB) showed a strong significant upregulation concomitantly to the increase in NH_4^+ load (Table 2.3). This finding corroborates the conclusions lately drawn for the functional role of mHAO in the verrucomicrobial methanotroph Methyloacidiphilum fumariolicum and other aerobic methanotrophs, namely that mHAO plays a crucial role in preventing the inhibition of MDH (Versantvoort et al., 2020). All subunits of the calcium-dependent Mxa-MDH (MxaFJGIRSACKLDH) were detectable in the SC2 proteome, with seven Mxa-MDH subunits (MxaFJCKLDH) being the only CH_4 oxidation pathway proteins significantly enriched at high (75 mM NH_4^+) load. The Mxa-MDH-associated cytochrome c_L (MxaG) was highly expressed constitutively. It is reasonable to assume that the significant enrichment of these seven Mxa-MDH subunits (including MxaF) is a proteomic response to compensate for the inhibitory effect of

hydroxylamine. By contrast the expression response of Xox-MDH varied, with XoxF being significantly downregulated at 30 and 50 mM NH_4^+ load (Table 2.3).

We observed a significant correspondence between the increase in NH_4^+ load and the accumulation of NO_2^- and, with delay, N_2O (Fig. 2.6). This accumulation pattern has already been observed for a few proteobacterial methanotrophs in previous research, with the presumption that NO_2^- is the final product of mHAO activity (Campbell et al., 2011; Kits et al., 2015; He et al., 2017; Mohammadi et al., 2017). However, recent purification of the mHAO from the verrucomicrobial methanotroph Methylacidiphilum fumariolicum provided biochemical evidence that rather than to NO_2^-, this enzyme rapidly oxidizes hydroxylamine to NO. Conserved structural elements among all known mHAOs led to the further conclusion that this reaction mechanism occurs in all aerobic methanotrophs (Versantvoort et al., 2020). Given that NO is an obligate free intermediate, one has to postulate either an yet unknown NO-oxidizing enzyme that converts NO to NO_2^- or the spontanenous reaction with O_2 to form NO_2^- (Gupta et al., 2016; Moller et al., 2019; Versantvoort et al., 2020). Significant production of N_2O only occurred after the oxygen concentration had dropped to low or unmeasurable levels (Fig. 2.6). This is in good agreement with previous reports that detoxification of hydroxylamine is directed towards increased production of N_2O at hypoxic conditions (Hoefman et al., 2014; Kits et al., 2015). Notably, the production of N_2O from NO in strain SC2 does not involve the prior reduction of NO_2^- to NO, because neither nirK nor nirS is encoded by its genome. This supports the authors' (Versantvoort et al., 2020) conclusion that NO is the end product of mHAO activity.

Candidate enzymes for the reduction of NO to N_2O are a putative NO reductase (NorB) and hybrid cluster proteins (Hcps). NorB is encoded on pBSC2-2 but was not detectable in the SC2 proteome. Previous transcriptome research had however shown that relative to 10 mM NH_4^+, the transcript expression of the plasmid-borne norB had significantly increased after 10-hour exposure of SC2 cells to 30 mM NH_4^+ (Dam et al., 2014). The inability to detect NorB in the SC2 proteome may be due to a large number of transmembrane domains, which makes it difficult to efficiently solubilize and digest NorB during the extraction of cellular proteins (Simon and Klotz, 2013). The chromosome-endoced Hcp (UniProt ID J7Q787) is one of the most highly expressed proteins in strain SC2 and significantly upregulated in response to increasing NH_4^+ levels (Table 2.3). Over the last decades, four different activities have been reported for Hcps

(Hagen, 2022). Among these is the activity as hydroxylamine reductase, which would lead to the production of NH_4^+/NH_3 and thereby directly contribute to the detoxification of hydroxylamine. Being historically the first activity proposed (Hagen, 2022), more recent research however suggests that the activity as hydroxylamine reductase has little or no physiological relevance. More likely is the conversion of NO to N_2O (NO reductase activity), which has been established as physiologically relevant (Hagen, 2022).

Notably, the pBSC2-2-encoded nitrous oxide reductase (NosZ) is constitutively expressed at high level (see Data Set S6 at https://doi.org/10.6084/m9.figshare.20750215.v2), thereby suggesting that N_2O may be further reduced to N_2. The nos operon is located on a 20-kb region of pBSC2-2, which also contains the genes encoding NorB and two Hcp proteins (Fig. S2.9). This proximity of nitrogen-cycling genes (norB, nosZ), but also involving those encoding Hcps, further substantiates the functional relevance of pBSC2-2 for strain SC2. One of the two Hcps (UniProt ID I4EBE8) was also significantly enriched in response to increasing NH_4^+ load, but its overall expression level was 1000-fold lower than that of the chromosome-encoded Hcp protein (Table 2.3).

2.5 Concluding remarks

In this study, we comprehensively assessed the cellular ability of *Methylocystis* to acclimatize to high NH_4^+ load. Our results provide detailed insights into how *Methylocystis* spp. adjust their cells to cope with the dual effect of NH_4^+, namely ionic and osmotic stress and competitive interaction between CH_4 and NH_3 (Fig. 2.7). Indeed, our results show that *Methylocystis* has the capacity to precisely acclimatize to changes in NH_4^+ concentration by exact physiological rebalancing enzymes and osmolyte composition, thereby enabling maintenance of a suitable cellular homeostasis for growth. The maximum NH_4^+ tolerance of *Methylocystis* sp. strain SC2 (75 mM NH_4^+) was in the same range as previously shown for *Methylosinus sporium* (71 mM NH_4^+) (He et al., 2017). The need to simultaneously combat both ionic-osmotic stress and the toxic effects of hydroxylamine and nitrite is presumably the limiting factor for the cellular acclimatization of *Methylocystis* spp. to higher NH_4^+ concentrations (Fig. 2.7).

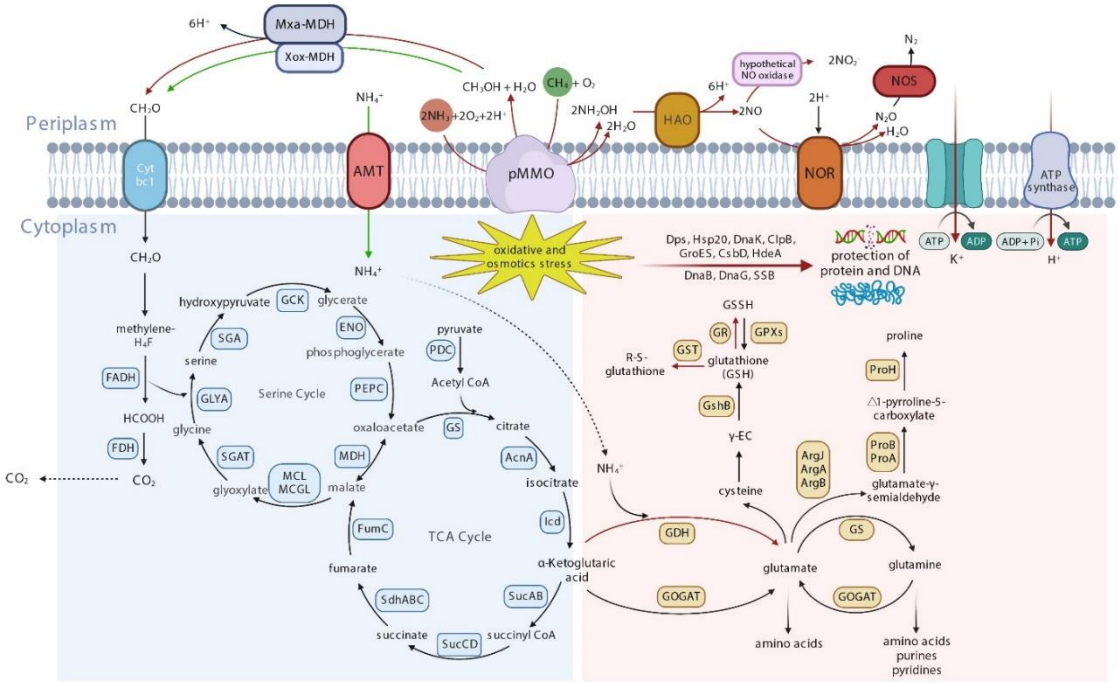

Fig. 2.7 Scheme of the metabolic pathways and processes proposed to be involved in the acclimatization of *Methylocystis* sp. strain SC2 to high NH_4^+ load. Proteins (enzymatic steps) and pathways that were significantly up- and down-regulated are marked with red and green arrows respectively. Black arrows indicate proteins (enzymatic steps) detectable in the proteome across all five NH_4^+ treatments, but not

differentially regulated. The response of strain SC2 to high (50 mM and 75 mM) NH_4^+ load involved K^+ influx ("salt-in" strategy) coupled to glutamate accumulation, in addition to increased production of various stress-responsive proteins. The intracellular accumulation of glutamate was achieved by high expression level of glutamine synthetase and glutamate synthetase (GS-GOGAT) and significantly induced activity of glutamate dehydrogenase (GDH), which furtherly fueled the biosynthesis of proline and other amino acids. Concomitantly, synthesis of the ammonium transporter (Amt) and nitrogen regulatory protein P-II was significantly downregulated. After initiation of growth, competitive interaction between CH_4 and NH_3 led to a significant increase in both $K_{m(app)}$ value for CH_4 oxidation and production of toxic hydroxylamine. Its detoxification involved the production and accumulation of nitrite (NO_2^-) and nitrous oxide (N_2O) under high NH_4^+ load, with NO as a putative intermediate (Versantvoort et al., 2020). In addition, intermediates of reactive nitrogen species (Ernst et al.) may have triggered antioxidant response involving the conversion of glutathione (GSH) into glutathione disulfide (GSSG) via the activity of glutathione peroxidase (GPX) and glutathione S-transferase (GST).

2.6 Materials and methods

Strain. The genome of *Methylocystis* sp. strain SC2 was found to comprise a 3.77 Mb chromosome and two large plasmids (Dam et al., 2012a; Dam et al., 2012b). Their nucleotide sequences are publicly available in EMBL, GenBank, and DDBJ databases under the accession numbers HE956757 (chromosome), FO000001, and FO000002 (plasmids). Genomic analysis revealed the presence of a complete denitrification pathway in strain SC2 (Dam et al., 2013). Strain SC2 has the ability to produce low- and high-affinity pMMO isozymes and can thus oxidize CH_4 across a wide concentration range (Ricke et al., 2004; Baani and Liesack, 2008). The low-affinity pMMO1 is encoded by two *pmoCAB1* gene clusters, while the high-affinity pMMO2 is encoded by a single *pmoCAB2* gene cluster (Dam et al., 2012c). In addition, the genome of strain SC2 encodes two chromosome-encoded monocistronic *pmoC* genes ($pmoC1_{Gs}$, $pmoC2_{Gs}$) and a single plasmid-borne *pmoC* gene ($pmoC_{Ps}$) (Dam et al., 2012b).

Experimental procedures. Strain SC2 cells were firstly inoculated into 40 ml nitrate-containing mineral salts medium (NMS) in 120-ml serum bottles and grown to an optical density

at 600 nm (OD_{600}) of 0.25 ± 0.05 (Fig. 2.1). The composition of NMS growth medium was the same as previously reported (Heyer et al., 2002), containing 1 gram of KNO_3 per liter as the nitrogen source. Strain SC2 was pre-cultured in NMS medium at least twice and then used to investigate the effect of increasing ammonium concentrations in mineral salts (AMS) medium on its cell density, CH_4 consumption, and CO_2 production. A 1-ml aliquot of NMS pre-cultured SC2 cells was inoculated into 120-ml serum bottles containing 40 ml AMS medium. The initial OD_{600} was 0.01 ± 0.003. The composition of AMS was the same as NMS, with the exception that 1 gram of KNO_3 (10 mM) was replaced by increasing amounts of NH_4Cl. This resulted in treatment concentrations of 1, 10, 30, 50, 75, and 100 mM NH_4Cl in the medium (Fig. 2.1), corresponding to a total ionic strength ranging from 40 mM (1 mM NH_4Cl) to 139 mM (100 mM NH_4Cl) (Table S2). The headspace of the batch cultures was filled with 0.20-μm filter-sterilized CH_4 and air in a 20:80 (v/v) ratio. The serum bottles were sealed with rubber stoppers and incubated on a rotary shaker at 130 rpm and 25 °C. Both OD_{600} and changes in the headspace concentrations of CH_4 and CO_2 were regularly monitored during the whole incubation period (Fig. 2.1).

Physiological parameters. The OD_{600} was determined using an Eppendorf Biophotometer UV/Vis spectrophotometer (Eppendorf, Germany). Cell dry weight (CDW) was calculated based on the following relationship: biomass (g CDW) = OD_{600} × 0.261 × volume (Hakobyan et al., 2020). Biomass yield is shown as mg CDW / mmol CH_4. Methane consumption and CO_2 production were analyzed by gas chromatography (SRI Instruments, Earl St. Torrance, CA). Methane consumption rate is indicated as mmol CH_4 consumed / g CDW / day. All rate calculations are based on parameter values measured during exponential growth. The production of N_2O was monitored using a N_2O microsensor with piercing-needle. The microsensor was connected to the Microsensor Multimeter (Unisens A/S, Denmark). The O_2 concentration in the headspace was monitored with a Fibox 4 trace meter using SP-PSt3 sensor spots. This yielded an oxygen detection limit as low as 0.002 vol % (PreSens; https://www.presens.de/). The production of NO_2^- was determined using the Griess Reagent System following the manufacturer`s instruction (Promega Corporation, Madison, WI).

Methane oxidation kinetics [$K_{m(app)}$ and $V_{max(app)}$] calculations. To test for the inhibitory effect of NH_4^+/NH_3 on CH_4 oxidation, SC2 cells were grown at the following CH_4:air mixing ratios: 20:80, 15:85, 10:90, 5:95, and 2.5:97.5 (v/v). Each CH_4:air mixing

ratio was tested in triplicate incubation under three different ammonium concentrations (10 mM, 30 mM, and 50 mM NH_4^+). Cell density (OD_{600}) and CH_4 concentration in the headspace were regularly measured over the whole incubation period. Cell density were converted into cell numbers as described previously (Baani and Liesack, 2008). An OD_{600} value of 1 corresponds to about 1.5×10^8 cells ml^{-1} in the exponential growth phase. The exponential decrease of CH_4 over incubation time was used to estimate $K_{m(app)}$ and $V_{max(app)}$ of SC2 cultures using nonlinear regression to the Michaelis–Menten equation. Multiplication by the Oswald constant (0.03395 at 25 °C) gave the $K_{m(app)}$ as the methane concentration in water (Baani and Liesack, 2008; Brindha and Vasudevan, 2018).

Sample preparation for proteomics. Samples for proteomics were collected from the same cultures. Strain SC2 was inoculated into 300 ml mineral salts medium (initial OD_{600} of 0.01 ± 0.003) supplemented with 1, 10, 30, 50, or 75 mM NH_4^+ (Fig. 2.1). Cells were grown to the mid-exponential phase (OD_{600} = 0.25 ± 0.02) and then collected by centrifugation at 7000 × *g* and 4 °C for 20 min. The cells were thoroughly washed twice with 1 × phosphate buffer (5.4 g $Na_2HPO_4 \times 7\ H_2O$ and 2.6 g KH_2PO_4 per liter distilled H_2O) to remove medium traces. The washed cell pellets were transferred to 2 ml sterile safe-lock microcentrifuge tubes (Eppendorf) and stored at -80 °C for subsequent protein extraction. Each NH_4^+ concentration involved the analysis of triplicate cultures.

Protein extraction, LC-MS/MS analyses, peptide/protein identification, and LFQ quantification. The extraction of total SC2 proteins was done as described previously, using an efficient tandem LysC/trypsin digestion in detergent condition (Hakobyan et al., 2018). The LC-MS/MS analysis of protein digests was performed on a Q-Exactive Plus mass spectrometer connected to an electrospray ion source (Thermo Fisher Scientific). Peptide separation was carried out using the Ultimate 3000 nanoLC-system (Thermo Fisher Scientific) equipped with an in-house packed C18 resin column (Magic C18 AQ 2.4 μm, Dr. Maisch). The peptides were first loaded onto a C18 precolumn (preconcentration set-up) and then eluted in backflush mode using a gradient from 96% solvent A (0.15% formic acid) and 4% solvent B (99.85% acetonitrile, 0.15% formic acid) to 30% solvent B over 115 min. The flow rate was set to 300 nL/min. The data acquisition mode for the initial LFQ study was set to obtain one high-resolution MS scan at a resolution of 60,000 (m/z 200) with a scanning range from 375 to 1500 m/z followed by MS/MS scans of the 10 most intense ions. To increase the efficiency of MS/MS acquisition, the charged state screening modus was activated to exclude unassigned and singly charged ions. The dynamic exclusion duration was set to 30 s. The

ion accumulation time was set to 50 ms (both MS and MS/MS). The automatic gain control (AGC) was set to 3×10^6 for MS survey scans and 1×10^5 for MS/MS scans (for details see (Hakobyan et al., 2018)).

Statistical and functional analysis of differentially regulated proteins. Discovery-LFQ was done using Progenesis QI software (Nonlinear Dynamics, version 2.0) as described before (for details see (Hakobyan et al., 2018)). Next, the data obtained from Progenesis were evaluated using SafeQuant R package, version 2.2.2 (Glatter et al., 2012). Hereby, a 1% identification and quantification false discovery rate (FDR) was calculated. Differentially regulated proteins (DRPs) with $\log_2$-fold change ≥ 1 (upregulated) or ≤ -1 (downregulated), *q*-value ≤ 0.01 were submitted to the Kyoto Encyclopedia of Genes and Genomes (KEGG) database for enrichment function analysis.

Sampling and extraction of intracellular metabolites. SC2 cells were grown to mid-exponential phase in 120-ml serum bottles containing 40 mL mineral salt medium supplemented with 1 mM, 10 mM, 30 mM, 50 mM, amd 75 mM NH_4^+ (Fig. 2.1). Aliquots (36 mL) of 60% methanol (v/v) in a 50-mL conical centrifuge tube were cooled down to −80 °C for 48 h and then used as quenching solution. Twelve-mL culture aliquots (n=4) were pipetted into the quenching solution and the quenched cells were immediately pelleted in an Eppendorf 5430R centrifuge for 10 min at 10,000 × *g* and −10 °C, using a fixed angel rotor. After centrifugation, the supernantant was removed, and the cell pellets were stored at −80 °C until further extraction of the endometabolome.

The endometabolome was extracted by suspending the frozen cell pellets in equal volumes of extraction fluid (−20 °C) and chloroform (−20 °C). The extraction volume was adapted to sample biomass, using 1 ml of extraction fluid and an equal volume of chloroform per 1 ml of sample of $OD_{600} = 1$. The extraction fluid consisted of 50% (v/v) methanol at LCMS grade and 50% (v/v) TE-buffer (10 mM TRIZMA, 1 mM EDTA). The resulting cell suspension was incubated in a ThermoMixer C shaker (Eppendorf) at 4 °C for 2 h (1500 rpm), followed by a two-phase separation of the suspension in an Eppendorf 5430R centrifuge for 10 min at 12,000 × *g* and −10 °C, using a fixed angel rotor. The upper phase was filtered through a 0.20-µm PTFE membrane filter (Phenomenex) into 2 ml sterile safelock microcentrifuge tubes (Eppendorf). The metabolite extracts were stored at −80 °C until downstream analysis.

Measurement of amino acids. Quantitative determination of amino acids was performed using LC-MS/MS. The chromatographic separation was performed on an Agilent Infinity II 1260 HPLC system using a ZicHILIC SeQuant column (150 × 2.1 mm, 3.5 µm particle size, 100 Å pore size) connected to a ZicHILIC guard column (20 × 2.1 mm, 5 µm particle size) (Merck KgAA), with a constant flow rate of 0.3 ml/min with mobile phase A being 0.1 % formic acid in 99:1 water:acetonitrile (Honeywell, Morristown, New Jersey, USA) and phase B being 0.1 % formic acid in 99:1 water:acetonitrile (Honeywell, Morristown, New Jersey, USA) at 25° C.

The injection volume was 1 µl. The mobile phase profile consisted of the following steps and linear gradients: 0 – 8 min from 80 to 60 % B; 8 – 10 min from 60 to 10 % B; 10 – 12 min constant at 10 % B; 12 – 12.1 min from 10 to 80 % B; 12.1 to 14 min constant at 80 % B. An Agilent 6470 mass spectrometer was used in positive mode with an electrospray ionization source and the following conditions: ESI spray voltage 4500 V, nozzle voltage 1500 V, sheath gas 400°C at 12 l/min, nebulizer pressure 30 psig, and drying gas 250 °C at 11 l/min. Compounds were identified based on their mass transition and retention time compared to standards. Chromatograms were integrated using MassHunter software (Agilent, Santa Clara, CA, USA). Absolute concentrations were calculated based on an external calibration curve prepared in sample matrix.

Computational analysis. Hierarchical heatmap analysis was performed on Z-score normalized LFQ intensities of the total of 438 DRPs. Creation of both hierarchical heatmap and Venn diagram, but also conduct of the principal component analysis (PCA), were done using the free online platform for data analysis and visualization available at http://www.bioinformatics.com.cn/. The Volcano plots were created using VolcaNoseR (Goedhart and Luijsterburg, 2020). The STRING database was used to construct the protein-protein interaction (PPI) network based on the Uniprot IDs of total DRPs, thereby resulting in automated calculation of edges and nodes using the default value for the minimum interaction score (0.4). Gephi (version 0.9.2), an open-source software, was used for modularity calculation and visualization (Bastian et al., 2009). Nodes with no or less than four edges were omitted, thereby resulting in a PPI network of 121 nodes (proteins) that are connected by a total of 431 edges. The final presentation layout of the PPI network was created with Fruchterman Reingold, a method implemented in Gephi.

Software used for preparation of figures and graphs. Figures and graphs were created with (i) Sigmaplot version 14.0; (ii) OriginPro 2020; (iii) GraphPad Prism 9.0.2 (iv) commercial software TIBCO Spotfire; and (v) and Adobe Illustrator 2020.

Raw Files and Associated Data Deposition.

Various supplemental figures (S1 - S9), tables (S3, S4), and data sets (S2 – S6) are available at https://figshare.com/projects/Methylocystis_sp_Strain_SC2_Acclimatizes_to_Increasing_NH4_Levels_by_a_Precise_Rebalancing_of_Enzymes_and_Osmolyte_Composition_-_supplementary_files/147147. The mass spectrometry proteomics data have been deposited with the ProteomeXchange Consortium via the PRIDE (Vizcaino et al., 2016) partner repository with the dataset identifier PXD032347.

2.7 Acknowledgments

The authors are grateful to Peter Klaus and Jörg Kahnt for technical support. Kangli Guo receives a PhD stipend from the Chinese Scholarship Council (CSC) and is a member of the International Max Planck Research School for Environmental, Cellular, and Molecular Microbiology (IMPRS-Mic). The research was supported in part by the Deutsche Forschungsgemeinschaft (DFG) through Collaborative Research Center SFB987 and the Max Planck Society. Prof. Dr. Andreas Brune is acknowledged for providing Unisense Multimeter instrument to conduct N_2O measurements.

We declare that we have no competing interests.

Table 2.3 Differentially regulated proteins involved in the proten-protein interaction (PPI) network[1]

Function category	Uniprot	Gene	Protein Description	Median Value					log_2ratio_Value[2]				*q*Value[2]			
				1mM	10mM	30mM	50mM	75mM	10mM	30mM	50mM	75mM	10mM	30mM	50mM	75mM
Methane metabolism																
Methane oxidation	J7QM98	*pmoC1*	Particulate methane monooxygenase (PmoC1)	1.83E+08	2.04E+08	2.30E+08	2.62E+08	2.61E+08	0.163	0.334	0.519	0.515	0.072	0.001	0.001	0.001
	Q70EF3	*pmoA1*	Particulate methane monooxygenase (PmoA1)	3.10E+08	3.51E+08	3.85E+08	4.26E+08	4.44E+08	0.178	0.311	0.456	0.516	0.036	0.001	0.001	0.003
	Q70EF2	*pmoB1*	Particulate methane monooxygenase (PmoB1)	1.41E+10	1.63E+10	1.98E+10	2.09E+10	2.11E+10	0.206	0.488	0.566	0.583	0.012	0.000	0.000	0.005
	Q6MZ16	*pmoB2*[3]	Particulate methane monooxygenase (PmoB2)	2.80E+06	2.71E+06	3.63E+06	2.76E+06	1.72E+06	-0.046	0.375	-0.024	-0.707	0.980	0.000	0.366	0.000
	J7QLZ6	$pmoC2_{Gs}$	Chromosome-encoded $PmoC2_{Gs}$	4.50E+05	8.10E+05	9.95E+05	1.67E+06	2.23E+06	0.848	**1.145**	**1.894**	**2.309**	0.036	0.005	0.001	0.000
	I4EB56[4]	$pmoC3_{Ps}$	Plasmid-borne $PmoC3_{Ps}$	5.76E+07	5.60E+07	2.07E+07	2.07E+06	2.57E+06	-0.040	-1.477	-4.800	-4.487	0.601	0.000	0.000	0.000
Methanol metabolism	J7Q447	*xoxF*	PQQ-dependent dehydrogenase, methanol/ethanol family	1.97E+08	1.43E+08	7.08E+07	9.45E+07	1.48E+08	-0.463	-1.473	-1.057	-0.409	0.001	0.000	0.003	0.064
	J7QNA0	*xoxG*	Putative cytochrome c protein	1.01E+07	8.33E+06	6.54E+06	5.32E+06	4.12E+06	-0.276	-0.624	-0.923	-1.290	0.182	0.001	0.002	0.002

J7Q898	*xoxJ*	Extracellular solute-binding protein family 3	9.69E+05	6.89E+05	4.60E+05	5.17E+05	8.72E+05	-0.492	-1.075	-0.907	-0.153	0.006	0.000	0.003	0.401
J7QHX8	*mxaF*	Methanol dehydrogenase MxaF	5.64E+09	6.84E+09	9.08E+09	1.04E+10	1.14E+10	0.279	0.688	0.879	**1.022**	0.003	0.000	0.000	0.000
J7Q9K7	*mxaJ*	Extracellular solute-binding protein family 3	2.87E+08	4.54E+08	6.79E+08	6.45E+08	7.15E+08	0.662	**1.242**	**1.170**	**1.318**	0.000	0.000	0.001	0.000
J7QR86	*mxaG*	Cytochrome c class I	2.64E+08	2.81E+08	2.75E+08	2.33E+08	2.25E+08	0.089	0.056	-0.183	-0.235	0.053	0.264	0.009	0.104
J7Q4V7	*mxaI*	Methanol dehydrogenase [cytochrome c] subunit 2	2.99E+08	3.54E+08	5.11E+08	5.75E+08	5.28E+08	0.246	0.774	0.945	0.820	0.087	0.001	0.000	0.001
J7QUZ4	*mxaR*	ATPase associated with various cellular activities AAA_3	3.76E+07	3.95E+07	4.51E+07	5.05E+07	5.83E+07	0.071	0.263	0.427	0.632	0.328	0.025	0.001	0.000
J7QHY1	*mxaS*	Uncharacterized protein	8.32E+05	7.81E+05	9.26E+05	1.19E+06	1.41E+06	-0.092	0.155	0.522	0.766	0.279	0.199	0.001	0.000
J7Q9K9	*mxaA*	MxaA protein, putative	6.81E+06	7.70E+06	9.41E+06	1.09E+07	1.30E+07	0.177	0.465	0.681	0.936	0.022	0.000	0.000	0.000
J7QR90	*mxaC*	von Willebrand factor type A	9.12E+05	1.09E+06	1.37E+06	1.55E+06	1.87E+06	0.261	0.586	0.764	**1.034**	0.003	0.000	0.000	0.000
J7Q4V8	*mxaK*	Uncharacterized protein	2.59E+06	2.91E+06	3.71E+06	4.60E+06	5.62E+06	0.167	0.519	0.829	**1.117**	0.799	0.019	0.003	0.000
J7QUZ9	*mxaL*	von Willebrand factor type A	9.13E+05	1.04E+06	1.36E+06	1.59E+06	2.07E+06	0.186	0.574	0.803	**1.183**	0.016	0.000	0.000	0.000
J7QHY3	*mxaD*	MxaD protein/polyketide cyclase/dehydrase	2.08E+08	2.44E+08	3.28E+08	4.14E+08	4.72E+08	0.235	0.660	0.995	**1.186**	0.008	0.000	0.000	0.000

	J7Q9L1	*mxaH*	Uncharacterized protein	1.20E+06	1.49E+06	2.17E+06	2.69E+06	3.41E+06	0.315	0.856	**1.168**	**1.511**	0.010	0.000	0.000	0.000
Stress response protein																
	J7QR19	*kdpC*	Potassium-transporting ATPase KdpC subunit	4.98E+06	4.25E+06	5.24E+06	7.86E+06	1.49E+07	-0.229	0.073	0.658	**1.583**	0.010	0.102	0.000	0.000
	J7Q4U0	*kdpB*	Potassium-transporting ATPase ATP-binding subunit	4.19E+06	4.26E+06	5.25E+06	8.35E+06	1.61E+07	0.023	0.326	0.994	**1.946**	0.998	0.000	0.000	0.000
Potassium transport	J7QUT1	*kdpA*	Potassium-transporting ATPase potassium-binding subunit	1.21E+06	1.07E+06	1.27E+06	1.78E+06	3.63E+06	-0.176	0.064	0.548	**1.579**	0.019	0.470	0.002	0.000
	J7Q9H9	*BN69_2486*	Osmosensitive K channel His kinase sensor	1.12E+05	1.46E+05	1.80E+05	3.19E+05	5.11E+05	0.393	0.691	**1.514**	**2.196**	0.061	0.005	0.000	0.000
	J7QQ02	*BN69_2097*	Stress response DNA-binding protein (Dps)	9.02E+06	8.97E+06	1.39E+07	5.04E+07	6.11E+07	-0.008	0.628	**2.483**	**2.759**	0.366	0.000	0.002	0.000
	J7QF27	*BN69_0580*	Heat shock protein Hsp20	5.17E+07	3.09E+07	6.47E+07	1.63E+08	2.52E+08	-0.744	0.323	**1.656**	**2.283**	0.000	0.002	0.001	0.000
	J7QJH1	*BN69_3580*	Heat shock protein Hsp20	1.03E+07	8.09E+06	6.06E+06	5.01E+06	6.47E+06	-0.344	-0.762	-1.035	-0.667	0.002	0.000	0.000	0.000
General stress-induced proteins	J7QM64	*htpG*	Chaperone protein HtpG	1.92E+08	1.50E+08	1.14E+08	9.54E+07	9.36E+07	-0.356	-0.744	-1.006	-1.033	0.001	0.000	0.000	0.000
	J7QPM2	*hdeA*	Probable acid stress chaperone HdeA	2.42E+07	3.26E+07	4.32E+07	5.79E+07	6.73E+07	0.428	0.834	**1.257**	**1.474**	0.007	0.000	0.000	0.000
	J7Q5H9	*BN69_3658*	Alcohol dehydrogenase GroES domain protein	1.20E+04	1.17E+04	1.72E+04	9.07E+04	4.12E+04	-0.035	0.521	**2.920**	**1.783**	0.883	0.651	0.028	0.114
	J7QV15	*BN69_2599*	CsbD family protein	9.87E+05	1.19E+06	1.43E+06	3.12E+06	1.00E+07	0.274	0.531	**1.659**	**3.342**	0.183	0.009	0.010	0.000

	J7QPM2	*hdeA*	Probable acid stress chaperone HdeA	2.42E+07	3.26E+07	4.32E+07	5.79E+07	6.73E+07	0.428	0.834	**1.257**	**1.474**	0.007	0.000	0.000	0.000
	J7QHI8	*BN69_2205*	Stress-induced protein	2.74E+05	3.18E+05	3.44E+05	2.20E+06	1.71E+06	0.212	0.327	**3.000**	**2.637**	0.189	0.024	0.001	0.000
	J7QSL3	*BN69_1574*	Glutathione peroxidase	2.47E+06	2.67E+06	3.86E+06	5.68E+06	7.39E+06	0.115	0.646	**1.202**	**1.582**	0.315	0.000	0.000	0.000
	J7QTI3	*BN69_1939*	Glutathione S-transferase, N-terminal domain	1.44E+05	1.73E+05	2.37E+05	5.12E+05	6.53E+05	0.260	0.716	**1.825**	**2.176**	0.082	0.010	0.002	0.000
	J7QHL1	*BN69_2280*	Glutathione S-transferase domain protein	1.82E+05	2.21E+05	2.05E+05	2.69E+05	4.66E+05	0.283	0.178	0.569	**1.361**	0.147	0.016	0.163	0.000
Glutathione metabolism	J7Q532	*BN69_2948*	Glutathione S-transferase domain protein	8.02E+04	1.13E+05	1.62E+05	1.78E+05	1.44E+05	0.495	**1.013**	**1.151**	0.842	0.045	0.003	0.002	0.003
	J7QIW6	*BN69_3230*	Glutathione S-transferase domain protein	3.56E+07	2.48E+07	1.67E+07	1.26E+07	1.02E+07	-0.522	-1.088	-1.501	-1.800	0.000	0.000	0.000	0.000
	J7QA29	*BN69_3006*	ChaC family protein	5.05E+05	6.39E+05	8.44E+05	9.33E+05	1.15E+06	0.339	0.740	0.886	**1.190**	0.007	0.000	0.000	0.000
	J7QQ61	*BN69_0634*	Glutamate/cysteine ligase	4.98E+07	4.86E+07	3.86E+07	2.96E+07	2.30E+07	-0.035	-0.366	-0.749	-1.117	0.495	0.000	0.000	0.000
	J7QVE2	*argD*	Acetylornithine aminotransferase	7.62E+04	8.88E+04	1.17E+05	1.81E+05	2.11E+05	0.220	0.623	**1.251**	**1.469**	0.775	0.009	0.002	0.000
Synthesis of amino acids/ compatible solutes	J7QHB7	*BN69_2040*	Glycine dehydrogenase (aminomethyl-transferring)	9.20E+05	6.17E+05	6.61E+05	1.52E+06	2.50E+06	-0.577	-0.478	0.725	**1.440**	0.005	0.003	0.005	0.002
	J7QPV5	*BN69_2037*	Aminomethyltransferase	4.52E+05	3.38E+05	3.23E+05	7.33E+05	1.12E+06	-0.418	-0.484	0.699	**1.311**	0.003	0.003	0.002	0.001

	J7Q4N1	*BN69_2223*	5-aminolevulinate synthase	2.82E+06	3.34E+06	7.16E+06	8.20E+06	9.09E+06	0.241	**1.341**	**1.537**	**1.685**	0.079	0.000	0.053	0.036
Nitrogen metabolism																
	J7QLT5	*BN69_0652*	Glutamine synthetase	1.65E+09	1.61E+09	1.61E+09	1.56E+09	1.57E+09	-0.039	-0.034	-0.082	-0.077	0.212	0.266	0.100	0.343
	J7QQX7	*BN69_0914*	Nitrogen regulatory protein P-II	4.89E+06	3.55E+06	2.47E+06	1.99E+06	2.38E+06	-0.464	-0.987	-1.295	-1.042	0.027	0.000	0.000	0.000
	J7QFK3	*BN69_0915*	Ammonium transporter	1.06E+06	5.86E+05	6.69E+05	4.75E+05	6.70E+05	-0.857	-0.664	-1.159	-0.663	0.050	0.010	0.002	0.015
Ammonium transport and assimilation	J7QFL3	*BN69_0930*	Nitrogen regulatory protein P-II	2.11E+06	9.85E+05	8.62E+05	7.17E+05	9.07E+05	-1.101	-1.292	-1.559	-1.220	0.000	0.000	0.000	0.000
	J7QR56	*BN69_0999*	Glutamate dehydrogenase	4.30E+04	2.97E+04	1.14E+05	2.78E+05	4.04E+05	-0.534	**1.406**	**2.693**	**3.231**	0.689	0.001	0.002	0.000
	J7QTS4	*BN69_3582*	Glutamate synthase [NADH], amyloplastic	1.71E+08	1.79E+08	1.80E+08	1.83E+08	1.93E+08	0.065	0.077	0.096	0.173	0.323	0.141	0.064	0.018
	J7QX35	*BN69_3584*	Glutamate synthase, NADH/NADPH, small subunit	7.65E+07	7.81E+07	7.73E+07	7.78E+07	8.57E+07	0.030	0.014	0.025	0.163	0.942	0.908	0.944	0.054
	J7Q787	*hcp*	Hybrid cluster protein	3.29E+08	8.67E+08	1.05E+09	1.12E+09	1.08E+09	**1.399**	**1.674**	**1.763**	**1.722**	0.000	0.000	0.000	0.000
	I4EBE8[ǂ]	*hcp*	Hybrid cluster protein	1.93E+05	5.50E+05	6.87E+05	7.27E+05	5.60E+05	**1.515**	**1.835**	**1.917**	**1.538**	0.001	0.000	0.000	0.001
Hydroxylamine detoxification	J7QAB0	*haoB*	Putative HaoB	1.78E+07	3.78E+07	4.71E+07	5.09E+07	5.55E+07	**1.086**	**1.404**	**1.516**	**1.638**	0.000	0.000	0.000	0.000
	J7QSX9	*haoA*	Hydroxylamine oxidase, HaoA	5.62E+06	1.76E+07	2.40E+07	3.01E+07	3.37E+07	**1.646**	**2.095**	**2.420**	**2.584**	0.000	0.000	0.000	0.000

[1] The complete list of the 121 PPI network proteins is shown in Data Set S4 at https://doi.org/10.6084/m9.figshare.20556651.v1. Significantly upregulated proteins are shown in bold, while significantly downregulated proteins are underlined. ǂ Proteins encoded by plasmid-borne genes.

[2] Both log_2ratio_Values and *q*Values are given in relation to the 1 mM treatment.

[3] Note that the LFQ values of PmoB2 were three to four orders of magnitude lower than those of PmoB1. The LFQ values of PmoC2 and PmoA2 were below detection limit arcoss all NH_4^+ treatments. Compared to PmoB, the lower LFQ values of PmoC and PmoA subunits, as observed for both pMMO isozymes (pMMO1, pMMO2), may be due the fact that PmoA and PmoC are integral membrane subunits; thereby resulting in low solubilization efficiency. By contrast, PmoB comprises two periplasmic domains connected by two transmembrane helices (Lieberman and Rosenzweig, 2005; Smith et al., 2011). A significant downregulation of *pmoCAB2* at the transcriptome level was observed after transfer of a batch of mid-log phase SC2 cells pregrown on 10 mM NMS (nitrate-based mineral medium) to the same medium containing 15 mM $(NH_4)_2SO_4$ (30 mM NH_4^+) instead of 10 mM NO_3^-. The SC2 cells were incubated for 10 hours on 15 mM $(NH_4)_2SO_4$ prior to sampling for RNA extraction (Dam et al., 2014).

2.8 References

Al-Fageeh, M.B., and Smales, C.M. (2006) Control and regulation of the cellular responses to cold shock: the responses in yeast and mammalian systems. *The Biochemical journal* **397**: 247-259.

Allocati, N., Federici, L., Masulli, M., and Di Ilio, C. (2009) Glutathione transferases in bacteria. *FEBS J* **276**: 58-75.

Allocati, N., Federici, L., Masulli, M., and Di Ilio, C. (2012) Distribution of glutathione transferases in Gram-positive bacteria and Archaea. *Biochimie* **94**: 588-596.

Almirón, M., Link, A.J., Furlong, D., and Kolter, R. (1992) A novel DNA-binding protein with regulatory and protective roles in starved *Escherichia coli*. *Genes Dev* **6**: 2646-2654.

Antony, E., and Lohman, T.M. (2019) Dynamics of E. coli single stranded DNA binding (SSB) protein-DNA complexes. *Semin Cell Dev Biol* **86**: 102-111.

Baani, M., and Liesack, W. (2008) Two isozymes of particulate methane monooxygenase with different methane oxidation kinetics are found in *Methylocystis* sp. strain SC2. *Proceedings of the National Academy of Sciences* **105**: 10203-10208.

Bastian, M., Heymann, S., and Jacomy, M. (2009) Gephi: An open source software for exploring and manipulating networks. *Proceedings of the International AAAI Conference on Web and Social Media* **3**.

Bédard, C., and Knowles, R. (1989) Physiology, biochemistry, and specific inhibitors of CH_4, NH_4^+, and CO oxidation by methanotrophs and nitrifiers. *Microbiological Reviews* **53**: 68-84.

Bepperling, A., Alte, F., Kriehuber, T., Braun, N., Weinkauf, S., Groll, M. et al. (2012) Alternative bacterial two-component small heat shock protein systems. *Proceedings of the National Academy of Sciences* **109**: 20407-20412.

Bremer, E. (2000) Coping with osmotic challenges: osmoregulation through accumulation and release of compatible solutes in *B. subtilis*. *Comparative Biochemistry and Physiology Part A: Molecular & Integrative Physiology* **126**: 17.

Bremer, E., and Kramer, R. (2019) Responses of microorganisms to osmotic stress. *Annu Rev Microbiol* **73**: 313-334.

Bremer, E., and Krämer, R. (2019) Responses of microorganisms to osmotic stress. *Annual Review of Microbiology* **73**: 313-334.

Brindha, R.K., and Vasudevan, N. (2018) Methane oxidation capacity of methanotrophs isolated from different soil ecosystems. *International Journal of Environmental Science and Technology* **15**: 1931-1940.

Cabezón, E., Montgomery, M.G., Leslie, A.G.W., and Walker, J.E. (2003) The structure of bovine F1-ATPase in complex with its regulatory protein IF1. *Nat Struct Mol Biol* **10**: 744-750.

Campbell, M.A., Nyerges, G., Kozlowski, J.A., Poret-Peterson, A.T., Stein, L.Y., and Klotz, M.G. (2011) Model of the molecular basis for hydroxylamine oxidation and nitrous oxide production in methanotrophic bacteria. *FEMS Microbiology Letters* **322**: 82-89.

Cébron, A., Bodrossy, L., Chen, Y., Singer, A.C., Thompson, I.P., Prosser, J.I., and Murrell, J.C. (2007) Identity of active methanotrophs in landfill cover soil as revealed by DNA-stable isotope probing. *FEMS Microbiology Ecology* **62**: 12-23.

Christie, P.J. (2004) Type IV secretion: the *Agrobacterium* VirB/D4 and related conjugation systems. *Biochimica et biophysica acta* **1694**: 219-234.

Christie, P.J., Whitaker, N., and González-Rivera, C. (2014) Mechanism and structure of the bacterial type IV secretion systems. *Biochimica et Biophysica Acta (BBA) - Molecular Cell Research* **1843**: 1578-1591.

Conrad, R. (2009) The global methane cycle: recent advances in understanding the microbial processes involved. *Environ Microbiol Rep* **1**: 285-292.

Costa, T.R.D., Felisberto-Rodrigues, C., Meir, A., Prevost, M.S., Redzej, A., Trokter, M., and Waksman, G. (2015) Secretion systems in Gram-negative bacteria: structural and mechanistic insights. *Nature Reviews Microbiology* **13**: 343-359.

Dam, B., Dam, S., Blom, J., and Liesack, W. (2013) Genome analysis coupled with physiological studies reveals a diverse nitrogen metabolism in *Methylocystis* sp strain SC2. *Plos One* **8**: e74767.

Dam, B., Dam, S., Kim, Y., and Liesack, W. (2014) Ammonium induces differential expression of methane and nitrogen metabolism-related genes in *Methylocystis* sp strain SC2. *Environmental Microbiology* **16**: 3115-3127.

Dam, B., Dam, S., Kube, M., Reinhardt, R., and Liesack, W. (2012a) Complete genome sequence of *Methylocystis* sp Strain SC2, an aerobic methanotroph with high-affinity methane oxidation potential. *Journal of Bacteriology* **194**: 6008-6009.

Dam, B., Kube, M., Dam, S., Reinhardt, R., and Liesack, W. (2012b) Complete sequence analysis of two methanotroph-specific repABC-containing plasmids from *Methylocystis* sp. Strain SC2. *Applied and Environmental Microbiology* **78**: 4373-4379.

Dam, B., Dam, S., Kube, M., Reinhardt, R., and Liesack, W. (2012c) Complete Genome Sequence of Methylocystis sp. Strain SC2, an Aerobic Methanotroph with High-Affinity Methane Oxidation Potential. *Journal of Bacteriology* **194**: 6008-6009.

Deckers-Hebestreit, G., and Altendorf, K. (1996) The F0F1-type ATP synthases of bacteria: structure and function of the F0 complex. *Annu Rev Microbiol* **50**: 791-824.

Deng, Y., Cui, X., Lüke, C., and Dumont, M.G. (2013) Aerobic methanotroph diversity in Riganqiao peatlands on the Qinghai-Tibetan Plateau. *Environ Microbiol Rep* **5**: 566-574.

Duine, J.A., and Frank, J., Jr. (1980) Studies on methanol dehydrogenase from *Hyphomicrobium X*. Isolation of an oxidized form of the enzyme. *The Biochemical journal* **187**: 213-219.

Dumont, M.G., Luke, C., Deng, Y.C., and Frenzel, P. (2014) Classification of *pmoA* amplicon pyrosequences using BLAST and the lowest common ancestor method in MEGAN. *Frontiers in Microbiology* **5**: 34.

Dunfield, P., and Knowles, R. (1995) Kinetics of inhibition of methane oxidation by nitrate, nitrite, and ammonium in a humisol. *Applied and Environmental Microbiology* **61**: 3129-3135.

Ernst, L., Steinfeld, B., Barayeu, U., Klintzsch, T., Kurth, M., Grimm, D. et al. (2022) Methane formation driven by reactive oxygen species across all living organisms. *Nature* **603**: 482-+.

Fichman, Y., Gerdes, S.Y., Kovacs, H., Szabados, L., Zilberstein, A., and Csonka, L.N. (2015) Evolution of proline biosynthesis: enzymology, bioinformatics, genetics, and transcriptional regulation. *Biological Reviews* **90**: 1065-1099.

Fronzes, R., Christie, P.J., and Waksman, G. (2009) The structural biology of type IV secretion systems. *Nat Rev Microbiol* **7**: 703-714.

Glatter, T., Ludwig, C., Ahrné, E., Aebersold, R., Heck, A.J.R., and Schmidt, A. (2012) Large-scale quantitative assessment of different in-solution protein digestion protocols reveals superior cleavage efficiency of tandem Lys-C/Trypsin proteolysis over trypsin digestion. *Journal of Proteome Research* **11**: 5145-5156.

Goedhart, J., and Luijsterburg, M.S. (2020) VolcaNoseR is a web app for creating, exploring, labeling and sharing volcano plots. *Scientific Reports* **10**: 20560.

Guerrero-Cruz, S., Vaksmaa, A., Horn, M.A., Niemann, H., Pijuan, M., and Ho, A. (2021) Methanotrophs: discoveries, environmental relevance, and a perspective on current and future applications. *Frontiers in Microbiology* **12**: 678057.

Gunde-Cimerman, N., Plemenitaš, A., and Oren, A. (2018) Strategies of adaptation of microorganisms of the three domains of life to high salt concentrations. *FEMS Microbiol Rev* **42**: 353-375.

Guo, H., Suzuki, T., and Rubinstein, J.L. (2019) Structure of a bacterial ATP synthase. *Elife* **8**.

Gupta, P., Lakes, A., and Dziubla, T. (2016) Chapter One - A free radical primer. In *Oxidative Stress and Biomaterials*. Dziubla, T., and Butterfield, D.A. (eds): Academic Press, pp. 1-33.

Hagen, W.R. (2022) Structure and function of the hybrid cluster protein. *Coordination Chemistry Reviews* **457**: 214405.

Haikarainen, T., and Papageorgiou, A.C. (2010) Dps-like proteins: structural and functional insights into a versatile protein family. *Cell Mol Life Sci* **67**: 341-351.

Hakobyan, A., Liesack, W., and Glatter, T. (2018) Crude-MS strategy for in-depth proteome analysis of the methane-oxidizing *Methylocystis* sp. strain SC2. *J Proteome Res* **17**: 3086-3103.

Hakobyan, A., Zhu, J., Glatter, T., Paczia, N., and Liesack, W. (2020) Hydrogen utilization by *Methylocystis* sp. strain SC2 expands the known metabolic versatility of type IIa methanotrophs. *Metabolic Engineering* **61**: 181-196.

Han, D., Link, H., and Liesack, W. (2017) Response of Methylocystis sp. Strain SC2 to Salt Stress: Physiology, Global Transcriptome, and Amino Acid Profiles. *Appl Environ Microbiol* **83**: e00866-00817.

Hanson, R.S., and Hanson, T.E. (1996) Methanotrophic bacteria. *Microbiological Reviews* **60**: 439-671.

He, R., Chen, M., Ma, R.-C., Su, Y., and Zhang, X. (2017) Ammonium conversion and its feedback effect on methane oxidation of *Methylosinus sporium*. *Journal of Bioscience and Bioengineering* **123**: 466-473.

Heyer, J., Galchenko, V.F., and Dunfield, P.F. (2002) Molecular phylogeny of type II methane-oxidizing bacteria isolated from various environments. *Microbiology (Reading)* **148**: 2831-2846.

Ho, A., Mendes, L.W., Lee, H.J., Kaupper, T., Mo, Y., Poehlein, A. et al. (2020) Response of a methane-driven interaction network to stressor intensification. *FEMS Microbiol Ecol* **96**: fiaa180.

Hoefman, S., van der Ha, D., Boon, N., Vandamme, P., De Vos, P., and Heylen, K. (2014) Niche differentiation in nitrogen metabolism among methanotrophs within an operational taxonomic unit. *BMC Microbiology* **14**: 83.

Hoffmann, F., and Rinas, U. (2004) Stress induced byrecombinant protein production in *Escherichia coli*. In *Physiological Stress Responses in Bioprocesses: -/-*. Berlin, Heidelberg: Springer Berlin Heidelberg, pp. 73-92.

Hoffmann, T., and Bremer, E. (2017) Guardians in a stressful world: the Opu family of compatible solute transporters from *Bacillus subtilis*. *Biological Chemistry* **398**: 193-214.

Hoffmann, T., Blohn, C.v., Stanek, A., Moses, S., Barzantny, H., and Bremer, E. (2012) Synthesis, release, and recapture of compatible solute proline by osmotically stressed *Bacillus subtilis* Cells. *Applied and Environmental Microbiology* **78**: 5753-5762.

Issa, K.H.B., Phan, G., and Broutin, I. (2018) Functional mechanism of the efflux pumps transcription regulators from *Pseudomonas aeruginosa* based on 3D structures. *Frontiers in Molecular Biosciences* **5**.

Johnstone, A.H. (2007) CRC handbook of chemistry and physic" 69th edition editor in chief R. C. Weast, CRC Press Inc., Boca Raton, Florida, 1988, pp. 2400. *Journal of Chemical Technology & Biotechnology* **50**: 294-295.

Karas, V.O., Westerlaken, I., Meyer, A.S., and Gourse, R.L. (2015) The DNA-binding protein from starved cells (Dps) utilizes dual functions to defend cells against multiple stresses. *Journal of Bacteriology* **197**: 3206-3215.

Kempf, B., and Bremer, E. (1998) Uptake and synthesis of compatible solutes as microbial stress responses to high-osmolality environments. *Archives of Microbiology* **170**: 319-330.

Kim, E.H., Nies, D.H., McEvoy, M.M., and Rensing, C. (2011) Switch or funnel: how RND-type transport systems control periplasmic metal homeostasis. *J Bacteriol* **193**: 2381-2387.

Kits, K.D., Campbell, D.J., Rosana, A.R., and Stein, L.Y. (2015) Diverse electron sources support denitrification under hypoxia in the obligate methanotroph *Methylomicrobium album* strain BG8. *Front Microbiol* **6**: 1072.

Knief, C. (2015) Diversity and habitat preferences of cultivated and uncultivated aerobic methanotrophic bacteria evaluated based on *pmoA* as molecular marker. *Frontiers in Microbiology* **6**: 1346.

Knief, C., and Dunfield, P.F. (2005) Response and adaptation of different methanotrophic bacteria to low methane mixing ratios. *Environ Microbiol* **7**: 1307-1317.

Knief, C., Lipski, A., and Dunfield, P.F. (2003) Diversity and activity of methanotrophic bacteria in different upland soils. *Applied and environmental microbiology* **69**: 6703-6714.

Knief, C., Vanitchung, S., Harvey, N.W., Conrad, R., Dunfield, P.F., and Chidthaisong, A. (2005) Diversity of methanotrophic bacteria in tropical upland soils under different land uses. *Applied and environmental microbiology* **71**: 3826-3831.

Kohlstedt, M., Sappa, P.K., Meyer, H., Maass, S., Zaprasis, A., Hoffmann, T. et al. (2014) Adaptation of *Bacillus subtilis* carbon core metabolism to simultaneous nutrient limitation and osmotic challenge: a multi-omics perspective. *Environ Microbiol* **16**: 1898-1917.

Kunzelmann, S., Morris, C., Chavda, A.P., Eccleston, J.F., and Webb, M.R. (2010) Mechanism of interaction between single-stranded DNA binding protein and DNA. *Biochemistry* **49**: 843-852.

Liberek, K., Lewandowska, A., and Zietkiewicz, S. (2008) Chaperones in control of protein disaggregation. *EMBO J* **27**: 328-335.

Lieberman, R.L., and Rosenzweig, A.C. (2005) Crystal structure of a membrane-bound metalloenzyme that catalyses the biological oxidation of methane. *Nature* **434**: 177-182.

Lin, H.-C., Lu, J.-J., Lin, L.-C., Ho, C.-M., Hwang, K.-P., Liu, Y.-C., and Chen, C.-J. (2019) Identification of a proteomic biomarker associated with invasive ST1, serotype VI Group

B *Streptococcus* by MALDI-TOF MS. *Journal of Microbiology, Immunology and Infection* **52**: 81-89.

Lindner, A.S., Pacheco, A., Aldrich, H.C., Costello Staniec, A., Uz, I., and Hodson, D.J. (2007) *Methylocystis hirsuta* sp. nov., a novel methanotroph isolated from a groundwater aquifer. *Int J Syst Evol Microbiol* **57**: 1891-1900.

Liu, G., Vijayaraman, S.B., Dong, Y., Li, X., Andongmaa, B.T., Zhao, L. et al. (2020) *Bacillus velezensis* LG37: transcriptome profiling and functional verification of GlnK and MnrA in ammonia assimilation. *BMC Genomics* **21**: 215.

Lopez, J.C., Porca, E., Collins, G., Clifford, E., Quijano, G., and Munoz, R. (2019) Ammonium influences kinetics and structure of methanotrophic consortia. *Waste Manag* **89**: 345-353.

Lucht, J.M., and Bremer, E. (1994) Adaptation of *Escherichia coli* to high osmolarity environments: osmoregulation of the high-affinity glycine betaine transport system proU. *FEMS Microbiol Rev* **14**: 3-20.

Ludwig, W., Strunk, O., Westram, R., Richter, L., Meier, H., Yadhukumar, a. et al. (2004) ARB: a software environment for sequence data. *Nucleic acids research* **32**: 1363-1371.

Mohammadi, S.S., Pol, A., van Alen, T., Jetten, M.S.M., and den Camp, H.J.M.O. (2017) Ammonia oxidation and nitrite reduction in the verrucomicrobial methanotroph *Methylacidiphilum fumariolicum* SoIV. *Frontiers in Microbiology* **8**: 1901.

Mohanty, S.R., Bodelier, P.L.E., Floris, V., and Conrad, R. (2006) Differential Effects of Nitrogenous Fertilizers on Methane-Consuming Microbes in Rice Field and Forest Soils. *Applied and Environmental Microbiology* **72**: 1346-1354.

Moller, M.N., Rios, N., Trujillo, M., Radi, R., Denicola, A., and Alvarez, B. (2019) Detection and quantification of nitric oxide-derived oxidants in biological systems. *J Biol Chem* **294**: 14776-14802.

Mustakhimov, I.I., Rozova, O.N., Solntseva, N.P., Khmelenina, V.N., Reshetnikov, A.S., and Trotsenko, Y.A. (2017) The properties and potential metabolic role of glucokinase in halotolerant obligate methanotroph *Methylomicrobium alcaliphilum* 20Z. *Antonie Van Leeuwenhoek* **110**: 375-386.

Nair, S., and Finkel, S.E. (2004) Dps protects cells against multiple stresses during stationary phase. *Journal of Bacteriology* **186**: 4192-4198.

Narberhaus, F., and Balsiger, S. (2003) Structure-function studies of *Escherichia coli* RpoH (sigma32) by in vitro linker insertion mutagenesis. *J Bacteriol* **185**: 2731-2738.

Nies, D.H. (2003) Efflux-mediated heavy metal resistance in prokaryotes. *FEMS Microbiol Rev* **27**: 313-339.

Niu, X.-N., Wei, Z.-Q., Zou, H.-F., Xie, G.-G., Wu, F., Li, K.-J. et al. (2015) Complete sequence and detailed analysis of the first indigenous plasmid from *Xanthomonas oryzae* pv. *oryzicola*. *BMC Microbiology* **15**: 233.

Nyerges, G., and Stein, L.Y. (2009) Ammonia cometabolism and product inhibition vary considerably among species of methanotrophic bacteria. *FEMS Microbiology Letters* **297**: 131-136.

Oren, A. (2013) Life at high salt concentrations, intracellular KCl concentrations, and acidic proteomes. *Frontiers in Microbiology* **4**.

Pragai, Z., and Harwood, C.R. (2002) Regulatory interactions between the Pho and sigma(B)-dependent general stress regulons of *Bacillus subtilis*. *Microbiology (Reading)* **148**: 1593-1602.

Ricke, P., Erkel, C., Kube, M., Reinhardt, R., and Liesack, W. (2004) Comparative analysis of the conventional and novel *pmo* (particulate methane monooxygenase) operons from *Methylocystis* Strain SC2. *Applied and Environmental Microbiology* **70**: 3055-3063.

Roe, A.J., McLaggan, D., O'Byrne, C.P., and Booth, I.R. (2000) Rapid inactivation of the *Escherichia coli* Kdp K^+ uptake system by high potassium concentrations. *Molecular Microbiology* **35**: 1235-1243.

Rye, H.S., Roseman, A.M., Chen, S., Furtak, K., Fenton, W.A., Saibil, H.R., and Horwich, A.L. (1999) GroEL-GroES cycling: ATP and nonnative polypeptide direct alternation of folding-active rings. *Cell* **97**: 325-338.

Sadeghi, A., Soltani, B.M., Nekouei, M.K., Jouzani, G.S., Mirzaei, H.H., and Sadeghizadeh, M. (2014) Diversity of the ectoines biosynthesis genes in the salt tolerant Streptomyces and evidence for inductive effect of ectoines on their accumulation. *Microbiological Research* **169**: 699-708.

Saum, S.H., and Müller, V. (2007) Salinity-dependent switching of osmolyte strategies in a moderately halophilic bacterium: glutamate induces proline biosynthesis in *halobacillus halophilu*. *Journal of Bacteriology* **189**: 6968-6975.

Schnell, S., and King, G.M. (1994) Mechanistic Analysis of Ammonium Inhibition of Atmospheric Methane Consumption in Forest Soils. *Applied and Environmental Microbiology* **60**: 3514-3521.

Shiau, Y.-J., Cai, Y., Jia, Z., Chen, C.-L., and Chiu, C.-Y. (2018) Phylogenetically distinct methanotrophs modulate methane oxidation in rice paddies across Taiwan. *Soil Biol Biochem* **124**: 59-69.

Simon, J., and Klotz, M.G. (2013) Diversity and evolution of bioenergetic systems involved in microbial nitrogen compound transformations. *Biochimica et Biophysica Acta (BBA) - Bioenergetics* **1827**: 114-135.

Sleator, R.D., and Hill, C. (2002) Bacterial osmoadaptation: the role of osmolytes in bacterial stress and virulence. *FEMS Microbiol Rev* **26**: 49-71.

Smirnova, G.V., and Oktyabrsky, O.N. (2005) Glutathione in bacteria. *Biochemistry (Moscow)* **70**: 1199-1211.

Smirnova, G.V., Krasnykh, T.A., and Oktyabrsky, O.N. (2001) Role of Glutathione in the Response of *Escherichia coli* to Osmotic Stress. *Biochemistry (Moscow)* **66**: 973-978.

Smith, S.M., Rawat, S., Telser, J., Hoffman, B.M., Stemmler, T.L., and Rosenzweig, A.C. (2011) Crystal Structure and Characterization of Particulate Methane Monooxygenase from Methylocystis species Strain M. *Biochemistry* **50**: 10231-10240.

Spooren, A.A., and Evelo, C.T. (1998) Only the glutathione dependent antioxidant enzymes are inhibited by haematotoxic hydroxylamines. *Human & Experimental Toxicology* **17**: 554-559.

Stein, L.Y., and Klotz, M.G. (2011a) Nitrifying and denitrifying pathways of methanotrophic bacteria. *Biochemical Society Transactions* **39**: 1826-1831.

Stein, L.Y., and Klotz, M.G. (2011b) Nitrifying and denitrifying pathways of methanotrophic bacteria. *Biochem Soc Trans* **39**: 1826-1831.

Stein, L.Y., Yoon, S., Semrau, J.D., DiSpirito, A.A., Crombie, A., Murrell, J.C. et al. (2010) Genome sequence of the obligate methanotroph *Methylosinus trichosporium* strain OB3b. *Journal of Bacteriology* **192**: 6497-6498.

Täumer, J., Marhan, S., Groß, V., Jensen, C., Kuss, A.W., Kolb, S., and Urich, T. (2022) Linking transcriptional dynamics of CH4-cycling grassland soil microbiomes to seasonal gas fluxes. *The ISME Journal* **16**: 1788-1797.

Tharmalingam, S., Alhasawi, A., Appanna, V.P., Lemire, J., and Appanna, V.D. (2017) Reactive nitrogen species (RNS)-resistant microbes: adaptation and medical implications. *Biological Chemistry* **398**: 1193-1208.

Tikhonova, E.N., Grouzdev, D.S., Avtukh, A.N., and Kravchenko, I.K. (2021) *Methylocystis silviterrae* sp.nov., a high-affinity methanotrophic bacterium isolated from the boreal forest soil. *Int J Syst Evol Microbiol* **71**.

Valdez-Cruz, N.A., Ramírez, O.T., and Trujillo-Roldán, M.A. (2011) Molecular responses of E. coli caused by heat stress and recombinant protein production during temperature induction. *Bioengineered Bugs* **2**: 105-110.

Valencia, E.Y., Braz, V.S., Guzzo, C., and Marques, M.V. (2013) Two RND proteins involved in heavy metal efflux in *Caulobacter crescentus* belong to separate clusters within proteobacteria. *BMC Microbiology* **13**: 79.

van Dijk, H., Kaupper, T., Bothe, C., Lee, H.J., Bodelier, P.L.E., Horn, M.A., and Ho, A. (2021) Discrepancy in exchangeable and soluble ammonium-induced effects on aerobic methane oxidation: a microcosm study of a paddy soil. *Biol Fertil* **57**: 873-880.

van Heeswijk, W.C., Westerhoff, H.V., and Boogerd, F.C. (2013) Nitrogen assimilation in *Escherichia coli*: putting molecular data into a systems perspective. *Microbiology and molecular biology reviews : MMBR* **77**: 628-695.

Versantvoort, W., Pol, A., Jetten, M.S.M., Niftrik, L.v., Reimann, J., Kartal, B., and Camp, H.J.M.O.d. (2020) Multiheme hydroxylamine oxidoreductases produce NO during ammonia oxidation in methanotrophs. *Proceedings of the National Academy of Sciences* **117**: 24459-24463.

Viljoen, A.J., Kirsten, C.J., Baker, B., van Helden, P.D., and Wiid, I.J. (2013) The role of glutamine oxoglutarate aminotransferase and glutamate dehydrogenase in nitrogen metabolism in *Mycobacterium bovis* BCG. *PLoS One* **8**: e84452.

Vizcaino, J.A., Csordas, A., del-Toro, N., Dianes, J.A., Griss, J., Lavidas, I. et al. (2016) 2016 update of the PRIDE database and its related tools. *Nucleic Acids Research* **44**: 447-456.

Wallden, K., Rivera-Calzada, A., and Waksman, G. (2010) Type IV secretion systems: versatility and diversity in function. *Cell Microbiol* **12**: 1203-1212.

Watanabe, Y.H., Motohashi, K., Taguchi, H., and Yoshida, M. (2000) Heat-inactivated proteins managed by DnaKJ-GrpE-ClpB chaperones are released as a chaperonin-recognizable non-native form. *J Biol Chem* **275**: 12388-12392.

Whatmore, A.M., Chudek, J.A., and Reed, R.H. (1990) The Effects of Osmotic Upshock on the Intracellular Solute Pools of *Bacillus-Subtilis*. *Journal of General Microbiology* **136**: 2527-2535.

Whittenbury, R., and Dalton, H. (1981) The Methylotrophic Bacteria. In *The Prokaryotes: A Handbook on Habitats, Isolation, and Identification of Bacteria*. Starr, M.P., Stolp, H., Trüper, H.G., Balows, A., and Schlegel, H.G. (eds). Berlin, Heidelberg: Springer Berlin Heidelberg, pp. 894-902.

Yan, D. (2007) Protection of the glutamate pool concentration in enteric bacteria. *Proceedings of the National Academy of Sciences* **104**: 9475-9480.

Yan, D.L., Ikeda, T.P., Shauger, A.E., and Kustu, S. (1996) Glutamate is required to maintain the steady-state potassium pool in *Salmonella typhimurium*. *Proceedings of the National Academy of Sciences of the United States of America* **93**: 6527-6531.

Yang, N., Lü, F., He, P., and Shao, L. (2011) Response of methanotrophs and methane oxidation on ammonium application in landfill soils. *Applied Microbiology and Biotechnology* **92**: 1073-1082.

Yang, S., Hao, D., Jin, M., Li, Y., Liu, Z., Huang, Y. et al. (2020) Internal ammonium excess induces ROS-mediated reactions and causes carbon scarcity in rice. *BMC Plant Biology* **20**: 143.

Yer, E.N., Baloglu, M.C., and Ayan, S. (2018) Identification and expression profiling of all Hsp family member genes under salinity stress in different poplar clones. *Gene* **678**: 324-336.

Yimga, M.T., Dunfield, P.F., Ricke, P., Heyer, J., and Liesack, W. (2003) Wide distribution of a novel *pmoA*-like gene copy among type II methanotrophs, and its expression in *Methylocystis* strain SC2. *Applied and Environmental Microbiology* **69**: 5593-5602.

Zaprasis, A., Bleisteiner, M., Kerres, A., Hoffmann, T., and Bremer, E. (2015) Uptake of Amino Acids and Their Metabolic Conversion into the Compatible Solute Proline Confers Osmoprotection to *Bacillus subtilis*. *Applied and Environmental Microbiology* **81**: 250-259.

Zhang, Y., Burkhardt, D.H., Rouskin, S., Li, G.-W., Weissman, J.S., and Gross, C.A. (2018) A Stress Response that Monitors and Regulates mRNA Structure Is Central to Cold Shock Adaptation. *Mol Cell* **70**: 274-286.

Zietkiewicz, S., Krzewska, J., and Liberek, K. (2004) Successive and synergistic action of the Hsp70 and Hsp100 chaperones in protein disaggregation. *J Biol Chem* **279**: 44376-44383.

Zuñiga, C., Morales, M., and Revah, S. (2013) Polyhydroxyalkanoates accumulation by *Methylobacterium organophilum* CZ-2 during methane degradation using citrate or propionate as cosubstrates. *Bioresource Technology* **129**: 686-689.

2.9 Supplemental information

2.9.1 Supplemental discussion

Ammonium effects on the expression of stress-responsive proteins

Dps. The DNA-binding protein (Dps) is widely distributed among bacteria (e.g., *Escherichia coli*, *Bacillus subtilis*, *Thermosynechococcus elongatus*), and its vital role in contributing to stress survival is remarkably conserved (Almirón et al., 1992; Haikarainen and Papageorgiou, 2010; Karas et al., 2015). In strain SC2, the expression of Dps was significantly induced upon exposure to high NH_4^+ levels. Dps has a significant structural homology to ferritins and possesses the ability to sequester iron and ferroxidase activity (Nair and Finkel, 2004). Its iron-binding activity plays a significant role in protecting the chromosome from oxidative damage during exponential growth of *E. coli*, but Dps has been shown to also protect *E. coli* cells during the stationary growth phase against UV, iron toxicity, heat and pH stress (Nair and Finkel, 2004).

CsbD. CsbD is a bacterial general stress response protein. Its expression is mediated by sigma-B, an alternative sigma factor (Pragai and Harwood, 2002). However, the role of CsbD in stress response remains elusive. In strain SC2, two CsbD family proteins and, in agreement with literature data, one sigma factor of CsbD (RpoH [σ^{32}]) were co-upregulated under high NH_4^+ load. Sigma factor RpoH is the key regulator of the heat shock response in *E. coli* (Narberhaus and Balsiger, 2003).

Heat shock response system. In strain SC2, global proteomics identified the expression of the following heat shock response (HSR) systems: Hsp10 (GroES), Hsp20, Hsp60 (GroEL), Hsp70 (DnaK/DnaJ/GrpE), Hsp90, and Hsp100 (ClpB). The expression of Hsp20, also known as small heat shock proteins (sHSPs), was significantly upregulated in response to high NH_4^+ load (Table 2.3). sHSPs play an important role in maintaining cell proteostasis. Their most widespread and evolutionarily conserved function is binding to denaturing polypeptides, thereby acting as protein chaperones. Indeed, sHSPs serve as an efficient binding reservoir for unstable protein-folding intermediates during stress. Once cells are exposed to sudden proteotoxic stress, Hsp20s encage and shield accumulated aggregation-prone nonnative proteins to ensure their correct folding in near-native conformations. Refolding occurs via the activity of the Hsp70 and Hsp100 systems as soon as environmental conditions become favorable. The assemblies are recognized

by Hsp70 and further processed by both Hsp70 and Hsp100, which leads in an ATPase-dependent manner to the extraction of single polypeptides from aggregates and their subsequent refolding (Zietkiewicz et al., 2004). In strain SC2, none of the Hsp70 (DnaK/DnaJ/GrpE) and Hsp100 (ClpB) proteins showed a differential expression response to increasing NH_4^+ load. However, DnaK (Hsp70) and Hsp100 (ClpB) were constitutively expressed at high level. In summary, while the refolding machinery is constitutively expressed in SC2 cells, the Hsp20 machinery to prevent aggregation and misfolding of client proteins is expressed only upon exposure to a stressor such as high NH_4^+ load (Table 2.3). Hsp60 (GroEL) is another chaperone system that prevents aggregation of misfolded proteins in an ATP-dependent manner (Watanabe et al., 2000). In *E. coli*, Hsp60 (GroEL) binds nonnative protein and sequesters it into the central cavity surrounded by the inside wall of a heptamer ring and capped by Hsp10 (GroES), a co-chaperonin (Rye et al., 1999). In strain SC2, both Hsp10 and Hsp60 were constitutively expressed at high level under all NH_4^+ conditions.

Potassium metabolism ("salt-in strategy"). In strain SC2, high (50 mM and 75 mM) NH_4^+ levels significantly induced expression of the K^+ channel histidine kinase sensor (UniProt ID H7QQ02). This two-component system is involved in sensing and responding to changes in environmental osmolarity. It was already shown decades ago that a sudden osmotic upshock triggers potassium uptake, thereby raising the cytoplasmic K^+ pool (Whatmore et al., 1990). Potassium accumulation is believed to act as an (initial) emergency stress reaction to limit water efflux in high osmolality conditions and, in consequence, to adapt the cell proteins and enzymes to the presence of high extracellular ion concentrations (Hoffmann and Bremer, 2017; Gunde-Cimerman et al., 2018). For instance, *E. coli* possesses four constitutively expressed low affinity K^+ transport systems [TrkG, TrkH, TrkF, and Kup (formerly TrkD)] and, in addition, a single inducible high affinity ATP-driven K^+ uptake system, Kdp (Roe et al., 2000). While Trk is not encoded by the SC2 genome, Kup is constitutively expressed at low level under all NH_4^+ conditions. Thus, like in *E. coli* (Sleator and Hill, 2002), Kup expression is not involved in the osmoregulation in strain SC2. By contrast, the expression level of the entire protein complex (KdpABC) of the high-affinity K^+ uptake system significantly increased under high (75 mM) NH_4^+ load (Table 2.3). In summary, the significant increase in the expression level of both K^+ sensing (H7QQ02) and high-affinity uptake (KdpABC)

system indicates that strain SC2 operates the "salt in" strategy (Bremer, 2000; Oren, 2013) to cope with the conditions of elevated osmolarity under high NH_4^+ load.

Ammonium assimilation and glutamate/glutamine metabolism. *Methylocystis* spp. have been reported to assimilate NH_4^+ through the GOGAT system, involving glutamine synthetase and glutamine-oxoglutarate amidotransferase (Zuñiga et al., 2013; Mustakhimov et al., 2017). Indeed, the intracellular accumulation of glutamate was presumably achieched by ammonia assimilation using the high-affinity GOGAT pathway, given that GOGAT was constitutively expressed at high level under all NH_4^+ conditions (Table 2.3). A high steady-state pool of negatively charged glutamate is presumably employed to neutralize the charge equibilibrium of highly detrimental cation of "salt in" K^+ in the cell (Sleator and Hill, 2002; Yan, 2007; Sadeghi et al., 2014) but also to act, in addition to glutamine, as a nitrogen donor for biosynthesis of other amino acids (van Heeswijk et al., 2013; Viljoen et al., 2013; Liu et al., 2020). Glutamine showed the same intracellular accumulation pattern as did glutamate but on a tenfold lower level (Fig. 2.4).

Among the canonical amino acids, the intracellular concentrations of threonine and lysine were also significantly increased at high (75 mM) NH_4^+ load (Fig. 2.4). While the exact functional reason for this pool size increase remains elusive, it may point to a supplementary role of amino acids in improving molecular structure and metabolic function of SC2 cells under unfavorable conditions, such as high ionic strength (Zaprasis et al., 2015).

Glutathione metabolism. The functional role of glutathione transferases (GSTs) and glutathione peroxidase (GPX) is to maintain an optimal cytoplasmic redox state, in both bacterial and eukaryotic cells. Following a burst of reactive oxygen species (ROS) or reactive nitrogen species (Ernst et al.), GST expression and activity is induced to catalyze the transfer of reactive species to reduced glutathione (GSH), thereby leading to the detoxification of the oxidants and oxidized glutathione (GSSG) (Allocati et al., 2009, 2012). In fact, it has been shown that different types of abiotic stress (e.g., osmotic stress, acidity, oxidative stress) trigger elevated cytoplasmic levels of glutathione in bacteria (Smirnova et al., 2001), plants (Yang et al., 2020), and mammals (Al-Fageeh and Smales, 2006). In strain SC2, high NH_4^+ load induced a significant increase in the expression level of three isoforms of the GST superfamily and GPX (Table 2.3). In a parallel experiment,

we found that NaCl stress induced the significant upregulation of two GST isoforms with the UniProt IDs J7QAL3 and J7QTI3 (unpublished proteome data). The ionic strength (IS) applied in that experiment was with 153 mM (equal to 0.75% NaCl) even higher than under 50 mM (90 mM IS) and 75 mM (114 mM IS) NH_4^+ load. Nonetheless, in addition to GST J7QTI3, the expression of GST isoforms with the UniProt IDs J7QHL1 and J7Q532 were specifically and significantly upregulated in response to increasing NH_4^+ load (Table 2.3). Their increase in expression level may be induced by the increased production of both hydroxylamine (Spooren and Evelo, 1998) and RNS such as nitrite (Stein and Klotz, 2011b; Tharmalingam et al., 2017), given that the expression of both GST isoforms specifically responded to increasing NH_4^+ load. GST J7QAL3 was undetectable under all NH_4^+ conditions. High cellular levels of glutathione may also be required for the retention of K^+ in the initial stage of osmotic adaptation (Smirnova and Oktyabrsky, 2005).

Notably, the glutathione metabolism pathway has multiple stress-responsive functions in methanotrophs, among these formaldehyde detoxification. A significant upregulation of glutathione (GSH)-dependent formaldehyde detoxification was observed in methanol-grown cultures of *Methylomicrobium album* BG8. During the detoxification response, GSH is condensed with formaldehyde either spontaneously or via formaldehyde-activated enzyme to yield S-hydroxymethylglutathione, which is subsequently converted to formate through a multistep reaction that releases GSH for another round of formaldehyde detoxification (34).

Differential regulation of proteins encoded on pBSC2-1 and pBSC2-2

Strain SC2 harbors two large, low-copy-number plasmids of 229.6 kb (pBSC2-1) and 143.5 kb (pBSC2-2) in size (Dam et al., 2012). Various plasmid-encoded proteins were differentially regulated in response to increasing NH_4^+ load: 26 of 53 proteins on pBSC2-1 and 24 of 45 proteins on pBSC2-2, with most of them being significantly upregulated (Table S10).

pBSC2-1

In particular, the single-stranded DNA-binding protein (SBB), three-component CzcCBA complex, and subunits of the F_0F_1 ATPase complex were among the differentially regulated proteins. The SBB protein showed a gradual increase in the expression level with increasing NH_4^+ load. Indeed, SBB was the most significantly

upregulated (3.95-fold) plasmid-encoded protein at 75 mM NH_4^+ (Table S10). The SBB protein plays a major role in DNA replication, recombination, and repair. SSB binds to ssDNA in order to (i) keep the individual strands separated by holding them in place so that each strand can serve as a template for new DNA synthesis, (ii) protect ssDNA from being broken down by nucleases during repair and (iii) remove the secondary structure of ssDNA so that other enzymes are able to access them and act effectively upon the strands (Kunzelmann et al., 2010; Antony and Lohman, 2019). In transcriptomics, the *ssb* gene also showed significantly increased expression level when SC2 cells were exposed to 0.75 % NaCl (Han et al., 2017). Thus, it is reasonable to conclude that the SBB protein plays an important biological role in the cellular response of strain SC2 to high ionic strength.

The *czcCBA* gene cluster is found on diverse plasmids (Niu et al., 2015) and encodes three proteins: CzcA (the RND family specific protein), two-subunit CzcB (membrane fusion protein, MFP), and CzcC (outer membrane protein, OMF). The three proteins constitute a membrane-bound tripartite complex of the RND family (Hoffmann and Rinas, 2004). This efflux system has been reported to confer resistance to metal cations, including but not limited to zinc, cadmium, and cobalt (Valencia et al., 2013). Its expression is regulated through metal ions (Nies, 2003). Tripartite RND efflux systems are known to be involved in maintaining cellular homeostasis by removal of toxic compounds (Kim et al., 2011; Issa et al., 2018). All three proteins (CzcA, CzcB, CzcC) were detected in the pBSC2-1 proteome, but the regulation of their expression in response to increasing NH_4^+ load differed. While the expression level of CzcA and both subunits of CzcB were found to be significantly upregulated under high (50 mM and 75 mM) NH_4^+ levels, CzcC was constitutively expressed at low level under all NH_4^+ conditions. It has been shown that CzcA transports metal cations from the cytoplasm to the periplasmic substrate-binding sites, where the outer membrane protein (CzcC) and membrane fusion protein (CzcB) contribute to the periplasmic efflux of the metal ions (Kim et al., 2011). CzcA, localized in the inner membrane, is active through proton motive force, which is an ATP-dependent process (Issa et al., 2018).

Both the overall structure and the amino acid sequence homology of ATP synthases are conserved among all organisms. The ATP synthase of *E. coli,* which has been most intensively studied, is composed of eight different subunits; with three subunits (a, b, and c) constituting the membrane-integrated ion-translocating F_0 complex. The other five subunits (α, β, γ, δ, and ε) belong to the peripheral F_1 complex. The F_0F_1-ATPases of

bacteria serve two important physiological functions. The enzyme catalyzes the synthesis of ATP from ADP and inorganic phosphate utilizing the energy of an electrochemical ion gradient. On the other hand, under conditions of low driving force, ATP synthases function as ATPases, thereby generating a transmembrane ion gradient at the expense of ATP hydrolysis (Deckers-Hebestreit and Altendorf, 1996; Cabezón et al., 2003; Guo et al., 2019). In our study, all ATPase subunits, including *a*, *b*, *c* subunits of F_0 complex and α, β, γ, δ, ε subunits of F_1 complex, are encoded by pBSC2-1 and were detectable in the SC2 proteome at low level under standard growth conditions with 1 mM NH_4^+. In particular, the *b* and *c* subunits of F_0 complex, but also α, β, γ subunits of F_1 complex, were significantly upregulated in response to high (50 mM and 75 mM) NH_4^+ levels. This increase in expression level, concurrently with CzcA, may suggest that the pBSC2-1 encoded F_0F_1 ATPase provides the energy for the efflux transporter activity of CzcA.

pBSC2-2

In particular, the type IV secretion system (T4SS) was among the differentially regulated proteins. T4SS is a secretion protein complex with versatile functions found in both gram-negative and gram-positive bacteria, and archaea (Fronzes et al., 2009; Wallden et al., 2010; Christie et al., 2014). Three main functions of T4SS are known: conjugation, DNA exchange with the extracellular space, and delivery of proteins to target cells (Wallden et al., 2010). The T4SS system of many gram-negative bacteria comprises 12 proteins (Fronzes et al., 2009; Costa et al., 2015), whose encoding genes were all detected on both plasmids, pBSC2-1 and pBSC2-2 (Dam et al., 2012). According to the UniProt database of *Methylocystis* sp. strain SC2, their designation is VirB1 to VirB11 (pBSC2-1) and AvhB1 to AvhB11 (pBSC2-2). The twelfth T4SS protein differs between the two plasmids and is TraG (pBSC2-1) and VirD4 (pBSC2-2). Nine T4SS proteins (AvhB1, AvhB4, AvhB5, AvhB7, AvhB8, AvhB9, AvhB10, AvhB11, VirD4) were identified in the pBSC2-2 proteome, of which seven T4SS proteins were significantly overexpressed at high (75 mM) NH_4^+ load (Table S10). Among these are AvhB4, AvhB11, and VirD4, which all participate in the synthesis of ATPase powering pilus assembly. The other four upregulated proteins are the inner (AvhB8, AvhB10) and outer (AvhB7, AvhB9) membrane channel proteins (Christie, 2004; Fronzes et al., 2009).

All the T4SS proteins encoded by pBSC2-1 and pBSC2-2 have a conjugative transfer function (Dam et al., 2012), but showed an opposite expression pattern when SC2 cells

were exposed to either 0.75% NaCl or high NH_4^+ load. The pBSC2-1 encoded T4SS proteins were significantly upregulated in response to the incubation treatment with 0.75% NaCl (Han et al., 2017), but not under high NH_4^+ load (this study). By contrast, the pBSC2-2 encoded T4SS proteins were significantly upregulated in response to high NH_4^+ load, but not in the incubation treatment with 0.75% NaCl. These findings suggest that the T4SS systems encoded by either pBSC2-1 or pBSC2-2 differ in their conjugative transfer function. The TraG (pBSC2-1) and VirD4 (pBSC2-2) proteins have the fundamental function to recruit substrates to the T4SS system for secretion through the translocation channel (Fronzes et al., 2009), but substrate recognition may differ between TraG and VirD4 (Christie, 2004). This may explain the opposite expression response of the pBSC2-1 and pBSC2-2 encoded T4SS proteins to 075% NaCl and high NH_4^+ load.

In summary, proteins located on pBSC2-1 and pBSC2-2 showed a strong differential regulation in response to increasing NH_4^+ load, thereby suggesting a molecular cross-talk between the two plasmids and the SC2 chromosome. Notably, previous attempts to cure plasmids pBSC2-1 and pBSC2-2 in strain SC2 failed (Dam et al., 2012). Both the failure to cure the two plasmids and the stress-induced proteome adjustments may indicate a stability relationship between the SC2 chromosome and the two plasmids, pBSC2-1 and pBSC2-2; not just for surviving, but also for conferring *Methylocystis* sp. strain SC2 with improved ability to cope with environmental stress. This view is further supported by the differential regulation of a single PmoC subunit uniquely encoded on pBSC2-2 (Table 2.3) and the constitutive expression of a *nos* operon located on the same plasmid (Fig. S2.9). Indeed, the PmoC subunit showed the greatest downregulation (-4.8-fold) among all differentially regulated proteins in response to high NH_4^+ load.

2.9.2 Supplemental References

Al-Fageeh, M.B., and Smales, C.M. (2006) Control and regulation of the cellular responses to cold shock: the responses in yeast and mammalian systems. *The Biochemical journal* **397**: 247-259.

Allocati, N., Federici, L., Masulli, M., and Di Ilio, C. (2009) Glutathione transferases in bacteria. *FEBS J* **276**: 58-75.

Allocati, N., Federici, L., Masulli, M., and Di Ilio, C. (2012) Distribution of glutathione transferases in Gram-positive bacteria and Archaea. *Biochimie* **94**: 588-596.

Almirón, M., Link, A.J., Furlong, D., and Kolter, R. (1992) A novel DNA-binding protein with regulatory and protective roles in starved *Escherichia coli*. *Genes Dev* **6**: 2646-2654.

Antony, E., and Lohman, T.M. (2019) Dynamics of E. coli single stranded DNA binding (SSB) protein-DNA complexes. *Semin Cell Dev Biol* **86**: 102-111.

Bremer, E. (2000) Coping with osmotic challenges: osmoregulation through accumulation and release of compatible solutes in *B. subtilis*. *Comparative Biochemistry and Physiology Part A: Molecular & Integrative Physiology* **126**: 17.

Cabezón, E., Montgomery, M.G., Leslie, A.G.W., and Walker, J.E. (2003) The structure of bovine F1-ATPase in complex with its regulatory protein IF1. *Nat Struct Mol Biol* **10**: 744-750.

Christie, P.J. (2004) Type IV secretion: the *Agrobacterium* VirB/D4 and related conjugation systems. *Biochimica et biophysica acta* **1694**: 219-234.

Christie, P.J., Whitaker, N., and González-Rivera, C. (2014) Mechanism and structure of the bacterial type IV secretion systems. *Biochimica et Biophysica Acta (BBA) - Molecular Cell Research* **1843**: 1578-1591.

Costa, T.R.D., Felisberto-Rodrigues, C., Meir, A., Prevost, M.S., Redzej, A., Trokter, M., and Waksman, G. (2015) Secretion systems in Gram-negative bacteria: structural and mechanistic insights. *Nature Reviews Microbiology* **13**: 343-359.

Dam, B., Kube, M., Dam, S., Reinhardt, R., and Liesack, W. (2012) Complete sequence analysis of two methanotroph-specific repABC-containing plasmids from *Methylocystis* sp. strain SC2. *Applied and Environmental Microbiology* **78**: 4373-4379.

Deckers-Hebestreit, G., and Altendorf, K. (1996) The F0F1-type ATP synthases of bacteria: structure and function of the F0 complex. *Annu Rev Microbiol* **50**: 791-824.

Fronzes, R., Christie, P.J., and Waksman, G. (2009) The structural biology of type IV secretion systems. *Nat Rev Microbiol* **7**: 703-714.

Gunde-Cimerman, N., Plemenitaš, A., and Oren, A. (2018) Strategies of adaptation of microorganisms of the three domains of life to high salt concentrations. *FEMS Microbiol Rev* **42**: 353-375.

Guo, H., Suzuki, T., and Rubinstein, J.L. (2019) Structure of a bacterial ATP synthase. *Elife* **8**.

Haikarainen, T., and Papageorgiou, A.C. (2010) Dps-like proteins: structural and functional insights into a versatile protein family. *Cell Mol Life Sci* **67**: 341-351.

Han, D.F., Link, H., and Liesack, W. (2017) Response of *Methylocystis* sp strain SC2 to salt stress: physiology, global transcriptome, and amino acid profiles. *Applied and Environmental Microbiology* **83**.

Hoffmann, F., and Rinas, U. (2004) Stress induced byrecombinant protein production in *Escherichia coli*. In *Physiological Stress Responses in Bioprocesses: -/-*. Berlin, Heidelberg: Springer Berlin Heidelberg, pp. 73-92.

Hoffmann, T., and Bremer, E. (2017) Guardians in a stressful world: the Opu family of compatible solute transporters from *Bacillus subtilis*. *Biological Chemistry* **398**: 193-214.

Issa, K.H.B., Phan, G., and Broutin, I. (2018) Functional mechanism of the efflux pumps transcription regulators from *Pseudomonas aeruginosa* based on 3D structures. *Frontiers in Molecular Biosciences* **5**.

Karas, V.O., Westerlaken, I., Meyer, A.S., and Gourse, R.L. (2015) The DNA-binding protein from starved cells (Dps) utilizes dual functions to defend cells against multiple stresses. *Journal of Bacteriology* **197**: 3206-3215.

Kim, E.H., Nies, D.H., McEvoy, M.M., and Rensing, C. (2011) Switch or funnel: how RND-type transport systems control periplasmic metal homeostasis. *J Bacteriol* **193**: 2381-2387.

Kunzelmann, S., Morris, C., Chavda, A.P., Eccleston, J.F., and Webb, M.R. (2010) Mechanism of interaction between single-stranded DNA binding protein and DNA. *Biochemistry* **49**: 843-852.

Liu, G., Vijayaraman, S.B., Dong, Y., Li, X., Andongmaa, B.T., Zhao, L. et al. (2020) *Bacillus velezensis* LG37: transcriptome profiling and functional verification of GlnK and MnrA in ammonia assimilation. *BMC Genomics* **21**: 215.

Mustakhimov, I.I., Rozova, O.N., Solntseva, N.P., Khmelenina, V.N., Reshetnikov, A.S., and Trotsenko, Y.A. (2017) The properties and potential metabolic role of glucokinase in halotolerant obligate methanotroph *Methylomicrobium alcaliphilum* 20Z. *Antonie Van Leeuwenhoek* **110**: 375-386.

Nair, S., and Finkel, S.E. (2004) Dps protects cells against multiple stresses during stationary phase. *Journal of Bacteriology* **186**: 4192-4198.

Narberhaus, F., and Balsiger, S. (2003) Structure-function studies of *Escherichia coli* RpoH (sigma32) by in vitro linker insertion mutagenesis. *J Bacteriol* **185**: 2731-2738.

Nies, D.H. (2003) Efflux-mediated heavy metal resistance in prokaryotes. *FEMS Microbiol Rev* **27**: 313-339.

Niu, X.-N., Wei, Z.-Q., Zou, H.-F., Xie, G.-G., Wu, F., Li, K.-J. et al. (2015) Complete sequence and detailed analysis of the first indigenous plasmid from *Xanthomonas oryzae* pv. *oryzicola*. *BMC Microbiology* **15**: 233.

Oren, A. (2013) Life at high salt concentrations, intracellular KCl concentrations, and acidic proteomes. *Frontiers in Microbiology* **4**.

Pragai, Z., and Harwood, C.R. (2002) Regulatory interactions between the Pho and sigma(B)-dependent general stress regulons of *Bacillus subtilis*. *Microbiology (Reading)* **148**: 1593-1602.

Roe, A.J., McLaggan, D., O'Byrne, C.P., and Booth, I.R. (2000) Rapid inactivation of the *Escherichia coli* Kdp K^+ uptake system by high potassium concentrations. *Molecular Microbiology* **35**: 1235-1243.

Rye, H.S., Roseman, A.M., Chen, S., Furtak, K., Fenton, W.A., Saibil, H.R., and Horwich, A.L. (1999) GroEL-GroES cycling: ATP and nonnative polypeptide direct alternation of folding-active rings. *Cell* **97**: 325-338.

Sadeghi, A., Soltani, B.M., Nekouei, M.K., Jouzani, G.S., Mirzaei, H.H., and Sadeghizadeh, M. (2014) Diversity of the ectoines biosynthesis genes in the salt tolerant Streptomyces and evidence for inductive effect of ectoines on their accumulation. *Microbiological Research* **169**: 699-708.

Sleator, R.D., and Hill, C. (2002) Bacterial osmoadaptation: the role of osmolytes in bacterial stress and virulence. *FEMS Microbiol Rev* **26**: 49-71.

Smirnova, G.V., and Oktyabrsky, O.N. (2005) Glutathione in bacteria. *Biochemistry (Moscow)* **70**: 1199-1211.

Smirnova, G.V., Krasnykh, T.A., and Oktyabrsky, O.N. (2001) Role of Glutathione in the Response of *Escherichia coli* to Osmotic Stress. *Biochemistry (Moscow)* **66**: 973-978.

Spooren, A.A., and Evelo, C.T. (1998) Only the glutathione dependent antioxidant enzymes are inhibited by haematotoxic hydroxylamines. *Human & Experimental Toxicology* **17**: 554-559.

Stein, L.Y., and Klotz, M.G. (2011) Nitrifying and denitrifying pathways of methanotrophic bacteria. *Biochem Soc Trans* **39**: 1826-1831.

Tharmalingam, S., Alhasawi, A., Appanna, V.P., Lemire, J., and Appanna, V.D. (2017) Reactive nitrogen species (RNS)-resistant microbes: adaptation and medical implications. *Biological Chemistry* **398**: 1193-1208.

Valencia, E.Y., Braz, V.S., Guzzo, C., and Marques, M.V. (2013) Two RND proteins involved in heavy metal efflux in *Caulobacter crescentus* belong to separate clusters within proteobacteria. *BMC Microbiology* **13**: 79.

van Heeswijk, W.C., Westerhoff, H.V., and Boogerd, F.C. (2013) Nitrogen assimilation in *Escherichia coli*: putting molecular data into a systems perspective. *Microbiology and molecular biology reviews : MMBR* **77**: 628-695.

Viljoen, A.J., Kirsten, C.J., Baker, B., van Helden, P.D., and Wiid, I.J. (2013) The role of glutamine oxoglutarate aminotransferase and glutamate dehydrogenase in nitrogen metabolism in *Mycobacterium bovis* BCG. *PLoS One* **8**: e84452.

Wallden, K., Rivera-Calzada, A., and Waksman, G. (2010) Type IV secretion systems: versatility and diversity in function. *Cell Microbiol* **12**: 1203-1212.

Watanabe, Y.H., Motohashi, K., Taguchi, H., and Yoshida, M. (2000) Heat-inactivated proteins managed by DnaKJ-GrpE-ClpB chaperones are released as a chaperonin-recognizable non-native form. *J Biol Chem* **275**: 12388-12392.

Whatmore, A.M., Chudek, J.A., and Reed, R.H. (1990) The Effects of Osmotic Upshock on the Intracellular Solute Pools of *Bacillus-Subtilis*. *Journal of General Microbiology* **136**: 2527-2535.

Yan, D. (2007) Protection of the glutamate pool concentration in enteric bacteria. *Proceedings of the National Academy of Sciences* **104**: 9475-9480.

Yang, S., Hao, D., Jin, M., Li, Y., Liu, Z., Huang, Y. et al. (2020) Internal ammonium excess induces ROS-mediated reactions and causes carbon scarcity in rice. *BMC Plant Biology* **20**: 143.

Zaprasis, A., Bleisteiner, M., Kerres, A., Hoffmann, T., and Bremer, E. (2015) Uptake of Amino Acids and Their Metabolic Conversion into the Compatible Solute Proline Confers Osmoprotection to *Bacillus subtilis*. *Applied and Environmental Microbiology* **81**: 250-259.

Zietkiewicz, S., Krzewska, J., and Liberek, K. (2004) Successive and synergistic action of the Hsp70 and Hsp100 chaperones in protein disaggregation. *J Biol Chem* **279**: 44376-44383.

Zuñiga, C., Morales, M., and Revah, S. (2013) Polyhydroxyalkanoates accumulation by *Methylobacterium organophilum* CZ-2 during methane degradation using citrate or propionate as cosubstrates. *Bioresource Technology* **129**: 686-689.

2.9.3 Supplemental figures

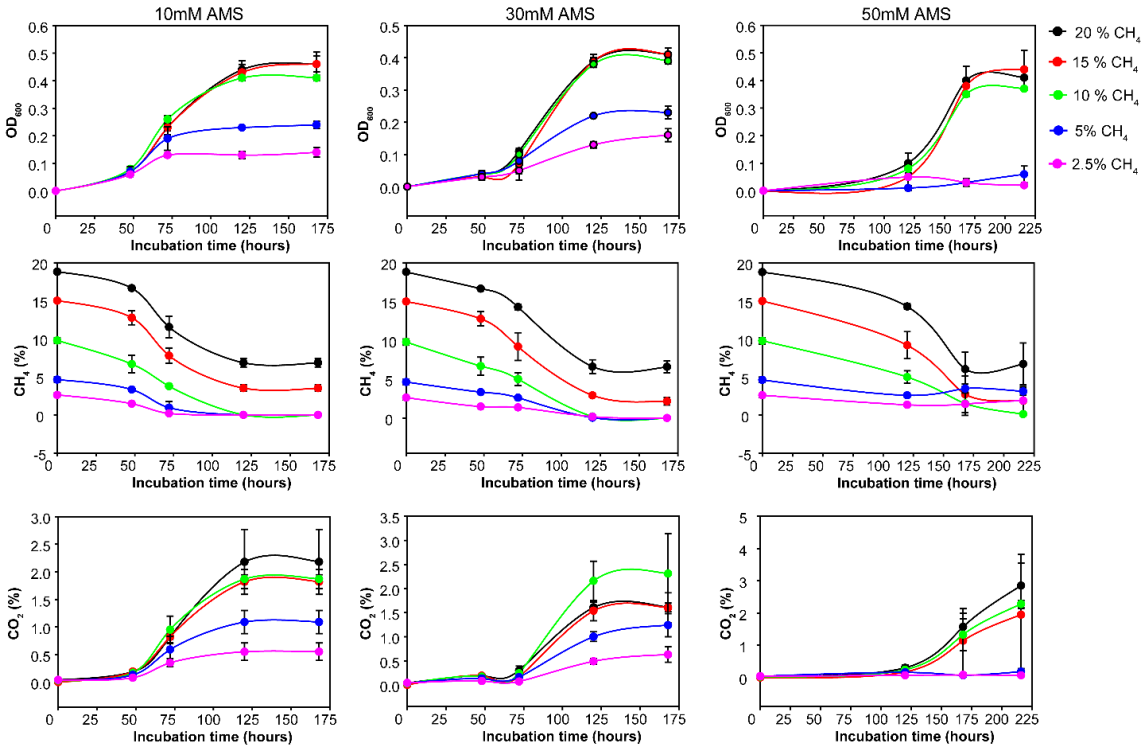

Fig. S2.1. Physiological parameter of Methylocystis sp. strain SC2 in response to varying CH_4:air mixing ratios under increasing NH_4^+ concentrations. Growth (OD_{600}) of strain SC2, CH_4 consumption, and CO_2 evolution were repeatedly monitored over the complete incubation period. Five different CH_4 headspace concentrations (20%, 15%, 10%, 5%, and 2.5%) under three different NH_4^+ concentrations were tested. The error bars show standard deviations of triplicate cultures. See Table S-1 for further details.

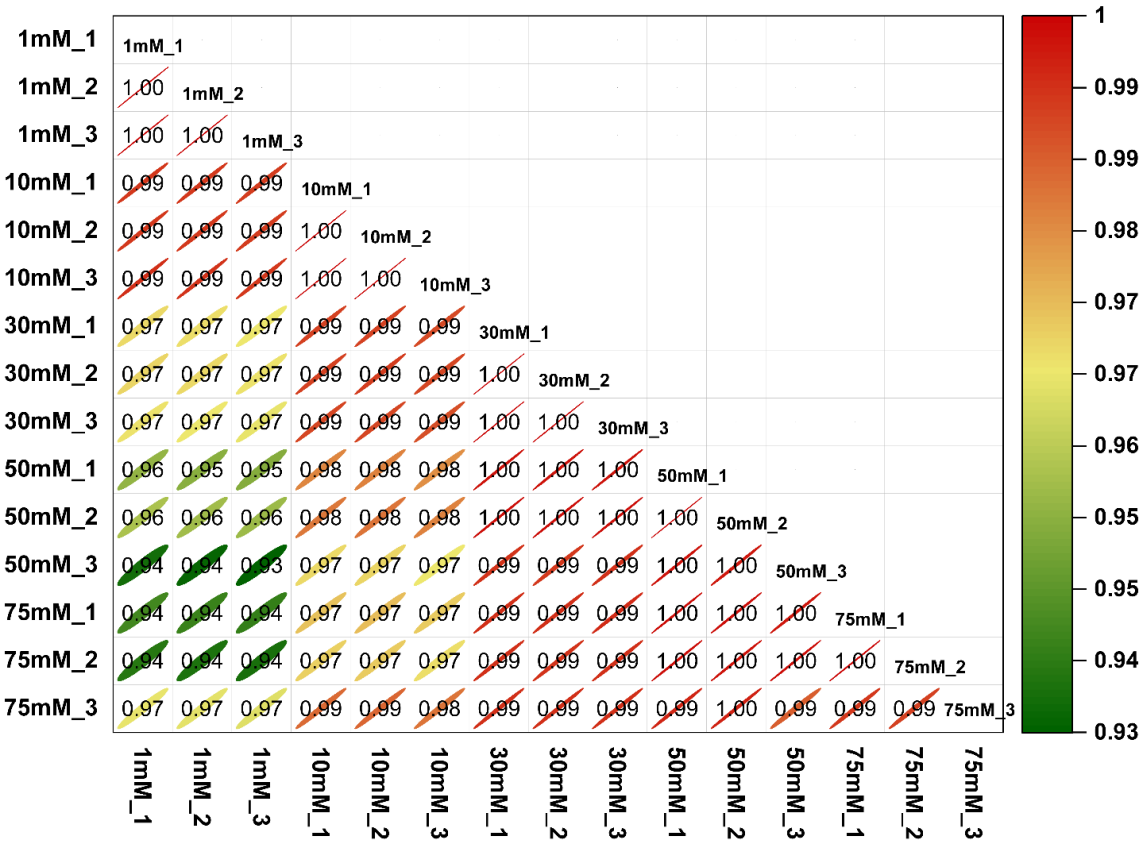

Fig. S2.2. Correlation analysis of LFQ intensities in global proteomics. The matrix of 105 correlation plots revealed very high correlations between the LFQ intensities in triplicate analysis, with Pearson correlation coefficient values of 0.99 or 1.00. The color of the ellipses highlights the correlation coefficient level between 0.93 and 1.00.

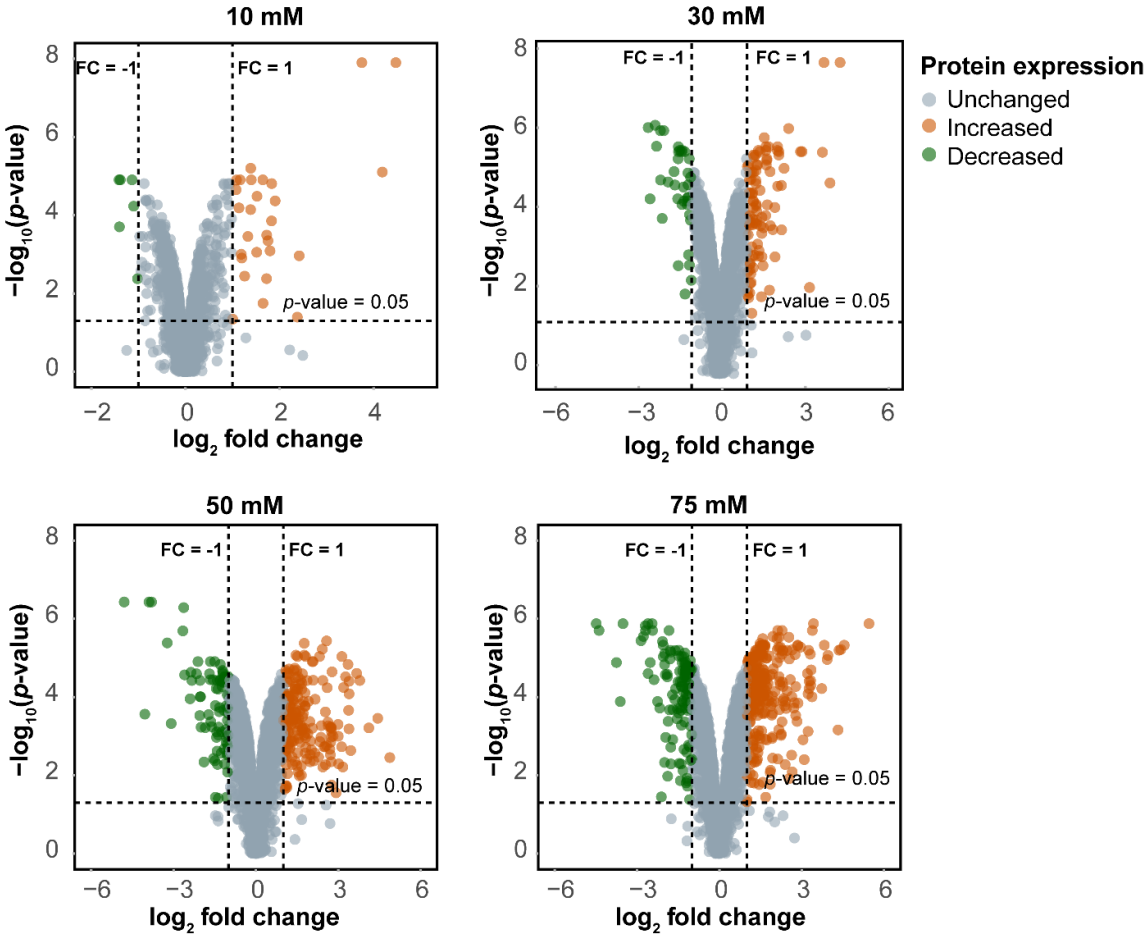

Fig. S2.3. Volcano plots illustrating the correspondence between the number of DRPs and increasing NH_4^+ level (10 mM, 30 mM, 50 mM, and 75 mM) relative to the control treatment (1 mM NH_4^+). The x-axis shows the $\log_2$ fold changes in protein abundance, while the y-axis indicates the negative $\log_{10}$ p-values. Significantly up- and down-regulated proteins are highlighted by orange and green color, respectively (further details in Table S3). Areas highlighted in grey color indicate those proteins whose expression level was not significantly affected by the increased NH_4^+ concentrations relative to the control.

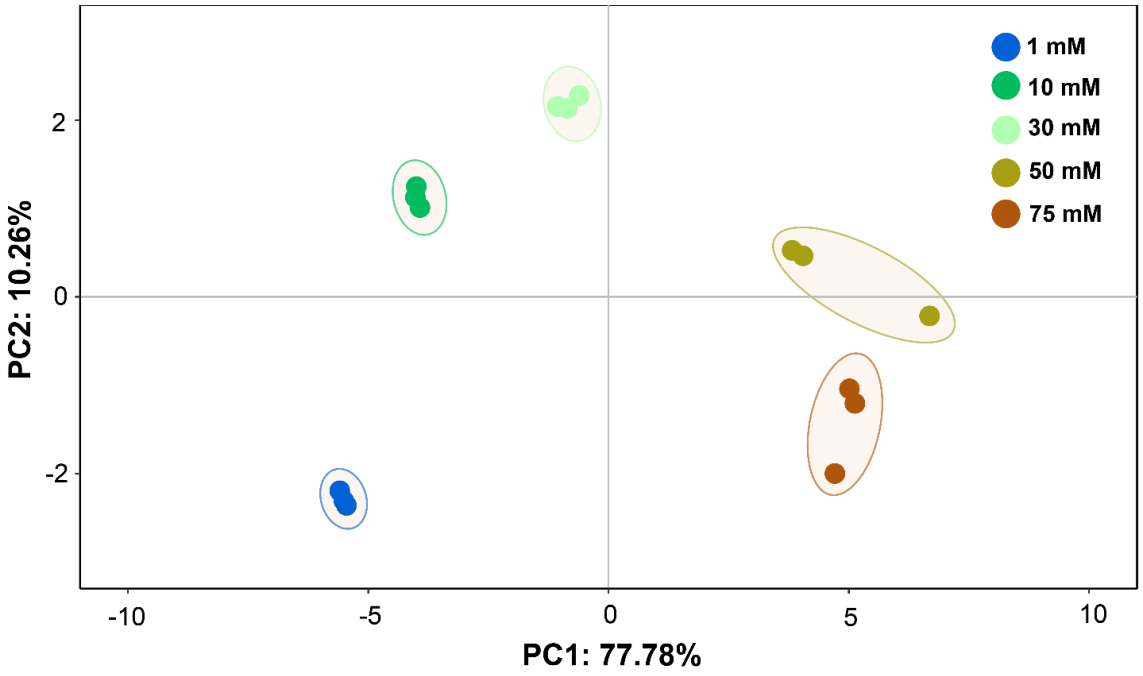

Fig. S2.4. Two-component principal component analysis (PCA) of the intensity values of the total of 438 DRPs. The PCA is based on the three biological replicate datasets obtained for each of the five different NH_4^+ treatments. A total of 88.04% of data variability was explained by PCA. The first component (PC1), accounting for 77.78% of data variance, was mainly influenced by the NH_4^+ concentration, while the second component (PC2) covered the remaining 10.26% of data variance.

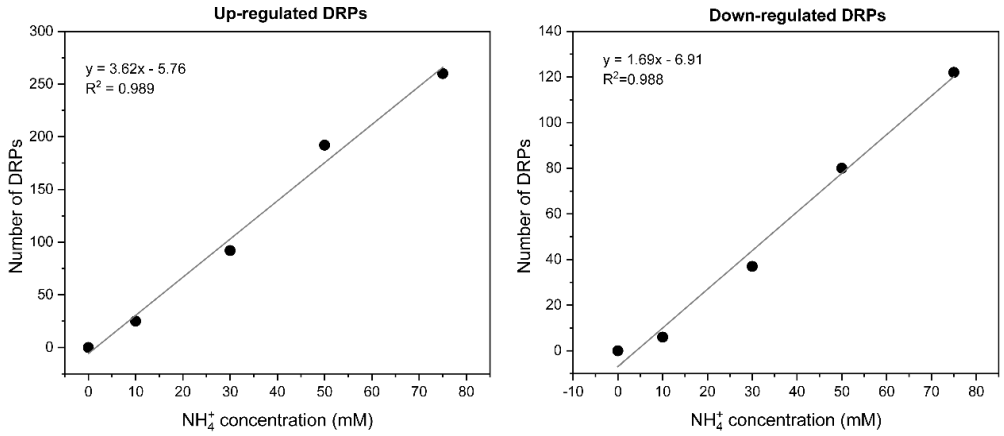

Fig. S2.5. Linear regression analysis of up- and down-regulated proteins. The graphs show the relationship between the number of differentially regulated proteins (DRPs) and NH_4^+ concentrations. The numbers of up- and down-regulated proteins were calculated in comparison to the control treatment (1 mM NH_4^+).

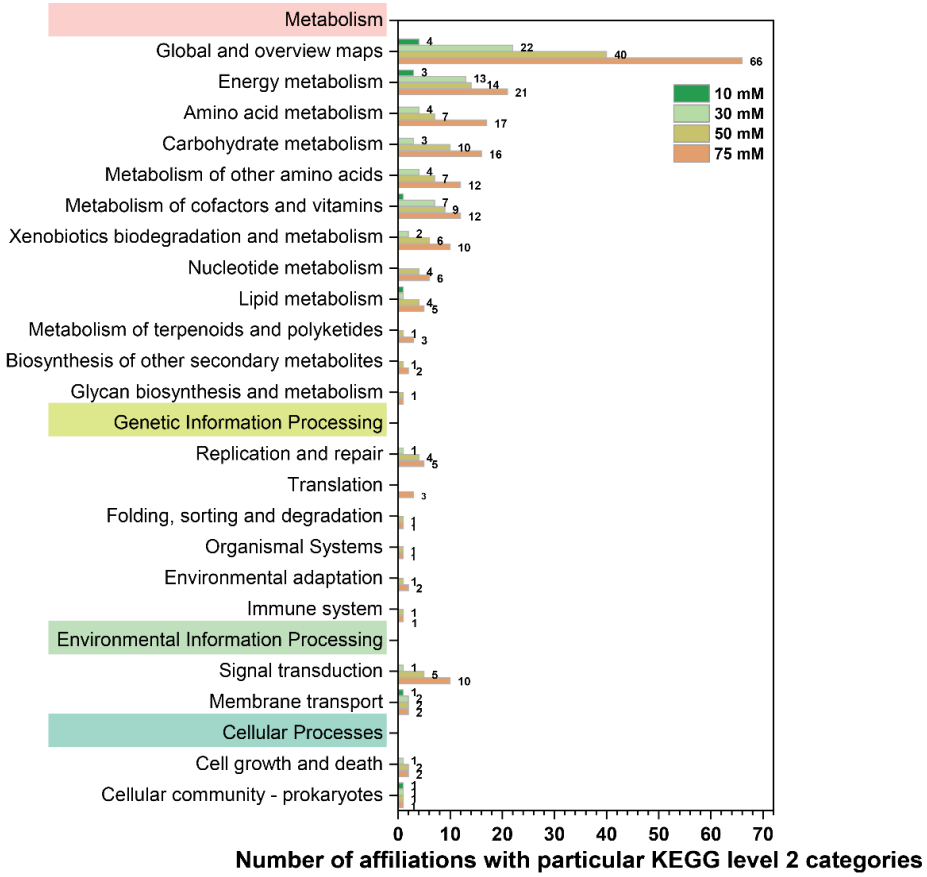

Fig. S2.6. Enrichment of 95 DRPs in KEGG level 2 comparison groups in response to increasing (10 mM, 30 mM, 50 mM, 75 mM) NH_4^+ load relative to the control treatment (1 mM NH_4^+). Note that various DRPs are affiliated with multiple KEGG level 2 categories (Table S5). The four higher-ranked KEGG level 1 categories are highlighted in color.

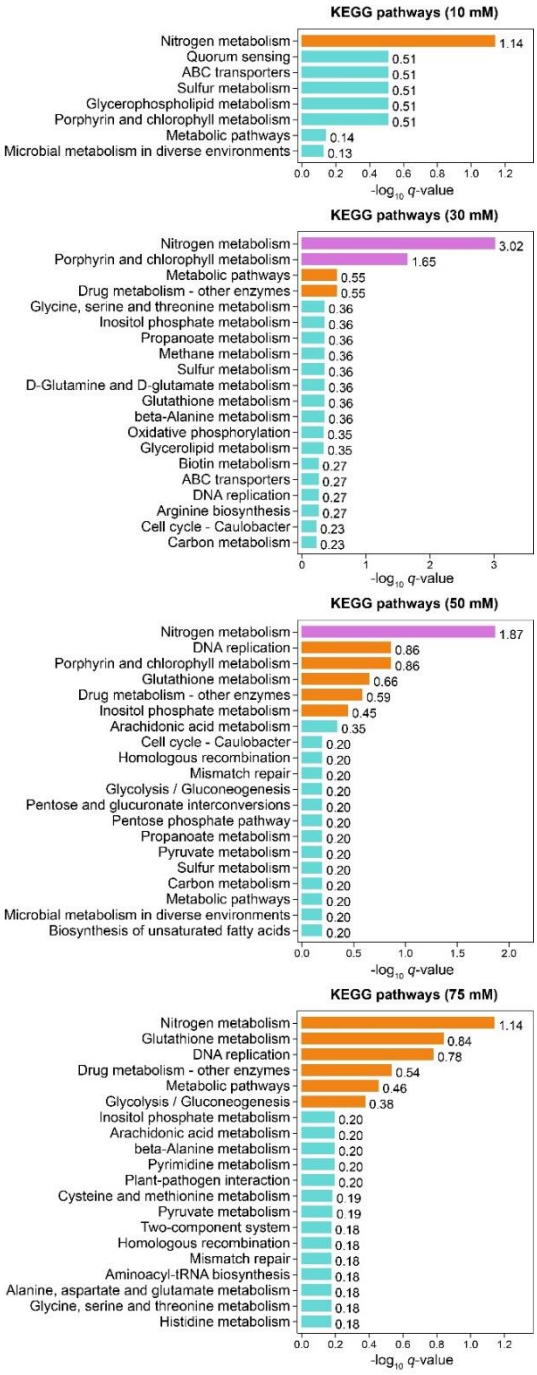

Fig. S2.7. The top 20 KEGG level 3 categories that showed enrichment of DRPs in response to increasing NH_4^+ concentrations. The numbers indicate $-\log_{10}$ p-values. The values given for 10 mM, 30 mM, 50 mM, and 75 mM NH_4^+ are shown in comparison to the control treatment (1 mM NH_4^+). Significance of pathway enrichments is shown color-coded: purple ($q < 0.05$ using Benjamini-Hochberg (BH) method); orange ($p < 0.05$); blue (enrichment insignificant).

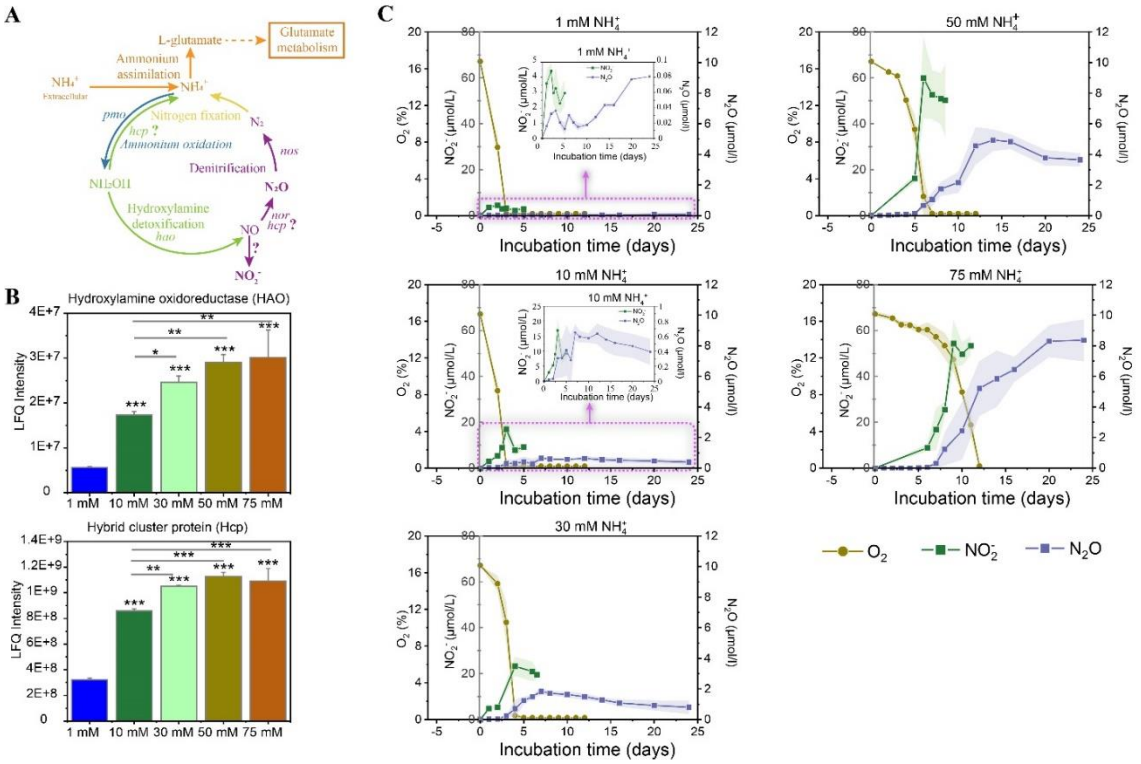

Fig. S2.8. Nitrogen oxidation and hydroxylamine detoxification. (A) Genetic potential for nitrogen metabolism pathways in strain SC2. (B) Differential regulation of hydroxylamine oxidoreductase (HaoA) and chromosome-encoded hybrid cluster protein (Hcp) in response to increasing NH_4^+ load. The lower asterisks (*) indicate significant difference relative to the control treatment (1 mM NH_4^+). The upper asterisks (*) indicate significant difference between the comparison groups. Significant difference is calculated using one-way ANOVA Holm-Sidak method: *p-value ≤ 0.05; **p-value ≤ 0.01; ***p-value ≤ 0.001. (C) Accumulation of nitrite (NO_2^-) and nitrous oxide (N_2O) over incubation time at each of the five NH_4^+ treatments. The inset figures in the graphs for 1 mM and 10 mM NH_4^+ treatments zoom into the minor accumulation of NO_2^- and N_2O over incubation time.

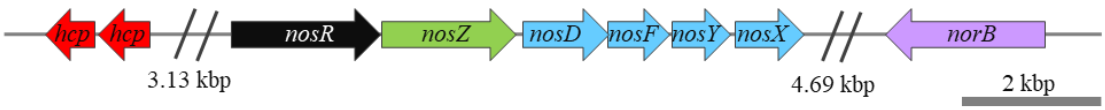

Fig. S2.9. Schematic diagram of the genetic organization of hcp genes, nos operon, and norB on plasmid pBSC2-2. Two hcp genes are located upstream of nosRZDFYX. The nosZ gene encodes nitrous oxide reductase, while nosRDFYX code for Nos-accessory proteins. The norB gene encodes nitric oxide reductase large subunit and is located downstream of the nos operon. The (//) sign indicates that the nitrogen-cycling genes are separated by several coding sequences. Scale bar = 2 kbp.

Chapter 3:

Asparagine Uptake: a Cellular Strategy of *Methylocystis* spp. to Combat Severe Salt Stress

Kangli Guo[1], Timo Glatter[2], Nicole Paczia[3*], Werner Liesack[1,4*]

*Corresponding authors

Chapter 3 is written in research manuscript style. It was submitted as research article in *Science of the Total Environment* in October, 2022. My contribution to the chapter 3 involved the experimental design, laboratory experiments, the proteomics and metabolomics data analysis, the writing and the revision of corresponding parts of the manuscript, including the design of the figures.

[1]Research group "Methanotrophic Bacteria and Environmental Genomics/Transcriptomics", Max Planck Institute for Terrestrial Microbiology, Marburg, D-35043, Germany

[2]*Core Facility for Mass Spectrometry and Proteomics, Max Planck Institute for Terrestrial Microbiology, Marburg, D-35043, Germany*

[3]*Core Facility for Metabolomics and Small Molecule Mass Spectrometry, Max Planck Institute for Terrestrial Microbiology, Marburg, D-35043, Germany*

[4]*Center for Synthetic Microbiology (SYNMIKRO), Philipps-Universität Marburg, Marburg, D-35043, Germany*

3.1 Abstract

Sodium chloride is an important ionic-osmotic stressor in bulk and rhizosphere soils. Members of the alphaproteobacterial methanotroph genus *Methylocystis* are known to have a low tolerance to osmotic and salt stress (≤ 1.0% NaCl), despite the fact that these methane oxidizers are soil inhabitants. We therefore tested various amino acids and other well-known osmolytes for their potential to act as a compatible solute or osmoprotectant under otherwise inhibitory NaCl conditions. Besides ornithine, the addition of 10 mM asparagine to the growth medium had the greatest stress relief effect under severe salinity (1.5% NaCl), leading to a partial growth recovery of strain SC2. Analysis of the exo-metabolome revealed that asparagine was taken up quantitatively by strain SC2. This resulted in an intracellular concentration of 264 ± 57 mM asparagine, with a certain portion hydrolysed to aspartate (4.20 ± 1.41 mM). Compared to severe salinity (1.5% NaCl), the uptake of asparagine induced major proteome rearrangements related to the KEGG level 2 categories energy metabolism, amino acid metabolism, and cell growth and death. In particular, various proteins involved in cell division (e.g., ChpT, CtrA, PleC, FtsA, FtsH1) and peptidoglycan synthesis showed a positive expression response. Asparagine-derived ^{13}C-carbon was incorporated into nearly all amino acids. Exo-metabolome and labeling degree with ^{13}C-carbon suggests that in addition to aspartate, the amino acids glutamate, glycine, serine, and alanine, but also pyruvate and malate, were most crucially involved in the osmoprotective effect of asparagine, with glutamate being a major hub between central carbon and amino acid pathways. In summary, asparagine induced major changes in the flux of metabolites and amino acids through the central carbon and amino acid pathways and acted, in part, as a carbon and nitrogen source for the growth recovery of strain SC2 under severe salinity (1.5% NaCl).

Highlights

- Growth of *Methylocystis* strain SC2 is completely inhibited by 1.5% NaCl.
- *Methylocystis* strain SC2 was tested for its response to potential osmoprotectants.
- Asparagine triggered a partial growth recovery under severe salinity (1.5% NaCl).

- Quantitative uptake of asparagine induced major proteome rearrangements.
- Asparagine-derived ^{13}C-carbon was incorporated into nearly all amino acids.
- Asparagine acted, in part, as a carbon and nitrogen source during growth recovery.

3.2 Introduction

Methane (CH_4), as a potent greenhouse gas and a precursor for tropospheric ozone pollution (Prather and Holmes, 2017), with more than 20-30 times greater impact per molecule than carbon dioxide (CO_2), has increased from 0.720 to 1.91 p.p.m.v in the atmosphere since the beginning of the industrial era (NOAA, 2022). The primary sinks of atmospheric CH_4 are the abiotic oxidation by tropospheric hydroxyl radicals and the activity of aerobic methane-oxidizing bacteria (MOB), or methanotrophs, in unsaturated soils (Conrad, 2009).

Phylogenetic analyses of proteobacterial methanotrophs confirmed the initial classification into *Gammaproteobacteria* (type I) and *Alphaproteobacteria* (type II). Their key enzyme is particular methane monooxygenase (pMMO), which is housed in an extensive intracytoplasmic membrane (ICM) system. The pMMO converts CH_4 to CH_3OH. Both type I and type II MOB are known to be widely distributed in the aerobic interfaces of methanogenic environments, such as natural wetlands, rice paddies, and landfills (Knief and Dunfield, 2005). Here, methanotrophic activity acts as a biofilter that reduces the amount of CH_4 released to the atmosphere. Members of the well-known type IIa MOB genera *Methylocystis* and *Methylosinus* have also been shown to be widely distributed in upland soils where they oxidize atmospheric methane, in addition to members of two largely uncultured clades termed USCα and USCγ (Knief and Dunfield, 2005; Kolb et al., 2005; Täumer et al., 2022). Various *Methylocystis* and *Methylosinus* spp. possess a high-affinity form of pMMO, which is responsible for oxidizing CH_4 at low partial pressures (Tchawa Yimga et al., 2003; Baani and Liesack, 2008).

All free-living bacteria have to cope in their natural habitats with fluctuations in the osmolarity of their surroundings. Studies have shown that fluctuations in the environmental osmolarity will generally inevitably trigger water fluxes along the osmotic gradient into or out of the cell and thereby restricts, or even prevents, cell growth (Bremer, 2000). Moreover, dissolved Na^+ and Cl^- ions can be toxic to bacterial cells (e.g., interaction with binding sites of enzymes) (Serrano, 1996). Methanotrophs show different

degrees of resistance to salt stress (Osudar et al., 2018). Halophilic and halotolerant methanotrophs have been identified to be widespread in saline environments, e.g., soda lakes, mangroves, and alkaline lakes (Osudar et al., 2018). Their specialized mechanisms to cope with high salt-stress have been studied in detail and, among other, involve (i) the synthesis of low-molecular-weight osmoprotectants such as glutamate, ectoine, sucrose and 5-oxo-1-proline (Reshetnikov et al., 2006; 2019), (ii) structural and compositional changes in their cell membranes, and (iii) the production of glycoprotein S-layers that cover the external surface of the cell wall (Khmelenina et al., 1999). These methanotrophs are predominantly associated with the type Ia subgroup within the *Gammaproteobacteria*.

By contrast, the response of methanotrophs in non-saline environments to increasing salinity has received little attention. Indeed, the increased salinization of arable land is at high risk. Salinity has been shown to be the major environmental determinant of microbial community composition as well as microbial-mediated biogeochemical processes, including methane cycling in widespread seawater intrusion areas (Lozupone and Knight, 2007; Deng et al., 2017). Here, paddy soils may be particularly affected, considering that growing rice consumes up to two or three times more water per hectare than other crop (Williams, 2010). In paddy soils, the methanotrophic activity has been shown to be inhibited at salinity levels > 0.3 M NaCl and to be fully ceased at 0.6 M NaCl (seawater salinity) (Ho et al., 2018). Furthermore, the impact of salinity on methane oxidation is of major environmental significance in upland soils, which are important net sinks for atmospheric methane (Cai et al., 2016; Deng et al., 2019). In these soils, salinity fluctuations caused by drought and rainfall processes have a potential impact on methanotrophic activity. Recent pure cultures has evidenced that alphaproteobacterial type II MOB possess low tolerance to salt stress (< 1% NaCl) (Trotsenko and Murrell, 2008; Han et al., 2017), with the exception of *Methylocystis parvus* that is able to tolerate up to 2% NaCl (Han et al., 2017; Jung et al., 2020).

In our research, *Methylocystis* sp. strain SC2 was used as the model organism to decipher mechanisms to cope with increasing salinity. Its ability to produce two pMMO isozymes with different methane oxidation kinetics provides strain SC2 with a selective advantage to thrive or survive under a wide range of methane conditions, including in upland soils (Baani and Liesack, 2008; Dam et al., 2012). To cope with changes in soil salinity, we hypothesized that, in addition to *de novo* synthesis of compatible solutes such as glutamate and proline (Han et al., 2017), strain SC2 can acquire osmoprotectants from

the environment. These may be synthesized by plants and released into soil by root exudation and decaying plant tissues (Moe, 2013). Thus, we aimed at investigating the ability of *Methylocystis* sp. strain SC2 to acquire a broad spectrum of potential osmoprotectants from the environment. In order to understand the unexpected environmental resilience and metabolic versatility of *Methylocystis* sp. strain SC2, our research further focused on unraveling the cellular mechanisms that shape its physiological response and central metabolism under continued salt stress, with potential osmoprotectants being added to the growth medium. In our research, we combined the growth experiments with global proteomics and ^{13}C-tracing experiments (Fig 3.1).

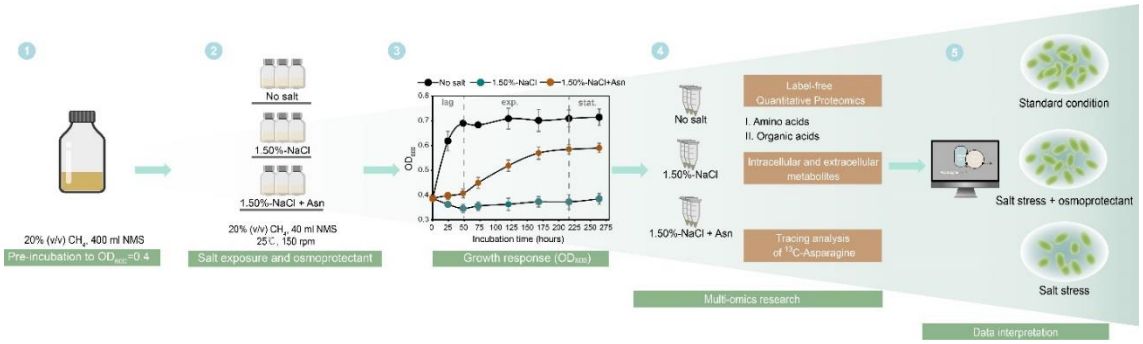

Fig 3.1 Outline of the experimental strategy.

3.3 Materials and methods

3.3.1 Growth conditions

Strain SC2 was routinely cultivated in nitrate mineral salt medium (NMS) with the same basic composition as reported earlier (Heyer et al., 2002). The synthetic medium contained 1 g KNO_3 (~ 10 mM NO_3^-) per liter as the nitrogen source. Cells of strain SC2 were grown twice to the early exponential growth phase (OD_{600} value of about 0.25). Aliquots (1 mL) of the pre-incubated culture were transferred to 120 serum bottles containing 40 mL of NMS. The culture headspace was adjusted to a filter-sterilized air: CH_4 mixing ratio of 80:20 % (v:v). The serum bottles were incubated on a rotary shaker at 150 rpm and 25 °C. These experimental SC2 cultures were grown to the mid-log phase (OD_{600} of 0.25 to 0.40) for salt stress exposure and the screening of potential osmoprotectants. The osmolarity of the growth medium was adjusted by adding NaCl from a 20% stock solution. The salt tolerance of strain SC2 was tested by exposing its mid-log phase cells (OD_{600} of 0.25) to 0% to 1.50% NaCl. Upon determining the salt tolerance range, SC2 cells were exposed to 1.00% NaCl in the presence or absence of potential osmoprotectants (each added at 1 mM concentration): alanine, arginine, asparagine, aspartate, cysteine, glutamate, glutamine, glycine, histone, lysine, methionine, proline, threonine, valine, ornithine, ectoine, and glycine betaine. The osmoprotective effect of each tested compound was analyzed by cell biomass measurement (OD_{600}) at the early stationary phase. SC2 cultures without the addition of NaCl and potential osmoprotectant were used as control.

Asparagine (Smirnova et al.) was chosen for further analysis. Its osmoprotective effect on strain SC2 was tested under three culture conditions: (i) no-salt; (ii) 1.50%-NaCl; and (iii) 1.50%-NaCl+Asn (Fig 3.1). The SC2 cells were pre-grown to the mid-log phase (OD_{600} of 0.40) as described above, after which NaCl (1.5%) and Asn (0.1, 1, 2, 5, 10, or 20 mM) were added. The osmoprotective effect of the increasing asparagine concentrations was analyzed by cell biomass measurement (OD_{600}) at the early stationary phase.

3.3.2 Physiological measurements

Cell optical density was monitored by spectrophotometry at 600 nm (OD_{600}) (Bio Photometer RS232C; Eppendorf AG, Hamburg, Germany). Cell dry weight (CDW) was calculated with 1 OD_{600} = 0.26 g CDW/L of strain SC2 culture (Hakobyan et al., 2020). Methane consumption was analyzed by gas chromatography (SRI Instruments, Earl St. Torrance, CA). Biomass yield is indicated as mg CDW/ mmol CH_4. The growth rate was calculated during the exponential growth.

3.3.3 Sampling and sample preparation for quantification of intracellular and extracellular metabolites

The SC2 cells were grown to the mid-log phase in 120-ml serum bottles under three conditions: (i) no-salt; (ii) 1.50%-NaCl; and (iii) 1.50%-NaCl+Asn (10 mM asparagine (Fig 3.1). Upon growth to the mid-log phase, an aliquot (1.2 mL) of each replicate culture was taken for various analytics applications. For the measurement of intracellular amino acids, a 1-ml aliquot was immediately transferred to a 2 mL Eppendorf tube, mixed with 1 mL quenching solution (70% MeOH [v/v], -80 °C) and centrifuged using a fixed angel rotor (10 min, −10 °C, 10,000 × *g*). After centrifugation, the supernatant was removed and the cell pellet was immediately stored at −80 ℃ for later extraction of the intracellular metabolites. These were extracted by suspending the frozen cell pellets in equal volumes of extraction fluid (−20 °C) and chloroform (−20 °C) based on sample biovolume. A 10-µl aliquot was used to measure the biovolume of SC2 cells usng a Multisizer 4e Coulter Counter (Beckman Coulter, Inc.). The residual aliquot (0.19 mL) was filtered through a 22 µm HPLC/ GC approved RC membrane filter (Phenomenex) into a 0.5 mL sterile safe-lock microcentrifuge tube (Eppendorf) and stored at -20 °C for subsequent measurement of the extracellular metabolites.

3.3.4 Quantification of metabolites

The quantitative analysis of amino acids was performed using LC-MS/MS. The chromatographic separation was done on an Agilent Infinity II 1260 HPLC system using a ZicHILIC SeQuant column (150 × 2.1 mm, 3.5 µm particle size, 100 Å pore size) connected to a ZicHILIC guard column (20 × 2.1 mm, 5 µm particle size) (Merck KgAA). The constant flow rate was 0.3 ml/min carried out with a mobile phase A being 0.1 %

formic acid in 99:1 water: acetonitrile (Honeywell, Morristown, New Jersey, USA) and a phase B being 0.1 % formic acid in 99:1 water:acetonitrile (Honeywell, Morristown, New Jersey, USA) at 25° C.

The injection volume was 3 µl. The mobile phase profile consisted of the following steps and linear gradients: 0 – 8 min from 80 to 60 % B; 8 – 10 min from 60 to 10 % B; 10 – 12 min constant at 10 % B; 12 – 12.1 min from 10 to 80 % B; 12.1 to 14 min constant at 80 % B. An Agilent 6470 mass spectrometer was used in positive mode with an electrospray ionization source and the following conditions: ESI spray voltage 4500 V, nozzle voltage 1500 V, sheath gas 400°C at 12 l/min, nebulizer pressure 30 psig, and drying gas 250 °C at 11 l/min. Compounds were identified based on their mass transition and retention time compared to standards. Chromatograms were integrated using MassHunter software (Agilent, Santa Clara, CA, USA). Absolute concentrations were calculated based on an external calibration curve prepared in sample matrix.

3.3.5 Comparative proteomics analysis

As for the metabolites analysis, the proteomics samples were collected at the mid-log phase after the incubation under no-salt, 1.50%-NaCl, and 1.50%-NaCl+Asn conditions. Here, strain SC2 was grown in triplicate per treatment in 300 ml NMS medium using 1 L Duran laboratory bottles with gas-tight caps (Merck, Germany). The gas headspace concentration and incubation conditions were as described in section 3.1. Each replicate culture was processed separately. A total of 150 mL cell culture was collected by centrifugation for 20 min at 7000 × g and 4 °C. The cell pellets were thoroughly washed twice with 1 × phosphate buffer to remove medium traces. The washed cells were transferred to 2 ml sterile safe-lock microcentrifuge tubes (Eppendorf) and stored at -80 °C until further processing. Every condition was conducted in triplicate cultures.

Sample preparation and proteins measurement were carried out as described previously (for details see (Hakobyan et al., 2018). Discovery-LFQ was done using the Progenesis QI software (Nonlinear Dynamics, version 2.0). Next, the data obtained from Progenesis were evaluated using SafeQuant R package, version 2.2.2 (Glatter et al., 2012). Hereby, 1% identification and quantification false discovery rate (FDR) were calculated. The data were analyzed using MASCOT (version 2.3.02), and the protein identification was performed using the most recent UniProt database version set up for

Methylocystis sp. strain SC2. Quantification was carried out with Proteome Discoverer (v.1.4, Thermo Fisher Scientific). Significantly regulated proteins (DRPs) (log_2 fold change ≥1 or ≤1, *q*-value ≤ 0.01) were searched against the Gene Ontology (GO) and Kyoto Encyclopedia of Genes and Genomes (KEGG) databases for protein annotation and functional enrichment analysis.

3.3.6 Computational proteome analysis

The Volcano plots were created using VolcaNoseR (Goedhart and Luijsterburg, 2020). Hierarchical heatmap analysis was performed on Z-score normalized LFQ intensities of all DRPs. Creation of both hierarchical heatmap and Venn diagram were done using the free online platform for data analysis and visualization available at http://www.bioinformatics.com.cn/. The STRING database was used to construct the protein-protein interaction (Ludwig et al.) network based on the Uniprot IDs of DRPs in three comparison groups: (i) 1.50%-NaCl/no-salt; (ii) 1.50%-NaCl+Asn/Asn; (iii) 1.50%-NaCl+Asn/1.50%-NaCl. This resulted in an automated calculation of edges and nodes using the default value for the minimum interaction score (0.4). Gephi (version 0.9.2), an open-source software, was used for modularity calculation and visualization (Bastian et al., 2009). Nodes with no or less than six edges were omitted in the 1.50%-NaCl/no-salt and 1.50%-NaCl+Asn/Asn comparison groups, while all the nodes were maintained in the 1.50%-NaCl+Asn/1.50%-NaCl comparison group. The final presentation layout of the PPI network was created with Fruchterman Reingold, a method implemented in Gephi.

3.3.7 ^{13}C-Asn labeling experiment

SC2 cells were grown to the mid-log phase as described above, after which 1.5%-NaCl and 10 mM ^{13}C-Asn (1.5%-NaCl+Asn) was added to the cultures. Cultures with no salt but ^{13}C-Asn addition (no-salt+Asn) were used as control treatment. Cells were harvested when the cultures were at both metabolic steady state and isotopic steady state. A culture aliquot (1.2 mL) was taken for the extraction of intracellular metabolites and measurement of the cell biovolume, using procedures described in **section 3.3**. The extracts of intracellular metabolites were stored at - 80°C for later measurement. The labeling distributions were determined using the same instrumentation and chromatographic method as described in section 3.4. To increase the sensitivity to a level

sufficient for detection of low-abundant metabolite fractions, the labeling patterns of alanine, proline, asparagine, aspartate, glutamate, leucine, isoleucine, glycine, serine, and methionine were determined in separate runs. The incorporation rate of asparagine-derived ^{13}C into intermediates of the central carbon metabolism was estimated based on their relative mass isotopomer distribution and the proportion of ^{13}C. The values for mass transitions, collision energies, fragmentor and accelerator voltages are shown in Supplemental Table S3.1.

3.3.8 Software used for preparation of figures and graphs

Data statistic differences were tested by Sigmaplot version 14.0. Figures and graphs were created with OriginPro 2020 and Adobe Illustrator 2020.

3.4 Results

3.4.1 Growth of *Methylocystis* sp. strain SC2 under salt stress

Growth experiments were conducted to determine the effect of increasing NaCl stress on the physiological activity of strain SC2. No difference in the growth rate occurred between no salt (1.57 mg CDW/d) and 0.50% NaCl (1.45 mg CDW/d), while 0.75% NaCl (0.66 mg CDW/d) and 1.00% NaCl (0.28 mg CDW/d) significantly decreased the growth rate ($p < 0.001$). The addition of 1.25% NaCl inhibited the growth of strain SC2 during the first 2 days of incubation, while it slightly recovered thereafter. Final biomass (0.50 OD_{600}) showed no significant difference between the no-salt control and the treatments with 0.50% NaCl and 0.75% NaCl (Fig S3.1A). Further increase in salinity significantly decreased the final biomass, with OD_{600} values of 0.46 (1% NaCl) and 0.35 (1.25% NaCl). Nearly no growth occurred with 1.50% NaCl in the medium (Fig S3.1A).

The osmoprotective effect of a series of potential compatible solutes and osmoprotectants was tested in SC2 cultures grown with 1% NaCl in the medium. The addition of alanine, asparagine, lysine, and ornithine led to a stress relief and, compared to salt-only condition, restored the biomass production by 12%, 21%, 14%, and 33%, respectively. The other compounds had no effect (cysteine, glycine betaine) or a negative effect (arginine, aspartate, cysteine, glutamate, glutamine, glycine, histone, methionine, proline, threonine, valine, ectoine) effect on the growth of strain SC2 (Fig S3.1B). Incubated under 1.5%-NaCl condition, the addition of 10 mM asparagine restored the biomass production significantly greater (57%) than the addition of 10 mM ornithine (14%), with CH_4 consumption, growth rate, and biomass yield being significantly increased ($p \leq 0.001$, Fig S3.1C, Fig 3.2 and Table S3.2). Therefore, asparagine was chosen for further analysis.

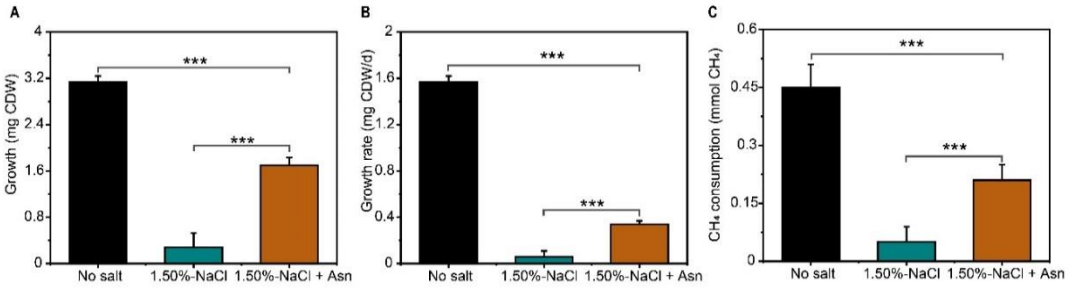

Fig 3.2 Growth parameters of *Methylocystis* sp. strain SC2 under the conditions of (i) no-salt, (ii) 1.50%-NaCl, and (iii) 1.50%-NaCl+Asn. All the growth parameters were calculated based on the mid-log phase. Asterisks indicate significant difference with **p*-value ≤ 0.05; ***p*-value ≤ 0.01; and ****p*-value ≤ 0.001, using Tukey's method with one-way ANOVA. Measurements were done in triplicate cultures. Error bars show standard deviations of triplicate cultures.

3.4.2 Comparative proteomics

Samples for global proteome analysis were taken during the mid-log phase, involving three treatment conditions: no-salt, 1.50%-NaCl, and 1.50%-NaCl+Asn (Fig 3.1). With $\log_2$-fold changes ≥ 1 or ≤ -1 and *q*-value ≤ 0.01, the total number of up- and down-regulated proteins were as follows: 1.50%-NaCl/no-salt (183 vs. 342), 1.50%-NaCl+Asn/no-salt (227 vs. 294), and 1.50%-NaCl+Asn/1.50%-NaCl (148 vs. 63) (Fig S3.2 and Table S3.3). Of the latter 148 DRPs, 45 DRPs were specifically upregulated in response to 1.5%-NaCl+Asn, with no differential expression effect in the comparison group 1.5%-NaCl/no-salt. The expression of another set of 18 DRPs were already

upregulated in the comparison group 1.50%-NaCl/no-salt and further significantly upregulated in response to asparagine (1.50%-NaCl+Asn/1.50%-NaCl). Finally, 85 DRPs showed a significant downregulation in the comparison group 1.50%-NaCl/no-salt, but upregulation in the comparison group 1.50%-NaCl+Asn/1.50%-NaCl (Fig 3.3). Triplicate proteome analysis confirmed high reproducibility, with Pearson correlation coefficients (PCC) ≥ 0.99 for each treatment condition (Fig S3.2). The protein-protein interaction (PPI) networks constructed for the comparison groups 1.50%-NaCl/no-salt, 1.50%-NaCl+Asn/no-salt, and 1.50%-NaCl+Asn/1.50%-NaCl revealed that proteins of the KEGG level 2 categories "energy metabolism", "carbohydrate metabolism", "amino acid metabolism", "cell growth and death", "replication and repair", and "signal transduction" were enriched in the 1.50%-NaCl and 1.50%-NaCl+Asn treatments relative to the no-salt treatment (Fig 3.3A and Table S3.4, 3.5, and 3.6).

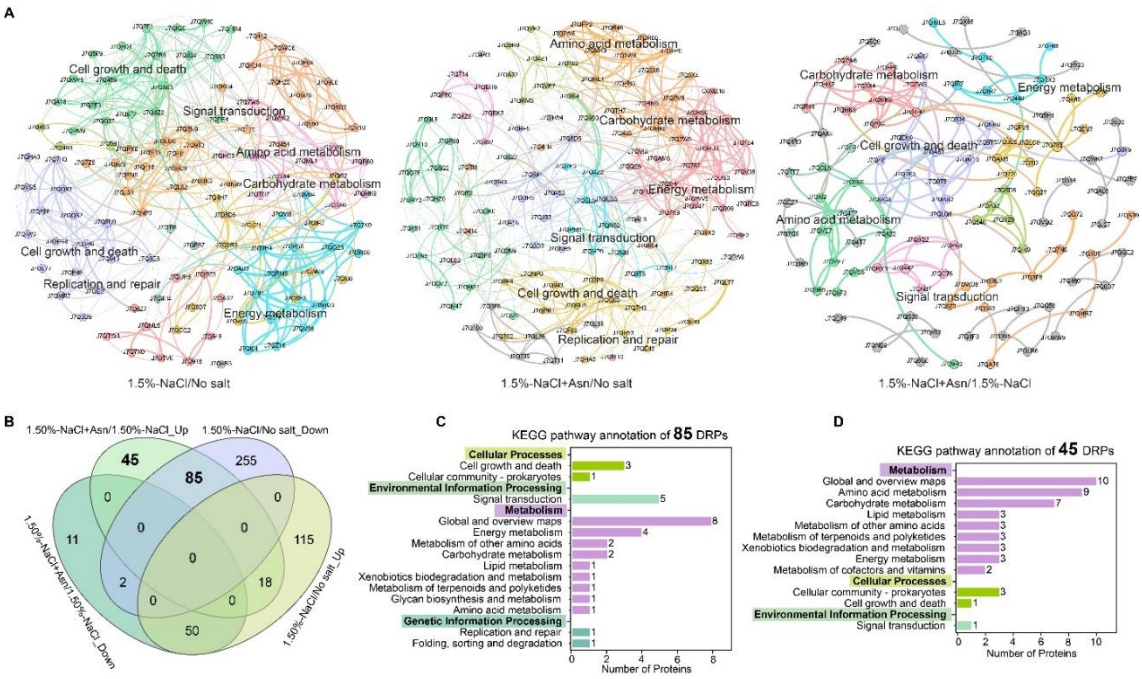

Fig 3.3 Comparative proteomics analysis under the conditions of no-salt, 1.50%-NaCl, and 1.50%-NaCl+Asn. (A) Protein-protein interaction networks in three comparison groups: "1.50%-NaCl/no-salt", "1.50%-NaCl+Asn/no-salt", and "1.50%-NaCl+Asn/1.50%-NaCl". The complex PPI networks show a remarkably high number of edges under salinity conditions: 926 (1.50%-NaCl/no-salt) and 907 (1.50%-NaCl+Asn/no-salt). The edges (157) were clearly less in number after the addition of asparagine (1.50%-NaCl+Asn/1.50%-NaCl), thereby resulting in a loose PPI network. Note that nodes with no or less than six edges were omitted in the PPI networks shown for the 1.50%-NaCl/no-salt and 1.50%-NaCl+Asn/Asn comparison groups, while all the nodes were maintained in the 1.50%-NaCl+Asn/1.50%-NaCl comparison group. The functional categorization of the modules is based on KEGG level 2. The size of nodes and edges

is proportional to the number of connections (its degree). The protein identity of each node is indicated by the UniProt ID. The network edges indicate both functional and physical protein associations based on active interaction sources including Textming, Experiments, Databases, Co-expression, Neighborhood, Gene Fusion, and Co-occurrence. See **Error! Reference source not found.**, S5, S6 for details on the 120, 126, and 111 DRPs used to construct the respective PPI network. (B) Venn diagram showing the number of DRPs for 1.50%-NaCl/no-salt and 1.50%-NaCl+Asn/1.50%-NaCl. (C) Pathway annotation on KEGG level 2 for 45 DRPs that had been identified to be exclusively upregulated in 1.50%-NaCl+Asn/1.50%-NaCl. (D) Pathway annotation on KEGG level 2 for 85 DRPs downregulated in 1.50%-NaCl/no-salt but upregulated in 1.50%-NaCl+Asn/1.50%-NaCl

3.4.3 Metabolites analysis

As for global proteomics, samples for the metabolites analysis were taken during the mid-log growth phase (Fig 3.2 and Fig S3.7). At 1.50%-NaCl, the addition of 10 mM asparagine to the medium significantly increased the intracellular pool size of most amino acids (Fig 3.4 and Table S3.7). While both asparagine and aspartate were not or barely detectable under no-salt and 1.50%-NaCl conditions, the intracellular levels of asparagine (264.43 mM) and aspartate (4.20 mM) significantly increased under the 1.50%-NaCl+Asn condition ($p \leq 0.001$, Fig 3.4). In addition, glutamate followed by glycine and serine significantly accumulated under 1.50%-NaCl+Asn relative to 1.50%-NaCl ($p \leq 0.01$, Fig 3.4 and Table S3.7). The pool sizes of glutamine and arginine were lower than that of glutamate under all three treatment conditions, but the addition of asparagine (1.50%-NaCl+Asn) significantly increased their intracellular concentration relative to 1.50%-NaCl ($p \leq 0.001$, Fig 3.4 and Table S3.7).

Analysis of the culture medium sampled at the mid-log phase showed no detectable concentration of aspartate, glutamate, glutamine, glycine, serine, or alanine under both conditions, 1.50%-NaCl and 1.50%-NaCl+Asn (Table S3.8). Asparagine was detectable only in low concentration (17.13 ± 0.69 µM) in the 1.50%-NaCl+Asn cultures but was below the detection level in the 1.5%-NaCl treatment (Table S3.8). All other amino acids were detectable under both conditions, 1.50%-NaCl and 1.50%-NaCl+Asn; with most of them in significantly larger amounts than under no-salt condition (Table S3.8). The concentration of metabolites in the culture medium was also measured under no-salt condition, but with the addition of 10 mM asparagine (no-salt+Asn) (Fig S3.3 Table S3.7, and Table S3.8). In particular, the extracellular concentrations of asparagine (628.12 ± 26.65 µM), aspartate (145.71 ± 13.18 µM), and glutamate (41.22 ± 1.45 µM) were

tremendously higher in the no-salt+Asn cultures than in the 1.5% NaCl+Asn cultures (Table S3.8). Similarly, the cellular efflux of various other amino acids into the culture medium, including alanine (19.06 ± 1.20 µM), glycine (11.5 ± 0.43 µM) and serine (7.82 ± 1.29 µM), was significantly increased compared to the 1.50%-NaCl+Asn treatment (Table S3.8).

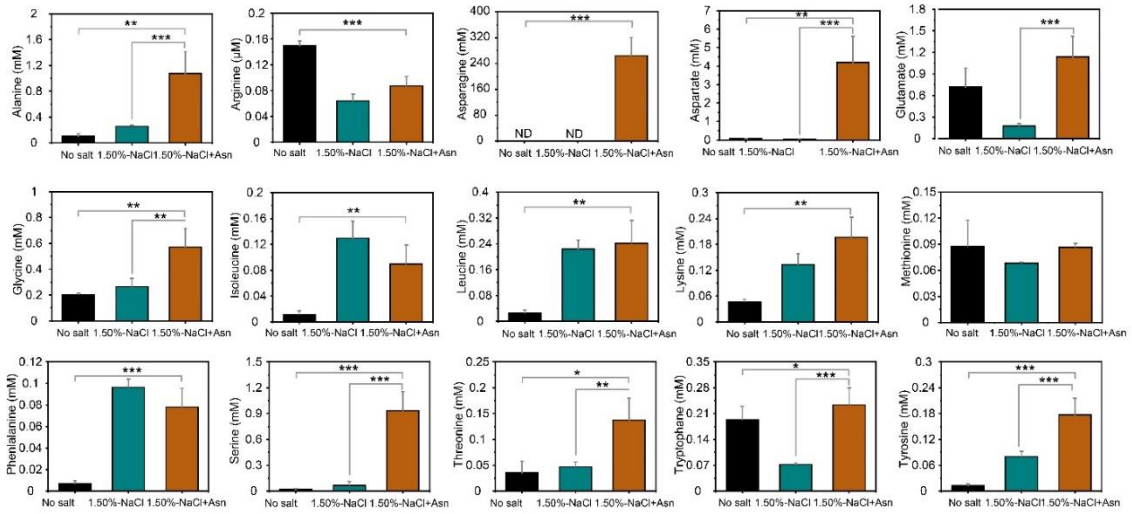

Fig 3.4 Absolute quantification of intracellular amino acids of *Methylocystis* sp. strain SC2 under the conditions of (i) no-salt, (ii) 1.50%-NaCl, and (iii) 1.50%-NaCl+Asn. SC2 biomass was collected at mid-phase phase. Asterisks indicate significant difference with **p*-value ≤ 0.05; ***p*-value ≤ 0.01; and ****p*-value ≤ 0.001, using Tukey's method with one-way ANOVA. Measurements were done in triplicate cultures. Error bars show standard deviations of triplicate cultures.

The intracellular concentrations of organic acids primarily showed a salinity (1.5% NaCl) effect (Table S3.9 and S3.10). In particular, the pool sizes of pyruvate, lactate, and glycolate tremendously declined, while those of malate and glyoxylate were nearly unaffected (Table S3.9). The addition of asparagine (1.5%-NaCl+Asn; no-salt+Asn) had no major effect on the intracellular metabolite concentrations (Table S3.9). All organic acids were detectable in the culture medium (Table S3.10).The extracellular concentrations of organic acids showed no significant difference between the 1.50%-NaCl and 1.50%-NaCl+Asn treatments (Table S3.10). The only exception was pyruvate. Its extracellular pool size was significantly greater under 1.50%-NaCl+Asn than 1.5%-NaCl ($p \leq 0.01$, Table S3.9). The cellular efflux of pyruvate was particularly high in the no-salt control, while the cellular efflux of malate into the culture medium (42.16 ± 8.66 µM) was strongly increased in the no-salt+Asn cultures relative to the other three

treatments (1.45 ± 0.01 to 1.87 ± 0.19 µM [no-salt; 1.5%-NaCl; and 1.5%-NaCl+Asn] (Table S3.10).

3.4.4 Tracing experiments with ^{13}C-labeled asparagine

The ^{13}C tracing analysis was carried out to locate metabolite fluxes that were altered by the uptake of asparagine under 1.50%-NaCl+Asn condition. No-salt+Asn was used as the reference condition. The intracellular asparagine was fully labeled, while all other amino acids and metabolites were only partially ^{13}C labeled. Most of the aspartate was ^{13}C-labeled in both treatment conditions, 1.50%-NaCl+Asn (86.2%) and no-salt+Asn (88.9%) (Fig 3.5). Glutamate ($p \leq 0.001$) and arginine ($p \leq 0.05$) were the only amino acids that showed a significantly higher degree of labeling under 1.50%-NaCl+Asn than under no-salt/Asn. The degree of labeling in glutamate was 71.8% (1.50%-NaCl+Asn) versus 41.5% (no-salt+Asn), while it was 31.9% (1.50%-NaCl+Asn) versus 23.0% (no-salt+Asn) for arginine (Fig 3.5, Table S3.11). In addition, methionine and serine showed, on average, a higher degree of labeling under 1.50%-NaCl+Asn than under no-salt/Asn, but the difference was insignificant (Fig 3.5, Table S3.11). The degree of labeling of the other intracellular amino acids was lower under 1.50%-NaCl+Asn than under no-salt/Asn, or showed no difference between the two experimental treatments (**Table S3.11**). Likely due to low pool size, the mass isotopomer distribution of proline, which is synthesized from the same precursor as arginine, could not be accurately detected in the cell extracts.

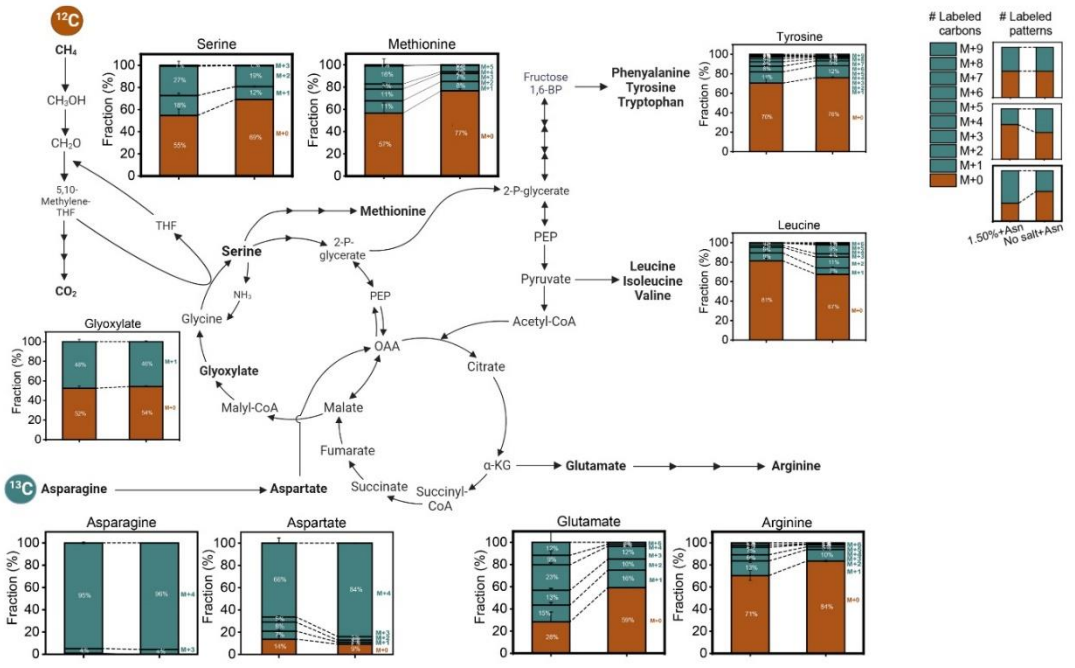

Fig 3.5 Labeling patterns of key metabolites under the conditions of 1.50%-NaCl+Asn and no-salt+Asn. Asterisks indicate significant difference with *p-value ≤ 0.05, **p-value ≤ 0.01, and ***p-value ≤ 0.001, using Tukey's method with one-way ANOVA. Measurements were done in triplicate cultures. Error bars show standard deviations of triplicate cultures.

3.5 Discussion

Various ion species can contribute to environmental salinity. Most research on the response of microorganisms to high salinity have, however, been conducted with NaCl as stressor (Osudar et al., 2017; Czech et al., 2018; Richter et al., 2019). In addition to the osmotic pressure, dissolved Na^+ and Cl^- ions can be toxic to bacterial cells by their interaction with the binding sites of the enzymes (Serrano, 1996). Alphaproteobacterial methanotrophs of the *Methylocystis* / *Methylosinus* group are known to have a low tolerance to salinity (Trotsenko and Murrell, 2008; Han et al., 2017). We confirmed that the addition of 1% and 1.25% NaCl to the medium leads to a partial inhibition of the growth of *Methylocystis* sp. strain SC2. The addition of 1.5% NaCl, to which we will refer as severe salinity, completely inhibited SC2 growth (Fig S3.1A). The low resilience of strain SC2 and other *Methylocystis* spp. to osmotic and salt stress prompted us to test a series of potential compatible solutes and osmoprotectants for their ability to have a

stress relief effect on the response of strain SC2 to partial inhibitory salinity (1% NaCl). When added in 1 mM concentration to the growth medium, asparagine and ornithine showed the greatest relief effect, while most other tested compounds had no or a negative effect (Fig S3.1B). The positive growth effect of asparagine showed to significantly increase with the amount added to the medium under severe salinity, with 10 mM asparagine having the greatest stress relief effect (Fig S3.1C). By contrast, the increase in the amount of ornithine added to the medium had even a decreasing relief effect on SC2 growth (Fig S3.1). Thus, we chose to analyze the relief effect of 10 mM asparagine with SC2 growth under severe salinity (1.5% NaCl) in greater detail. Quantitative metabolite analysis confirmed that the medium added asparagine was completely taken up by the SC2 cells within 1 to 2 days of incubation, thereby resulting in an intracellular pool size of 263.3 mM asparagine. By contrast, intracellular asparagine was nearly undetectable in SC2 cells grown with no salt (0.05 mM) or incubated with 1.5% NaCl (0.08 mM). Thus, maintenance of this very high intracellular level of asparagine was likely to be crucial for the effective acclimatization of strain SC2 to severe salinity (1.5% NaCl). In the following, we will first discuss the proteome response to severe salinity and how the proteome rearrangements were affected by the uptake of asparagine. This will be followed by a discussion of the metabolite response to unlabeled and ^{13}C-labeled asparagine, in part related to the observed proteome rearrangements.

3.5.1 The proteome of strain SC2

3.5.1.1 General aspects

Three PPI networks were constructed using the DRPs of the different treatments. The high density of the PPI networks constructed for the comparison groups 1.50%-NaCl/no-salt and 1.50%-NaCl+Asn/no-salt indicates that the protein-protein-interactions were primarily shaped by severe salinity. The high number of edges (926 respectively 907) clearly suggests that the functional roles of the DRPs were closely interrelated, which in turn governed the metabolic response to severe salinity. By contrast, the DRPs of the comparison group 1.50%-NaCl+Asn/1.50%-NaCl show a loose PPI network with a clearly less number of edges (157) than the other two PPI networks. Despite the major difference in network density, all three PPI networks were significantly enriched in DRPs affiliated with the same KEGG level 2 categories, namely energy metabolism, amino acid

metabolism, and cell growth and death. However, the proteins, whose differential regulation was specifically triggered by asparagine (1.5%-NaCl+Asn/1.5%NaCl), were not only less in number but also less closely interrelated than the proteins affected by severe salinity.

Thus, the impact of severe salinity and asparagine on the proteome rearrangements of strain SC2 greatly differed between functional categories. DRPs involved in general and oxidative stress response, but also some DRPs involved in amino acid turnover (e.g., glutamate dehydrogenase, acetlyornithine aminotransferase), primarily responded to severe salinity, with their expression level was only partly modulated by asparagine (Fig 3.6). However, the expression level of certain DRPs involved in methane oxidation, central carbon metabolism (e.g, glycine cleavage system, GCS), and synthesis of compatible solutes (i.e., ornithine cyclodeaminase), was majorly affected by asparagine (Fig 3.6). Most DRPs involved in the nitrogen metabolism were significantly downregulated in response to severe salinity (e.g., nitrogenase complex), with no significant effect of asparagine on their expression level (Fig 3.6).

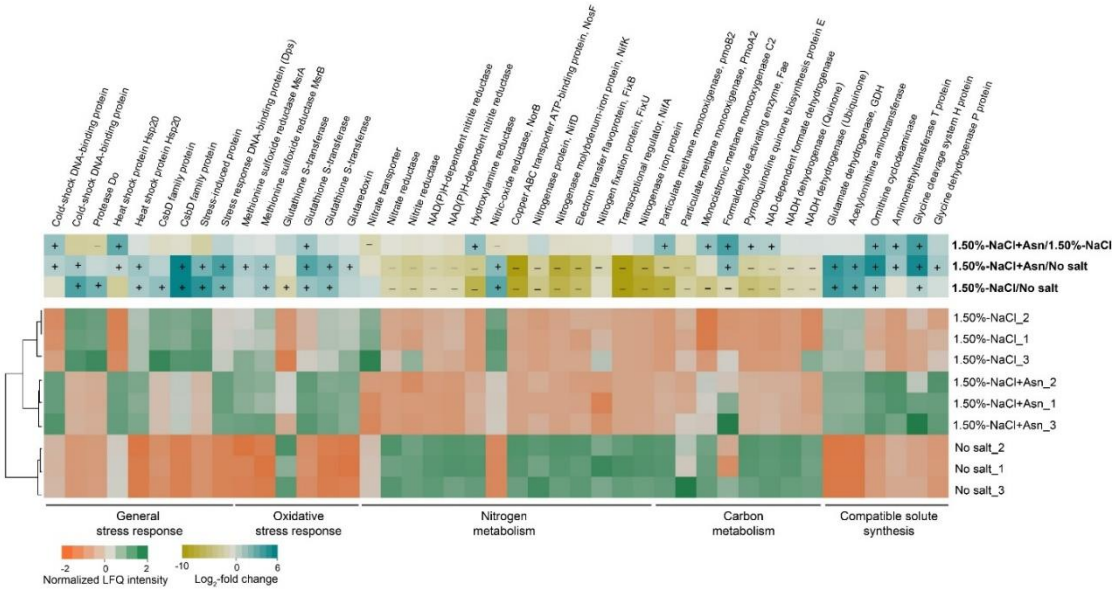

Fig 3.6 Heatmap showing proteins and functional categories differentially expressed under the conditions of no-salt, 1.50%-NaCl and 1.50%-NaCl+Asn. The protein expression values are indicated by Z-score normalized LFQ intensity values (lower panel). Log_2-fold changes are shown for the comparison groups "1.50%-NaCl/no-salt", "1.50%-NaCl+Asn/no-salt", and "1.50%-NaCl+Asn/1.50%-NaCl" (upper panel). The plus and minus symbols indicate proteins significantly up- or downregulated (log_2-fold change ≥ 1 or ≤ -1, q-value ≤ 0.01) in the respective comparison group.

3.5.1.2 General and oxidative stress

The cellular adjustment processes to severe salinity (1.5% NaCl) induced a significantly increased synthesis of stress-responsive proteins and antioxidant systems (Fig 3.6, Table S3.12). However, their increased cellular level did not promote growth unless 10 mM asparagine had been added to the medium. The expression of both the stress-induced protein (J7QHI8) and the stress response DNA-binding protein (Dps) (J7QQ02) were significantly upregulated. The stress-induced protein is known to be induced by environmental stress, but its functional role remains elusive (Iguchi et al., 2013). Dps has three intrinsic properties: DNA binding, iron sequestration, and ferroxidase activity. Thus, Dps production is crucial for bacterial cells to be able to cope with various types of stressors, including heat shock, starvation, oxidative stress, and overexposure to iron (Calhoun and Kwon, 2011; Karas et al., 2015). One CsbD protein (J7QV15) showed not only a high intracellular level but also was one of the proteins whose expression was most strongly upregulated, with a $\log_2$-fold change of 4.99 to 5.62 (4.18E+07 to ~2.05E+09). This agrees well with the results of a previous transcriptome study that had been conducted to assess the transient inhibitory effects of 0.75% NaCl on strain SC2 (Han et al., 2017) (Fig 3.6). The upregulation of these stress-responsive proteins occurs in strain SC2 regardless of the osmotic stressor (Guo et al., 2022) and follows an expression pattern that is widely distributed among bacteria (e.g., *Escherichia coli* and *Bacillus subtilis*) (Petersohn et al., 2001; Karas et al., 2015; Antipov et al., 2017).

The Hsp20 machinery prevents aggregation and misfolding of client proteins (Lindquist and Craig, 1988; Suss and Reichmann, 2015). This machinery is not only expressed upon exposure to heat shock but also in response to the toxic effects of osmotic stress (Liberek et al., 2008; Bepperling et al., 2012; Yer et al., 2018). One of two Hsp20 proteins (J7QJH1) was significantly upregulated in response to both 1.5%-NaCl/no-salt and 1.5%-NaCl+Asn/no-salt, while the second Hsp20 protein (J7QF27) belonged to those 85 DRPs that exhibited an expression reversal in response to asparagine.

Concomitantly to the upregulation of stress-responsive proteins, a great number of proteins involved in redox metabolism were significantly upregulated, including two glutathione S-transferases (GSTs), one glutaredoxin, and the peptide methionine sulfoxide reductases MsrA and MsrB (Fig 3.6, Table S3.12). GSTs have protective functions against oxidative stress and thus are widely distributed in aerobic prokaryotes

(Allocati et al., 2009). The particular increase in the expression level of two GSTs under 1.5%-NaCL+Asn conditions suggests that the asparagine-induced changes in the SC2 metabolism led to an increased presence of both reactive oxygen and nitrogen species (RONS) that needed to be transferred to reductive glutathione (GSH) and detoxified by GST activity (Allocati et al., 2009). The glutathione acts as a cofactor by glutaredoxins in cellular regulation (Vlamis-Gardikas et al., 2002). Similarly, the peptide methionine sulfoxide reductase catalyzes the reduction of methionine sulfoxide back to methionine which is particularly susceptible to oxidative species (John et al., 2001; Weissbach et al., 2002; Madeira et al., 2017).

3.5.1.3 Methane metabolism

Growth of strain SC2 under replete CH_4 conditions is due to the activity of the low-affinity pMMO1 (Baani and Liesack, 2008) and the methanol dehydrogenase (MDH). These two enzymes oxidize CH_4 first to methanol (pMMO1) and then to formaldehyde (MDH). The expression of its subunits (PmoCAB1) was not affected by severe salinity, regardless of whether asparagine had been added to the medium (Fig 3.6, Table S3.12). Presumably, the pMMO1 is one of the "housekeeping" enzymes whose expression level is generally maintained under osmotic and salt stress as it also was not differentially regulated in response to increasing NH_4Cl stress (Guo et al., 2022). This in contrast to subunits (PmoA2, PmoB2) of the high-affinity pMMO2 and the chromosome-encoded monocistronic $PmoC2_{Gs}$ whose expression responded to NaCl stress (Fig 3.6, Table S3.12). While the expression of the calcium-dependent MDH is not differentially regulated in response to increasing NaCl stress (Han et al., 2017; this study), increasing NH_4Cl stress induced an upregulation of the MDH complex; with the latter likely to overcome the toxic effect of hydroxylamine (Guo et al., 2022). The resulting formaldehyde can be either assimilated into cell carbon or further oxidized to gain energy for growth (Marx et al., 2005; Vorobev et al., 2014). While tetrahydromethanopterin (H_4MPT) is a crucial cofactor for direct oxidation of formaldehyde to formate, tetrahydrofolate (H_4F) (THF) acts a formaldehyde acceptor required for carbon assimilation via the serine cycle (Vorholt, 2002; Karthikeyan et al., 2015). The formaldehyde-activating enzyme (Fae) catalyzes the condensation of formaldehyde with methylene-H_4MPT, while formate dehydrogenase (FDH) catalyzes the terminal step of methane oxidation, thereby yielding redox equivalents ($NADH/H^+$) and CO_2 (Vorholt et

al., 2000). Both enzymes, Fae and FDH, were strongly downregulated in response to severe salt stress, but belonged to the 85 DRPs that showed an expression reversal after the addition of asparagine; thereby leading to a significant upregulation in the comparison group 1.5% NaCl+Asn/1.5%-NaCl (Fig 3.6, Table S3.12). Thus, while the expression of the C1 assimilation pathway was not differentially regulated, asparagine addition had a significant relief effect on the downregulation of the energy-yielding reactions involved in the oxidation of fomaldehyde to carbon dioxide via formate.

3.5.1.4 Nitrogen metabolism

Strain SC2 has been shown to be able to efficiently fix dinitrogen, in particular with a concentration of 8% to 10% oxygen in the culture headspace (Dam et al., 2014). The expression level of the nitrogenase complex, however, was relatively low already under no-salt condition due to the supply of 10 mM NO_3^- in the growth medium. Nonetheless, the expression of various proteins of the nitrogenase complex (e.g., NifD, NifK) was more than tenfold downregulated in response to severe salinity with no effect by asparagine (Fig 3.6, Table S3.12). Noteworthy, the nitrate transporter (UniProt ID J7Q4T7) showed, despite the presence of 10 mM nitrate in the culture medium, a specific downregulation in the comparison group 1.5%-NaCl+Asn/1.5%-NaCl (Fig 3.6, Table S3.12). This transporter is known to be transcriptionally and post-translationally regulated by intracellular ammonium (Rice and Tiedje, 1989). This led us speculate that its downregulation may be due an asparagine-derived nitrogen supply. Indeed, the results of our metabolites analysis evidenced sufficient nitrogen supply for growth of strain SC2 under severe salinity by the enzymatic hydrolysis of asparagine to aspartate (Meister, 1974) (**see section 4.3,** Fig 3.6, Table S3.12). Another noteworthy aspect is that the chromosome-encoded hydroxylamine reductase (Hcp, UniProt ID J7Q787) exhibited a specific upregulation in the comparison group 1.5%-NaCl+Asn/1.5% NaCl (Fig 3.6, Table S3.12). Most recent research, however, suggests that among other possible functions, the most likely physiological role of Hcp is the conversion of NO to N_2O (NO reductase activity) (Hagen et al., 2022).

3.5.1.5 Cell divisions

Severe salinity (1.5% NaCl) led to a significant downregulation of nearly all identified cell division proteins (Table S3.12), in good agreement with the knowledge that signaling

cascades induced by abiotic stress halt cell cycle progression through inhibiting the transcription process (Nepal and Kumar, 2020). In consequence, the growth of strain SC2 was completely inhibited under severe salinity (Fig 3.2). However, the addition of asparagine (1.5%-NaCl+Asn) specifically affected the differential regulation of various proteins involved in cell division, including the two-component transcriptional regulator (CtrA), the HPTransfase domain-containing protein (ChpT), the multi-sensor signal transduction histidine kinase (PleC), the ATP-dependent zinc metalloprotease (FtsH), and the cell division protein (FtsA). In consequence, these proteins showed a significant upregulation in the comparison group 1.5%-NaCl+Asn/1.5%-NaCl (Table S3.12).

The two-component transcriptional regulator (CtrA) is the key cell cycle regulator. Under optimal growth conditions, the membrane-bound multi-sensor hybrid histidine kinase (CckA) activates CtrA via the HPTransfase domain-containing protein (ChpT), with the latter responding to spatiotemporal cues that trigger the expression of genes required for cell division (Biondi et al., 2006; Iniesta et al., 2006). In addition, PleC, a phosphatase, plays a pivotal role in the developmental program by keeping cell cycle response regulator DivK and PleD phosphorylation levels low during G1 phase of the cell cycle, thereby preventing premature CtrA inactivation (Coppine et al., 2020).

The FtsH protease is highly sensitive to elevated salt concentrations (Deuerling et al., 1997). FtsH is unique owing to its anchoring to the inner membrane. It is a structural homologue of tubulin and known to polymerize into protofilaments at the division site. It participates, for example, in the cell division initiation in *Escherichia coli* and *Caulobacter crescentus* (Tomoyasu et al., 1995; Fischer et al., 2002; Langklotz et al., 2012). The absence of FtsH protease led to a severe cell division phenotype and sporulation defect in *C. crescentus*, emphasizing the sensitive response of the FtsH protease to salt stress (Fischer et al., 2002). The FtsA protein is the most highly conserved actin-related protein of the divisome and recruits the FtsZ protein to the membrane (Ma and Margolin, 1999; Loose and Mitchison, 2014; Mahone and Goley, 2020).

Thus, the addition of asparagine under severe salinity partly restored the intricate coordination between ChpT, CtrA, and Plec and in consequence the cell division process by increased relative expression of the FtsA and FtsH proteins, all of which corresponds well to the partial recovery of cell growth and biomass production. In good agreement, the enzyme alanine racemase was significantly upregulated in response to asparagine

addition. This enzyme converts L-alanine into D-alanine that is used for peptidoglycan synthesis.

3.5.2 The metabolome of strain SC2

The import of compounds that are compatible with cell physiology at high internal concentrations is a well-known capability of soil bacteria (e.g., *Bacillus* spp.) (Bremer and Kramer, 2019). This raised the question of whether non-saline methanotrophs, such as our model organism *Methylocystis* sp. strain SC2, are able to take up compatible solutes from the environment to enhance stress resilience under otherwise osmotically unfavorable NaCl conditions (Han et al., 2017; Leon et al., 2018; Sun et al., 2022). The addition of asparagine to the medium under severe salt stress (1.5% NaCl) significantly altered both exo-metabolome and the intracellular concentrations of various central carbon metabolites and free amino acids. Indeed, asparagine (264.43 ± 56.71 mM) was taken up quantitatively by strain SC2 under severe salt stress (1.5% NaCl), while the uptake of asparagine was significantly less under no-salt+Asn condition (202.29 ± 31.63 mM). The hydrolysis of asparagine to aspartate resulted in a high pool size of free intracellular aspartate (4.20 ± 1.41 mM). The released amino groups may have favored the conversion of α-ketoglutarate into glutamate by increased GDH activity, thereby explaining, in part, the strong accumulation of free glutamate (Meister, 1974).

The extracellular and intracellular concentrations of pyruvate were similar under all three treatment conditions (1.50%-NaCl, 1.50%-NaCl+Asn, no-salt+Asn), but significantly lower than in the no-salt control (**Table S3.9, Table S3.10**). Noteworthily, while undectable (1.50%-NaCl+Asn) or nearly undetectable (no-salt+Asn), intracellular pyruvate showed a high labeling degree (>70%) with ^{13}C-carbon, thereby suggesting a very low pool size but rapid turnover of pyruvate. The latter is corroborated by significantly increased expression of the pyruvate dehydrogenase complex under 1.5%-NaCl+Asn condition. This includes the acetyl-transferring E1 component (alpha and beta subunit) and the dihydrolipoyllysine-residue acetyltransferase [E2 component]) (Table S.3.12). This enzyme complex catalyses the irreversible carboxylation of pyruvate to acetyl-CoA plus CO_2 and thus feeds the citric acid cycle.

Oxaloacetate, an intermediate that replenishes both the TCA cycle and the serine cycle, is converted into malate which is subsequently used for the formation of malyl-

CoA by the activities of malate dehydrogenase and malate kinase (Vorobev et al., 2014; Chistoserdova, 2017). Then, malyl-CoA is cleaved into acetyl-CoA and glyoxylate by malyl-CoA lyase in the ethylmalonyl-CoA (EMC) pathway (Schneider et al., 2012). The high ^{13}C-carbon labeling degree of malate and glyoxylate indicates that a major portion of the asparagine was assimilated via TCA cycle and EMC pathway (Fig 3.5, Tables S3.11). This conclusion is further supported by the high excretion of malate into the medium under no-salt+Asn (42.16 µM) condition, but not under 1.50%-NaCl+Asn (1.69 µM) condition.

The composition of both exo- and intra-metabolome indicates that in addition to aspartate, high cytosolic pool sizes of glutamate, glycine, serine, and alanine were crucial for the stress relief effect of asparagine (Figs 3.4, 3.5; Tables S3.7, S3.8). This is particularly evidenced by the high excretion level of these amino acids under no-salt+Asn condition, while they were undetectable (glutamate, glycine, serine, alanine) or nearly not detectable (asparagine, 17.13 ± 0.69 µM) in the exo-bolome under 1.5%-NaCl+Asn condition (Table S3.8).

Under no-salt condition, the growth yield of strain SC2 was 7.35 (mg CDW/mmol CH_4), which agrees well with the maximum value that can be theoretically obtained with methane as sole source of carbon and energy (Bordel et al., 2019; Hakobyan et al., 2020). Intriguingly, we observed under 1.5%-NaCl+Asn condition an even greater methane-based growth yield than for standard growth condition without salt and asparagine (Fig S3.5). Thus, it is reasonable to conclude that in addition to methane, asparagine contributed as a supplemental carbon source to the partial growth recovery of strain SC2 under severe salinity. This conclusion is further corroborated by the incorporation of asparagine-derived ^{13}C-carbon into nearly all canonical amino acids (Fig 3.5; Table S3.11).

3.6 Final Remarks

In this work, we provide new insights into the metabolic potential of *Methylocystis* sp. strain SC2 to cope with severe salt stress. The relief effect of asparagine under otherwise completely inhibitory NaCl stress is a novel and unexpected finding. The uptake of asparagine led to a partial growth recovery with half of the biomass produced under standard growth condition. The tracing experiment with ^{13}C-labeled asparagine allowed

us to identify those organic acids (e.g., pyruvate, malate, glyoxylate) and amino acids (e.g., aspartate, glutamate, glycine, serine, alanine) whose intracellular pools were most affected by the uptake of asparagine. In particular, the high ^{13}C-labeling degree of glutamate suggests that it acted as a major hub between central carbon and amino acid pathways. However, our current research data may be insufficient to draw definite conclusions about how the asparagine uptake changed the flux of metabolites through these pathways. This would require additional research, such as metabolite flux measurements coupled to ^{13}C-labeling experiments with both methane and asparagine. Finally, we found that not only asparagine but also the amino acids ornithine, lysine, and alanine had a stress relief effect on strain SC2 under osmotically unfavorable conditions (1.0% NaCl). Thus, a comparative analysis of their stress relief effects on the proteomic and metabolomic level would be of interest. This should also address the question of whether these amino acids can act under severe salinity as the only external nitrogen source, in addition to their stress relief effect.

3.7 References

Allocati, N., Federici, L., Masulli, M., and Di Ilio, C. (2009) Glutathione transferases in bacteria. *FEBS J* **276**: 58-75.

Antipov, S., Turishchev, S., Purtov, Y., Shvyreva, U., Sinelnikov, A., Semov, Y. et al. (2017) The Oligomeric Form of the Escherichia coli Dps Protein Depends on the Availability of Iron Ions. *Molecules* **22**.

Baani, M., and Liesack, W. (2008) Two isozymes of particulate methane monooxygenase with different methane oxidation kinetics are found in *Methylocystis* sp. strain SC2. *Proceedings of the National Academy of Sciences* **105**: 10203-10208.

Bastian, M., Heymann, S., and Jacomy, M. (2009) Gephi: An open source software for exploring and manipulating networks. *Proceedings of the International AAAI Conference on Web and Social Media* **3**.

Bepperling, A., Alte, F., Kriehuber, T., Braun, N., Weinkauf, S., Groll, M. et al. (2012) Alternative bacterial two-component small heat shock protein systems. *Proceedings of the National Academy of Sciences* **109**: 20407-20412.

Biondi, E.G., Reisinger, S.J., Skerker, J.M., Arif, M., Perchuk, B.S., Ryan, K.R., and Laub, M.T. (2006) Regulation of the bacterial cell cycle by an integrated genetic circuit. *Nature* **444**: 899-904.

Bordel, S., Rodríguez, Y., Hakobyan, A., Rodríguez, E., Lebrero, R., and Muñoz, R. (2019) Genome scale metabolic modeling reveals the metabolic potential of three Type II methanotrophs of the genus Methylocystis. *Metabolic Engineering* **54**: 191-199.

Bremer, E. (2000) Coping with osmotic challenges: osmoregulation through accumulation and release of compatible solutes in *B. subtilis*. *Comparative Biochemistry and Physiology Part A: Molecular & Integrative Physiology* **126**: 17.

Bremer, E., and Kramer, R. (2019) Responses of microorganisms to osmotic stress. *Annu Rev Microbiol* **73**: 313-334.

Cai, Y., Zheng, Y., Bodelier, P.L.E., Conrad, R., and Jia, Z. (2016) Conventional methanotrophs are responsible for atmospheric methane oxidation in paddy soils. *Nature Communications* **7**: 11728.

Calhoun, L.N., and Kwon, Y.M. (2011) Structure, function and regulation of the DNA-binding protein Dps and its role in acid and oxidative stress resistance in Escherichia coli: a review. *J Appl Microbiol* **110**: 375-386.

Chistoserdova, L. (2017) Application of Omics Approaches to Studying Methylotrophs and Methylotroph Communities. *Curr Issues Mol Biol* **24**: 119-142.

Conrad, R. (2009) The global methane cycle: recent advances in understanding the microbial processes involved. *Environ Microbiol Rep* **1**: 285-292.

Coppine, J., Kaczmarczyk, A., Petit, K., Brochier, T., Jenal, U., and Hallez, R. (2020) Regulation of Bacterial Cell Cycle Progression by Redundant Phosphatases. *Journal of Bacteriology* **202**: e00345-00320.

Czech, L., Hermann, L., Stoveken, N., Richter, A.A., Hoppner, A., Smits, S.H.J. et al. (2018) Role of the Extremolytes Ectoine and Hydroxyectoine as Stress Protectants and Nutrients: Genetics, Phylogenomics, Biochemistry, and Structural Analysis. *Genes (Basel)* **9**.

Dam, B., Dam, S., Kim, Y., and Liesack, W. (2014) Ammonium induces differential expression of methane and nitrogen metabolism-related genes in *Methylocystis* sp strain SC2. *Environmental Microbiology* **16**: 3115-3127.

Dam, B., Dam, S., Kube, M., Reinhardt, R., and Liesack, W. (2012) Complete Genome Sequence of Methylocystis sp. Strain SC2, an Aerobic Methanotroph with High-Affinity Methane Oxidation Potential. *Journal of Bacteriology* **194**: 6008-6009.

de Vries, S.T., Yilmaz, S., Bar-Even, A., Claassens, N.J., Bordanaba-Florit, G., Cotton, C.A.R. et al. (2020) Replacing the Calvin cycle with the reductive glycine pathway in Cupriavidus necator. *Metabolic Engineering* **62**: 30-41.

Deng, Y., Liu, Y., Dumont, M., and Conrad, R. (2017) Salinity Affects the Composition of the Aerobic Methanotroph Community in Alkaline Lake Sediments from the Tibetan Plateau. *Microbial Ecology* **73**: 101-110.

Deng, Y., Che, R., Wang, F., Conrad, R., Dumont, M., Yun, J. et al. (2019) Upland Soil Cluster Gamma dominates methanotrophic communities in upland grassland soils. *Science of The Total Environment* **670**: 826-836.

Deuerling, E., Mogk, A., Richter, C., Purucker, M., and Schumann, W. (1997) The ftsH gene of Bacillus subtilis is involved in major cellular processes such as sporulation, stress adaptation and secretion. *Molecular Microbiology* **23**: 921-933.

Fischer, B., Rummel, G., Aldridge, P., and Jenal, U. (2002) The FtsH protease is involved in development, stress response and heat shock control in Caulobacter crescentus. *Mol Microbiol* **44**: 461-478.

Glatter, T., Ludwig, C., Ahrné, E., Aebersold, R., Heck, A.J.R., and Schmidt, A. (2012) Large-scale quantitative assessment of different in-solution protein digestion protocols reveals superior cleavage efficiency of tandem Lys-C/Trypsin proteolysis over trypsin digestion. *Journal of Proteome Research* **11**: 5145-5156.

Goedhart, J., and Luijsterburg, M.S. (2020) VolcaNoseR is a web app for creating, exploring, labeling and sharing volcano plots. *Scientific Reports* **10**: 20560.

Gontijo, J.B.A.U.P.F.S.A.U.V.A.M.A.U.M.J.A.A.U.B.P.L.E. (2022). [WWW document].

Gunde-Cimerman, N., Plemenitaš, A., and Oren, A. (2018) Strategies of adaptation of microorganisms of the three domains of life to high salt concentrations. *FEMS Microbiol Rev* **42**: 353-375.

Hahne, H., Mäder, U., Otto, A., Bonn, F., Steil, L., Bremer, E. et al. (2010) A comprehensive proteomics and transcriptomics analysis of Bacillus subtilis salt stress adaptation. *Journal of bacteriology* **192**: 870-882.

Hakobyan, A., Liesack, W., and Glatter, T. (2018) Crude-MS strategy for in-depth proteome analysis of the methane-oxidizing *Methylocystis* sp. strain SC2. *J Proteome Res* **17**: 3086-3103.

Hakobyan, A., Zhu, J., Glatter, T., Paczia, N., and Liesack, W. (2020) Hydrogen utilization by *Methylocystis* sp. strain SC2 expands the known metabolic versatility of type IIa methanotrophs. *Metabolic Engineering* **61**: 181-196.

Han, D., Link, H., and Liesack, W. (2017) Response of Methylocystis sp. Strain SC2 to Salt Stress: Physiology, Global Transcriptome, and Amino Acid Profiles. *Appl Environ Microbiol* **83**: e00866-00817.

Harper, C.J., Hayward, D., Kidd, M., Wiid, I., and van Helden, P. (2010) Glutamate dehydrogenase and glutamine synthetase are regulated in response to nitrogen availability in Myocbacterium smegmatis. *BMC Microbiology* **10**: 138.

Heyer, J., Galchenko, V.F., and Dunfield, P.F. (2002) Molecular phylogeny of type II methane-oxidizing bacteria isolated from various environments. *Microbiology-Sgm* **148**: 2831-2846.

Ho, A., Mo, Y.L., Lee, H.J., Sauheitl, L., Jia, Z.J., and Horn, M.A. (2018) Effect of salt stress on aerobic methane oxidation and associated methanotrophs; a microcosm study of a natural community from a non-saline environment. *Soil Biol Biochem* **125**: 210-214.

Hoffmann, T., Bleisteiner, M., Sappa, P.K., Steil, L., Mader, U., Volker, U., and Bremer, E. (2017) Synthesis of the compatible solute proline by Bacillus subtilis: point mutations rendering the osmotically controlled proHJ promoter hyperactive. *Environmental Microbiology* **19**: 3700-3720.

Iguchi, H., Sato, I., Yurimoto, H., and Sakai, Y. (2013) Stress resistance and C1 metabolism involved in plant colonization of a methanotroph Methylosinus sp. B4S. *Archives of Microbiology* **195**: 717-726.

Iniesta, A.A., McGrath, P.T., Reisenauer, A., McAdams, H.H., and Shapiro, L. (2006) A phospho-signaling pathway controls the localization and activity of a protease complex critical for bacterial cell cycle progression. *Proceedings of the National Academy of Sciences* **103**: 10935-10940.

John, G.S., Brot, N., Ruan, J., Erdjument-Bromage, H., Tempst, P., Weissbach, H., and Nathan, C. (2001) Peptide methionine sulfoxide reductase from *Escherichia coli* and *Mycobacterium tuberculosis* protects bacteria against oxidative damage from reactive nitrogen intermediates. *Proceedings of the National Academy of Sciences* **98**: 9901-9906.

Jung, G.Y., Rhee, S.K., Han, Y.S., and Kim, S.J. (2020) Genomic and Physiological Properties of a Facultative Methane-Oxidizing Bacterial Strain of Methylocystis sp. from a Wetland. *Microorganisms* **8**.

Karas, V.O., Westerlaken, I., and Meyer, A.S. (2015) The DNA-Binding Protein from Starved Cells (Dps) Utilizes Dual Functions To Defend Cells against Multiple Stresses. *J Bacteriol* **197**: 3206-3215.

Karthikeyan, O.P., Chidambarampadmavathy, K., Cirés, S., and Heimann, K. (2015) Review of Sustainable Methane Mitigation and Biopolymer Production. *Crit Rev Environ Sci Technol* **45**: 1579-1610.

Khmelenina, V.N., Kalyuzhnaya, M.G., Sakharovsky, V.G., Suzina, N.E., Trotsenko, Y.A., and Gottschalk, G. (1999) Osmoadaptation in halophilic and alkaliphilic methanotrophs. *Archives of Microbiology* **172**: 321-329.

Kikuchi, G., Motokawa, Y., Yoshida, T., and Hiraga, K. (2008) Glycine cleavage system: reaction mechanism, physiological significance, and hyperglycinemia. *Proceedings of the Japan Academy Series B-Physical and Biological Sciences* **84**: 246-263.

Knief, C., and Dunfield, P.F. (2005) Response and adaptation of different methanotrophic bacteria to low methane mixing ratios. *Environmental Microbiology* **7**: 1307-1317.

Kohlstedt, M., Sappa, P.K., Meyer, H., Maaß, S., Zaprasis, A., Hoffmann, T. et al. (2014) Adaptation of Bacillus subtilis carbon core metabolism to simultaneous nutrient limitation and osmotic challenge: a multi-omics perspective. *Environ Microbiol* **16**: 1898-1917.

Kolb, S., Knief, C., Dunfield, P.F., and Conrad, R. (2005) Abundance and activity of uncultured methanotrophic bacteria involved in the consumption of atmospheric methane in two forest soils. *Environmental Microbiology* **7**: 1150-1161.

Langklotz, S., Baumann, U., and Narberhaus, F. (2012) Structure and function of the bacterial AAA protease FtsH. *Biochimica et Biophysica Acta (BBA) - Molecular Cell Research* **1823**: 40-48.

Leon, M.J., Hoffmann, T., Sanchez-Porro, C., Heider, J., Ventosa, A., and Bremer, E. (2018) Compatible Solute Synthesis and Import by the Moderate Halophile Spiribacter salinus: Physiology and Genomics. *Frontiers in Microbiology* **9**.

Liberek, K., Lewandowska, A., and Zietkiewicz, S. (2008) Chaperones in control of protein disaggregation. *EMBO J* **27**: 328-335.

Lindquist, S., and Craig, E.A. (1988) THE HEAT-SHOCK PROTEINS. *Annu Rev Genet* **22**: 631-677.

Loose, M., and Mitchison, T.J. (2014) The bacterial cell division proteins FtsA and FtsZ self-organize into dynamic cytoskeletal patterns. *Nat Cell Biol* **16**: 38-46.

Lozupone, C.A., and Knight, R. (2007) Global patterns in bacterial diversity. *Proceedings of the National Academy of Sciences* **104**: 11436-11440.

Ludwig, W., Strunk, O., Westram, R., Richter, L., Meier, H., Yadhukumar, a. et al. (2004) ARB: a software environment for sequence data. *Nucleic acids research* **32**: 1363-1371.

Ma, X., and Margolin, W. (1999) Genetic and Functional Analyses of the Conserved C-Terminal Core Domain of Escherichia coli FtsZ. *Journal of Bacteriology* **181**: 7531-7544.

Madeira, J.P., Alpha-Bazin, B.M., Armengaud, J., and Duport, C. (2017) Methionine Residues in Exoproteins and Their Recycling by Methionine Sulfoxide Reductase AB Serve as an Antioxidant Strategy in Bacillus cereus. *Frontiers in Microbiology* **8**.

Mahone, C.R., and Goley, E.D. (2020) Bacterial cell division at a glance. *J Cell Sci* **133**.

Mandal, M., Lee, M., Barrick, J.E., Weinberg, Z., Emilsson, G.M., Ruzzo, W.L., and Breaker, R.R. (2004) A glycine-dependent riboswitch that uses cooperative binding to control gene expression. *Science* **306**: 275-279.

Marx, C.J., Van Dien, S.J., and Lidstrom, M.E. (2005) Flux analysis uncovers key role of functional redundancy in formaldehyde metabolism. *PLoS Biol* **3**: 244-253.

Meister, A. (1974) 17. Asparagine Synthesis. In *The Enzymes*. Boyer, P.D. (ed): Academic Press, pp. 561-580.

Moe, L.A. (2013) Amino acids in the rhizosphere: from plants to microbes. *Am J Bot* **100**: 1692-1705.

Nepal, S., and Kumar, P. (2020). Growth, Cell Division, and Gene Expression of Escherichia coli at Elevated Concentrations of Magnesium Sulfate: Implications for Habitability of Europa and Mars [WWW document].

Osudar, R., Klings, K.W., Wagner, D., and Bussmann, I. (2017) Effect of salinity on microbial methane oxidation in freshwater and marine environments. *Aquatic Microbial Ecology* **80**: 181-192.

Osudar, R., Klings, K.W., Wagner, D., and Bussmann, I. (2018) Effect of salinity on microbial methane oxidation in freshwater and marine environments. *Aquatic Microbial Ecology* **80**: 181-192.

Petersohn, A., Brigulla, M., Haas, S., Hoheisel, J.D., Volker, U., and Hecker, M. (2001) Global analysis of the general stress response of Bacillus subtilis. *Journal of Bacteriology* **183**: 5617-5631.

Prather, M.J., and Holmes, C.D. (2017) Overexplaining or underexplaining methane's role in climate change. *Proceedings of the National Academy of Sciences* **114**: 5324.

Reitzer, L. (2004) Biosynthesis of Glutamate, Aspartate, Asparagine,L-Alanine, and D-Alanine. *EcoSal Plus* **1**.

Reshetnikov, A.S., Khmelenina, V.N., and Trotsenko, Y.A. (2006) Characterization of the ectoine biosynthesis genes of haloalkalotolerant obligate methanotroph "Methylomicrobium alcaliphilum 20Z". *Archives of Microbiology* **184**: 286-297.

Riba, L., Becerril, B., Servingonzalez, L., Valle, F., and Bolivar, F. (1988) Identification of a Functional Promoter for the Escherichia-Coli Gdha Gene and Its Regulation. *Gene* **71**: 233-246.

Rice, C.W., and Tiedje, J.M. (1989) Regulation of nitrate assimilation by ammonium in soils and in isolated soil microorganisms. *Soil Biol Biochem* **21**: 597-602.

Richter, A.A., Mais, C.N., Czech, L., Geyer, K., Hoeppner, A., Smits, S.H.J. et al. (2019) Biosynthesis of the Stress-Protectant and Chemical Chaperon Ectoine: Biochemistry of the Transaminase EctB. *Frontiers in Microbiology* **10**.

Schneider, K., Peyraud, R., Kiefer, P., Christen, P., Delmotte, N., Massou, S. et al. (2012) The Ethylmalonyl-CoA Pathway Is Used in Place of the Glyoxylate Cycle by Methylobacterium extorquens AM1 during Growth on Acetate*. *Journal of Biological Chemistry* **287**: 757-766.

Serrano, R. (1996) Salt tolerance in plants and microorganisms: toxicity targets and defense responses. *Int Rev Cytol* **165**: 1-52.

Smirnova, G.V., Krasnykh, T.A., and Oktyabrsky, O.N. (2001) Role of Glutathione in the Response of *Escherichia coli* to Osmotic Stress. *Biochemistry (Moscow)* **66**: 973-978.

Sun, X.X., Zhao, J., Zhou, X., Bei, Q.C., Xia, W.W., Zhao, B.Z. et al. (2022) Salt tolerance-based niche differentiation of soil ammonia oxidizers. *Isme Journal* **16**: 412-422.

Suss, O., and Reichmann, D. (2015) Protein plasticity underlines activation and function of ATP-independent chaperones. *Front Mol Biosci* **2**: 43.

Täumer, J., Marhan, S., Groß, V., Jensen, C., Kuss, A.W., Kolb, S., and Urich, T. (2022) Linking transcriptional dynamics of CH4-cycling grassland soil microbiomes to seasonal gas fluxes. *The ISME Journal* **16**: 1788-1797.

Tchawa Yimga, M., Dunfield Peter, F., Ricke, P., Heyer, J., and Liesack, W. (2003) Wide Distribution of a Novel pmoA-Like Gene Copy among Type II Methanotrophs, and Its Expression in Methylocystis Strain SC2. *Applied and Environmental Microbiology* **69**: 5593-5602.

Tomoyasu, T., Gamer, J., Bukau, B., Kanemori, M., Mori, H., Rutman, A.J. et al. (1995) Escherichia coli FtsH is a membrane-bound, ATP-dependent protease which degrades the heat-shock transcription factor sigma 32. *Embo j* **14**: 2551-2560.

Vlamis-Gardikas, A., Potamitou, A., Zarivach, R., Hochman, A., and Holmgren, A. (2002) Characterization of Escherichia coli Null Mutants for Glutaredoxin 2. *Journal of Biological Chemistry* **277**: 10861-10868.

Vorholt, J.A. (2002) Cofactor-dependent pathways of formaldehyde oxidation in methylotrophic bacteria. *Arch Microbiol* **178**: 239-249.

Vorholt, J.A., Marx, C.J., Lidstrom, M.E., and Thauer, R.K. (2000) Novel Formaldehyde-Activating Enzyme in *Methylobacterium extorquens* AM1 Required for Growth on Methanol. *Journal of Bacteriology* **182**: 6645-6650.

Vorobev, A., Jagadevan, S., Jain, S., Anantharaman, K., Dick Gregory, J., Vuilleumier, S., and Semrau Jeremy, D. (2014) Genomic and Transcriptomic Analyses of the Facultative Methanotroph Methylocystis sp. Strain SB2 Grown on Methane or Ethanol. *Applied and Environmental Microbiology* **80**: 3044-3052.

Weissbach, H., Etienne, F., Hoshi, T., Heinemann, S.H., Lowther, W.T., Matthews, B. et al. (2002) Peptide Methionine Sulfoxide Reductase: Structure, Mechanism of Action, and Biological Function. *Archives of Biochemistry and Biophysics* **397**: 172-178.

Williams, V. (2010) Identifying the economic effects of salt water intrusion after Hurricane Katrina. *Journal of Sustainable Development* **3**: 29-37.

Yang, S., Matsen, J.B., Konopka, M., Green-Saxena, A., Clubb, J., Sadilek, M. et al. (2013) Global Molecular Analyses of Methane Metabolism in Methanotrophic Alphaproteobacterium, Methylosinus trichosporium OB3b. Part II. Metabolomics and 13C-Labeling Study. *Front Microbiol* **4**: 70.

Yer, E.N., Baloglu, M.C., and Ayan, S. (2018) Identification and expression profiling of all Hsp family member genes under salinity stress in different poplar clones. *Gene* **678**: 324-336.

Zaprasis, A., Bleisteiner, M., Kerres, A., Hoffmann, T., and Bremer, E. (2015) Uptake of Amino Acids and Their Metabolic Conversion into the Compatible Solute Proline Confers Osmoprotection to *Bacillus subtilis*. *Applied and Environmental Microbiology* **81**: 250-259.

3.8 Supplemental information

3.8.1 Supplemental figures

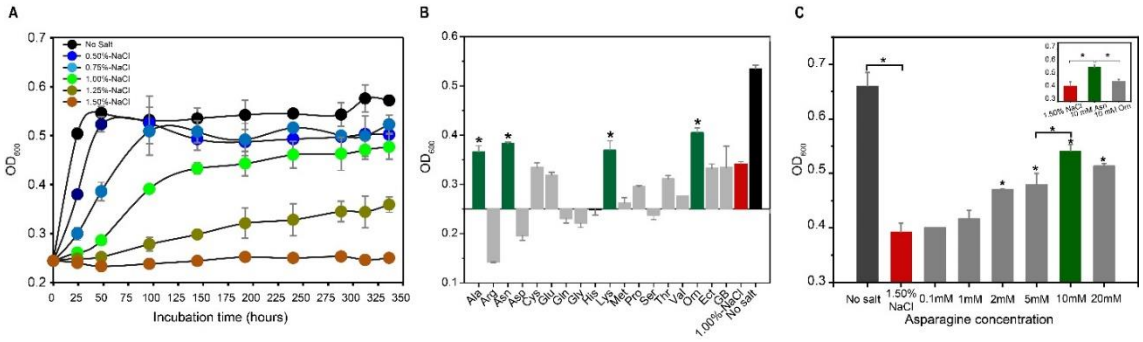

Fig S3.1 Effect of increasing NaCl stress (A), potential osmoprotectants (B), and increasing asparagine concentrations (C) on the growth of Methylocystis sp. strain SC2. (A) The growth dynamics of strain SC2 were repeatedly monitored at OD_{600} during the whole incubation period. The starting OD_{600} was 0.25. (B) The effect of potential osmoprotectants (1 mM) was tested using 1.0% NaCl in the medium. The starting OD_{600} was 0.21. The osmoprotective effect of each compound was assessed using OD_{600} measurements after an incubation period of 88 h. (C) The concentration triggering the greatest osmoprotective effect of asparagine was tested using 1.50%-NaCl in the medium. Incubations with no salt and 1.50% NaCl in the medium were used as controls. The starting OD_{600} was 0.40. Measurements were done in triplicate cultures. Error bars show standard deviations of triplicate cultures.

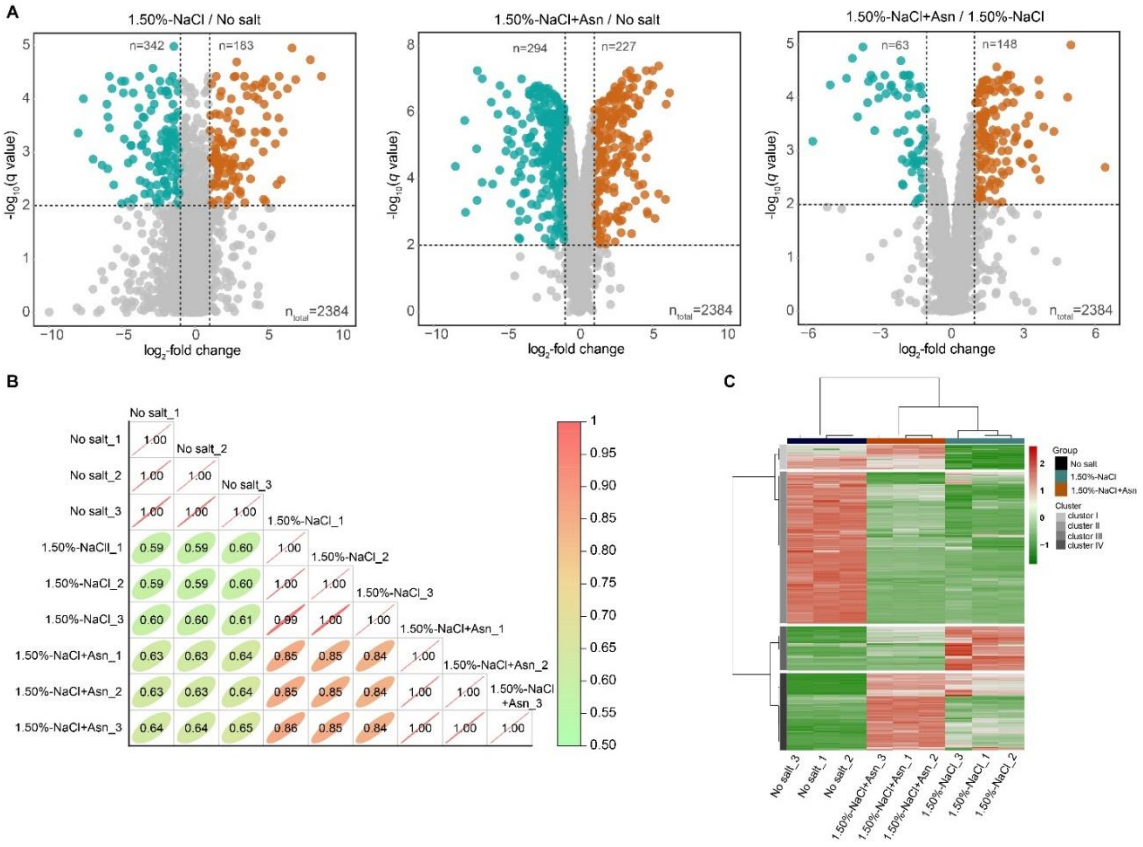

Fig S3.2 Differential protein expression in response to high-salinity condition with and without the addition of 10 mM asparagine (no-salt vs. 1.5%-NaCl vs. 1.50%-NaCl+Asn). (A) Volcano plots of total proteome, showing the differential expression of proteins under the conditions of no-salt, 1.50%-NaCl, and 1.50%-NaCl+Asn. (B) Pearson correlation coefficient (PCC) matrix of the three treatment conditions. The correlation coefficient is indicated by colors and numbers. (C) Hierarchical cluster analysis summarizing the differential expression modes of identified DRPs.

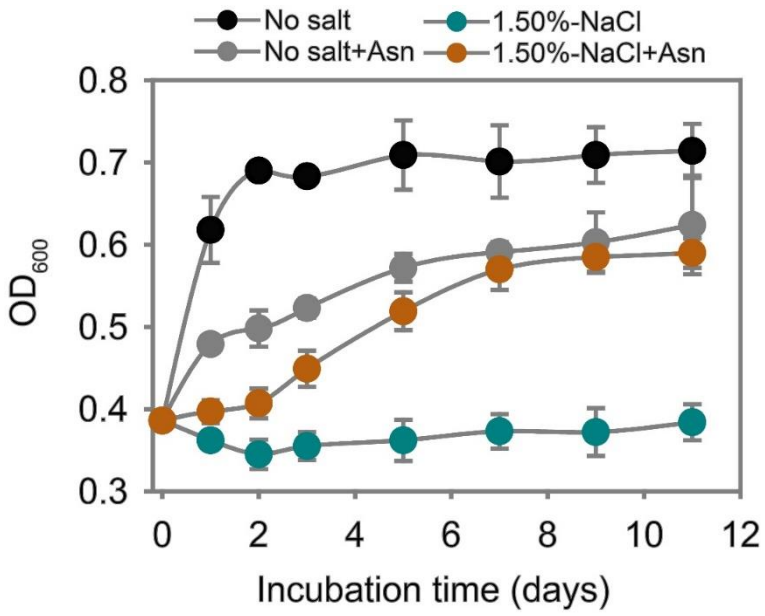

Fig S3.3 Growth of strain SC2 under the conditions of no-salt, 1.50%-NaCl, 1.50%-NaCl+Asn, and no-salt+Asn.

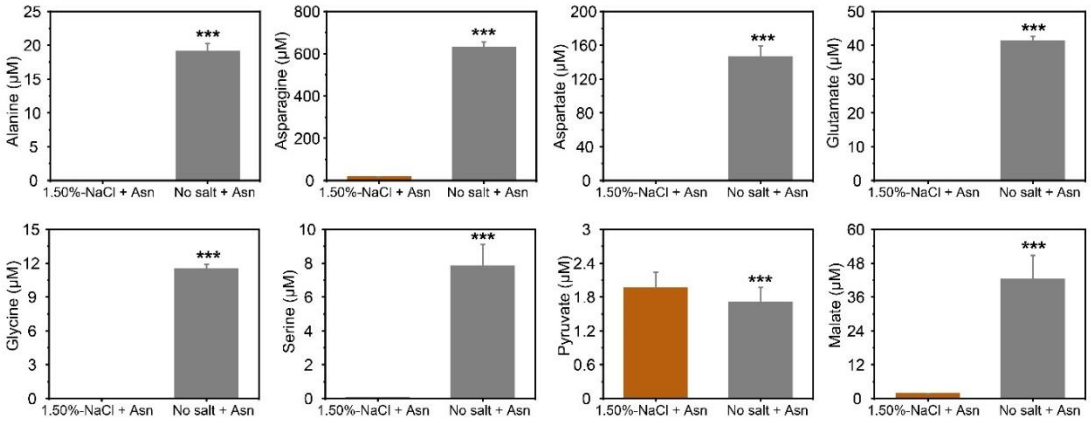

Fig S3.4 Absolute quantification of extracellular amino acids and organic acids of Methylocystis sp. strain SC2 under the conditions of (i) 1.50%-NaCl+Asn and (ii) no-salt+Asn. See full list at Table S4 and S6. SC2 biomass was collected at mid-phase phase. Asterisks indicate significant difference with ***p-value ≤ 0.001, using Tukey's method with one-way ANOVA. Measurements were done in triplicate cultures. Error bars show standard deviations of triplicate cultures.

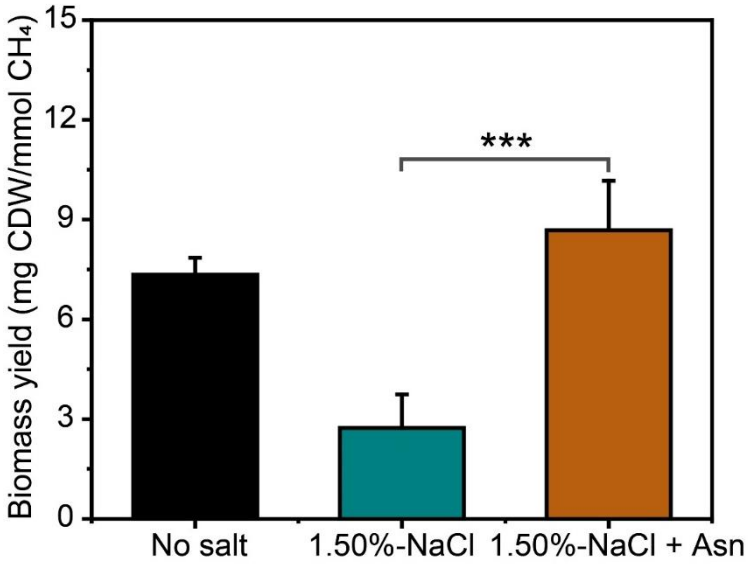

Fig S3.5 Methane-based biomass yield of Methylocystis sp. strain SC2 under the conditions of (i) no salt, (ii) 1.50%-NaCl, and (iii) 1.50%-NaCl+Asn. All the growth parameters were calculated based on the total CH_4 consumptions at the mid-log phase. The biomass yield calculation for 1.5%-NaCl+Asn is based on the hypothetical assumption that methane acted as the only carbon source for cell biomass production. Asterisks indicate significant difference with *p-value ≤ 0.05; **p-value ≤ 0.01; and ***p-value ≤ 0.001, using Tukey's method with one-way ANOVA. Measurements were done in triplicate cultures. Error bars show standard deviations of triplicate cultures.

3.8.2 Supplemental Tables

The supplemental tables (S3.1 to S3.12) are available at https://figshare.com/articles/dataset/Supplement_tables_pdf/213834

Chapter 4:
Discussion and Outlook

4 Discussion and Outlook

4.1 Discussion

Methane is the second most important greenhouse gas contributing to the rise in global warming since the industrial revolution (Jackson et al., 2020; Arias et al., 2021). It is also a promising carbon feedstock for the biological production of value-added chemicals. Methanotrophic bacteria are a unique group of microorganisms able to use CH_4 as the sole source of energy. Proteobacterial methanotrophs play a key role in reducing methane emissions to the atmosphere from methanogenic habitats (Hanson and Hanson, 1996; Gebert et al., 2004; Reim et al., 2012) and contribute to the atmospheric methane oxidation in grassland and forest soils (Conrad, 1996; Knief and Dunfield, 2005; Kolb et al., 2005; Cai et al., 2016; Täumer et al., 2022). Various abiotic factors in their native environment can affect methane oxidation (Conrad, 2007; Kaupper et al., 2020). Methane and nitrogen are the most well-studied factors. Fluctuations in their availability strongly shape the composition and activity of methanotrophic communities. Site-specific environmental parameters have, however, been shown to more greatly affect the composition of methanotroph communities than substrate availability (Kaupper et al., 2022).

In particular, the cellular mechanisms allowing non-saline methanotrophs to cope with high NH_4^+ load have not yet been well understood. The effect of inorganic nitrogen on aerobic methanotrophs has been widely studied, particularly in agricultural soils where ammonium- or nitrate-based fertilizers may influence CH_4 oxidation and affect the global CH_4 budget (Noll et al. 2008). Alphaproteobacterial methanotrophs of the *Methylocystis*/*Methylosinus* group were shown to possess a diverse nitrogen metabolism, including the reduction of nitrate to nitrite (Bowman et al. 1993), the fixation of atmospheric dinitrogen (Dam et al., 2013; Hoefman et al. 2014; Tays et al. 2018), the cometabolic oxidation of NH_3 (Nyerges and Stein 2009), and the detoxification of hydroxylamine and nitrite (Nyerges and Stein 2009; Nyerges et al. 2010). In particular, however, the physiological results of pure culture studies on the effect of NH_4^+ on methanotrophic activity were partly in conflict with environmental research demonstrating either inhibition or stimulation of CH_4 oxidation (Dunfield and Knowles

1995; Bodelier et al. 2000; Bodelier and Laanbroek 2004; Hoefman et al. 2014). State-of-the-art omics approaches applied to alphaproteobacterial methanotrophs of the genus *Methylocystis* may thus help to gain a deeper understanding of the underlying mechanisms driving their acclimatization to high NH_4Cl load. Similarly, such research may allow us to uncover metabolic potential of *Methylocystis* spp. to effectively combat severe NaCl stress.

This prompted our research, with *Methylocystis* sp. strain SC2 being the model organism. Strain SC2 was isolated in 1978 from the highly polluted river Saale near Wichmar, Germany (Dunfield et al., 2002; Heyer et al., 2002). A specific trait of strain SC2 is the expression of two pMMO isozymes with different methane oxidation kinetics, the low-affinity pMMO1 and the high-affinity pMMO2 (Baani and Liesack, 2008). The genome of *Methylocystis* sp. strain SC2 was found to comprise a 3.77 Mb chromosome and two large plasmids (Dam et al., 2012; Dam et al., 2013). Genomic analysis revealed not only all genes required for a methanotrophic lifestyle but also a diverse nitrogen metabolism including a complete denitrification pathway (Dam et al., 2013). Furthermore, the genome harbors a complete set of genes encoding polyhydroxybutyrate (PHB) metabolism. Indeed, strain SC2 has been shown to be a strong PHB producer. The maximum PHB content can be up to 30% of the cell weight under N_2 fixation condition (Pieja et al., 2011).

A unique characteristic of strain SC2 and other members of the *Methylocystis/Methylosinus* group is that their key enzyme (pMMO) and other associated membrane proteins are housed in an extensive system of copper-induced intracytoplasmic membranes (ICMs) (Zhu et al., 2022). In consequence, effective proteome analysis of *Methylocystis* spp. requires the efficient solubilization and digestion of their ICM system. A newly developed proteome workflow, termed crude-lysate-MS approach, proved to increase protein quantification accuracy and proteome coverage of strain SC2. It captured 62% of the predicted SC2 proteome, with up to 10-fold increase in membrane-associated proteins relative to less effective conditions (Hakobyan et al., 2018). Later, this workflow was used to provide proteomic evidence that strain SC2 is able to utilize hydrogen as an alternative energy source under oxygen-limited conditions (Hakobyan et al., 2020).

In our first project, we used this proteome workflow to elucidate the cellular mechanisms underlying the acclimatization of strain SC2 to high NH_4^+ load (**Chapter 2**). We predicted that increase in NH_4^+ load will have a dual effect on the activity of strain

SC2, with one being the general phenomenon of ionic-osmotic stress and the other being the competitive inhibition effect of NH_3 on pMMO-based methane oxidation. The research combined SC2 growth experiments under increasing NH_4^+ load (1 to 100 mM) with global proteomics, analysis of intracellular amino acids (metabolomics), and measurement of NO_2^- and N_2O release to the medium .

Relative to 1 mM NH_4^+, high (50 mM and 75 mM) NH_4^+ load under CH_4-replete conditions significantly increased the lag phase duration required for proteome adjustment. The number of differentially regulated proteins was highly significantly correlated with the increase in NH_4^+ load. The cellular responses involved the significant upregulation of stress-responsive proteins, the K^+ "salt-in" strategy, the synthesis of compatible solutes (glutamate and proline), and the induction of the glutathione metabolism pathway. This response pattern is common to most bacteria (e.g., *Escherichia coli*, *Bacillus subtilis*) and indicative of ionic-osmotic stress phenomena (Hoffmann et al., 2002; Imlay, 2015; Gregory and Boyd, 2021).

The apparent K_m value for CH_4 oxidation significantly increased with the NH_4^+ concentration. This observation was indicative of an increased pMMO-based oxidation of NH_3 to toxic hydroxylamine. In consequence, the detoxifying activity of hydroxlyamine oxidoreductase (HAO) increased with the NH_4^+ load and led to a significant accumulation of NO_2^- and, with delay, N_2O. Recent purification of the mHAO from the verrucomicrobial methanotroph Methylacidiphilum fumariolicum provided biochemical evidence that this enzyme oxidizes hydroxylamine to NO rather than to NO_2^- (Moller et al., 2019; Versantvoort et al., 2020). Given that NO is an obligate free intermediate, one has to postulate either an as-yet-unknown NO-oxidizing enzyme that converts NO to NO_2^- or the spontanenous reaction with O_2 to form NO_2^- (Gupta et al., 2016). Significant production of N_2O occurred only after the oxygen concentration had dropped to low or unmeasurable levels. Candidate enzymes in strain SC2 for the reduction of NO to N_2O are a putative NO reductase (NorB) and hybrid cluster proteins (Hcps). Nitric oxide reductase and Hcps were significantly upregulated. Among the various functional roles historically proposed for Hcps, most likely is the conversion of NO to N_2O (NO reductase activity), which has been established as physiologically relevant (Hagen, 2022).

In summary, strain SC2 has the capacity to precisely rebalance enzymes and osmolyte composition in response to increasing NH_4^+ exposure, but the need to simultaneously combat both ionic-osmotic stress and the toxic effects of hydroxylamine may be the reason why its acclimatization capacity is limited to 75 mM NH_4^+.

Starting point of my second project was the knowledge that the growth of strain SC2 is completely inhibited at medium concentrations of 1.5% NaCl (Han et al., 2017) (**Chapter 3**). Sodium chloride is an important ionic-osmotic stressor in bulk and rhizosphere soils (Osudar et al., 2017). Thus, we tested a series of external compounds (amino acids and other potential osmolytes) to act as a compatible solute or osmoprotectant under otherwise inhibitory NaCl conditions (Roberts, 2005; Reshetnikov et al., 2006). Besides ornithine, the addition of 1 mM asparagine to the growth medium showed a major stress relief effect under 1% NaCl. Further analysis revealed that the addition of 10 mM asparagine had the greatest stress relief effect under 1.5% NaCl, thereby leading to a partial growth recovery of strain SC2. Thus, we decided to investigate the stress relief effect of 10 mM asparagine under 1.5% NaCl condition in greater detail. This involved global proteomics and metabolomics, including a tracing experiment with ^{13}C-labeled asparagine. Analysis of the exo-metabolome revealed that asparagine was taken up by strain SC2 quantitatively, resulting in an intracellular concentration of 264.43 mM. Compared to severe salinity (1.5% NaCl), the uptake of asparagine induced major proteome rearrangements. In particular, various proteins affiliated with the following KEGG level 2 categories showed a significant and positive expression response to the asparagine uptake: energy metabolism, amino acid metabolism, and cell growth and death. This involved cell-division-related proteins such as the two-component transcriptional regulator (CtrA), the HPTransfase domain-containing protein (ChpT), the multi-sensor signal transduction histidine kinase (PleC), the ATP-dependent zinc metalloprotease (FtsH), and the cell division protein (FtsA). Among other factors, this explains well the partial growth recovery of strain SC2. Presumably, the intracellular asparagine also acted as a nitrogen source due to hydrolytic conversion of asparagine into aspartate. The released NH_4^+ may have favored the conversion of α-ketoglutarate into glutamate by glutamate dehydrogenase (GDH) whose expression was highly upregulated. Significant downregulation of the nitrate transporter (UniProt ID J7Q4T7) provided further evidence for a switch in the nitrogen source from nitrate to asparagine. This transporter is known to be transcriptionally and post-translationally regulated by intracellular NH_4^+ (Rice and Tiedje, 1989). The distribution of ^{13}C-carbon across nearly

all canonical amino acids, but also theoretical calculations, suggests that asparagine-derived carbon was incorporated into cell biomass. In addition to asparagine and aspartate, amino acids (glutamate, alanine) and metabolites (pyruvate) closely associated with the citric acid cycle were most strongly ^{13}C-labeled.

4.2 Concluding remarks and outlook

In this work, we provide new insights into the metabolic potential of *Methylocystis* sp. strain SC2 to cope with environmental stress. This involved the cellular acclimatization of strain SC2 to high NH_4^+ load and a newly uncovered metabolic potential to combat severe NaCl stress. Knowledge of these metabolic capabilities is of importance considering that *Methylocystis* spp. reside in agricultural soils, which may be treated with NH_4^+-based fertilizers, and in soils that are globally at risk of salinization (e.g., rice paddies, grasslands). The intracellular accumulation of compatible solutes through *de novo* synthesis or import is known to be an effective mechanism to cope with osmotic and salt stress. Here, we showed that with increasing NH_4^+ load, strain SC2 accumulates glutamate and, at higher osmotic pressure, proline in addition. This is a typical stress response pattern that has previously been shown for a variety of model organisms such *E. coli* and *B. subtilis*. However, the relief effect of asparagine under otherwise completely inhibitory NaCl stress was a novel and unexpected finding. The uptake of asparagine led to a partial growth recovery with half of the biomass produced under standard growth condition. The tracing experiment with ^{13}C-labeled asparagine allowed us to identify those organic acids (e.g., pyruvate, malate, glyoxylate) and amino acids (e.g., aspartate, glutamate, alanine) whose intracellular pools were most affected by the uptake of asparagine. In particular, the high ^{13}C-labeling degree of glutamate suggests that it acted as a major hub between central carbon and amino acid pathways. However, our current research data are insufficient to draw definite conclusions about how the asparagine uptake changed the flux of metabolites through these pathways. This would require additional research, such as metabolite flux measurements coupled to ^{13}C-labeling experiments with both methane and asparagine (**the future project I**). In particular, elucidation of the functional role of the glycine cleavage system, whose expression was specifically upregulated by the uptake of asparagine under severe salinity (1.5% NaCl), would be of major interest (**the future project II**). Finally, we found that not only asparagine but also the amino acids ornithine, lysine, and alanine had a stress relief effect

on strain SC2 under osmotically unfavorable conditions (1.0% NaCl). Thus, a comparative analysis of their stress relief effects on the proteomic and metabolomic level would be of interest. This should also address the question of whether these amino acids can act under severe salinity as the only external nitrogen source, in addition to their stress relief effect (**the future project III**).

4.3 References

Arias, P., Bellouin, N., Coppola, E., Jones, R., Krinner, G., Marotzke, J. et al. (2021) Climate Change 2021: The Physical Science Basis. Contribution of Working Group14 I to the Sixth Assessment Report of the Intergovernmental Panel on Climate Change; Technical Summary.

Baani, M., and Liesack, W. (2008) Two isozymes of particulate methane monooxygenase with different methane oxidation kinetics are found in *Methylocystis* sp. strain SC2. *Proceedings of the National Academy of Sciences* **105**: 10203-10208.

Balch, W., Fox, G.E., Magrum, L.J., Woese, C.R., and Wolfe, R. (1979) Methanogens: reevaluation of a unique biological group. *Microbiological reviews* **43**: 260-296.

Cai, Y., Zheng, Y., Bodelier, P.L.E., Conrad, R., and Jia, Z. (2016) Conventional methanotrophs are responsible for atmospheric methane oxidation in paddy soils. *Nature Communications* **7**: 11728.

Conrad, R. (1996) Soil microorganisms as controllers of atmospheric trace gases (H2, CO, CH4, OCS, N2O, and NO). *Microbiological reviews* **60**: 609-640.

Conrad, R. (2007) Microbial Ecology of Methanogens and Methanotrophs. In *Advances in Agronomy*: Academic Press, pp. 1-63.

Dam, B., Dam, S., Blom, J., and Liesack, W. (2013) Genome analysis coupled with physiological studies reveals a diverse nitrogen metabolism in *Methylocystis* sp strain SC2. *Plos One* **8**: e74767.

Dam, B., Dam, S., Kube, M., Reinhardt, R., and Liesack, W. (2012) Complete genome sequence of *Methylocystis* sp Strain SC2, an aerobic methanotroph with high-affinity methane oxidation potential. *Journal of Bacteriology* **194**: 6008-6009.

Dunfield, P.F., Yimga, M.T., Dedysh, S.N., Berger, U., Liesack, W., and Heyer, J. (2002) Isolation of a Methylocystis strain containing a novel pmoA-like gene. *Fems Microbiology Ecology* **41**: 17-26.

Fei, Q., Guarnieri, M.T., Tao, L., Laurens, L.M.L., Dowe, N., and Pienkos, P.T. (2014) Bioconversion of natural gas to liquid fuel: Opportunities and challenges. *Biotechnol Adv* **32**: 596-614.

Gebert, J., Gröngröft, A., Schloter, M., and Gattinger, A. (2004) Community structure in a methanotroph biofilter as revealed by phospholipid fatty acid analysis. *FEMS Microbiology Letters* **240**: 61-68.

Gregory, G.J., and Boyd, E.F. (2021) Stressed out: Bacterial response to high salinity using compatible solute biosynthesis and uptake systems, lessons from Vibrionaceae. *Computational and Structural Biotechnology Journal* **19**: 1014-1027.

Gupta, P., Lakes, A., and Dziubla, T. (2016) Chapter One - A free radical primer. In *Oxidative Stress and Biomaterials*. Dziubla, T., and Butterfield, D.A. (eds): Academic Press, pp. 1-33.

Hagen, W.R. (2022) Structure and function of the hybrid cluster protein. *Coordination Chemistry Reviews* **457**: 214405.

Hakobyan, A., Liesack, W., and Glatter, T. (2018) Crude-MS strategy for in-depth proteome analysis of the methane-oxidizing *Methylocystis* sp. strain SC2. *J Proteome Res* **17**: 3086-3103.

Hakobyan, A., Zhu, J., Glatter, T., Paczia, N., and Liesack, W. (2020) Hydrogen utilization by *Methylocystis* sp. strain SC2 expands the known metabolic versatility of type IIa methanotrophs. *Metabolic Engineering* **61**: 181-196.

Han, D., Link, H., and Liesack, W. (2017) Response of Methylocystis sp. Strain SC2 to Salt Stress: Physiology, Global Transcriptome, and Amino Acid Profiles. *Appl Environ Microbiol* **83**: e00866-00817.

Hanson, R.S., and Hanson, T.E. (1996) Methanotrophic bacteria. *Microbiological Reviews* **60**: 439-671.

Heyer, J., Galchenko, V.F., and Dunfield, P.F. (2002) Molecular phylogeny of type II methane-oxidizing bacteria isolated from various environmentsThe GenBank accession numbers for the nearly complete 16S rRNA gene sequences for the isolates are AJ458466 to AJ458510. Partial sequences of the pmoA, mxaF and mmoX genes have been deposited under the accession numbers AJ458994–AJ459052, AJ459053–AJ459100 and AJ458511–AJ458535, respectively. Where multiple strains contained identical sequences, only one has been deposited. *Microbiology* **148**: 2831-2846.

Hoffmann, T., Schütz, A., Brosius, M., Völker, A., Völker, U., and Bremer, E. (2002) High-salinity-induced iron limitation in Bacillus subtilis. *J Bacteriol* **184**: 718-727.

Imlay, J.A. (2015) Diagnosing oxidative stress in bacteria: not as easy as you might think. *Curr Opin Microbiol* **24**: 124-131.

Jackson, R.B., Saunois, M., Bousquet, P., Canadell, J.G., Poulter, B., Stavert, A.R. et al. (2020) Increasing anthropogenic methane emissions arise equally from agricultural and fossil fuel sources. *Environmental Research Letters* **15**: 071002.

Kaupper, T., Luehrs, J., Lee, H.J., Mo, Y., Jia, Z., Horn, M.A., and Ho, A. (2020) Disentangling abiotic and biotic controls of aerobic methane oxidation during re-colonization. *Soil Biol Biochem* **142**: 107729.

Kaupper, T., Mendes, L.W., Poehlein, A., Frohloff, D., Rohrbach, S., Horn, M.A., and Ho, A. (2022) The methane-driven interaction network in terrestrial methane hotspots. *Environmental Microbiome* **17**: 15.

Knief, C., and Dunfield, P.F. (2005) Response and adaptation of different methanotrophic bacteria to low methane mixing ratios. *Environ Microbiol* **7**: 1307-1317.

Kolb, S., Knief, C., Dunfield, P.F., and Conrad, R. (2005) Abundance and activity of uncultured methanotrophic bacteria involved in the consumption of atmospheric methane in two forest soils. *Environmental Microbiology* **7**: 1150-1161.

Moller, M.N., Rios, N., Trujillo, M., Radi, R., Denicola, A., and Alvarez, B. (2019) Detection and quantification of nitric oxide-derived oxidants in biological systems. *J Biol Chem* **294**: 14776-14802.

Osudar, R., Klings, K.W., Wagner, D., and Bussmann, I. (2017) Effect of salinity on microbial methane oxidation in freshwater and marine environments. *Aquatic Microbial Ecology* **80**: 181-192.

Pieja, A.J., Sundstrom, E.R., and Criddle, C.S. (2011) Poly-3-hydroxybutyrate metabolism in the type II methanotroph Methylocystis parvus OBBP. *Applied and environmental microbiology* **77**: 6012-6019.

Reim, A., Lüke, C., Krause, S., Pratscher, J., and Frenzel, P. (2012) One millimetre makes the difference: high-resolution analysis of methane-oxidizing bacteria and their specific activity at the oxic–anoxic interface in a flooded paddy soil. *The ISME journal* **6**: 2128-2139.

Reshetnikov, A.S., Khmelenina, V.N., and Trotsenko, Y.A. (2006) Characterization of the ectoine biosynthesis genes of haloalkalotolerant obligate methanotroph "Methylomicrobium alcaliphilum 20Z". *Archives of Microbiology* **184**: 286-297.

Rice, C.W., and Tiedje, J.M. (1989) Regulation of nitrate assimilation by ammonium in soils and in isolated soil microorganisms. *Soil Biol Biochem* **21**: 597-602.

Roberts, M.F. (2005) Organic compatible solutes of halotolerant and halophilic microorganisms. *Saline Systems* **1**: 5.

Rodríguez, Y., Firmino, P.I.M., Pérez, V., Lebrero, R., and Muñoz, R. (2020) Biogas valorization via continuous polyhydroxybutyrate production by Methylocystis hirsuta in a bubble column bioreactor. *Waste Manage* **113**: 395-403.

Saratale, G.D., and Oh, M.-K. (2015) Characterization of poly-3-hydroxybutyrate (PHB) produced from Ralstonia eutropha using an alkali-pretreated biomass feedstock. *International journal of biological macromolecules* **80**: 627-635.

Täumer, J., Marhan, S., Groß, V., Jensen, C., Kuss, A.W., Kolb, S., and Urich, T. (2022) Linking transcriptional dynamics of CH4-cycling grassland soil microbiomes to seasonal gas fluxes. *The ISME Journal* **16**: 1788-1797.

Trotsenko, Y.A., and Murrell, J.C. (2008) Metabolic aspects of aerobic obligate methanotrophy. *Advances in Applied Microbiology, Vol 63* **63**: 183-229.

Versantvoort, W., Pol, A., Jetten, M.S.M., Niftrik, L.v., Reimann, J., Kartal, B., and Camp, H.J.M.O.d. (2020) Multiheme hydroxylamine oxidoreductases produce NO during ammonia oxidation in methanotrophs. *Proceedings of the National Academy of Sciences* **117**: 24459-24463.

Wang, Y., Yin, J., and Chen, G.Q. (2014) Polyhydroxyalkanoates, challenges and opportunities. *Curr Opin Biotechnol* **30**: 59-65.

Yeo, J.C.C., Muiruri, J.K., Thitsartarn, W., Li, Z., and He, C. (2018) Recent advances in the development of biodegradable PHB-based toughening materials: Approaches, advantages and applications. *Materials Science and Engineering: C* **92**: 1092-1116.

Zhu, Y., Koo, C.W., Cassidy, C.K., Spink, M.C., Ni, T., Zanetti-Domingues, L.C. et al. (2022) Structure and activity of particulate methane monooxygenase arrays in methanotrophs. *Nature Communications* **13**: 5221.

Acknowledgements

From 2018 to 2022, this 4 years PhD study was a challenging and highly rewarding journey that prepared me for my future career as a scientist. There are many faculties and friends for me to express sincere thankfulness.

First and foremost, I would like to thank my supervisor **Dr. Werner Liesack** for giving me the opportunity to work on these exciting projects in his lab. He provided support since the first email contact in November 2017 and continued supervision and guidance from day one when I arrived in Germany in October 2018. My doctoral studies and this thesis would never be possible to be accomplished without his professional guidance. I thank him for spending so much time training my way of thinking on lab experiments, scientific presentations, manuscript preparation and revision. His preciseness on scientific research will affect my whole life.

I am thankful to my thesis advisory committee members, **Prof. Dr. Andreas Brune, Prof. Dr. Tobias Erb** and **Dr. Timo Glatter**, for their precious time, helpful guidance, and valuable suggestions. In particular, I am very grateful to my second supervisor **Prof. Dr. Andreas Brune** for his insightful comments on my research projects and for sharing his knowledge in biochemistry during our joint seminars and FISH workshop. I am grateful to **Dr. Timo Glatter** for providing training on Proteomics.

I would like to give lot of thanks again to **Dr. Werner Liesack**, **Prof. Dr. Martin Thanbichler**, **Prof. Dr. Gert Bange**, and **Prof. Dr. Lennart Randau** to be my thesis committee members.

I would like to specially thank **Dr. Nicole Paczia**. I am very happy to collaborate with her a lot in my projects. During my PhD study, I was able to interact with her frequently, which helped me to learn many valuable insights into metabolomics and ^{13}C tracing analysis. Dr. Paczia shared her extensive knowledge of metabolomics and taught me how to design experiments, collect samples, and analyze the data.

Furthermore, I would like to thank all members of the AG Liesack. In particular, I would like to thank **Dr. Anna Hakobyan**, an excellent PhD student and now a postdoc at the INRES Molecular Biology of the Rhizosphere, University of Bonn (Bonn, Germany). Anna provided the essential support in the beginning of my lab work and showed me how to grow our model organism - *Methylocystis* sp. strain SC2. She provided

me with much help during my proteomics experiments. Thanks to **Dr. Qicheng Bei** for his support in my research and for sharing his thoughts on science and life. Thanks to **Xin Li** for four years of great companionship in the lab.

I am grateful to the **China Scholarship Council (CSC)** for providing me with three years of scholarship to study and live in Marburg.

Last but not least, I sincerely thank **my parents**, **my sister**, and my whole family in China for their unfailing support. Thanks to my beloved parents for your encouragement and support of my academic and life abroad.